DIFFERENT WHIRLIN SPLICING ISOFORMS PLAY UNIQUE ROLES IN THE INNER EAR AND RETINA

by

Pranav Dinesh Mathur

A dissertation submitted to the faculty of
The University of Utah
in partial fulfillment of the requirements for the degree of

Doctor of Philosophy

Department of Neurobiology and Anatomy

The University of Utah

August 2016

The University of Utah Graduate School

STATEMENT OF DISSERTATION APPROVAL

The dissertation of **Pranav Dinesh Mathur**

has been approved by the following supervisory committee members

Jun Yang	, Chair	**5/10/2016** Date Approved
Gary C. Schoenwolf	, Member	**5/09/2016** Date Approved
Wolfgang Baehr	, Member	**5/09/2016** Date Approved
Suzanne L. Mansour	, Member	**5/09/2016** Date Approved
Michael Robert Deans	, Member	**5/12/2016** Date Approved
Yukio Saijoh	, Member	**5/10/2016** Date Approved

and by **Monica L. Vetter**, Chair of

the Department/College/School of **Neurobiology and Anatomy**

and by David B. Kieda, Dean of The Graduate School.

ABSTRACT

Usher Syndrome (USH) is the leading cause of deaf-blindness worldwide. Patients with USH have hearing loss, balance problems, and retinal degeneration. To date, eleven genes have been associated with USH. Interestingly, mutations in several USH genes lead to discrete diseases as well. Despite extensive studies on USH in the past, over one-hundred years since USH was originally identified, the molecular function of USH genes remains understudied. This incomplete understanding greatly limits therapeutic development for USH. To understand the molecular mechanisms underlying variable disease manifestations, I studied an USH2 gene, *DFNB31,* which causes USH2D when mutated in its N-terminal region, and autosomal recessive nonsyndromic deafness type 31 (DFNB31) when mutated towards its C-terminal region. *DFNB31* encodes a protein called whirlin that was previously shown to have multiple mRNA variants in human and mouse tissues. I hypothesized that whirlin isoforms have unique functions and disruption of different whirlin isoforms is the cause of various disease manifestations. To test this hypothesis, I utilized region-specific whirlin antibodies and *Dfnb31* mouse models that mimic human *DFNB31* mutations and disease outcomes. I found that alternative splicing and alternative use of promoters produce several *Dfnb31* mRNA variants that are translated to full-length (FL), N-terminal and C-terminal whirlin isoforms, which localize at different subcellular positions in the inner ear hair cells and retinal photoreceptors. Studies in *Dfnb31* mutants show that FL-whirlin isoform is required at the hair cell stereociliary bases and retinal

photoreceptor periciliary membrane complex to form a stable USH2 protein complex, whereas C-whirlin isoform is required at the stereocilia tips for stereociliary elongation. I found that mutations in N-terminal region of *Dfnb31* lead to loss of FL- and N-whirlin isoforms and cause USH2D-like symptoms. On the other hand, mutations in the C-terminal region of *Dfnb31* lead to loss of FL- and C-whirlin isoforms and cause DFNB31-like symptoms. Considering the presence of multiple splicing isoforms for several other USH genes and the variable phenotypes caused by mutations in these genes, differential disruption of the splicing isoforms is likely the mechanism underlying different disease manifestations upon mutation in these USH genes. In addition, I found vestibular deficits in *Dfnb31* mutants, which was surprising because USH2 patients were thought to have normal vestibular function. My findings present a rationale for vestibular analysis of all USH2 patients at the clinics to comprehend the pathogenesis and mechanism of USH. In summary, my findings will help improve differential diagnosis between USH and its related diseases and is expected to contribute to the development of USH therapies.

“Be more dedicated to making solid achievements than in running after swift but synthetic happiness.”

Late Dr. APJ Abdul Kalam

TABLE OF CONTENTS

ABSTRACT……...iii

ACKNOWLEDGEMENTS……..……...viii

Chapters

1. PROLOGUE……1

References……6

2. USHER SYNDROME: HEARING LOSS, RETINAL DEGENERATION AND ASSOCIATED ABNORMALITIES……..…….…...8

Abstract……9
Introduction……..9
Genes and loci identified in USH patients…….……11
Expression of USH genes……...12
USH proteins exist in multiprotein complexes……...14
Functional studies of USH gene products……...15
Insights from current literatures about USH genes in various tissues…….17
Current progress in therapeutic studies on USH……17
Current gaps in understanding and treating USH……18
Summary……19
Acknowledgements……19
References……..19

3. DISTINCT EXPRESSION AND FUNCTION OF WHIRLIN ISOFORMS IN THE INNER EAR AND RETINA: AN INSIGHT INTO PATHOGENESIS OF USH2D AND DFNB31……..…….24

Abstract……..25
Introduction ...……25
Results ...……26
Discussion……..……34
Materials and methods……...37
Acknowledgements ……...……....38
References ……..……38

4. A STUDY OF WHIRLIN ISOFORMS IN THE MOUSE VESTIBULAR SYSTEM SUGGESTS POTENTIAL VESTIBULAR DYSFUNCTION IN DFNB31-DEFICIENT PATIENTS……...41

Abstract……..……42
Introduction ……...…….…..……..42
Results ……...…….…..43
Discussion…….…….……48
Materials and methods…….…….……52
Acknowledgements ……...…...53
References…….……....53

5. DISCUSSION…….…..……..56

Introduction…….……..57
Mutations in DFNB31 cause variable disease manifestations .……...61
Dfnb31 mouse models recapitulate USH2D and DFNB31 diseases……..……..…..63
Whirlin has different spatiotemporal expression patterns in the inner ear and retina ..……...……....69
Whirlin forms different multiprotein complexes in the inner ear and retina..…….…...74
Correlation of genotypes with phenotypes conveys the function of different whirlin isoforms ……...……....…79
Whirlin isoforms have functions outside the inner ear and retina……82
Previous attempts to rescue Dfnb31 mutant phenotypes were only partially successful……...83
Conclusion and future directions……...84
References……..……88

ACKNOWLEDGEMENTS

First and foremost I would like to thank, with all my heart, my mentor Dr. Jun Yang for accepting me in her laboratory and giving me this incredible project to work on. I always wanted to do a research with high translational significance and Jun gave me this beautiful project that I was able to develop and contribute to science. Her guidance, persistence, and cooperation helped me throughout my research. She always welcomed my ideas and provided me the freedom to experiment out and test my hypothesis. In addition, she helped me improve my train of thought, which will help me become an independent scientist one day.

I would like to specially acknowledge Dr. Yukio Saijoh, my previous employer and current thesis committee member. I worked in Yukio's lab as a laboratory technician for about a year. This experience not only helped me get into the graduate school, but also trained me to understand how science is done. Over the past several years, he has been more than a mentor to me. He is someone to whom I can run anytime with my problems. He always found time to listen to me and provided me a valid and most appropriate solution for my scientific/nonscientific worries. I would also like to thank other members of my supervisory committee, Drs. Suzanne Mansour, Gary Schoenwolf, Michael Deans and Wolfgang Baehr, who have given me valuable inputs and have been generous with their time.

I would also like to take this opportunity to thank my undergraduate mentor, Dr. Arun Sirothia from the Nagpur Veterinary College, MAFSU, and my master's mentors, Drs. GVPPS Ravi Kumar and Gurvinder Singh Brah from the College of Veterinary Sciences, GADVASU in India. They were the ones who instilled in me a desire to do research in Cell Biology and Genetics. They also provided me with basic concepts of Genetics and my first hands-on experience with several molecular biology techniques.

A great deal of thanks goes to my current and previous lab-mates, Junhuang, Qian, Ali Sharif, Cris, Jesse and Christin, who helped me with experiments and were always enthusiastic to talk about science. I would also like to thank Ali Almishaal, my scientific collaborator-cum-friend who helped me in my project by doing ABRs and DPOAE tests. Eventually, I also helped him in several experiments on his project. This gave me an idea about how collaboration works. I hope we both benefited by this collaboration and get more publications.

I am sincerely thankful to my parents and parents-in-law, who always stood by me through thick and thin. My parents were my first source of inspiration. My father provided me my first ever understanding about Biology and Mathematics, and always encouraged me to pursue a scientific career. Ever since I met my parents-in-law, they have always motivated me and kept praying for my success. Last, but certainly not the least, I am thankful for my best friend and wife Deepti for her love, patience and endless support. Deepti moved to Salt Lake with me when I started my PhD program in 2010. She cooperated with me and always helped me, especially those days when I was terribly busy and stressed. She always believed in me and stood by me during this entire process. I will always be grateful to her kindness.

CHAPTER 1

PROLOGUE

Background and significance of the study in this dissertation

The overall goal of the research in this dissertation is to address the molecular functions of Usher syndrome (USH) proteins, and Chapters 2 to 4 represent my specific accomplishments in the process. Diseases that affect the retina and inner ear, two main sensory organs of the human body, significantly affect the patient's social life and psychological health. USH accounts for more than 50% of inherited deaf-blindness cases, with an estimated frequency of 1:6000 (Kimberling et al., 2010). USH patients exhibit a variety of symptoms. Based on the severity of hearing loss, USH is categorized into three clinical types, namely, USH1, USH2 and USH3. USH1 patients have congenital profound sensorineural hearing loss; USH2 patients display moderate to severe levels of congenital sensorineural hearing loss; and USH3 patients have progressive deafness. All USH patients undergo retinal degeneration (RD). However, the onset of RD is variable, with adolescence being the earliest age reported.

There are eleven known genes that can cause USH. Most proteins encoded by these USH genes interact with one another to form complexes that carry out various functions in the inner ear and retina. To comprehend the complexity of USH genes, their known functions, available animal models, and current research progress, I co-authored a review paper that will serve as Chapter 2 of this dissertation (Mathur & Yang, 2015). Chapter 2 will thoroughly introduce the readers to various USH proteins, their functions, interaction complexes, disease outcomes, unsolved problems in USH research, and the current state of therapeutic advancement. A major limitation in the path of therapeutic advancement is the lack of complete knowledge of USH protein functions at the molecular level. Specifically, the function of USH proteins, in complex with other proteins at different subcellular

locations of various sensory organs, remains obscure. Furthermore, it remains unknown how mutations in most USH genes cause multiple discrete diseases. Addressing these questions is important since, despite several efforts to study USH genes and to develop therapies, there is no cure for USH to date. An understanding of the molecular function of USH proteins will aid disease treatment, early differential diagnosis, and patient rehabilitation. Moreover, it will advance our understanding of the cell-specific function of USH proteins.

Study design and results

To reveal the molecular mechanisms underlying USH, I studied an USH2 gene, *DFNB31*, which encodes a protein called whirlin. Mutations in the 5' region of *DFNB31* are associated with USH2D, a subtype of USH, while mutations in the 3' region cause DFNB31, a subtype of nonsyndromic autosomal recessive deafness (DFNB) (Audo et al., 2011; Besnard et al., 2012; Ebermann et al., 2007; Mburu et al., 2003; Nishiguchi et al., 2013; Tlili et al., 2005). The variation in the disease outcome upon mutations within the same gene impacts differential diagnosis and development of therapies. Therefore, the objective of my research in Chapter 3 was to understand the genotype-phenotype correlation upon mutations in *Dfnb31*. To address this question, I utilized *Dfnb31* mouse mutants that mimic the region and outcome of human *DFNB31* mutations. A mouse *Dfnb31*$^{neo/neo}$ mutant, generated by replacing the 5' region of *Dfnb31* exon1 including the translation start codon with a *Neo*^{r} cassette, mimics the mutation region and disease outcome of USH2D (Yang et al., 2010), whereas a *Dfnb31*$^{wi/wi}$ mutant mouse that harbors a 592-bp deletion in the coding region of *Dfnb31* exons 6-9 mimics DFNB31 patients

(Mburu et al., 2003). Furthermore, similar to human *DFNB31*, mouse *Dfnb31* is also known to yield multiple mRNA transcripts, likely as a result of alternative splicing and/or presence of multiple promoters in the gene (Belyantseva et al., 2005; Mburu et al., 2003; Wright, Hong, & Perkins, 2012). In my study, I found different spatiotemporal expressions and subcellular localizations of *Dfnb31* mRNA variants and whirlin protein isoforms in the organ of Corti hair cells and retinal photoreceptors. My studies show that a mutation in *Dfnb31* leads to loss of different whirlin protein isoforms, depending upon the site of the mutation (Mathur, Zou et al., 2015). As a result, inner ear hair cells and/or retinal photoreceptors are differentially affected, resulting in either DFNB31 or USH2D. My study, combined with previous findings showing multiple splicing isoforms of several other USH genes and variable phenotypes caused by mutations of these USH genes, suggests that a parallel mechanism plays a role in those cases as well.

Dfnb31 was previously reported to have multiple mRNA variants in the mouse vestibular hair cells (Belyantseva et al., 2005). In addition, a *Dfnb31* mutant (*Dfnb31*$^{wi/wi}$) shows circling and head-bobbing behaviors, suggestive of vestibular deficits (Holme et al., 2002). Since patients with mutations in *DFNB31* do not report any balance issues, the role of whirlin in the vestibular system remains understudied. To understand the role of whirlin in the vestibular system, I examined the *Dfnb31*$^{neo/neo}$ and *Dfnb31*$^{wi/wi}$ vestibular hair cells. My studies revealed for the first time that a mutation in *Dfnb31* leads to vestibular impairment, suggesting a possibility that USH2D and DFNB31 patients may have vestibular abnormalities (Mathur, Vijayakumar, et al., 2015). These results were published in *Human Molecular Genetics* and form Chapter 4 of this dissertation. The study described in Chapter 4 is significant, since, to date, vestibular abnormalities are thought to be

restricted only to USH1 and USH3 patients. My study suggests that USH2 patients need to be tested for vestibular problems in the clinics in the future. My findings have been further supported by a recent clinical study that reported the presence of vestibular pathologies in a majority of USH2 patients studied (Magliulo et al., 2015). Finally, my study in Chapter 4 also elucidates the molecular functions of *Dfnb31* in the murine vestibular system.

Conclusion

Overall, I found that disruption of different whirlin isoforms by different mutations is the molecular basis underlying the genotype-phenotype correlation in mice, suggesting that a similar mechanism underlies the different disease manifestations in *DFNB31*-deficient humans. Differential isoform disruption could also be the cause for a wide spectrum of disease manifestation in patients carrying mutations in other USH genes. For example, a mutation in CDH23, known to express three different protein isoforms, can cause either USH1D or DFNB12 (Lagziel et al., 2005; Schultz et al., 2005, 2011). Furthermore, I found that *DFNB31*-deficient patients may also have vestibular deficits in addition to hearing and/or vision defects. These findings are discussed in a broader context in Chapter 5 of this dissertation, written in a stand-alone review format. In addition, Chapter 5 explains how my research, described in Chapters 3 and 4, will inform accurate clinical diagnosis and therapeutic progress. Accurate differential diagnosis of patients with mutated USH genes is critical for parental counselling and initiation of rehabilitation and treatment.

References

Audo, I., Bujakowska, K., Mohand-Saïd, S., Tronche, S., Lancelot, M.-E., Antonio, A., … Zeitz, C. (2011). A novel DFNB31 mutation associated with Usher type 2 syndrome showing variable degrees of auditory loss in a consanguineous Portuguese family. *Molecular Vision*, *17*, 1598–606. Retrieved from http://www.pubmedcentral.nih.gov/articlerender.fcgi?artid=3123164&tool=pmcentrez&rendertype=abstract

Belyantseva, I. a, Boger, E. T., Naz, S., Frolenkov, G. I., Sellers, J. R., Ahmed, Z. M., … Friedman, T. B. (2005). Myosin-XVa is required for tip localization of whirlin and differential elongation of hair-cell stereocilia. *Nature Cell Biology*, *7*(2), 148–156. http://doi.org/10.1038/ncb1219

Besnard, T., Vaché, C., Baux, D., Larrieu, L., Abadie, C., Blanchet, C., … Roux, A.-F. (2012). Non-USH2A mutations in USH2 patients. *Human Mutation*, *33*(3), 504–10. http://doi.org/10.1002/humu.22004

Ebermann, I., Scholl, H. P. N., Charbel Issa, P., Becirovic, E., Lamprecht, J., Jurklies, B., … Bolz, H. (2007). A novel gene for Usher syndrome type 2: Mutations in the long isoform of whirlin are associated with retinitis pigmentosa and sensorineural hearing loss. *Human Genetics*, *121*(2), 203–211. http://doi.org/10.1007/s00439-006-0304-0

Holme, R. H., Kiernan, B. W., Brown, S. D. M., & Steel, K. P. (2002). Elongation of hair cell stereocilia is defective in the mouse mutant whirler. *The Journal of Comparative Neurology*, *450*(1), 94–102. http://doi.org/10.1002/cne.10301

Kimberling, W. J., Hildebrand, M. S., Shearer, A. E., Jensen, M. L., Halder, J. A., Trzupek, K., … Smith, R. J. H. (2010). Frequency of Usher syndrome in two pediatric populations: Implications for genetic screening of deaf and hard of hearing children. *Genetics in Medicine: Official Journal of the American College of Medical Genetics*, *12*(8), 512–6. http://doi.org/10.1097/GIM.0b013e3181e5afb8

Lagziel, A., Ahmed, Z. M., Schultz, J. M., Morell, R. J., Belyantseva, I. A., & Friedman, T. B. (2005). Spatiotemporal pattern and isoforms of cadherin 23 in wild type and waltzer mice during inner ear hair cell development. *Developmental Biology*, *280*(2), 295–306. http://doi.org/10.1016/j.ydbio.2005.01.015

Magliulo, G., Iannella, G., Gagliardi, S., Plateroti, R., Plateroti, P., Iozzo, N., & Vingolo, E. M. (2015). Usher's syndrome: Evaluation of the vestibular system with Cervical and Ocular Vestibular Evoked Myogenic Potentials and the Video Head Impulse Test. *Otology & Neurotology*, *36*(2), 1421–1427. http://doi.org/10.1097/MAO.0000000000000613

Mathur, P. D., Vijayakumar, S., Vashist, D., Jones, S. M., Jones, T. A., & Yang, J. (2015). A study of whirlin isoforms in the mouse vestibular system suggests potential vestibular dysfunction in *DFNB31* -deficient patients. *Human Molecular Genetics*, (September), ddv403. http://doi.org/10.1093/hmg/ddv403

Mathur, P. D., Zou, J., Zheng, T., Almishaal, A., Wang, Y., Chen, Q., … Yang, J. (2015). Distinct expression and function of whirlin isoforms in the inner ear and retina: an insight into pathogenesis of USH2D and DFNB31. *Human Molecular Genetics*, *24*(21), 6213–28. http://doi.org/10.1093/hmg/ddv339

Mathur, P., & Yang, J. (2015). Usher syndrome: Hearing loss, retinal degeneration and associated abnormalities. *Biochimica et Biophysica Acta*, *1852*(3), 406–420. http://doi.org/10.1016/j.bbadis.2014.11.020

Mburu, P., Mustapha, M., Varela, A., Weil, D., El-Amraoui, A., Holme, R. H., … Brown, S. D. M. (2003). Defects in whirlin, a PDZ domain molecule involved in stereocilia elongation, cause deafness in the whirler mouse and families with DFNB31. *Nature Genetics*, *34*(4), 421–8. http://doi.org/10.1038/ng1208

Nishiguchi, K. M., Tearle, R. G., Liu, Y. P., & et al. (2013). Whole genome sequencing in patients with retinitis pigmentosa reveals pathogenic DNA structural changes and NEK2 as a new disease gene. *Proceedings of the National Academy of Sciences of the United States of America*, *110*(40), 16139–44. http://doi.org/10.1073/pnas.1308243110

Schultz, J. M., Bhatti, R., Madeo, A. C., Turriff, A., Muskett, J. a, Zalewski, C. K., … Friedman, T. B. (2011). Allelic hierarchy of CDH23 mutations causing non-syndromic deafness DFNB12 or Usher syndrome USH1D in compound heterozygotes. *Journal of Medical Genetics*, *48*(11), 767–75. http://doi.org/10.1136/jmedgenet-2011-100262

Schultz, J. M., Yang, Y., Caride, A. J., Filoteo, A. G., Penheiter, A. R., Lagziel, A., … Griffith, A. J. (2005). Modification of human hearing loss by plasma-membrane calcium pump PMCA2. *The New England Journal of Medicine*, *352*(15), 1557–64. http://doi.org/10.1056/NEJMoa043899

Tlili, A., Charfedine, I., Lahmar, I., Benzina, Z., Mohamed, B. A., Weil, D., … Ayadi, H. (2005). Identification of a novel frameshift mutation in the DFNB31/WHRN gene in a Tunisian consanguineous family with hereditary non-syndromic recessive hearing loss. *Human Mutation*, *25*(5), 503. http://doi.org/10.1002/humu.9333

Wright, R. N., Hong, D.-H., & Perkins, B. (2012). RpgrORF15 connects to the usher protein network through direct interactions with multiple whirlin isoforms. *Investigative Ophthalmology & Visual Science*, *53*(3), 1519–29. http://doi.org/10.1167/iovs.11-8845

Yang, J., Liu, X., Zhao, Y., Adamian, M., Pawlyk, B., Sun, X., … Li, T. (2010). Ablation of whirlin long isoform disrupts the USH2 protein complex and causes vision and hearing loss. *PLoS Genetics*, *6*(5), e1000955. http://doi.org/10.1371/journal.pgen.1000955

CHAPTER 2

USHER SYNDROME: HEARING LOSS, RETINAL DEGENERATION AND ASSOCIATED ABNORMALITIES

Jun Yang wrote this review. My role was to read more literature and find out additional information that need to be incorporated. In addition, I generated figures for this review and helped revise each version of the manuscript.

Biochimica et Biophysica Acta 1852 (2015) 406–420

Contents lists available at ScienceDirect

Biochimica et Biophysica Acta

journal homepage: www.elsevier.com/locate/bbadis

Review

Usher syndrome: Hearing loss, retinal degeneration and associated abnormalities☆

Pranav Mathur [a,b], Jun Yang [a,b,c,*]

[a] Department of Ophthalmology and Visual Sciences, John A. Moran Eye Center, University of Utah, Salt Lake City, UT 84132, USA
[b] Department of Neurobiology and Anatomy, University of Utah, Salt Lake City, UT 84132, USA
[c] Department of Otolaryngology Head and Neck Surgery, University of Utah, Salt Lake City, UT 84132, USA

ARTICLE INFO

Article history:
Received 1 September 2014
Received in revised form 25 November 2014
Accepted 26 November 2014
Available online 4 December 2014

Keywords:
Retina photoreceptor
Inner ear hair cell
Hair bundle link
Periciliary membrane complex
USH multiprotein complex
Therapy

ABSTRACT

Usher syndrome (USH), clinically and genetically heterogeneous, is the leading genetic cause of combined hearing and vision loss. USH is classified into three types, based on the hearing and vestibular symptoms observed in patients. Sixteen loci have been reported to be involved in the occurrence of USH and atypical USH. Among them, twelve have been identified as causative genes and one as a modifier gene. Studies on the proteins encoded by these USH genes suggest that USH proteins interact among one another and function in multiprotein complexes in vivo. Although their exact functions remain enigmatic in the retina, USH proteins are required for the development, maintenance and function of hair bundles, which are the primary mechanosensitive structure of inner ear hair cells. Despite the unavailability of a cure, progress has been made to develop effective treatments for this disease. In this review, we focus on the most recent discoveries in the field with an emphasis on USH genes, protein complexes and functions in various tissues as well as progress toward therapeutic development for USH.

1. Introduction

In mammals, the inner ear and retina are the two sensory organs responsible for hearing, balance and vision. The inner ear contains the cochlea and vestibular system for sensing sounds and position changes, respectively (Fig. 1A). In the cochlea, the organ of Corti, the main sound-sensitive structure, has three rows of outer hair cells (OHCs) and one row of inner hair cells (IHCs) (Fig. 1B). OHCs receive and amplify sound-evoked vibrations of the sensory epithelium, whereas IHCs convert the amplified mechanical signals into electrical responses [1]. The vestibular system includes the utricle and saccule for detection of linear acceleration as well as semicircular canal ampullae for detection of angular acceleration (Fig. 1A) [2,3]. Two types of hair cells, named I and II, exist in these vestibular sensory organs (Fig. 1C). In both cochlear and vestibular systems, hair cells are neurons possessing a specialized mechanosensitive structure, the hair bundle, on their cellular apices (Fig. 1D). Each hair bundle consists of well-organized, actin-based stereocilia graded in lengths and a long microtubule-based kinocilium, although the latter is missing in mature mammalian cochlear hair cells. Responding to sound, movement or gravity, the hair bundle deflects in the excitatory direction toward the longest stereocilia, which induces the opening of ion channels at the tip of shorter stereocilia. Influx of cations leads to membrane potential changes, thereby converting the mechanical stimuli into electrical responses (Fig. 1E), a process referred to as mechanoelectrical transduction (MET) [1,4,5].

In the retina, photoreceptors (Fig. 2A) are light-sensitive neurons that are highly compartmentalized. Their outer segment, a modified sensory cilium, contains many tightly-packed flat membrane disks harboring proteins involved in phototransduction (Fig. 2B). This segment undergoes active and continuous renewal with their proteins and membranes synthesized in the inner segment and transported to the outer

Abbreviations: USH, Usher syndrome; USH1, Usher syndrome type 1; USH2, Usher syndrome type 2; USH3, Usher syndrome type 3; *RP*, *retinitis pigmentosa*; DFNB, nonsyndromic autosomal recessive deafness; DFNA, nonsyndromic autosomal dominant deafness; IHC, inner hair cell; OHC, outer hair cell; RPE, retinal pigment epithelium; UTLD, upper tip link density; LTLD, lower tip link density; MET, mechanoelectrical transduction; ERG, electroretinogram; ER, endoplasmic reticulum; *MYO7A*, myosin VIIa; *USH1C*, harmonin; *CDH23*, cadherin 23; *PCDH15*, protocadherin 15; SANS, scaffold protein containing ankyrin repeats and sam domain; *CIB2*, calcium- and integrin-binding protein 2; *USH2A*, usherin; *GPR98*, G protein-coupled receptor 98; *DFNB31*, autosomal recessive deafness 31; *WHRN*, whirlin; *CLRN1*, clarin-1; *HARS*, histidyl-tRNA synthetase; *PDZD7*, PDZ domain containing 7; VLGR1, very large G protein-coupled receptor 1; SPAG5, sperm-associated antigen 5; Magi2, membrane-associated guanylate kinase inverted-2; DYSC, dyschronic; PDZ, PSD95/Dlg1/ZO1 domain; PBM, PDZ-binding motif; SAM, sterile alpha motif; CEN, central domain; FERM, band 4.1/ezrin/radixin/moesin domain; MyTH4, myosin tail homology 4 domain; ASO, antisense oligonucleotide; AAV, adeno-associated virus; iPSCs, induced pluripotent stem cells; HIV, human immunodeficiency virus; EIAV, equine infectious anemia virus

☆ Grant support: National Eye Institute (EY020853 and EY014800), Research to Prevent Blindness, Foundation Fighting Blindness, the E. Matilda Ziegler Foundation for the Blind, Inc., and Hope for Vision.

* Corresponding author at: John A Moran Eye Center, University of Utah, 65 Mario Capecchi Drive, Bldg. 523, Salt Lake City, UT 84132, USA. Tel.: +1 801 213 2591; fax: +1 801 587 8314.
E-mail address: jun.yang@hsc.utah.edu (J. Yang).

http://dx.doi.org/10.1016/j.bbadis.2014.11.020
0925-4439/

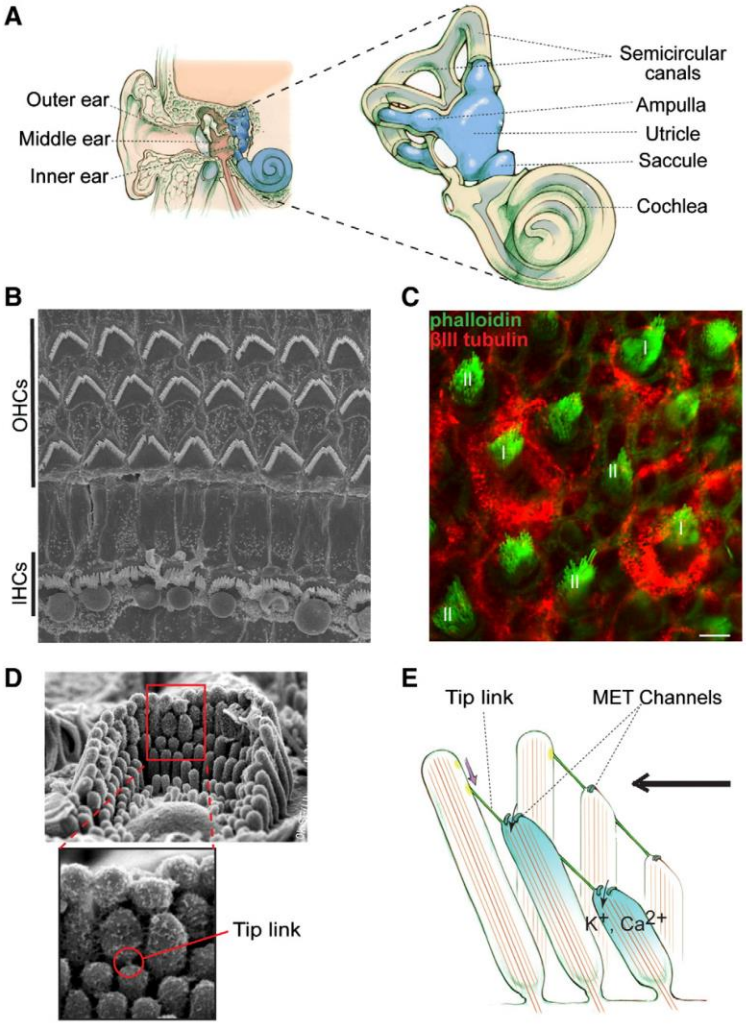

Fig. 1. Inner ear anatomy and mechanoelectrical transduction (MET). (A) The position and structure of the inner ear. The inner ear is the most inner part of the ear (left). It contains the cochlea and vestibular system. The vestibular system includes the utricle, saccule and semicircular canal ampullae (right). (B) Top view of the murine organ of Corti shown by scanning electron microscopy. The organ of Corti has one row of inner hair cells (IHCs) and three rows of outer hair cells (OHCs). (C) Type I (I) and type II (II) hair cells in the murine utricular extrastriola shown by immunofluorescence. Phalloidin signal (green) indicates actin bundles in stereocilia. βIII tubulin (red) labels calyx afferents of type I hair cells. Scale bar, 5 μm. (D) A hair bundle shown by scanning electron microscopy. Top, an entire bundle with a staircase pattern of stereociliary organization. Bottom, an amplified view of the boxed area on the top showing a tip link. (E) MET occurs when the hair bundle is deflected toward the longest stereocilium (excitatory direction, black arrow). Deflection of hair bundles in this direction stretches tip links, which subsequently regulates the gating of MET channels and leads to hair cell depolarization. Note that this is a simplified model and tip links may associate with MET channels indirectly.

segment by intraflagellar transport through the connecting cilium. Addition of new disks proximally is balanced by shedding of old disks distally. Retinal pigment epithelium (RPE) cells (Fig. 2A) phagocytose and digest the shed photoreceptor outer segment tips and participate in visual pigment regeneration. Proximal to photoreceptors are bipolar cells, horizontal cells, amacrine cells and ganglion cells (Fig. 2A). Electrical impulses, generated from phototransduction in the photoreceptor outer segment, are transmitted to the above-mentioned downstream retinal neurons at the photoreceptor ribbon synapse. Müller cells, the major glial cells in the retina (Fig. 2A), have large and long radial cellular processes and form adherens junctions with photoreceptors at the proximal inner segment. Compromised photoreceptors, RPE cells and Müller cells are now thought to be the cellular basis underlying pathogenesis of *retinitis pigmentosa* (*RP*) (reviewed in [6]).

Usher syndrome (USH), an autosomal recessive genetic disease, is characterized by hearing loss, vision loss and occasional balance problems. USH, first described by the Scottish ophthalmologist, Charles Usher, is the leading genetic cause of deaf-blindness with a prevalence in the range of 1–4 per 25,000 people [7–10]. Based on diverse clinical symptoms observed in patients, USH is classified into three types. USH type I (USH1) patients are defined as having congenital severe-to-profound deafness, vestibular areflexia and onset of *RP* within the first decade of life. USH2 patients show congenital moderate-to-severe hearing loss, normal vestibular function and onset of *RP* within the

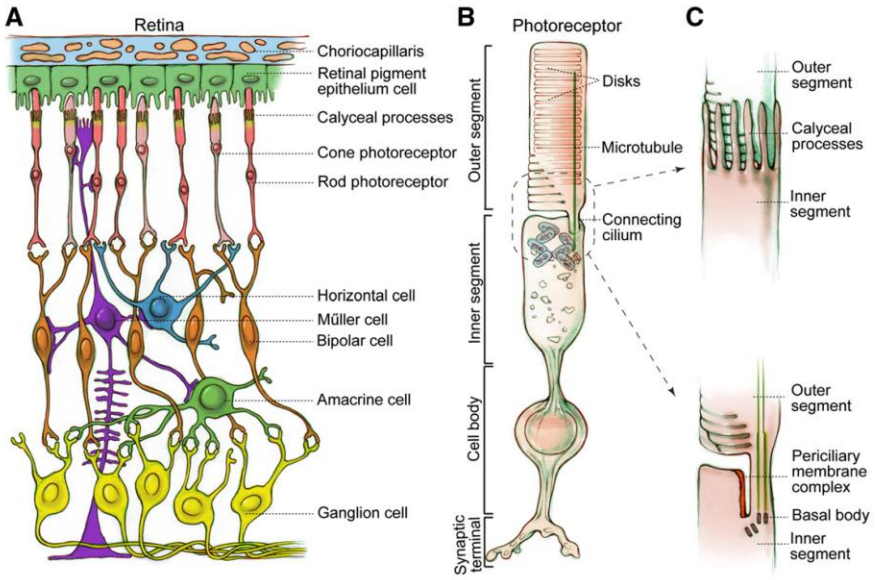

Fig. 2. Schematic diagrams of the retina and photoreceptor. (A) Cellular organization of the retina. Retinal neurons are arranged into different layers. Photoreceptors and RPE cells are located in the outer retina, while horizontal cells, bipolar cells, amacrine cells and ganglion cells are downstream neurons of photoreceptors in the inner retina. Müller cells are glial cells spanning all cell layers of the retina. (B) Photoreceptor structure exemplified by a rod. Photoreceptors are ciliated cells with several specialized subcellular compartments, consisting of an outer segment having tightly packed membrane disks, a connecting cilium with microtubules, calyceal processes with actin bundles (not shown), an inner segment having all organelles for energy and protein synthesis, a cell body containing the nucleus, and a synaptic terminus for signal transmission to bipolar and horizontal cells. (C) Magnified drawings of calyceal processes (top) and periciliary membrane complex (bottom) around the photoreceptor connecting cilium. In order to show the periciliary membrane complex, calyceal processes are omitted in the bottom drawing.

second decade of life. In USH3 patients, the hearing loss, vestibular dysfunction and onset of *RP* are progressive, sporadic and variable, respectively. Early symptoms of *RP* are night blindness and loss of peripheral vision, caused by degeneration of rod photoreceptors. Upon progression of *RP*, cone photoreceptors also degenerate [8]. Loss of central (cone-mediated) vision results in USH patients becoming legally or completely blind with no known cure [11,12].

Significant progress has been made recently toward the identification of USH causative genes. Through extensive study of these genes in various animal models, evidence suggests that defects in inner ear hair cell development and photoreceptor maintenance probably underlie USH pathogenesis. In this review, we will summarize the current knowledge of USH causative genes, disease mechanisms and potential treatments. We will focus on new discoveries regarding USH etiology, because several excellent and comprehensive reviews already exist in the literature [13–22].

2. Genes and loci identified in USH patients

To date, sixteen loci have been associated with USH: nine are involved in USH1, three in USH2, two in USH3 and two not specified (Table 1) [9,23–27]. From these loci, thirteen genes have been identified. They include six USH1, three USH2, two USH3, one USH modifier and one atypical USH genes. The USH1 genes are *MYO7A* (myosin VIIa) [28], *USH1C* (harmonin) [29,30], *CDH23* (cadherin 23) [31,32], *PCDH15* (protocadherin 15) [33,34], *USH1G* (SANS, scaffold protein containing ankyrin repeats and sam domain) [35] and *CIB2* (calcium- and integrin-binding protein 2) [36]. The USH2 genes are *USH2A* (usherin)

Table 1
USH loci and genes with predicted protein function.

USH type	Locus	gene name	Protein name	Predicted function	References
USH1	USH1B	*MYO7A*	myosin VIIa	Actin-based motor protein	[28]
	USH1C	*USH1C*	harmonin	PDZ scaffold protein	[29,30]
	USH1D	*CDH23*	cadherin 23	Cell adhesion	[31,32]
	USH1E	n/a	n/a	Unknown	[212]
	USH1F	*PCDH15*	protocadherin 15	Cell adhesion	[33,34]
	USH1G	*USH1G*	SANS	Scaffold protein	[35]
	USH1H	n/a	n/a	Unknown	[213]
	USH1J	*CIB2*	CIB2	Ca^{2+} and integrin binding	[36]
	USH1K	n/a	n/a	Unknown	[214]
USH2	USH2A	*USH2A*	usherin	Cell adhesion	[37]
	USH2C	*GPR98*	VLGR1 (aka GPR98, MASS1)	G-protein coupled receptor	[38]
	USH2D	*DFNB31* (*Whrn* in mice)	whirlin	PDZ scaffold protein	[39]
USH3	USH3A	*CLRN1*	Clarin-1	Auxiliary subunit of ion channels?	[40–42]
n/a	n/a	*PDZD7*	PDZD7	PDZ scaffold protein	[26]

Table 2
Different diseases caused by USH gene mutations.

Gene name	USH subtype	Other diseases involved	References
Myo7a	USH1B	DFNB2, DFNA11, atypical USH	[47–51]
USH1C	USH1C	DFNB18	[52,53]
CDH23	USH1D	DFNB12	[32,54,55]
PCDH15	USH1F	DFNB23	[56,57]
CIB2	USH1J	DFNB48	[36]
USH2A	USH2A	Nonsyndromic RP	[37,59]
GPR98	USH2C	Febrile and afebrile seizures	[38,60]
DFNB31	USH2D	DFNB31	[39,58]
PDZD7	Digenic USH	DFNB	[26,215]

DFNB: nonsyndromic recessive deafness.
DFNA: nonsyndromic dominant deafness.

[37], *GPR98* (G protein-coupled receptor 98) [38] and *DFNB31* (autosomal recessive deafness 31) [39]. *CLRN1* (Clarin-1) and *HARS* (histidyl-tRNA synthetase) are the USH3 genes [25,40–42]. Furthermore, *PDZD7* (PDZ domain containing 7) was recently discovered as an USH modifier and digenic USH contributor gene [26], and *CEP250* as an atypical USH gene [27]. Among these genes, *HARS* is debatable as an USH3 gene, because patients carrying mutations in this gene develop episodic psychosis as well as progressive hearing loss and *RP* [25], which could be clinical symptoms of other rare syndromes. The atypical USH patients carrying the homozygous *CEP250* nonsense mutation exhibit early-onset hearing loss and mild *RP*. They all have a heterozygous C2orf71 nonsense mutation. Although C2orf71is an autosomal recessive *RP* gene [43–46], it is unclear whether its heterozygous mutation also contributes to the disease development of these atypical USH patients.

In addition to involvement in USH, different mutations in nine USH genes have been reported to cause other discrete diseases (Table 2). For example, different mutations in *MYO7A* are the causes of USH1, nonsyndromic recessive deafness 2 (DFNB2), nonsyndromic dominant deafness 11 (DFNA11) and atypical USH [47–51]. Other examples include mutations in *USH1C*, *CDH23*, *PCDH15*, *CIB2* and *DFNB31*, which lead to either USH or nonsyndromic recessive deafness (DFNB) [32,36, 39,52–58], mutations in *USH2A* which have been found in patients with either USH2 or nonsyndromic *RP* [37,59] and mutations in *GPR98* which are responsible for either USH2 or seizures [38,60]. For at least four USH1 genes, *MYO7A*, *CDH23*, *PCDH15* and *USH1C*, there appears to be a genotype–phenotype correlation in patients [50,54]. Nonsense, frameshift and splice site mutations resulting in truncation of USH1 proteins are usually responsible for the occurrence of USH1, while 'leaky' splice site and some missense mutations lead only to DFNB. It is hypothesized that mutant alleles causing DFNB and USH1 are hypomorphic and functionally null alleles, respectively, and that residual function of USH1 proteins from the DFNB alleles spare normal retinal and vestibular functions in patients [50,54,61]. Additionally, most USH genes have multiple splice isoforms with different spatial and temporal expression patterns in the inner ear and retina [29,62–68]. These USH splice isoforms could have slightly different cellular functions. Thus, the differential disruption of USH splice isoforms due to mutations in different USH gene regions may also contribute to the genotype–phenotype correlation found in patients [53].

3. Expression of USH genes

USH genes are expressed in various tissues [69–74]. This section addresses their protein expressions in the inner ear and retina (Table 3).

3.1. USH proteins are mainly localized to the hair bundle and synapse of inner ear hair cells.

Various dynamically-changing proteinaceous filamentous links (Fig. 3) exist in hair cell bundles, where USH proteins are localized. These interstereociliary links are essential for bundle development, maintenance and function [75–77]. During early development, kinociliary links connect the kinocilium to its neighboring stereocilia, and transient lateral links connect adjacent stereocilia along their entire length [75,76]. Later, ankle links and tip links emerge at the stereociliary base and tip, respectively [76]. Tip links connect the tip of shorter stereocilia to the lateral wall of taller stereocilia (Figs. 1D and 3) and mediate gate opening of ion channels during MET (Fig. 1E). Electron dense structures, upper (UTLD) and lower (LTLD) tip link densities (Fig. 3), are observed at the upper and lower insertion sites of tip links in stereocilia, respectively. Kinociliary links, transient lateral links and ankle links disappear after maturation of mammalian cochlear hair cells, but some are permanent in the vestibular system [75,76]. Tip

Table 3
USH protein distributions in hair cells and photoreceptors.

Protein name	Subcellular distribution	References
Hair cells		
Myosin VIIa	Cytoplasm and stereocilia	[86–90]
Harmonin	UTLD[a] and synapse	[84,85,90,99,104]
Cadherin 23	Transient lateral link, kinociliary link, tip link and synapse	[79–82,90,101,103]
Protocadherin 15	Transient lateral link, kinociliary link, tip link and synapse	[63,79,83,90,102,103]
SANS	UTLD[a] and stereociliary tip	[86,139]
CIB2	stereocilia	[36]
Usherin	Ankle link and synapse	[68,77,99,100]
VLGR1	Ankle link and synapse	[77,93,99,100,102,103]
Whirlin	Ankle link, stereociliary tip and synapse	[66,68,77,94–96,100]
Clarin-1	hair bundle, apical cytoplasm and synapse	[97,98]
PDZD7	Ankle link	[68,94]
Photoreceptors		
Myosin VIIa	Connecting cilium, periciliary membrane, calyceal process and synapse	[19,20,105,109,112]
Harmonin	Outer segment, calyceal process and synapse	[19,99,105,112,113]
Cadherin 23	Inner segment, calyceal process and synapse	[19,105,112]
Protocadherin 15	Base of outer segment, calyceal process and synapse	[19,105,112]
SANS	Connecting cilium, basal body, calyceal process and synapse	[105,111,133]
CIB2	Inner and outer segment	[36]
Usherin	Periciliary membrane complex and synapse	[17,19,68,99,100,105,106,116,117]
VLGR1	Periciliary membrane complex and synapse	[19,68,99,100,105,106,117]
Whirlin	Periciliary membrane complex	[17,68,100,105,106,111,117]
Clarin-1	Connecting cilium, inner segment, adherens junction and synapse	[97,118]
PDZD7	unclear	[26,68]

[a] UTLD: upper tip link density.

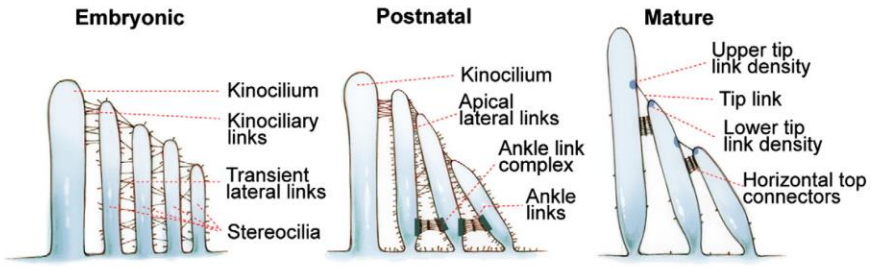

Fig. 3. Dynamic changes of various interstereociliary links in the hair bundle during and after development. During embryogenesis, emerging stereocilia are bundled by transient lateral links and connected with the kinocilium through kinociliary links. Postnatally, the transient lateral links are gradually replaced by tip links, apical lateral links and ankle links. After maturation, the apical lateral links are replaced by horizontal top connectors. Upper tip link density (UTLD) and lower tip link density (LTLD) are electron-dense structures at the insertion sites of tip links in the taller and shorter stereocilia, respectively. In mature rodent cochlear hair cells, the ankle links, kinociliary links and kinocilium disappear.

links remain in mature cochlear and vestibular hair cells throughout life [78,79].

Among USH1 proteins, cadherin 23 and protocadherin 15 are localized to transient lateral links and kinociliary links during development and to tip links in adulthood [63,80–83]. Harmonin and SANS are part of the UTLD [84–86]. CIB2 was found in both hair cells and supporting cells [36]. In hair cells, CIB2 is localized along stereocilia and more concentrated near the tip. Myosin VIIa is distributed throughout hair cells including the cytoplasm and hair bundle [87–89]. This protein has been shown to be at the tip, base, shaft or entire length of stereocilia by different research laboratories [86,87,90–92]. These inconsistent myosin VIIa signal patterns may result from 1) different detection approaches, such as immunostaining of the endogenous protein or overexpression of a tagged exogenous protein; 2) different myosin VIIa antibodies, which could have variable quality and/or detect different myosin VIIa isoforms; 3) different hair cell types, such as the cochlear IHCs, OHCs or vestibular hair cells, examined at different developing time points; and 4) various sample processing procedures.

The protein of the USH2 gene *GPR98*, VLGR1 (very large G protein-coupled receptor 1), has been shown to be a major component of ankle links [77,93]. Other USH2 proteins usherin and whirlin (*DFNB31*), together with PDZD7, are colocalized with VLGR1 at the ankle link complex [68,77,93,94]. Additionally, whirlin is also present at the stereociliary tip [66,95,96]. Among USH3 proteins, clarin-1 is relatively well studied in the inner ear. While clarin-1 could not be found in the hair bundle of zebrafish mechanosensory hair cells [97], its presence in mouse cochlear hair bundles was suggested [98].

USH proteins are also found in the synapse of hair cells, where the electrical responses generated from MET are transmitted to second-order neurons in the inner ear. Protocadherin 15, cadherin 23, harmonin, clarin-1, usherin, VLGR1 and whirlin have all been reported in the synapses of developing and mature hair cells [97,99–104].

3.2. USH proteins are localized in photoreceptors and other retinal cell types.

Cellular distributions of USH proteins in the retina are less well-defined, owing to inconsistent reports in the literature. These inconsistent reports might result from different antibodies, different sample processing procedures and/or different species used in the studies. In general, USH proteins have been localized in photoreceptors and some other retinal cells, and may have distinct distribution patterns in retinas of different species. In photoreceptors, they tend to be positioned to some specific subcellular structures (Table 3).

One such structure is the calyceal process of long actin-based, microvilli-like thin projection (Fig. 2C). Calyceal processes extend from the inner segment apex toward the outer segment, and wrap tightly around the basolateral outer segment. Calyceal processes exist in primate, amphibian and avian photoreceptors, but are absent and vestigial in rodent rods and cones, respectively [105]. Although differing in function, calyceal processes and the outer segment of photoreceptors are considered structurally similar to stereocilia and the kinocilium of hair cells. Another structure related to USH proteins is the periciliary membrane complex in mammalian photoreceptors (Fig. 2C), which is a specialized plasma membrane region at the inner segment apex facing the connecting cilium. The periciliary membrane complex is thought to be analogous to the periciliary ridge complex [106], which likely participates in protein trafficking between frog photoreceptor inner and outer segments [107].

In mice, USH1 protein myosin VIIa exists mostly in RPE cells [89,108]. Its localization in photoreceptors at the connecting cilium and periciliary membrane remains open to debate [20,109,110]. Other USH1 proteins were localized to various photoreceptor compartments, including the outer segment, connecting cilium, inner segment and synapse [36,56,99,111–113]. Some of these findings are inconsistent among different research groups [99,105,113]. Apart from photoreceptors, CIB2 was found in RPE and other retinal cells [36]. Recently, Sahly et al. reported that USH1 proteins, except CIB2 (not examined), are all located at calyceal processes of human, monkey and frog photoreceptors [105] . The USH1 protein localization in photoreceptor calyceal processes, to some extent, corresponds with their localization in hair cell stereocilia. Additionally, studies in zebrafish illustrate that cadherin 23 and harmonin are localized in a small subset of GABAergic amacrine cells and Müller cells, respectively [114,115]. In summary, USH1 proteins may have variable cellular and subcellular distributions in retinas of different species.

USH2 proteins usherin, VLGR1 and whirlin were initially positioned in the inner segment, connecting cilium, basal bodies, synaptic terminus and adherens junction of mouse photoreceptors [17,19,100,111]. Using antibodies whose specificities have been verified stringently, the three USH2 proteins are now localized to the periciliary membrane/ridge complex of mouse and frog photoreceptors [106,116,117]. USH2 protein localizations at the periciliary membrane complex were further confirmed in monkey photoreceptors [105].

Distribution of USH3 protein clarin-1 in the retina has been reported by three research groups and remains inconclusive [97,118,119]. In mouse retinas, one group showed that clarin-1 protein is present in the photoreceptor connecting cilium, inner segment and synaptic terminus [118], whereas others demonstrated that clarin-1 mRNA exists only during development in Müller cells but not photoreceptors [119]. In zebrafish retinas, Phillips et al. found that the clarin-1 protein is distributed in photoreceptors and other retinal cells, which could be amacrine cells, Müller cells and ganglion cells, during development and adulthood; in photoreceptors, clarin-1 is localized to the inner segment lateral membrane, adherens junctions with Müller cells and synaptic terminus [97].

4. USH proteins exist in multiprotein complexes

Individual USH proteins are predicted to accomplish various functions including actin-based intracellular trafficking, cell adhesion, scaffolds in multiprotein complexes, and G protein- or Ca^{2+}-mediated signaling (Table 1). For example, myosin VIIa is revealed as an unconventional motor protein with a motor domain, actin-binding domain and long tail region [120,121]. Harmonin, whirlin and PDZD7 are paralogs belonging to the same protein family. These three proteins and SANS each have several protein–protein interaction domains and thus are thought to be scaffold proteins [18,68,99,106,117,122,123]. Cadherin 23, protocadherin 15 and usherin are transmembrane proteins with a long extracellular region containing various cell adhesion domains, suggesting a potential function of binding cell surface proteins and/or extracellular matrix proteins [79,83,124]. CIB2 has several Ca^{2+}-binding EF-hand domains and is able to bind to integrin [36], while VLGR1 is a very large adhesion G protein-coupled receptor with multiple extracellular Ca^{2+}-binding motifs [70]. Recent colocalization, in vitro interaction and mouse genetic studies on USH proteins suggest that proteins within the same USH clinical type interact to form multiprotein complexes (Fig. 4) and that mutations in USH genes lead to protein complex disruption and disease development [18,77,90,106]. Therefore, the distinct functions of individual USH proteins probably contribute to the function of USH multiprotein complexes as a whole in various subcellular regions of hair cells and photoreceptors [17–19,21,22,125]. Here, we present one USH1 complex and one USH2 complex to exemplify USH multiprotein complexes.

USH1 proteins harmonin, SANS and myosin VIIa are suggested to form a complex (Fig. 4) at the UTLD in mature inner ear hair cells by several lines of evidence. Genetic and cell biological studies have revealed interdependence of these proteins for their normal localizations at the UTLD in mice [84,86]. Structural and biochemical studies further show that harmonin and SANS, the two scaffold proteins, form a complex through the harmonin PDZ1 domain and SANS SAM region and PDZ-binding motif (PBM) [123]. The harmonin N-domain in the harmonin/SANS complex is open and available to interact with the cadherin 23 short cytoplasmic region [91,126,127], and the CEN domain of SANS is able to bind to the FERM and MyTH4 domains of myosin VIIa [122,128]. Thus, the USH1 complex of harmonin, SANS and myosin VIIa is thought to anchor the cadherin 23 component of tip links to actin filaments inside taller stereocilia [84]. Latest studies in zebrafish hair cells also found that cadherin 23, myosin VIIa and harmonin are likely preassembled into a complex at the endoplasmic reticulum (ER), where the proteins are synthesized [129]. Defects in any of the three proteins affect trafficking of the complex to hair bundles and induce ER stress and apoptosis in hair cells [129].

USH2 proteins usherin, VLGR1 and whirlin are able to interact in vitro through PDZ domains of whirlin and PBMs of usherin and VLGR1 (Fig. 4) [65,100,106]. They are colocalized at the photoreceptor periciliary membrane complex (Fig. 2C) [105,106,111,116,117] and the developing hair cell ankle link complex (Fig. 3) [65,77,93]. Loss of one USH2 protein affects the normal localizations of other USH2 proteins in photoreceptors [106] and hair cells ([77] and our unpublished data), and whirlin is able to recruit usherin and VLGR1 to the photoreceptor periciliary membrane complex [117]. These findings indicate that USH2 proteins exist as a multiprotein complex in vivo. USH modifier protein PDZD7 also interacts directly with the three USH2 proteins (Fig. 4) [26,68] and colocalizes with VLGR1 and whirlin at the hair cell ankle link complex [68,94]. PDZD7 and the three USH2 proteins are mutually dependent for normal localizations in cochlear hair cells [68,77]. However, localization of PDZD7 at the photoreceptor periciliary membrane complex could not be determined [26,68]. Ablation of PDZD7 did not affect the integrity of the USH2 complex in mouse photoreceptors [68]. Therefore, PDZD7 is probably a component of the USH2 multiprotein complex in hair cells but not photoreceptors. Currently,

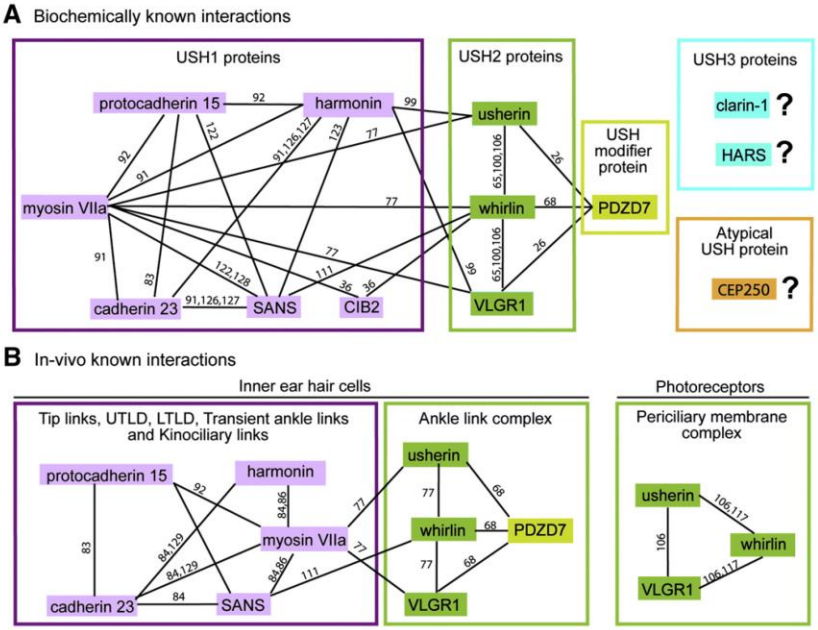

Fig. 4. Known interaction networks among USH proteins. (A) Interactions among USH1 (pink), USH2 (green) and PDZD7 proteins found and confirmed by various in vitro biochemical assays. Interactions among the two USH3 (blue), atypical USH (CEP250) and other USH proteins have not yet been revealed. (B) Interactions of USH proteins confirmed in inner ear hair cells (left) and photoreceptors (right) by genetic studies. Reference numbers are given along each line.

three-dimensional structural data of the USH2 multiprotein complex are unavailable.

Linkage between USH1 and USH2 multiprotein complexes appears likely (Fig. 4). For instance, USH1 protein CIB2 was shown to be capable of binding to both USH1 protein myosin VIIa and USH2 protein whirlin in vitro [36]. Another in vitro biochemical study demonstrated molecular interactions between USH1 scaffold protein harmonin and USH2 proteins usherin and VLGR1 [99]. Therefore, USH proteins are currently thought to function cooperatively in vivo through the intertwined network of their multiprotein complexes. However, it is still elusive as to how these multiprotein complexes coordinate functionally at their distinct subcellular locations, although association among USH multiprotein complexes could occur transiently during trafficking from the ER to final destinations.

To thoroughly understand the biological functions of various USH multiprotein complexes, extensive efforts have been implemented to identify novel partners that interact with known USH proteins, mainly through yeast two-hybrid screen, in vitro biochemical confirmation and in vivo immunolocalization. Espin 1–3 isoforms, derived from alternative usage of transcriptional start sites and alternative splicing, were discovered to associate with the USH2 protein complex [74]. Espins bind to actin monomers and bundle actin filaments [130]. They colocalize partially with whirlin at the photoreceptor periciliary membrane and hair cell ankle link complexes. Interaction between espins and whirlin in vivo appears important for the maintenance of actin bundle geometry [74]. Other recent findings describe interactions of myomegalin with the SANS CEN domain [131], SPAG5 (sperm-associated antigen 5, also called astrin) with the usherin cytoplasmic region [132], and Magi2 (membrane-associated guanylate kinase inverted-2) with the SANS SAM region [133]. However, caution is needed when data from screens of USH protein-interacting partners are interpreted physiologically, because some of the interactions have not been confirmed in vivo [134,135].

5. Functional studies of USH gene products

5.1. USH genes in inner ear hair cells

5.1.1. USH1 genes

Mice and zebrafish carrying mutations in USH1 gene orthologs, except *CIB2* (not reported yet), share common morphological phenotypes of their hair bundles [81,90,115,136,137]. *Cdh23*$^{v2J/v2J}$, *Pcdh15*$^{av3J/av3J}$, *Ush1g*$^{js/js}$, *Myo7a*$^{4626SB/4626SB}$ and *Ush1c*$^{-/-}$ mice have fragmented hair bundles with planar cell polarity defects in both IHCs and OHCs [90], which are similar to the hair bundle phenotypes found in *myo7a*, *cdh23*, *pcdh15* and *ush1c* mutant zebrafish [81,115,136,137]. Such morphological defects caused by USH1 gene mutations could result from disconnection between the kinocilium and neighboring stereocilia, and among stereocilia themselves. Therefore, proteins encoded by USH1 genes probably function cooperatively in maintaining cohesion of stereocilia and kinocilium in developing and mature hair bundles as components of tip links, UTLD and other interstereociliary links.

Stereociliary tip links are absent in *Cdh23*$^{v2J/v2J}$, *Pcdh15*$^{av3J/av3J}$ and *Ush1g*$^{-/-}$ mice [138,139] and in *cdh23*$^{tc317e/tc317e}$, *cdh23*$^{tc300a/tc300a}$ and *cdh23*$^{tc370e/tc370e}$ zebrafish [81]. Consistently, various MET abnormalities have been reported in *Cdh23*, *Pcdh15*, *Myo7a*, *Ush1c* and *Ush1g* mutant mice (Table 4), which were recorded in vitro by either fluid jet or stiff glass probe stimulation. Among these USH1 mutant mice, *Ush1g*$^{fl/fl}$*Myo15-cre*$^{+/-}$ mice have intact hair bundle morphology. Thus, abnormal MET responses detected in USH1 mutant mice are probably primary and not secondary to bundle morphological defects. Knockdown of *cib2* in zebrafish causes reduced microphonic potentials of neuromasts, suggesting that CIB2, like other USH1 proteins, is also essential for MET responses in hair cells [36]. Therefore, USH1 proteins are either directly or indirectly involved in the MET process in the hair cell bundle.

Harmonin has also been found in synaptic termini of mouse, rat and zebrafish hair cells [99,104,115]. In mature cochlear IHC synapses, harmonin interacts with the cytoplasmic terminus of $Ca_v1.3$ α1 subunit, the pore-forming subunit of voltage-gated $Ca_v1.3$ Ca^{2+} channels, which is essential for Ca^{2+}-dependent glutamate release and synaptic transmission. Harmonin controls the amount of $Ca_v1.3$ α1 on the synaptic plasma membrane by increasing ubiquitination of $Ca_v1.3$ α1 subunit, improves voltage-dependent facilitation of $Ca_v1.3$ Ca^{2+} channels, and regulates exocytosis of vesicles containing readily releasable neurotransmitters at synaptic ribbons [104,140].

5.1.2. USH2 genes

Most mouse models carrying USH2 gene mutations share common phenotypes. In *Gpr98*$^{-/-}$ and *Gpr98*$^{del7TM/del7TM}$ mice, ankle links are completely missing, indicating that VLGR1 is a core protein of ankle links [77,93]. In all reported *Gpr98*, *Ush2a*, *Whrn* (mouse ortholog of *DFNB31*) and *Pdzd7* mutant mice, except *Whrn*$^{wi/wi}$ mice [58,141], abnormal stereociliary organization was observed in OHC but not IHC bundles [68,77,93,106,116,142,143]. Consistently, *Gpr98*$^{-/-}$, *Gpr98*$^{del7TM/del7TM}$ and *Pdzd7*$^{-/-}$ mice have reduced MET amplitude and sensitivity in OHCs, but normal MET responses in IHCs [68,77,93]. USH2 mutant mice, except *Whrn*$^{wi/wi}$ mice, exhibit no obvious behaviors of vestibular dysfunction. *Gpr98*$^{-/-}$, *Gpr98*$^{del7TM/del7TM}$ and *Pdzd7*$^{-/-}$ vestibular hair cells also have normal MET responses [68,77,93]. These findings indicate that USH2 proteins at the ankle link complex are important for organizing stereocilia into a V-shaped bundle during OHC development and raise a possibility that neither USH2 proteins nor the ankle link complex may function significantly in IHCs or vestibular hair cells.

By contrast, *Whrn*$^{wi/wi}$ mice show shortened stereocilia in both IHCs and OHCs as well as disorganized OHC bundles [58,141,144]. The mice have circling and head tossing phenotypes, indicative of vestibular dysfunction. It is currently hypothesized that the more severe phenotypes found in *Whrn*$^{wi/wi}$ mice are probably due to the combined defective *Whrn* expressions at both the tip and ankle link complex of stereocilia

Table 4
MET defects in USH1 mutant mice.

Mouse	MET defects	References
Cdh23$^{v2J/v2J}$	Reduced current and abnormal directional sensitivity	[138]
Pcdh15$^{av3J/av3J}$	Reduced or no current and abnormal directional sensitivity[a]	[92,138]
Pcdh15$^{av6J/av6J}$	Reduced current and abnormal directional sensitivity[a]	[138]
Myo7a$^{6J/6J}$	Increased current, decreased sensitivity and abnormal adaptation	[216]
Myo7a$^{4626SB/4626SB}$	Increased current, decreased sensitivity and abnormal adaptation	[216]
Ush1c$^{dfcr/dfcr}$	Decreased sensitivity of OHCs[a]	[84]
Ush1c$^{dfcr\text{-}2J/dfcr\text{-}2J}$	Reduced OHC current and abnormal adaptation of outer and vestibular hair cells[a]	[85]
USH1g$^{fl/fl}$;*Myo15-Cre*$^{+/-}$	Reduced current and normal sensitivity	[139]

[a] The discrepancy of MET defects found in USH1 mice carrying different mutant alleles of the same gene could result from differences in splice isoforms affected and/or conditions used for MET measurements, such as either fluid jet or stiff glass probe stimulation.

[106,141]. However, the OHC MET in *Whrn*$^{wi/wi}$ mice has been found to be normal [145].

5.1.3. USH3 genes

Similar to most USH2 mutant mice, *Clrn1*$^{-/-}$ mice show morphological defects of OHC but not IHC bundles [146], and they have reduced MET amplitude and sensitivity in OHCs but normal MET responses in IHCs [98] during development. However, unlike most USH2 mutant mice, *Clrn1*$^{-/-}$ mice exhibit progressive vestibular dysfunction with no overt circling or head tossing behaviors by one month of age but severe circling and head tossing behaviors by 6 months of age [146]. Additionally, MET responses in *Clrn1*$^{-/-}$ vestibular hair cells show reduced currents and less sensitivity [98]. Consequently, USH2 and USH3 proteins might participate in similar cellular processes of stereocilia organization in the cochlea, but play relatively distinct roles in the vestibular system during bundle development.

5.1.4. In summary

Proteins encoded by most USH genes, as various interstereociliary links, confer cohesive organization of stereocilia during bundle growth and differentiation. Some USH proteins remain functional in adult hair cells at important subcellular structures, e.g., tip links and tip link densities. The bundle morphological defects caused by USH gene mutations may affect establishment of the MET process, which is likely causal for hearing loss and, sometimes, vestibular areflexia. Thus, USH proteins are required for development, maintenance and function of inner ear hair cell bundles. Some USH proteins may additionally serve a synaptic transmission role from hair cells to downstream neurons.

5.2. USH genes in the retina

Current understanding of USH genes affecting retina health is fragmentary. The only relatively well-understood USH gene in the retina is *MYO7A*. Myosin VIIa in RPE cells is implicated in driving melanosomes into apical processes [147], delivering phagosomes to their cytoplasmic digestion site from apical processes [148], and translocating RPE65, an enzyme important for visual pigment regeneration [149]. In photoreceptors, delay of rhodopsin transport to the outer segment is shown in three different strains of *Myo7a* mutant mice and *myo7aa*$^{ty229d/ty229d}$ zebrafish (Zebrafish has two human *MYO7A* orthologs, *myo7aa* and *myo7ab*.) [150,151]. The role of myosin VIIa in rhodopsin transport is proposed to be achieved through direct interaction of myosin VIIa with spectrin-βV, an adaptor protein associating with rhodopsin, kinesin-II and the dynein complex [152]. Further, *Myo7a*$^{sh1\text{-}11J/sh1\text{-}11J}$ mice have a delay and increased threshold of transducin translocation from the outer to inner segment upon light stimulation [153]. Together, these findings suggest that myosin VIIa is important for protein and organelle transport in both RPE cells and photoreceptors of the retina.

Physiological and histological studies in various *Myo7a* mutant mouse and *myo7aa* mutant zebrafish retinas produced somewhat inconsistent results, possibly resulting from different mutant species and strains, genetic backgrounds, retinal pigmentation levels and light illumination levels used in the experiments [149,151,153–155]. Electroretinogram (ERG) recording is a non-invasive technique to measure retinal electrical responses to light stimuli with resulting a- and b-waves representing responses from photoreceptors and inner retinal neurons, respectively. *Myo7a*$^{4626SB/4626SB}$, *Myo7a*$^{816SB/816SB}$, *Myo7a*$^{7J/7J}$, *Myo7a*$^{8J/8J}$ and *Myo7a*$^{9J/9J}$ mice and *myo7aa*$^{ty229d/ty229d}$ mutant zebrafish exhibit reduced ERG a- and b-wave amplitudes but normal light sensitivity [151,155], while albino *Myo7a*$^{4626SB/4626SB}$ mice show an age-dependent reduction of ERG b-wave, less light sensitivity and slow recovery from light desensitization [154]. In *myo7aa*$^{ty229d/ty229d}$ zebrafish, mild retinal degeneration, indicated by photoreceptor loss, was observed at 10 days postfertilization [151], while no retinal degeneration occurs in all *Myo7a* mutant mice examined under normal husbandry conditions. Light illumination can induce retinal degeneration in *Myo7a*$^{sh1\text{-}11J/sh1\text{-}11J}$ [153] but not *Myo7a*$^{4626SB/4626SB}$ mice [149]. Although inconsistently observed by different research groups, most physiological and histological abnormalities can be rescued by delivery of *Myo7a* cDNAs into RPE and photoreceptor cells of *Myo7a* mutant mice using either adeno-associated virus (AAV) or lentivirus [154,156–159], suggesting that the above identified phenotypes are specific to *Myo7a* mutations.

The second well-studied USH genes in the retina are the group of USH2 genes. In *Ush2a*$^{-/-}$, *Gpr98*$^{del7TM/del7TM}$ and *Whrn*$^{neo/neo}$ mice, the integrity of the USH2 complex is disrupted at the photoreceptor periciliary membrane complex [106]. *Ush2a*$^{-/-}$ and *Whrn*$^{neo/neo}$ mice exhibit late-onset weak retinal degeneration [106,116]. Consistently, knockdown of *ush2a* and *gpr98* in zebrafish results in an increase of dying photoreceptors [26]. Therefore, the USH2 complex is important for photoreceptor survival. However, the exact biological function of the USH2 complex in photoreceptors remains elusive. Originally, the USH2 complex at the periciliary membrane complex was proposed to participate in protein trafficking through the connecting cilium [107], but no clear evidence demonstrates any defects in protein trafficking between the inner and outer segment in *Ush2a*$^{-/-}$ and *Whrn*$^{neo/neo}$ photoreceptors [106,116]. Interestingly, using *Whrn*$^{wi/wi}$ mice, which do not develop spontaneous retinal degeneration [106], Tian et al. demonstrated a defect in light-induced transducin translocation from photoreceptor outer to inner segment and light-induced retinal degeneration [160]. The molecular mechanisms underlying these phenotypes in *Whrn*$^{wi/wi}$ mice need to be further elucidated.

Among all reported USH1 and USH3 mouse models, the *Ush1c* knock-in mouse is the only one to have a spontaneous retinal degeneration phenotype [161], mimicking the *RP* symptoms of USH1 patients. In this knock-in mouse, a c.216G>A cryptic splice site mutation in *USH1C*, cloned from Acadian USH1 patients in Louisiana, was inserted into the mouse genome to replace the normal mouse *Ush1c* sequence [162]. It has been proposed that gain-of-function or dominant-negative effect of a truncated harmonin protein fragment from aberrant splicing account for the degeneration. Additionally, *ush1c*$^{fh293/fh293}$ zebrafish line was recently found to have progressive retinal degeneration through labeling of apoptotic marker caspase-3 [115]. Despite these findings, the function of harmonin in the retina remains unidentified.

In summary, little is known of USH protein function in the retina, except myosin VIIa. One of the reasons is that mouse models with mutant USH genes typically have no or weak retinal phenotypes and thus provide limited insight.

5.3. USH genes in other tissues

Three patients from two unrelated Arabic consanguineous families were found to have profound congenital deafness and enteropathy caused by a deletion in the *USH1C* gene [30], suggesting that *USH1C* may have a function in the intestine in addition to the inner ear and retina. Harmonin was recently localized at the tip of intestinal epithelial cell microvilli, which are structurally analogous to hair cell stereocilia [69]. At this place, harmonin is able to anchor protocadherin 24, mucin-like protocadherin and myosin VIIb through direct interactions. In *Ush1c*$^{-/-}$ mice, altered morphology and complete disappearance of microvilli were found in 10–40% of epithelial cells of the small intestine and proximal colon, suggesting an important role of harmonin in maintaining the structure of intestinal enterocytes. Even so, the intestinal physiology of *Ush1c*$^{-/-}$ mice appears normal [69], indicating a potential high tolerance of the intestine to loss of harmonin, which may explain the absence of enteropathy in most patients carrying *USH1C* mutations.

Whirlin protein has been localized in various neurons in the rat cerebrum, cerebellum and thalamus [73] in addition to hair cells and photoreceptors. This protein is required for maintenance of paranodal organization and prevention of subcellular organelle accumulation in myelinated axons of the central and peripheral nervous systems [163]. Another study involving a large-scale phenotyping screen unexpectedly

discovered a defective nociceptive response in *Whrn*$^{tm1a(EUCOMM)Wtsi}$ mutant mice [164]. Female *Whrn*$^{tm1a(EUCOMM)Wtsi}$ mutant mice at 10 weeks of age and fed on a high fat diet were able to stay on a 52 °C hot plate longer than controls, indicating that whirlin may be involved in thermal pain perception. In *Drosophila*, the closest homolog of *DFNB31*, *dysc* (*dyschronic*), was recently identified as a novel component of the circadian output pathway [165]. DYSC protein is present in the major neuronal tracks throughout the fly central brain. It probably functions through forming a complex with a calcium-activated potassium channel SLOWPOKE and regulating the expression of this channel. Several *dysc* mutants generated by the P-element insertions have normal central circadian machinery, but exhibit an arrhythmic locomotor behavior. These findings indicate a potential role of whirlin in regulation of circadian rhythm in the brain. *DFNB31* is known to have multiple alternatively-spliced isoforms, whirlin long and short isoforms [58,166]. Whirlin long isoforms are predicted to be disrupted in all the mutant mice and flies used in the above studies. Therefore, the potential whirlin functions in the brain are probably attributed to whirlin long isoforms.

USH2A was shown to be associated with touch sensitivity and acuity. Studies on two cohorts of USH patients from Germany and Spain have revealed that the tactile acuity and vibration detection threshold are compromised in patients carrying pathogenic *USH2A* mutations, but not in other USH2 patients [167]. Furthermore, patients with *USH2A* mutations in the study were found to have a slightly but significantly lower heat pain threshold. Therefore, the *USH2A* and *DFNB31* genes seem to be in the same neuronal sensory pathway as in vision and hearing, although the effects of the two genes on the heat pain threshold appear opposite. However, due to the small sample sizes in the two studies [164,167], involvement of the *DFNB31* and *USH2A* genes in the thermal pain perception needs to be further verified, and the underlying mechanisms need to be elucidated.

Before its discovery as the *USH2C* gene [38], *GPR98* and its ortholog were originally identified as a causative gene for febrile and afebrile seizures in humans [60] and for audiogenic epilepsy in mice [168]. *GPR98* ortholog mRNAs were detected in the mouse and zebrafish brains [67,169]. VLGR1 protein is highly enriched in the mouse midbrain superior and inferior colliculi [70], while inferior colliculus is known to participate in the occurrence of audiogenic seizures [170]. In oligodendrocytes of the mouse superior and inferior colliculi, VLGR1 regulates the stability of myelin-associated glycoprotein [70], a protein functioning in the axon–glial interaction at the periaxonal membrane of glial myelin sheaths [171]. As mentioned, whirlin is involved in the paranodal organization between the glial myelin sheaths and their wrapped axons [163]. Therefore, both VLGR1 and whirlin likely play a role in nerve axon myelination in the brain.

6. Insights from current literatures about USH genes in various tissues

USH proteins are generally localized to folded plasma membrane structures. For example, USH1 proteins are present at inner ear hair cell stereocilia (Fig. 3) [36,79,80,82–86,90,139], retinal photoreceptor calyceal processes (Fig. 2C) [105] and intestinal enterocyte microvilli [69]. USH2 proteins are present at the ankle link complex of the hair cell stereociliary base (Fig. 3) [68,77,93,94] and the periciliary membrane complex of the photoreceptor inner segment apex facing the connecting cilium (Fig. 2C) [68,105,106,116]. In the nervous system, although the exact cellular or subcellular localizations of whirlin and VLGR1 in myelinated nerves are unclear [70,163], it is possible that these two proteins are present in the myelin sheath, layers of the folded plasma membrane of oligodendrocytes or Schwann cells, to fulfill their functions. The folded plasma membrane structures, where USH proteins are localized, are likely highly dynamic. For example, the plasma membrane of hair cell stereocilia probably moves toward the tip when stereocilia grow rapidly during development; the plasma membrane of the photoreceptor connecting cilium and outer segment probably moves distally during outer segment renewal. Considering the cell adhesion, Ca^{2+}-binding and cell signaling domains predicted in several USH proteins and the localizations of most USH proteins on or near the plasma membrane, USH proteins may mediate signaling to regulate and maintain the dynamic organization of folded membranous structures.

USH proteins are believed to be assembled in multiprotein complexes with other USH and non-USH proteins. As scaffold proteins, harmonin, SANS, whirlin and PDZD7 are essential for organization of these multiprotein complexes. These scaffold proteins bind to their partners mostly through PDZ domains and PBMs with weak affinities in the micromolar range [172]. Therefore, interactions in USH multiprotein complexes are probably transient, consistent with the signaling and dynamic cell adhesion roles of these complexes. PDZ domain-mediated interactions are promiscuous [172]. Their specificity is usually regulated in spatial, temporal and cell type-specific manners. This may explain that the composition and organization of USH multiprotein complexes vary according to tissue. Compared with the harmonin-containing USH1 protein complex at the UTLD in hair cells [91,122,123,126–129], harmonin forms a complex with completely different proteins, protocadherin 24, mucin-like protocadherin and myosin VIIb, at the tip of microvilli in enterocytes [69]. Likewise, PDZD7 plays a crucial role in the USH2 protein complex formation in hair cells, but is dispensable for the complex formation in photoreceptors [68]. Despite the USH multiprotein complex variation in different tissues, individual USH proteins probably conduct similar functions among different complexes. VLGR1 protein was shown to sense the extracellular calcium changes and activate PKA and PKC through binding to Gαs and Gαq, respectively, in the superior and inferior colliculi [70]. This protein was also demonstrated to couple Gαi signaling in overexpressed cell cultures [173]. These signaling pathways could therefore co-exist at the VLGR1-containing USH2 protein complex in both hair cells and photoreceptors. Further, myosin VIIa transports cellular organelles and proteins in RPE cells and photoreceptors [147–151]. Thus, this protein could also participate in intracellular transport in hair cell stereocilia and cytoplasm, although myosin VIIa is generally proposed to anchor USH proteins to actin bundles in hair cell stereocilia. Based on dissimilarities of USH multiprotein complexes in various tissues and potential similarities of USH proteins in different multiprotein complexes, it is crucial to investigate USH proteins/multiprotein complexes in all tissues where present.

7. Current progress in therapeutic studies on USH

As mentioned, no cure for USH has been discovered so far. Present treatments mostly attempt to ameliorate hearing loss or retinal degeneration symptomatically. Here we describe therapeutic approaches that have been investigated with either success or promise.

7.1. Cochlear, vestibular and retinal implants

Cochlear implantation has proven to be a successful therapeutic approach for USH patients [174–176]. The majority of USH children receiving cochlear implants at their early age are able to hear open-set speech and develop oral communication skills at some level. Although enormous progress has been made in retinal prosthesis, the current implantation approach is less successful than cochlear implantation in terms of visual acuity that can be achieved [177]. Development of vestibular implants is still in its infancy [178,179].

7.2. Application of antisense oligonucleotides (ASO)

Striking progress in rescuing hearing and vestibular function has been achieved via application of ASOs in the *Ush1c* knock-in mouse model [180]. Peritoneal injection of an 18-bp ASO in *Ush1c* knock-in

mice at postnatal day 5 was able to restore vestibular function up to 9 months and hearing function up to 6 months, the two longest time points tested [180]. In this study, 15–18 bp ASOs were designed to have base sequences complementary to the patient genomic DNA region containing the *USH1C* 216G>A mutation. These ASOs were able to block the cryptic 5′ splice site generated by the mutation, which leads to production of a small amount of normal harmonin protein. Investigators are now evaluating the rescue effect of ASOs in the retina. This technique is currently limited to a specific class of mutations that generate cryptic splice sites.

7.3. Gene replacement therapy using viral vectors

Viral-mediated gene replacement therapy has attracted favor due to its encouraging efficacy and safety results obtained from clinical trials for an early-onset retinal degenerative disease, Leber's congenital amaurosis, using serotype 2 AAV [181–183]. However, AAVs have a cargo packing limit of 4.7 kb while the most common causative USH1 and USH2 genes, *MYO7A* and *USH2A*, respectively, are much larger than this packing limit. Recent studies on the gene replacement therapy for USH have focused mainly on finding ways to deliver a large gene, especially *MYO7A*, into target retinal cells using various viral vectors.

Four strategies have been reported using AAVs [154,157–159,184,185]. One is to pack the entire 7-kb human *MYO7A* cDNA into single AAV particles, even though this cDNA is significantly larger than the AAV packing limit [154,157]. These oversized AAV particles are able to induce myosin VIIa protein expression in both RPE and photoreceptor cells after subretinal injection, rescue the molecular and cellular defects in these retinal cells, and improve the functional recovery of $Myo7a^{4626SB/4626SB}$ retinas after light desensitization [154,157]. However, oversized single AAV vectors tend to have heterogeneous genomes, raising safety concerns during clinical application. The other three strategies entail application of dual AAV overlapping, trans-splicing and hybrid vectors [157,158,184,185]. In these, N- and C-terminal halves of *MYO7A* cDNA, packed into two separate AAV vectors, are designed to reconnect inside target cells through homologous recombination (overlapping), trans-splicing, or both (hybrid) [158,185]. It was found that dual AAV trans-splicing and hybrid vectors have better transduction efficiencies for both RPE and photoreceptor cells, compared with oversized single AAV and dual AAV overlapping vectors [158]. Subretinal injection of dual AAV trans-splicing and hybrid vectors in $Myo7a^{4626SB/4626SB}$ mice was shown to lead to robust myosin VIIa protein expression in the retina and to rescue the normal localizations of melanosome in RPE cells and rhodopsin in photoreceptors [158].

Lentiviral vectors are able to pack a transgene up to 7.5 kb long [186]. HIV (human immunodeficiency virus)- and EIAV (equine infectious anemia virus)-based lentiviral vectors are capable of delivering the *MYO7A* gene into mouse photoreceptors and RPE cells to provide 'rescue' of phenotypes in *Myo7a* mutant mice [156,159]. A phase I/IIa clinical trial using the EIAV-based lentiviral vector carrying the human *MYO7A* gene, UshStat® (Oxford BioMedica), is being conducted by Dr. Richard Weleber's group at the Oregon Health & Science University (http://www.ohsu.edu/xd/health/services/casey-eye/research/ushersyndrome-study.cfm). This clinical trial is still ongoing and results are yet unpublished.

7.4. Other therapeutic approaches

Translational read-through small molecule drugs for nonsense mutations and genome editing are two approaches with no necessity to pack large genes into a viral vector and no risk of mutagenesis caused by random insertion of viral vectors into the host genome. These two approaches are also able to keep intact the endogenous gene expression regulatory machinery. Translational read-through drugs can insert a random amino acid at the nonsense mutation site by changing mRNA conformation, thereby preventing translation premature stop. Among these drugs, molecules NB54 and PTC124 have been tested to suppress a nonsense mutation, p.R31X, of the *USH1C* gene in vivo [187]. Subretinal injection of NB54 and PTC124 is able to restore protein expression of full-length harmonin in mice. However, the amount of corrected harmonin protein relative to its endogenous protein level was not reported, and the ability of PTC124 to read through the premature stop codon was recently challenged [188]. On the other hand, genome editing is a newly emerging technique to correct gene mutations at the genomic DNA level using artificially-engineered nucleases [189–191]. Two zinc-finger nucleases, designed for different cutting sites around the p.R31X mutation of *USH1C*, are able to correct the DNA error through homologous recombination with a normal DNA template and eventually induce full-length harmonin protein expression without affecting cell viability in cultured cells [192]. At present, this technique is untested in the retina of animal models.

Despite these encouraging findings with translational read-through drugs and genome editing, limitations exist with both approaches. If successful in clinical trials, the translational read-through drugs can only be applied to treat patients carrying nonsense mutations in USH genes, which account for only ~12% of all USH mutations [193]. The genome editing technique has been investigated mainly to correct mutations ex vivo in induced pluripotent stem cells (iPSCs), which are eventually returned to the affected tissue of same patients where the iPSCs are derived [189–191]. Up to now, only two studies have attempted to edit genome in vivo by directly delivering engineered nucleases into the mouse liver [194,195]. One showed some success in correcting the mutant gene, generating a small amount of normal protein and partially rescuing the phenotype [194]. Therefore, for future clinical application of genome editing in USH patients, direct ways to deliver engineered nucleases and DNA templates into photoreceptors and hair cells need to be explored. As genome editing is subject to off-target toxicity and low efficiency problems [189–191,194], the mechanisms underlying genome editing need to be elucidated in detail.

8. Current gaps in understanding and treating USH

Despite identification and extensive study of USH genes using various biochemical, cellular and genetic approaches, knowledge of gene functions at the molecular level is far from full elucidation, especially in the retina, which poses a major hurdle for us to understand the pathogenic mechanisms of USH. The major reason is that phenotypes observed in retinas of USH patients are not faithfully replicated in mice, the historically gold standard animal model for studying human diseases. Several explanations were discussed previously [22,196]. Recently, more hypotheses have been proposed. One is that human and mouse photoreceptors have different subcellular structural requirements for their survival. Localization of USH1 proteins in human photoreceptor calyceal processes [105] and the retinal degeneration symptoms manifested in USH1 patients suggest that calyceal processes are essential for human photoreceptor survival. However, the absence of real calyceal processes and unclear localizations of USH1 proteins in mouse photoreceptors implies that this structure and USH1 proteins are dispensable for rodent photoreceptor survival. Another hypothesis is that USH genes are expressed and required differently for human and animal photoreceptor survival. For instance, expressions of primate *CDH23* and mouse *Cdh23* isoforms are not the same in the retina [101]. Further, cadherin 23, harmonin and clarin-1 proteins of various species show significantly different retinal cellular and subcellular patterns [97,99,112,114,115,118,119]. A third hypothesis is that light illumination is necessary to induce retinal degeneration in USH mouse models [153,160], although the underlying mechanism is unclear. Recently, zebrafish models carrying USH gene mutations have emerged to exhibit early retinal degeneration phenotypes, such as $myo7aa^{ty229d/ty229d}$ and $ush1c^{fh293/fh293}$ zebrafish [115,151], indicating that zebrafish models could be useful for understanding functions of USH genes in the retina

and testing potential treatments. However, evolutionary distance of zebrafish from humans and duplication of human gene orthologs may pose problems, when findings in zebrafish are interpreted and applied to humans. Therefore, development of animal models exhibiting retinal characteristics similar to USH patients is of prime importance.

Current knowledge of USH genes in the vestibular system is scarce. Direct assessment of vestibular function in humans is challenging in terms of both techniques and patients' experience [197]. Furthermore, additional contribution of eyes and proprioceptive organs to balance maintenance [3,198] may mask balance problems in USH patients. These factors possibly lead to research more focused on the cochlea/hearing than the vestibular system/balance. But USH1 and some USH3 patients usually experience more severe balance problems when their vision deteriorates with age. Considering the potential differences of USH multiprotein complexes across different tissues, investigation of USH genes in vestibular organs should be strengthened.

Many case reports on USH patients showing mental disorders exist in the literature [199–211]. Two recent reports also imply that usherin and whirlin may be associated with other sensory modalities, touch and pain [164,167]. Thus, these reports raise a question whether USH patients may have other symptoms in addition to hearing, vision and balance abnormalities. However, all these reports have a limitation due to small sample sizes of patients and mice examined. Further well-designed studies to evaluate the mental health and other senses in USH patients need to be considered.

Therapeutic approaches, such as viral-mediated gene replacement, ASO therapy, translational read-through chemical drugs and genome editing, have been actively explored, while therapeutic research using various types of stem cells is relatively stagnant. Most approaches are now targeted to rescue either hearing or vision loss but not both. Except the cochlear implantation and EIAV-based lentiviral-mediated replacement of the *MYO7A* gene, other approaches are still in their early stage in terms of eventual application in USH patients. Finally, further investigation into the genotype–phenotype correlations of USH genes and elucidation of their molecular basis are imperative for early and appropriate diagnosis, genetic counseling, prognosis and therapy as well as for comprehensive understanding of the USH gene functions in vivo.

9. Summary

USH is an incurable autosomal recessive genetic disease. USH patients exhibit various degrees of hearing, vision and balance impairment. Currently, thirteen genes have been identified to be associated with USH. These genes encode proteins believed to conduct various cellular functions, including intracellular transport, organization of multiprotein complexes, cell adhesion and cell signaling. The USH proteins probably function in multiprotein complexes in vivo. Although required for the development, maintenance and function of hair cell stereocilia in the inner ear, USH multiprotein complexes are not well revealed at the molecular level, and understanding of disease mechanisms underlying USH is incomplete. At present, progress is being made actively to develop effective treatments for USH.

Acknowledgements

The authors thank anonymous reviewers, Dr. Suzanne L. Mansour, Dr. Gary C. Schoenwolf and Dr. Jeanne M. Frederick for their manuscript critiques. The authors also thank Mr. Chris Maggio for his professional artwork. The research on Usher syndrome conducted in the authors' laboratory has been supported by Hope for Vision, Foundation Fighting Blindness, the E. Matilda Ziegler Foundation for the Blind, Inc., National Eye Institute (EY020853 and EY014800), Research to Prevent Blindness and the Moran Eye Center at the University of Utah.

References

[1] M. LeMasurier, P.G. Gillespie, Hair-cell mechanotransduction and cochlear amplification, Neuron 48 (2005) 403–415.
[2] R.A. Eatock, J.E. Songer, Vestibular hair cells and afferents: two channels for head motion signals, Annu. Rev. Neurosci. 34 (2011) 501–534.
[3] S. Khan, R. Chang, Anatomy of the vestibular system: a review, NeuroRehabilitation 32 (2013) 437–443.
[4] P.G. Gillespie, U. Muller, Mechanotransduction by hair cells: models, molecules, and mechanisms, Cell 139 (2009) 33–44.
[5] M.A. Vollrath, K.Y. Kwan, D.P. Corey, The micromachinery of mechanotransduction in hair cells, Annu. Rev. Neurosci. 30 (2007) 339–365.
[6] E.L. Fletcher, A.I. Jobling, K.A. Vessey, C. Luu, R.H. Guymer, P.N. Baird, Animal models of retinal disease, Prog. Mol. Biol. Transl. Sci. 100 (2011) 211–286.
[7] J.A. Boughman, M. Vernon, K.A. Shaver, Usher syndrome: definition and estimate of prevalence from two high-risk populations, J. Chronic Dis. 36 (1983) 595–603.
[8] D.T. Hartong, E.L. Berson, T.P. Dryja, Retinitis pigmentosa, Lancet 368 (2006) 1795–1809.
[9] B.J. Keats, D.P. Corey, The usher syndromes, Am. J. Med. Genet. 89 (1999) 158–166.
[10] W.J. Kimberling, M.S. Hildebrand, A.E. Shearer, M.L. Jensen, J.A. Halder, K. Trzupek, E.S. Cohn, R.G. Weleber, E.M. Stone, R.J. Smith, Frequency of Usher syndrome in two pediatric populations: implications for genetic screening of deaf and hard of hearing children, Genet. Med. 12 (2010) 512–516.
[11] A. Edwards, G.A. Fishman, R.J. Anderson, S. Grover, D.J. Derlacki, Visual acuity and visual field impairment in Usher syndrome, Arch. Ophthalmol. 116 (1998) 165–168.
[12] G.A. Fishman, S. Bozbeyoglu, R.W. Massof, W. Kimberling, Natural course of visual field loss in patients with Type 2 Usher syndrome, Retina 27 (2007) 601–608.
[13] A. El-Amraoui, C. Petit, The retinal phenotype of Usher syndrome: pathophysiological insights from animal models, CR Biol. 337 (2014) 167–177.
[14] Z.M. Ahmed, G.I. Frolenkov, S. Riazuddin, Usher proteins in inner ear structure and function, Physiol. Genomics 45 (2013) 987–989.
[15] C. Bonnet, A. El-Amraoui, Usher syndrome (sensorineural deafness and retinitis pigmentosa): pathogenesis, molecular diagnosis and therapeutic approaches, Curr. Opin. Neurol. 25 (2012) 42–49.
[16] D. Cosgrove, M. Zallocchi, Usher protein functions in hair cells and photoreceptors, Int. J. Biochem. Cell Biol. 46 (2013) 80–89.
[17] H. Kremer, E. van Wijk, T. Marker, U. Wolfrum, R. Roepman, Usher syndrome: molecular links of pathogenesis, proteins and pathways, Hum. Mol. Genet. 15 (Spec No 2) (2006) R262–R270.
[18] L. Pan, M. Zhang, Structures of usher syndrome 1 proteins and their complexes, Physiology (Bethesda) 27 (2012) 25–42.
[19] J. Reiners, K. Nagel-Wolfrum, K. Jurgens, T. Marker, U. Wolfrum, Molecular basis of human Usher syndrome: deciphering the meshes of the Usher protein network provides insights into the pathomechanisms of the Usher disease, Exp. Eye Res. 83 (2006) 97–119.
[20] D.S. Williams, Usher syndrome: animal models, retinal function of Usher proteins, and prospects for gene therapy, Vis. Res. 48 (2008) 433–441.
[21] J. Yang, L. Wang, H. Song, M. Sokolov, Current understanding of usher syndrome type II, Front. Biosci. 17 (2012) 1165–1183.
[22] J. Yang, Usher syndrome: genes, proteins, models, molecular mechanisms, and therapies, in: S. Naz (Ed.), Hearing Loss, Intech Open Access, Croatia, 2012, pp. 293–328.
[23] B.J.B. Keats, J. Lentz, Usher syndrome type II, in: R.A. Pagon, M.P. Adam, T.D. Bird (Eds.), GeneReviews, University of Washington, Seattle1993–2014.
[24] B.J.B. Keats, J. Lentz, Usher syndrome type I, in: R.A. Pagon, M.P. Adam, T.D. Bird (Eds.), GeneReviews, University of Washington, Seattle1993–2014.
[25] E.G. Puffenberger, R.N. Jinks, C. Sougnez, K. Cibulskis, R.A. Willert, N.P. Achilly, R.P. Cassidy, C.J. Fiorentini, K.F. Heiken, J.J. Lawrence, M.H. Mahoney, C.J. Miller, D.T. Nair, K.A. Politi, K.N. Worcester, R.A. Setton, R. Dipiazza, E.A. Sherman, J.T. Eastman, C. Francklyn, S. Robey-Bond, N.L. Rider, S. Gabriel, D.H. Morton, K.A. Strauss, Genetic mapping and exome sequencing identify variants associated with five novel diseases, PLoS ONE 7 (2012) e28936.
[26] I. Ebermann, J.B. Phillips, M.C. Liebau, R.K. Koenekoop, B. Schermer, I. Lopez, E. Schafer, A.F. Roux, C. Dafinger, A. Bernd, E. Zrenner, M. Claustres, B. Blanco, G. Nurnberg, P. Nurnberg, R. Ruland, M. Westerfield, T. Benzing, H.J. Bolz, PDZD7 is a modifier of retinal disease and a contributor to digenic Usher syndrome, J. Clin. Invest. 120 (2010) 1812–1823.
[27] S. Khateb, L. Zelinger, L. Mizrahi-Meissonnier, C. Ayuso, R.K. Koenekoop, U. Laxer, M. Gross, E. Banin, D. Sharon, A homozygous nonsense CEP250 mutation combined with a heterozygous nonsense C2orf71 mutation is associated with atypical Usher syndrome, J. Med. Genet. 51 (2014) 460–469.
[28] D. Weil, S. Blanchard, J. Kaplan, P. Guilford, F. Gibson, J. Walsh, P. Mburu, A. Varela, J. Levilliers, M.D. Weston, et al., Defective myosin VIIA gene responsible for Usher syndrome type 1B, Nature 374 (1995) 60–61.
[29] E. Verpy, M. Leibovici, I. Zwaenepoel, X.Z. Liu, A. Gal, N. Salem, A. Mansour, S. Blanchard, I. Kobayashi, B.J. Keats, R. Slim, C. Petit, A defect in harmonin, a PDZ domain-containing protein expressed in the inner ear sensory hair cells, underlies Usher syndrome type 1C, Nat. Genet. 26 (2000) 51–55.
[30] M. Bitner-Glindzicz, K.J. Lindley, P. Rutland, D. Blaydon, V.V. Smith, P.J. Milla, K. Hussain, J. Furth-Lavi, K.E. Cosgrove, R.M. Shepherd, P.D. Barnes, R.E. O'Brien, P.A. Farndon, J. Sowden, X.Z. Liu, M.J. Scanlan, S. Malcolm, M.J. Dunne, A. Aynsley-Green, B. Glaser, A recessive contiguous gene deletion causing infantile hyperinsulinism, enteropathy and deafness identifies the Usher type 1C gene, Nat. Genet. 26 (2000) 56–60.
[31] H. Bolz, B. von Brederlow, A. Ramirez, E.C. Bryda, K. Kutsche, H.G. Nothwang, M. Seeliger, C.S.C.M. del, M.C. Vila, O.P. Molina, A. Gal, C. Kubisch, Mutation of

CDH23, encoding a new member of the cadherin gene family, causes Usher syndrome type 1D, Nat. Genet. 27 (2001) 108–112.
[32] J.M. Bork, L.M. Peters, S. Riazuddin, S.L. Bernstein, Z.M. Ahmed, S.L. Ness, R. Polomeno, A. Ramesh, M. Schloss, C.R. Srisailpathy, S. Wayne, S. Bellman, D. Desmukh, Z. Ahmed, S.N. Khan, V.M. Kaloustian, X.C. Li, A. Lalwani, M. Bitner-Glindzicz, W.E. Nance, X.Z. Liu, G. Wistow, R.J. Smith, A.J. Griffith, E.R. Wilcox, T.B. Friedman, R.J. Morell, Usher syndrome 1D and nonsyndromic autosomal recessive deafness DFNB12 are caused by allelic mutations of the novel cadherin-like gene CDH23, Am. J. Hum. Genet. 68 (2001) 26–37.
[33] Z.M. Ahmed, S. Riazuddin, S.L. Bernstein, Z. Ahmed, S. Khan, A.J. Griffith, R.J. Morell, T.B. Friedman, E.R. Wilcox, Mutations of the protocadherin gene PCDH15 cause Usher syndrome type 1 F, Am. J. Hum. Genet. 69 (2001) 25–34.
[34] K.N. Alagramam, H. Yuan, M.H. Kuehn, C.L. Murcia, S. Wayne, C.R. Srisailpathy, R.B. Lowry, R. Knaus, L. Van Laer, F.P. Bernier, S. Schwartz, C. Lee, C.C. Morton, R.F. Mullins, A. Ramesh, G. Van Camp, G.S. Hageman, R.P. Woychik, R.J. Smith, Mutations in the novel protocadherin PCDH15 cause Usher syndrome type 1 F, Hum. Mol. Genet. 10 (2001) 1709–1718.
[35] D. Weil, A. El-Amraoui, S. Masmoudi, M. Mustapha, Y. Kikkawa, S. Laine, S. Delmaghani, A. Adato, S. Nadifi, Z.B. Zina, C. Hamel, A. Gal, H. Ayadi, H. Yonekawa, C. Petit, Usher syndrome type I G (USH1G) is caused by mutations in the gene encoding SANS, a protein that associates with the USH1C protein, harmonin, Hum. Mol. Genet. 12 (2003) 463–471.
[36] S. Riazuddin, I.A. Belyantseva, A.P. Giese, K. Lee, A.A. Indzhykulian, S.P. Nandamuri, R. Yousaf, G.P. Sinha, S. Lee, D. Terrell, R.S. Hegde, R.A. Ali, S. Anwar, P.B. Andrade-Elizondo, A. Sirmaci, L.V. Parise, S. Basit, A. Wali, M. Ayub, M. Ansar, W. Ahmad, S.N. Khan, J. Akram, M. Tekin, T. Cook, E.K. Buschbeck, G.I. Frolenkov, S.M. Leal, T.B. Friedman, Z.M. Ahmed, Alterations of the CIB2 calcium- and integrin-binding protein cause Usher syndrome type 1 J and nonsyndromic deafness DFNB48, Nat. Genet. 44 (2012) 1265–1271.
[37] J.D. Eudy, M.D. Weston, S. Yao, D.M. Hoover, H.L. Rehm, M. Ma-Edmonds, D. Yan, I. Ahmad, J.J. Cheng, C. Ayuso, C. Cremers, S. Davenport, C. Moller, C.B. Talmadge, K.W. Beisel, M. Tamayo, C.C. Morton, A. Swaroop, W.J. Kimberling, J. Sumegi, Mutation of a gene encoding a protein with extracellular matrix motifs in Usher syndrome type IIa, Science 280 (1998) 1753–1757.
[38] M.D. Weston, M.W. Luijendijk, K.D. Humphrey, C. Moller, W.J. Kimberling, Mutations in the VLGR1 gene implicate G-protein signaling in the pathogenesis of Usher syndrome type II, Am. J. Hum. Genet. 74 (2004) 357–366.
[39] I. Ebermann, H.P. Scholl, P. Charbel Issa, E. Becirovic, J. Lamprecht, B. Jurklies, J.M. Millan, E. Aller, D. Mitter, H. Bolz, A novel gene for Usher syndrome type 2: mutations in the long isoform of whirlin are associated with retinitis pigmentosa and sensorineural hearing loss, Hum. Genet. 121 (2007) 203–211.
[40] A. Adato, S. Vreugde, T. Joensuu, N. Avidan, R. Hamalainen, O. Belenkiy, T. Olender, B. Bonne-Tamir, E. Ben-Asher, C. Espinos, J.M. Millan, A.E. Lehesjoki, J.G. Flannery, K.B. Avraham, S. Pietrokovski, E.M. Sankila, J.S. Beckmann, D. Lancet, USH3A transcripts encode clarin-1, a four-transmembrane-domain protein with a possible role in sensory synapses, Eur. J. Hum. Genet. 10 (2002) 339–350.
[41] R.R. Fields, G. Zhou, D. Huang, J.R. Davis, C. Moller, S.G. Jacobson, W.J. Kimberling, J. Sumegi, Usher syndrome type III: revised genomic structure of the USH3 gene and identification of novel mutations, Am. J. Hum. Genet. 71 (2002) 607–617.
[42] T. Joensuu, R. Hamalainen, B. Yuan, C. Johnson, S. Tegelberg, P. Gasparini, L. Zelante, U. Pirvola, L. Pakarinen, A.E. Lehesjoki, A. de la Chapelle, E.M. Sankila, Mutations in a novel gene with transmembrane domains underlie Usher syndrome type 3, Am. J. Hum. Genet. 69 (2001) 673–684.
[43] I. Audo, M.E. Lancelot, S. Mohand-Said, A. Antonio, A. Germain, J.A. Sahel, S.S. Bhattacharya, C. Zeitz, Novel C2orf71 mutations account for approximately 1% of cases in a large French arRP cohort, Hum. Mutat. 32 (2011) E2091–E2103.
[44] R.W. Collin, C. Safieh, K.W. Littink, S.A. Shalev, H.J. Garzozi, L. Rizel, A.H. Abbasi, F.P. Cremers, A.I. den Hollander, B.J. Klevering, T. Ben-Yosef, Mutations in C2ORF71 cause autosomal-recessive retinitis pigmentosa, Am. J. Hum. Genet. 86 (2010) 783–788.
[45] M. Hebrard, G. Manes, B. Bocquet, I. Meunier, D. Coustes-Chazalette, E. Herald, A. Senechal, A. Bolland-Auge, D. Zelenika, C.P. Hamel, Combining gene mapping and phenotype assessment for fast mutation finding in non-consanguineous autosomal recessive retinitis pigmentosa families, Eur. J. Hum. Genet. 19 (2011) 1256–1263.
[46] D.Y. Nishimura, L.M. Baye, R. Perveen, C.C. Searby, A. Avila-Fernandez, I. Pereiro, C. Ayuso, D. Valverde, P.N. Bishop, F.D. Manson, J. Urquhart, E.M. Stone, D.C. Slusarski, G.C. Black, V.C. Sheffield, Discovery and functional analysis of a retinitis pigmentosa gene, C2ORF71, Am. J. Hum. Genet. 86 (2010) 686–695.
[47] X.Z. Liu, C. Hope, J. Walsh, V. Newton, X.M. Ke, C.Y. Liang, L.R. Xu, J.M. Zhou, D. Trump, K.P. Steel, S. Bundey, S.D. Brown, Mutations in the myosin VIIA gene cause a wide phenotypic spectrum, including atypical Usher syndrome, Am. J. Hum. Genet. 63 (1998) 909–912.
[48] X.Z. Liu, J. Walsh, P. Mburu, J. Kendrick-Jones, M.J. Cope, K.P. Steel, S.D. Brown, Mutations in the myosin VIIA gene cause non-syndromic recessive deafness, Nat. Genet. 16 (1997) 188–190.
[49] X.Z. Liu, J. Walsh, Y. Tamagawa, K. Kitamura, M. Nishizawa, K.P. Steel, S.D. Brown, Autosomal dominant non-syndromic deafness caused by a mutation in the myosin VIIA gene, Nat. Genet. 17 (1997) 268–269.
[50] S. Riazuddin, S. Nazli, Z.M. Ahmed, Y. Yang, F. Zulfiqar, R.S. Shaikh, A.U. Zafar, S.N. Khan, F. Sabar, F.T. Javid, E.R. Wilcox, E. Tsilou, E.T. Boger, J.R. Sellers, I.A. Belyantseva, S. Riazuddin, T.B. Friedman, Mutation spectrum of MYO7A and evaluation of a novel nonsyndromic deafness DFNB2 allele with residual function, Hum. Mutat. 29 (2008) 502–511.
[51] D. Weil, P. Kussel, S. Blanchard, G. Levy, F. Levi-Acobas, M. Drira, H. Ayadi, C. Petit, The autosomal recessive isolated deafness, DFNB2, and the Usher 1B syndrome are allelic defects of the myosin-VIIA gene, Nat. Genet. 16 (1997) 191–193.
[52] Z.M. Ahmed, T.N. Smith, S. Riazuddin, T. Makishima, M. Ghosh, S. Bokhari, P.S. Menon, D. Deshmukh, A.J. Griffith, T.B. Friedman, E.R. Wilcox, Nonsyndromic recessive deafness DFNB18 and Usher syndrome type IC are allelic mutations of USHIC, Hum. Genet. 110 (2002) 527–531.
[53] X.M. Ouyang, X.J. Xia, E. Verpy, L.L. Du, A. Pandya, C. Petit, T. Balkany, W.E. Nance, X.Z. Liu, Mutations in the alternatively spliced exons of USH1C cause non-syndromic recessive deafness, Hum. Genet. 111 (2002) 26–30.
[54] J.M. Schultz, R. Bhatti, A.C. Madeo, A. Turriff, J.A. Muskett, C.K. Zalewski, K.A. King, Z.M. Ahmed, S. Riazuddin, N. Ahmad, Z. Hussain, M. Qasim, S.N. Kahn, M.R. Meltzer, X.Z. Liu, M. Munisamy, M. Ghosh, H.L. Rehm, E.T. Tsilou, A.J. Griffith, W.M. Zein, C.C. Brewer, T.B. Friedman, Allelic hierarchy of CDH23 mutations causing non-syndromic deafness DFNB12 or Usher syndrome USH1D in compound heterozygotes, J. Med. Genet. 48 (2011) 767–775.
[55] J.M. Schultz, Y. Yang, A.J. Caride, A.G. Filoteo, A.R. Penheiter, A. Lagziel, R.J. Morell, S.A. Mohiddin, L. Fananapazir, A.C. Madeo, J.T. Penniston, A.J. Griffith, Modification of human hearing loss by plasma-membrane calcium pump PMCA2, N. Engl. J. Med. 352 (2005) 1557–1564.
[56] Z.M. Ahmed, S. Riazuddin, J. Ahmad, S.L. Bernstein, Y. Guo, M.F. Sabar, P. Sieving, A.J. Griffith, T.B. Friedman, I.A. Belyantseva, E.R. Wilcox, PCDH15 is expressed in the neurosensory epithelium of the eye and ear and mutant alleles are responsible for both USH1F and DFNB23, Hum. Mol. Genet. 12 (2003) 3215–3223.
[57] L. Doucette, N.D. Merner, S. Cooke, E. Ives, D. Galutira, V. Walsh, T. Walsh, L. MacLaren, T. Cater, B. Fernandez, J.S. Green, E.R. Wilcox, L.I. Shotland, X.C. Li, M. Lee, M.C. King, T.L. Young, Profound, prelingual nonsyndromic deafness maps to chromosome 10q21 and is caused by a novel missense mutation in the Usher syndrome type IF gene PCDH15, Eur. J. Hum. Genet. 17 (2009) 554–564.
[58] P. Mburu, M. Mustapha, A. Varela, D. Weil, A. El-Amraoui, R.H. Holme, A. Rump, R.E. Hardisty, S. Blanchard, R.S. Coimbra, I. Perfettini, N. Parkinson, A.M. Mallon, P. Glenister, M.J. Rogers, A.J. Paige, L. Moir, J. Clay, A. Rosenthal, X.Z. Liu, G. Blanco, K.P. Steel, C. Petit, S.D. Brown, Defects in whirlin, a PDZ domain molecule involved in stereocilia elongation, cause deafness in the whirler mouse and families with DFNB31, Nat. Genet. 34 (2003) 421–428.
[59] C. Rivolta, E.A. Sweklo, E.L. Berson, T.P. Dryja, Missense mutation in the USH2A gene: association with recessive retinitis pigmentosa without hearing loss, Am. J. Hum. Genet. 66 (2000) 1975–1978.
[60] J. Nakayama, Y.H. Fu, A.M. Clark, S. Nakahara, K. Hamano, N. Iwasaki, A. Matsui, T. Arinami, L.J. Ptacek, A nonsense mutation of the MASS1 gene in a family with febrile and afebrile seizures, Ann. Neurol. 52 (2002) 654–657.
[61] Y. Miyasaka, S. Suzuki, Y. Ohshiba, K. Watanabe, Y. Sagara, S.P. Yasuda, K. Matsuoka, H. Shitara, H. Yonekawa, R. Kominami, Y. Kikkawa, Compound heterozygosity of the functionally null Cdh23(v-ngt) and hypomorphic Cdh23(ahl) alleles leads to early-onset progressive hearing loss in mice, Exp. Anim. 62 (2013) 333–346.
[62] Z.Y. Chen, T. Hasson, P.M. Kelley, B.J. Schwender, M.F. Schwartz, M. Ramakrishnan, W.J. Kimberling, M.S. Mooseker, D.P. Corey, Molecular cloning and domain structure of human myosin-VIIa, the gene product defective in Usher syndrome 1B, Genomics 36 (1996) 440–448.
[63] Z.M. Ahmed, R. Goodyear, S. Riazuddin, A. Lagziel, P.K. Legan, M. Behra, S.M. Burgess, K.S. Lilley, E.R. Wilcox, A.J. Griffith, G.I. Frolenkov, I.A. Belyantseva, G.P. Richardson, T.B. Friedman, The tip-link antigen, a protein associated with the transduction complex of sensory hair cells, is protocadherin-15, J. Neurosci. 26 (2006) 7022–7034.
[64] F. Di Palma, R. Pellegrino, K. Noben-Trauth, Genomic structure, alternative splice forms and normal and mutant alleles of cadherin 23 (Cdh23), Gene 281 (2001) 31–41.
[65] A. Adato, G. Lefevre, B. Delprat, V. Michel, N. Michalski, S. Chardenoux, D. Weil, A. El-Amraoui, C. Petit, Usherin, the defective protein in Usher syndrome type IIA, is likely to be a component of interstereocilia ankle links in the inner ear sensory cells, Hum. Mol. Genet. 14 (2005) 3921–3932.
[66] I.A. Belyantseva, E.T. Boger, S. Naz, G.I. Frolenkov, J.R. Sellers, Z.M. Ahmed, A.J. Griffith, T.B. Friedman, Myosin-XVa is required for tip localization of whirlin and differential elongation of hair-cell stereocilia, Nat. Cell Biol. 7 (2005) 148–156.
[67] D.R. McMillan, K.M. Kayes-Wandover, J.A. Richardson, P.C. White, Very large G protein-coupled receptor-1, the largest known cell surface protein, is highly expressed in the developing central nervous system, J. Biol. Chem. 277 (2002) 785–792.
[68] J. Zou, T. Zheng, C. Ren, C. Askew, X.P. Liu, B. Pan, J.R. Holt, Y. Wang, J. Yang, Deletion of PDZD7 disrupts the Usher syndrome type 2 protein complex in cochlear hair cells and causes hearing loss in mice, Hum. Mol. Genet. 23 (2014) 2374–2390.
[69] S.W. Crawley, D.A. Shifrin Jr., N.E. Grega-Larson, R.E. McConnell, A.E. Benesh, S. Mao, Y. Zheng, Q.Y. Zheng, K.T. Nam, B.A. Millis, B. Kachar, M.J. Tyska, Intestinal brush border assembly driven by protocadherin-based intermicrovillar adhesion, Cell 157 (2014) 433–446.
[70] D. Shin, S.T. Lin, Y.H. Fu, L.J. Ptacek, Very large G protein-coupled receptor 1 regulates myelin-associated glycoprotein via Galphas/Galphaq-mediated protein kinases A/C, Proc. Natl. Acad. Sci. U. S. A. 110 (2013) 19101–19106.
[71] G. Bhattacharya, C. Miller, W.J. Kimberling, M.M. Jablonski, D. Cosgrove, Localization and expression of usherin: a novel basement membrane protein defective in people with Usher's syndrome type IIa, Hear. Res. 163 (2002) 1–11.
[72] N. Pearsall, G. Bhattacharya, J. Wisecarver, J. Adams, D. Cosgrove, W. Kimberling, Usherin expression is highly conserved in mouse and human tissues, Hear. Res. 174 (2002) 55–63.
[73] C.C. Yap, F. Liang, Y. Yamazaki, Y. Muto, H. Kishida, T. Hayashida, T. Hashikawa, R. Yano, CIP98, a novel PDZ domain protein, is expressed in the central nervous system and interacts with calmodulin-dependent serine kinase, J. Neurochem. 85 (2003) 123–134.
[74] L. Wang, J. Zou, Z. Shen, E. Song, J. Yang, Whirlin interacts with espin and modulates its actin-regulatory function: an insight into the mechanism of Usher syndrome type II, Hum. Mol. Genet. 21 (2012) 692–710.

[75] C.M. Hackney, D.N. Furness, The composition and role of cross links in mechanoelectrical transduction in vertebrate sensory hair cells, J. Cell Sci. 126 (2013) 1721–1731.
[76] R.J. Goodyear, W. Marcotti, C.J. Kros, G.P. Richardson, Development and properties of stereociliary link types in hair cells of the mouse cochlea, J. Comp. Neurol. 485 (2005) 75–85.
[77] N. Michalski, V. Michel, A. Bahloul, G. Lefevre, J. Barral, H. Yagi, S. Chardenoux, D. Weil, P. Martin, J.P. Hardelin, M. Sato, C. Petit, Molecular characterization of the ankle-link complex in cochlear hair cells and its role in the hair bundle functioning, J. Neurosci. 27 (2007) 6478–6488.
[78] D.N. Furness, Y. Katori, B. Nirmal Kumar, C.M. Hackney, The dimensions and structural attachments of tip links in mammalian cochlear hair cells and the effects of exposure to different levels of extracellular calcium, Neuroscience 154 (2008) 10–21.
[79] A.A. Indzhykulian, R. Stepanyan, A. Nelina, K.J. Spinelli, Z.M. Ahmed, I.A. Belyantseva, T.B. Friedman, P.G. Barr-Gillespie, G.I. Frolenkov, Molecular remodeling of tip links underlies mechanosensory regeneration in auditory hair cells, PLoS Biol. 11 (2013) e1001583.
[80] J. Siemens, C. Lillo, R.A. Dumont, A. Reynolds, D.S. Williams, P.G. Gillespie, U. Muller, Cadherin 23 is a component of the tip link in hair-cell stereocilia, Nature 428 (2004) 950–955.
[81] C. Sollner, G.J. Rauch, J. Siemens, R. Geisler, S.C. Schuster, U. Muller, T. Nicolson, Mutations in cadherin 23 affect tip links in zebrafish sensory hair cells, Nature 428 (2004) 955–959.
[82] V. Michel, R.J. Goodyear, D. Weil, W. Marcotti, I. Perfettini, U. Wolfrum, C.J. Kros, G.P. Richardson, C. Petit, Cadherin 23 is a component of the transient lateral links in the developing hair bundles of cochlear sensory cells, Dev. Biol. 280 (2005) 281–294.
[83] P. Kazmierczak, H. Sakaguchi, J. Tokita, E.M. Wilson-Kubalek, R.A. Milligan, U. Muller, B. Kachar, Cadherin 23 and protocadherin 15 interact to form tip-link filaments in sensory hair cells, Nature 449 (2007) 87–91.
[84] N. Grillet, W. Xiong, A. Reynolds, P. Kazmierczak, T. Sato, C. Lillo, R.A. Dumont, E. Hintermann, A. Sczaniecka, M. Schwander, D. Williams, B. Kachar, P.G. Gillespie, U. Muller, Harmonin mutations cause mechanotransduction defects in cochlear hair cells, Neuron 62 (2009) 375–387.
[85] N. Michalski, V. Michel, E. Caberlotto, G.M. Lefevre, A.F. van Aken, J.Y. Tinevez, E. Bizard, C. Houbron, D. Weil, J.P. Hardelin, G.P. Richardson, C.J. Kros, P. Martin, C. Petit, Harmonin-b, an actin-binding scaffold protein, is involved in the adaptation of mechanoelectrical transduction by sensory hair cells, Pflugers Arch. 459 (2009) 115–130.
[86] M. Grati, B. Kachar, Myosin VIIa and sans localization at stereocilia upper tip-link density implicates these Usher syndrome proteins in mechanotransduction, Proc. Natl. Acad. Sci. U. S. A. 108 (2011) 11476–11481.
[87] P. Kussel-Andermann, A. El-Amraoui, S. Safieddine, S. Nouaille, I. Perfettini, M. Lecuit, P. Cossart, U. Wolfrum, C. Petit, Vezatin, a novel transmembrane protein, bridges myosin VIIA to the cadherin–catenins complex, EMBO J. 19 (2000) 6020–6029.
[88] U. Wolfrum, X. Liu, A. Schmitt, I.P. Udovichenko, D.S. Williams, Myosin VIIa as a common component of cilia and microvilli, Cell Motil. Cytoskeleton 40 (1998) 261–271.
[89] T. Hasson, M.B. Heintzelman, J. Santos-Sacchi, D.P. Corey, M.S. Mooseker, Expression in cochlea and retina of myosin VIIa, the gene product defective in Usher syndrome type 1B, Proc. Natl. Acad. Sci. U. S. A. 92 (1995) 9815–9819.
[90] G. Lefevre, V. Michel, D. Weil, L. Lepelletier, E. Bizard, U. Wolfrum, J.P. Hardelin, C. Petit, A core cochlear phenotype in USH1 mouse mutants implicates fibrous links of the hair bundle in its cohesion, orientation and differential growth, Development 135 (2008) 1427–1437.
[91] A. Bahloul, V. Michel, J.P. Hardelin, S. Nouaille, S. Hoos, A. Houdusse, P. England, C. Petit, Cadherin-23, myosin VIIa and harmonin, encoded by Usher syndrome type I genes, form a ternary complex and interact with membrane phospholipids, Hum. Mol. Genet. 19 (2010) 3557–3565.
[92] M. Senften, M. Schwander, P. Kazmierczak, C. Lillo, J.B. Shin, T. Hasson, G.S. Geleoc, P.G. Gillespie, D. Williams, J.R. Holt, U. Muller, Physical and functional interaction between protocadherin 15 and myosin VIIa in mechanosensory hair cells, J. Neurosci. 26 (2006) 2060–2071.
[93] J. McGee, R.J. Goodyear, D.R. McMillan, E.A. Stauffer, J.R. Holt, K.G. Locke, D.G. Birch, P.K. Legan, P.C. White, E.J. Walsh, G.P. Richardson, The very large G-protein-coupled receptor VLGR1: a component of the ankle link complex required for the normal development of auditory hair bundles, J. Neurosci. 26 (2006) 6543–6553.
[94] M. Grati, J.B. Shin, M.D. Weston, J. Green, M.A. Bhat, P.G. Gillespie, B. Kachar, Localization of PDZD7 to the stereocilia ankle-link associates this scaffolding protein with the Usher syndrome protein network, J. Neurosci. 32 (2012) 14288–14293.
[95] B. Delprat, V. Michel, R. Goodyear, Y. Yamasaki, N. Michalski, A. El-Amraoui, I. Perfettini, P. Legrain, G. Richardson, J.P. Hardelin, C. Petit, Myosin XVa and whirlin, two deafness gene products required for hair bundle growth, are located at the stereocilia tips and interact directly, Hum. Mol. Genet. 14 (2005) 401–410.
[96] Y. Kikkawa, P. Mburu, S. Morse, R. Kominami, S. Townsend, S.D. Brown, Mutant analysis reveals whirlin as a dynamic organizer in the growing hair cell stereocilium, Hum. Mol. Genet. 14 (2005) 391–400.
[97] J.B. Phillips, H. Vastinsalo, J. Wegner, A. Clement, E.M. Sankila, M. Westerfield, The cone-dominant retina and the inner ear of zebrafish express the ortholog of CLRN1, the causative gene of human Usher syndrome type 3A, Gene Expr. Patterns 13 (2013) 473–481.
[98] R. Geng, S. Melki, D.H. Chen, G. Tian, D.N. Furness, T. Oshima-Takago, J. Neef, T. Moser, C. Askew, G. Horwitz, J.R. Holt, Y. Imanishi, K.N. Alagramam, The mechanosensory structure of the hair cell requires clarin-1, a protein encoded by Usher syndrome III causative gene, J. Neurosci. 32 (2012) 9485–9498.
[99] J. Reiners, E. van Wijk, T. Marker, U. Zimmermann, K. Jurgens, H. te Brinke, N. Overlack, R. Roepman, M. Knipper, H. Kremer, U. Wolfrum, Scaffold protein harmonin (USH1C) provides molecular links between Usher syndrome type 1 and type 2, Hum. Mol. Genet. 14 (2005) 3933–3943.
[100] E. van Wijk, B. van der Zwaag, T. Peters, U. Zimmermann, H. Te Brinke, F.F. Kersten, T. Marker, E. Aller, L.H. Hoefsloot, C.W. Cremers, F.P. Cremers, U. Wolfrum, M. Knipper, R. Roepman, H. Kremer, The DFNB31 gene product whirlin connects to the Usher protein network in the cochlea and retina by direct association with USH2A and VLGR1, Hum. Mol. Genet. 15 (2006) 751–765.
[101] A. Lagziel, N. Overlack, S.L. Bernstein, R.J. Morell, U. Wolfrum, T.B. Friedman, Expression of cadherin 23 isoforms is not conserved: implications for a mouse model of Usher syndrome type 1D, Mol. Vis. 15 (2009) 1843–1857.
[102] M. Zallocchi, D. Delimont, D.T. Meehan, D. Cosgrove, Regulated vesicular trafficking of specific PCDH15 and VLGR1 variants in auditory hair cells, J. Neurosci. 32 (2012) 13841–13859.
[103] M. Zallocchi, D.T. Meehan, D. Delimont, J. Rutledge, M.A. Gratton, J. Flannery, D. Cosgrove, Role for a novel Usher protein complex in hair cell synaptic maturation, PLoS ONE 7 (2012) e30573.
[104] F.D. Gregory, K.E. Bryan, T. Pangrsic, I.E. Calin-Jageman, T. Moser, A. Lee, Harmonin inhibits presynaptic Cav1.3 Ca(2) channels in mouse inner hair cells, Nat. Neurosci. 14 (2011) 1109–1111.
[105] I. Sahly, E. Dufour, C. Schietroma, V. Michel, A. Bahloul, I. Perfettini, E. Pepermans, A. Estivalet, D. Carette, A. Aghaie, I. Ebermann, A. Lelli, M. Iribarne, J.P. Hardelin, D. Weil, J.A. Sahel, A. El-Amraoui, C. Petit, Localization of Usher 1 proteins to the photoreceptor calyceal processes, which are absent from mice, J. Cell Biol. 199 (2012) 381–399.
[106] J. Yang, X. Liu, Y. Zhao, M. Adamian, B. Pawlyk, X. Sun, D.R. McMillan, M.C. Liberman, T. Li, Ablation of whirlin long isoform disrupts the USH2 protein complex and causes vision and hearing loss, PLoS Genet. 6 (2010) e1000955.
[107] K.R. Peters, G.E. Palade, B.G. Schneider, D.S. Papermaster, Fine structure of a periciliary ridge complex of frog retinal rod cells revealed by ultrahigh resolution scanning electron microscopy, J. Cell Biol. 96 (1983) 265–276.
[108] T. Hasson, J. Walsh, J. Cable, M.S. Mooseker, S.D. Brown, K.P. Steel, Effects of shaker-1 mutations on myosin-VIIa protein and mRNA expression, Cell Motil. Cytoskeleton 37 (1997) 127–138.
[109] X. Liu, G. Vansant, I.P. Udovichenko, U. Wolfrum, D.S. Williams, Myosin VIIa, the product of the Usher 1B syndrome gene, is concentrated in the connecting cilia of photoreceptor cells, Cell Motil. Cytoskeleton 37 (1997) 240–252.
[110] A. el-Amraoui, I. Sahly, S. Picaud, J. Sahel, M. Abitbol, C. Petit, Human Usher 1B/mouse shaker-1: the retinal phenotype discrepancy explained by the presence/absence of myosin VIIA in the photoreceptor cells, Hum. Mol. Genet. 5 (1996) 1171–1178.
[111] T. Maerker, E. van Wijk, N. Overlack, F.F. Kersten, J. McGee, T. Goldmann, E. Sehn, R. Roepman, E.J. Walsh, H. Kremer, U. Wolfrum, A novel Usher protein network at the periciliary reloading point between molecular transport machineries in vertebrate photoreceptor cells, Hum. Mol. Genet. 17 (2008) 71–86.
[112] J. Reiners, T. Marker, K. Jurgens, B. Reidel, U. Wolfrum, Photoreceptor expression of the Usher syndrome type 1 protein protocadherin 15 (USH1F) and its interaction with the scaffold protein harmonin (USH1C), Mol. Vis. 11 (2005) 347–355.
[113] D.S. Williams, T.S. Aleman, C. Lillo, V.S. Lopes, L.C. Hughes, E.M. Stone, S.G. Jacobson, Harmonin in the murine retina and the retinal phenotypes of Ush1c-mutant mice and human USH1C, Invest. Ophthalmol. Vis. Sci. 50 (2009) 3881–3889.
[114] G. Glover, K.P. Mueller, C. Sollner, S.C. Neuhauss, T. Nicolson, The Usher gene cadherin 23 is expressed in the zebrafish brain and a subset of retinal amacrine cells, Mol. Vis. 18 (2012) 2309–2322.
[115] J.B. Phillips, B. Blanco-Sanchez, J.J. Lentz, A. Tallafuss, K. Khanobdee, S. Sampath, Z.G. Jacobs, P.F. Han, M. Mishra, D.S. Williams, B.J. Keats, P. Washbourne, M. Westerfield, Harmonin (Ush1c) is required in zebrafish Muller glial cells for photoreceptor synaptic development and function, Dis. Model. Mech. 4 (2011) 786–800.
[116] X. Liu, O.V. Bulgakov, K.N. Darrow, B. Pawlyk, M. Adamian, M.C. Liberman, T. Li, Usherin is required for maintenance of retinal photoreceptors and normal development of cochlear hair cells, Proc. Natl. Acad. Sci. U. S. A. 104 (2007) 4413–4418.
[117] J. Zou, L. Luo, Z. Shen, V.A. Chiodo, B.K. Ambati, W.W. Hauswirth, J. Yang, Whirlin replacement restores the formation of the USH2 protein complex in whirlin knockout photoreceptors, Invest. Ophthalmol. Vis. Sci. 52 (2011) 2343–2351.
[118] M. Zallocchi, D.T. Meehan, D. Delimont, C. Askew, S. Garige, M.A. Gratton, C.A. Rothermund-Franklin, D. Cosgrove, Localization and expression of clarin-1, the Clrn1 gene product, in auditory hair cells and photoreceptors, Hear. Res. 255 (2009) 109–120.
[119] S.F. Geller, K.I. Guerin, M. Visel, A. Pham, E.S. Lee, A.A. Dror, K.B. Avraham, T. Hayashi, C.A. Ray, T.A. Reh, O. Bermingham-McDonogh, W.J. Triffo, S. Bao, J. Isosomppi, H. Västinsalo, E.M. Sankila, J.G. Flannery, CLRN1 is nonessential in the mouse retina but is required for cochlear hair cell development, PLoS Genet. 5 (2009) e1000607.
[120] T. Sakai, N. Umeki, R. Ikebe, M. Ikebe, Cargo binding activates myosin VIIA motor function in cells, Proc. Natl. Acad. Sci. U. S. A. 108 (2011) 7028–7033.
[121] S.M. Heissler, D.J. Manstein, Functional characterization of the human myosin-7a motor domain, Cell. Mol. Life Sci. 69 (2012) 299–311.
[122] A. Adato, V. Michel, Y. Kikkawa, J. Reiners, K.N. Alagramam, D. Weil, H. Yonekawa, U. Wolfrum, A. El-Amraoui, C. Petit, Interactions in the network of Usher syndrome type 1 proteins, Hum. Mol. Genet. 14 (2005) 347–356.
[123] J. Yan, L. Pan, X. Chen, L. Wu, M. Zhang, The structure of the harmonin/sans complex reveals an unexpected interaction mode of the two Usher syndrome proteins, Proc. Natl. Acad. Sci. U. S. A. 107 (2010) 4040–4045.
[124] R.J. Goodyear, A. Forge, P.K. Legan, G.P. Richardson, Asymmetric distribution of cadherin 23 and protocadherin 15 in the kinocilial links of avian sensory hair cells, J. Comp. Neurol. 518 (2010) 4288–4297.

[125] Z. Saihan, A.R. Webster, L. Luxon, M. Bitner-Glindzicz, Update on Usher syndrome, Curr. Opin. Neurol. 22 (2009) 19–27.
[126] L. Pan, J. Yan, L. Wu, M. Zhang, Assembling stable hair cell tip link complex via multidentate interactions between harmonin and cadherin 23, Proc. Natl. Acad. Sci. U. S. A. 106 (2009) 5575–5580.
[127] L. Zheng, J. Zheng, D.S. Whitlon, J. Garcia-Anoveros, J.R. Bartles, Targeting of the hair cell proteins cadherin 23, harmonin, myosin XVa, espin, and prestin in an epithelial cell model, J. Neurosci. 30 (2010) 7187–7201.
[128] L. Wu, L. Pan, Z. Wei, M. Zhang, Structure of MyTH4-FERM domains in myosin VIIa tail bound to cargo, Science 331 (2011) 757–760.
[129] B. Blanco-Sanchez, A. Clement, J. Fierro Junior, P. Washbourne, M. Westerfield, Usher protein complexes preassemble at the endoplasmic reticulum and are required for trafficking and ER homeostasis, Dis. Model. Mech. 7 (2014) 547–559.
[130] G. Sekerkova, L. Zheng, P.A. Loomis, E. Mugnaini, J.R. Bartles, Espins and the actin cytoskeleton of hair cell stereocilia and sensory cell microvilli, Cell. Mol. Life Sci. 63 (2006) 2329–2341.
[131] N. Overlack, D. Kilic, K. Bauss, T. Marker, H. Kremer, E. van Wijk, U. Wolfrum, Direct interaction of the Usher syndrome 1G protein SANS and myomegalin in the retina, Biochim. Biophys. Acta 1813 (2011) 1883–1892.
[132] F.F. Kersten, E. van Wijk, L. Hetterschijt, K. Baubeta, T.A. Peters, M.G. Aslanyan, B. van der Zwaag, U. Wolfrum, J.E. Keunen, R. Roepman, H. Kremer, The mitotic spindle protein SPAG5/Astrin connects to the Usher protein network postmitotically, Cilia 1 (2013) 2.
[133] K. Bauss, B. Knapp, P. Jores, R. Roepman, H. Kremer, E.V. Wijk, T. Marker, U. Wolfrum, Phosphorylation of the Usher syndrome 1G protein SANS controls Magi2-mediated endocytosis, Hum. Mol. Genet. 23 (2014) 3923–3942.
[134] F. Kersten, E. van Wijk, J. van Reeuwijk, B. van der Zwaag, T. Maerker, T. Peters, N. Katsanis, U. Wolfrum, J. Keunen, R. Roepman, H. Kremer, Association of whirlin with Cav1.3 ({alpha}1D) channels in photoreceptors, defining a novel member of the Usher protein network, Invest. Ophthalmol. Vis. Sci. 51 (2010) 2338–2346.
[135] J. Zou, A. Lee, J. Yang, The expression of whirlin and Ca(v)1.3alpha(1) is mutually independent in photoreceptors, Vis. Res. 75 (2012) 53–59.
[136] C. Seiler, K.C. Finger-Baier, O. Rinner, Y.V. Makhankov, H. Schwarz, S.C. Neuhauss, T. Nicolson, Duplicated genes with split functions: independent roles of protocadherin15 orthologues in zebrafish hearing and vision, Development 132 (2005) 615–623.
[137] S. Ernest, G.J. Rauch, P. Haffter, R. Geisler, C. Petit, T. Nicolson, Mariner is defective in myosin VIIA: a zebrafish model for human hereditary deafness, Hum. Mol. Genet. 9 (2000) 2189–2196.
[138] K.N. Alagramam, R.J. Goodyear, R. Geng, D.N. Furness, A.F. van Aken, W. Marcotti, C.J. Kros, G.P. Richardson, Mutations in protocadherin 15 and cadherin 23 affect tip links and mechanotransduction in mammalian sensory hair cells, PLoS ONE 6 (2011) e19183.
[139] E. Caberlotto, V. Michel, I. Foucher, A. Bahloul, R.J. Goodyear, E. Pepermans, N. Michalski, I. Perfettini, O. Alegria-Prevot, S. Chardenoux, M. Do Cruzeiro, J.P. Hardelin, G.P. Richardson, P. Avan, D. Weil, C. Petit, Usher type 1G protein sans is a critical component of the tip–link complex, a structure controlling actin polymerization in stereocilia, Proc. Natl. Acad. Sci. U. S. A. 108 (2011) 5825–5830.
[140] F.D. Gregory, T. Pangrsic, I.E. Calin-Jageman, T. Moser, A. Lee, Harmonin enhances voltage-dependent facilitation of Cav1.3 channels and synchronous exocytosis in mouse inner hair cells, J. Physiol. 591 (2013) 3253–3269.
[141] R.H. Holme, B.W. Kiernan, S.D. Brown, K.P. Steel, Elongation of hair cell stereocilia is defective in the mouse mutant whirler, J. Comp. Neurol. 450 (2002) 94–102.
[142] K.R. Johnson, Q.Y. Zheng, M.D. Weston, L.J. Ptacek, K. Noben-Trauth, The Mass1frings mutation underlies early onset hearing impairment in BUB/BnJ mice, a model for the auditory pathology of Usher syndrome IIC, Genomics 85 (2005) 582–590.
[143] H. Yagi, H. Tokano, M. Maeda, T. Takabayashi, T. Nagano, H. Kiyama, S. Fujieda, K. Kitamura, M. Sato, Vlgr1 is required for proper stereocilia maturation of cochlear hair cells, Genes Cells 12 (2007) 235–250.
[144] M.M. Mogensen, A. Rzadzinska, K.P. Steel, The deaf mouse mutant whirler suggests a role for whirlin in actin filament dynamics and stereocilia development, Cell Motil. Cytoskeleton 64 (2007) 496–508.
[145] R. Stepanyan, I.A. Belyantseva, A.J. Griffith, T.B. Friedman, G.I. Frolenkov, Auditory mechanotransduction in the absence of functional myosin-XVa, J. Physiol. 576 (2006) 801–808.
[146] R. Geng, S.F. Geller, T. Hayashi, C.A. Ray, T.A. Reh, O. Bermingham-McDonogh, S.M. Jones, C.G. Wright, S. Melki, Y. Imanishi, K. Palczewski, K.N. Alagramam, J.G. Flannery, Usher syndrome IIIA gene clarin-1 is essential for hair cell function and associated neural activation, Hum. Mol. Genet. 18 (2009) 2748–2760.
[147] X. Liu, B. Ondek, D.S. Williams, Mutant myosin VIIa causes defective melanosome distribution in the RPE of shaker-1 mice, Nat. Genet. 19 (1998) 117–118.
[148] D. Gibbs, J. Kitamoto, D.S. Williams, Abnormal phagocytosis by retinal pigmented epithelium that lacks myosin VIIa, the Usher syndrome 1B protein, Proc. Natl. Acad. Sci. U. S. A. 100 (2003) 6481–6486.
[149] V.S. Lopes, D. Gibbs, R.T. Libby, T.S. Aleman, D.L. Welch, C. Lillo, S.G. Jacobson, R.A. Radu, K.P. Steel, D.S. Williams, The Usher 1B protein, MYO7A, is required for normal localization and function of the visual retinoid cycle enzyme, RPE65, Hum. Mol. Genet. 20 (2011) 2560–2570.
[150] X. Liu, I.P. Udovichenko, S.D. Brown, K.P. Steel, D.S. Williams, Myosin VIIa participates in opsin transport through the photoreceptor cilium, J. Neurosci. 19 (1999) 6267–6274.
[151] M.M. Wasfy, J.I. Matsui, J. Miller, J.E. Dowling, B.D. Perkins, myosin 7aa mutant zebrafish show mild photoreceptor degeneration and reduced electroretinographic responses, Exp. Eye Res. 122C (2014) 65–76.
[152] S. Papal, M. Cortese, K. Legendre, N. Sorusch, J. Dragavon, I. Sahly, S. Shorte, U. Wolfrum, C. Petit, A. El-Amraoui, The giant spectrin betaV couples the molecular motors to phototransduction and Usher syndrome type I proteins along their trafficking route, Hum. Mol. Genet. 22 (2013) 3773–3788.
[153] Y.W. Peng, M. Zallocchi, W.M. Wang, D. Delimont, D. Cosgrove, Moderate light induced degeneration of rod photoreceptors with delayed transducin translocation in shaker1 mice, Invest. Ophthalmol. Vis. Sci. 52 (2011) 6421.
[154] P. Colella, A. Sommella, E. Marrocco, U. Di Vicino, E. Polishchuk, M.G. Garrido, M.W. Seeliger, R. Polishchuk, A. Auricchio, Myosin7a deficiency results in reduced retinal activity which is improved by gene therapy, PLoS ONE 8 (2013) e72027.
[155] R.T. Libby, K.P. Steel, Electroretinographic anomalies in mice with mutations in Myo7a, the gene involved in human Usher syndrome type 1B, Invest. Ophthalmol. Vis. Sci. 42 (2001) 770–778.
[156] T. Hashimoto, D. Gibbs, C. Lillo, S.M. Azarian, E. Legacki, X.M. Zhang, X.J. Yang, D.S. Williams, Lentiviral gene replacement therapy of retinas in a mouse model for Usher syndrome type 1B, Gene Ther. 14 (2007) 584–594.
[157] V.S. Lopes, S.E. Boye, C.M. Louie, S. Boye, F. Dyka, V. Chiodo, H. Fofo, W.W. Hauswirth, D.S. Williams, Retinal gene therapy with a large MYO7A cDNA using adeno-associated virus, Gene Ther. 20 (2013) 824–833.
[158] I. Trapani, P. Colella, A. Sommella, C. Iodice, G. Cesi, S. De Simone, E. Marrocco, S. Rossi, M. Giunti, A. Palfi, G. Jane Farrar, R. Polishchuk, A. Auricchio, Effective delivery of large genes to the retina by dual AAV vectors, EMBO Mol. Med. 6 (2013) 194–211.
[159] M. Zallocchi, K. Binley, Y. Lad, S. Ellis, P. Widdowson, S. Iqball, V. Scripps, M. Kelleher, J. Loader, J. Miskin, Y.W. Peng, W.M. Wang, L. Cheung, D. Delimont, K.A. Mitrophanous, D. Cosgrove, EIAV-based retinal gene therapy in the shaker1 mouse model for usher syndrome type 1B: development of UshStat, PLoS ONE 9 (2014) e94272.
[160] M. Tian, W. Wang, D. Delimont, L. Cheung, M. Zallocchi, D. Cosgrove, Y.W. Peng, Photoreceptors in whirler mice show defective transducin translocation and are susceptible to short-term light/dark changes-induced degeneration, Exp. Eye Res. 118 (2014) 145–153.
[161] J.J. Lentz, W.C. Gordon, H.E. Farris, G.H. MacDonald, D.E. Cunningham, C.A. Robbins, B.L. Tempel, N.G. Bazan, E.W. Rubel, E.C. Oesterle, B.J. Keats, Deafness and retinal degeneration in a novel USH1C knock-in mouse model, Dev. Neurobiol. 70 (2010) 253–267.
[162] J. Lentz, F. Pan, S.S. Ng, P. Deininger, B. Keats, Ush1c216A knock-in mouse survives Katrina, Mutat. Res. 616 (2007) 139–144.
[163] J.A. Green, J. Yang, M. Grati, B. Kachar, M.A. Bhat, Whirlin, a cytoskeletal scaffolding protein, stabilizes the paranodal region and axonal cytoskeleton in myelinated axons, BMC Neurosci. 14 (2013) 96.
[164] J.K. White, A.K. Gerdin, N.A. Karp, E. Ryder, M. Buljan, J.N. Bussell, J. Salisbury, S. Clare, N.J. Ingham, C. Podrini, R. Houghton, J. Estabel, J.R. Bottomley, D.G. Melvin, D. Sunter, N.C. Adams, D. Tannahill, D.W. Logan, D.G. Macarthur, J. Flint, V.B. Mahajan, S.H. Tsang, I. Smyth, F.M. Watt, W.C. Skarnes, G. Dougan, D.J. Adams, R. Ramirez-Solis, A. Bradley, K.P. Steel, Genome-wide generation and systematic phenotyping of knockout mice reveals new roles for many genes, Cell 154 (2013) 452–464.
[165] J.E. Jepson, M. Shahidullah, A. Lamaze, D. Peterson, H. Pan, K. Koh, dyschronic, a *Drosophila* homolog of a deaf-blindness gene, regulates circadian output and Slowpoke channels, PLoS Genet. 8 (2012) e1002671.
[166] R.N. Wright, D.H. Hong, B. Perkins, RpgrORF15 connects to the usher protein network through direct interactions with multiple whirlin isoforms, Invest. Ophthalmol. Vis. Sci. 53 (2012) 1519–1529.
[167] H. Frenzel, J. Bohlender, K. Pinsker, B. Wohlleben, J. Tank, S.G. Lechner, D. Schiska, T. Jaijo, F. Ruschendorf, K. Saar, J. Jordan, J.M. Millan, M. Gross, G.R. Lewin, A genetic basis for mechanosensory traits in humans, PLoS Biol. 10 (2012) e1001318.
[168] S.L. Skradski, A.M. Clark, H. Jiang, H.S. White, Y.H. Fu, L.J. Ptacek, A novel gene causing a mendelian audiogenic mouse epilepsy, Neuron 31 (2001) 537–544.
[169] Y. Gibert, D.R. McMillan, K. Kayes-Wandover, A. Meyer, G. Begemann, P.C. White, Analysis of the very large G-protein coupled receptor gene (Vlgr1/Mass1/USH2C) in zebrafish, Gene 353 (2005) 200–206.
[170] N. Garcia-Cairasco, A critical review on the participation of inferior colliculus in acoustic–motor and acoustic–limbic networks involved in the expression of acute and kindled audiogenic seizures, Hear. Res. 168 (2002) 208–222.
[171] R.H. Quarles, Myelin-associated glycoprotein (MAG): past, present and beyond, J. Neurochem. 100 (2007) 1431–1448.
[172] G. Schreiber, A.E. Keating, Protein binding specificity versus promiscuity, Curr. Opin. Struct. Biol. 21 (2011) 50–61.
[173] Q.X. Hu, J.H. Dong, H.B. Du, D.L. Zhang, H.Z. Ren, M.L. Ma, Y. Cai, T.C. Zhao, X.L. Yin, X. Yu, T. Xue, Z.G. Xu, J.P. Sun, Constitutive galphai coupling activity of VLGR1 and its regulation by PDZD7, J. Biol. Chem. 289 (2014) 24215–24225.
[174] S.J. Broomfield, I.A. Bruce, L. Henderson, R.T. Ramsden, K.M. Green, Cochlear implantation in children with syndromic deafness, Int. J. Pediatr. Otorhinolaryngol. 77 (2013) 1312–1316.
[175] K.R. Jatana, D. Thomas, L. Weber, M.B. Mets, J.B. Silverman, N.M. Young, Usher syndrome: characteristics and outcomes of pediatric cochlear implant recipients, Otol. Neurotol. 34 (2013) 484–489.
[176] F. Imtiaz, K. Taibah, G. Bin-Khamis, S. Kennedy, A. Hemidan, F. Al-Qahtani, K. Tabbara, B. Al Mubarak, K. Ramzan, B.F. Meyer, M. Al-Owain, USH1G with unique retinal findings caused by a novel truncating mutation identified by genome-wide linkage analysis, Mol. Vis. 18 (2012) 1885–1894.
[177] A.T. Chuang, C.E. Margo, P.B. Greenberg, Retinal implants: a systematic review, Br. J. Ophthalmol. 98 (2014) 852–856.
[178] D.M. Merfeld, R.F. Lewis, Replacing semicircular canal function with a vestibular implant, Curr. Opin. Otolaryngol. Head Neck Surg. 20 (2012) 386–392.
[179] J.P. Guyot, A. Gay, M.I. Kos, M. Pelizzone, Ethical, anatomical and physiological issues in developing vestibular implants for human use, J. Vestib. Res. 22 (2012) 3–9.

[180] J.J. Lentz, F.M. Jodelka, A.J. Hinrich, K.E. McCaffrey, H.E. Farris, M.J. Spalitta, N.G. Bazan, D.M. Duelli, F. Rigo, M.L. Hastings, Rescue of hearing and vestibular function by antisense oligonucleotides in a mouse model of human deafness, Nat. Med. 19 (2013) 345–350.
[181] J.W. Bainbridge, A.J. Smith, S.S. Barker, S. Robbie, R. Henderson, K. Balaggan, A. Viswanathan, G.E. Holder, A. Stockman, N. Tyler, S. Petersen-Jones, S.S. Bhattacharya, A.J. Thrasher, F.W. Fitzke, B.J. Carter, G.S. Rubin, A.T. Moore, R.R. Ali, Effect of gene therapy on visual function in Leber's congenital amaurosis, N. Engl. J. Med. 358 (2008) 2231–2239.
[182] W.W. Hauswirth, T.S. Aleman, S. Kaushal, A.V. Cideciyan, S.B. Schwartz, L. Wang, T.J. Conlon, S.L. Boye, T.R. Flotte, B.J. Byrne, S.G. Jacobson, Treatment of leber congenital amaurosis due to RPE65 mutations by ocular subretinal injection of adeno-associated virus gene vector: short-term results of a phase I trial, Hum. Gene Ther. 19 (2008) 979–990.
[183] A.M. Maguire, F. Simonelli, E.A. Pierce, E.N. Pugh Jr., F. Mingozzi, J. Bennicelli, S. Banfi, K.A. Marshall, F. Testa, E.M. Surace, S. Rossi, A. Lyubarsky, V.R. Arruda, B. Konkle, E. Stone, J. Sun, J. Jacobs, L. Dell'Osso, R. Hertle, J.X. Ma, T.M. Redmond, X. Zhu, B. Hauck, O. Zelenaia, K.S. Shindler, M.G. Maguire, J.F. Wright, N.J. Volpe, J.W. McDonnell, A. Auricchio, K.A. High, J. Bennett, Safety and efficacy of gene transfer for Leber's congenital amaurosis, N. Engl. J. Med. 358 (2008) 2240–2248.
[184] P. Colella, I. Trapani, G. Cesi, A. Sommella, A. Manfredi, A. Puppo, C. Iodice, S. Rossi, F. Simonelli, M. Giunti, M.L. Bacci, A. Auricchio, Efficient gene delivery to the cone-enriched pig retina by dual AAV vectors, Gene Ther. 21 (2014) 450–456.
[185] F.M. Dyka, S.L. Boye, V.A. Chiodo, W.W. Hauswirth, S.E. Boye, Dual adeno-associated virus vectors result in efficient in vitro and in vivo expression of an oversized gene, MYO7A, Hum. Gene Ther. Methods 25 (2014) 166–177.
[186] S. Benedetti, H. Hoshiya, F.S. Tedesco, Repair or replace? Exploiting novel gene and cell therapy strategies for muscular dystrophies, FEBS J. 280 (2013) 4263–4280.
[187] T. Goldmann, N. Overlack, F. Moller, V. Belakhov, M. van Wyk, T. Baasov, U. Wolfrum, K. Nagel-Wolfrum, A comparative evaluation of NB30, NB54 and PTC124 in translational read-through efficacy for treatment of an USH1C nonsense mutation, EMBO Mol. Med. 4 (2012) 1186–1199.
[188] S.P. McElroy, T. Nomura, L.S. Torrie, E. Warbrick, U. Gartner, G. Wood, W.H. McLean, A lack of premature termination codon read-through efficacy of PTC124 (Ataluren) in a diverse array of reporter assays, PLoS Biol. 11 (2013) e1001593.
[189] M. Li, K. Suzuki, N.Y. Kim, G.H. Liu, J.C. Izpisua Belmonte, A cut above the rest: targeted genome editing technologies in human pluripotent stem cells, J. Biol. Chem. 289 (2014) 4594–4599.
[190] L.T. Cheng, L.T. Sun, T. Tada, Genome editing in induced pluripotent stem cells, Genes Cells 17 (2012) 431–438.
[191] D.J. Segal, J.F. Meckler, Genome engineering at the dawn of the golden age, Annu. Rev. Genomics Hum. Genet. 14 (2013) 135–158.
[192] N. Overlack, T. Goldmann, U. Wolfrum, K. Nagel-Wolfrum, Gene repair of an Usher syndrome causing mutation by zinc-finger nuclease mediated homologous recombination, Invest. Ophthalmol. Vis. Sci. 53 (2012) 4140–4146.
[193] R. Kellermayer, Translational readthrough induction of pathogenic nonsense mutations, Eur. J. Med. Genet. 49 (2006) 445–450.
[194] H. Li, V. Haurigot, Y. Doyon, T. Li, S.Y. Wong, A.S. Bhagwat, N. Malani, X.M. Anguela, R. Sharma, L. Ivanciu, S.L. Murphy, J.D. Finn, F.R. Khazi, S. Zhou, D.E. Paschon, E.J. Rebar, F.D. Bushman, P.D. Gregory, M.C. Holmes, K.A. High, In vivo genome editing restores haemostasis in a mouse model of haemophilia, Nature 475 (2011) 217–221.
[195] A. Gouble, J. Smith, S. Bruneau, C. Perez, V. Guyot, J.P. Cabaniols, S. Leduc, L. Fiette, P. Ave, B. Micheau, P. Duchateau, F. Paques, Efficient in toto targeted recombination in mouse liver by meganuclease-induced double-strand break, J. Gene Med. 8 (2006) 616–622.
[196] A. El-Amraoui, C. Petit, Usher I syndrome: unravelling the mechanisms that underlie the cohesion of the growing hair bundle in inner ear sensory cells, J. Cell Sci. 118 (2005) 4593–4603.
[197] S.M. Jones, T.A. Jones, Genetics of peripheral vestibular dysfunction: lessons from mutant mouse strains, J. Am. Acad. Audiol. 25 (2014) 289–301.
[198] A. Gramsbergen, Postural control in man: the phylogenetic perspective, Neural Plast. 12 (2005) 77–88 (discussion 263–272).
[199] A. Jumaian, K. Fergusson, Psychosis in a patient with Usher syndrome: a case report, East Mediterr. Health J. 9 (2003) 215–218.
[200] M. Mangotich, J. Misiaszek, Atypical psychosis in Usher's syndrome, Psychosomatics 24 (1983) 674–675.
[201] J. Hess-Rover, J. Crichton, K. Byrne, A.J. Holland, Diagnosis and treatment of a severe psychotic illness in a man with dual severe sensory impairments caused by the presence of Usher syndrome, J. Intellect. Disabil. Res. 43 (Pt 5) (1999) 428–434.
[202] N. Rijavec, V.N. Grubic, Usher syndrome and psychiatric symptoms: a challenge in psychiatric management, Psychiatr. Danub. 21 (2009) 68–71.
[203] A. Viala, T. Nicot, F. Levy, M.N. Vacheron, A case of Usher's syndrome associated with psychotic symptoms: diagnosis and follow-up in a psychiatric unit, Encéphale 35 (2009) 286–291.
[204] D. Domanico, S. Fragiotta, P. Trabucco, M. Nebbioso, E.M. Vingolo, Genetic analysis for two Italian siblings with usher syndrome and schizophrenia, Case Rep. Ophthalmol. Med. 2012 (2012) 380863.
[205] J. Koizumi, K. Ofuku, K. Sakuma, H. Shiraishi, M. Iio, S. Nawano, CNS changes in Usher's syndrome with mental disorder: CT, MRI and PET findings, J. Neurol. Neurosurg. Psychiatry 51 (1988) 987–990.
[206] N.P. Rao, V. Danivas, G. Venkatasubramanian, R.V. Behere, B.N. Gangadhar, Comorbid bipolar disorder and Usher syndrome, Prim Care Companion, J. Clin. Psychiatry 12 (2010).
[207] C.Y. Wu, C.C. Chiu, Usher syndrome with psychotic symptoms: two cases in the same family, Psychiatry Clin. Neurosci. 60 (2006) 626–628.
[208] J. Grondahl, S. Mjoen, Usher syndrome in four Norwegian counties, Clin. Genet. 30 (1986) 14–28.
[209] B. Hallgren, Retinitis pigmentosa combined with congenital deafness; with vestibulo-cerebellar ataxia and mental abnormality in a proportion of cases: a clinical and genetico-statistical study, Acta Psychiatr. Scand. Suppl. 34 (1959) 1–101.
[210] A. Nuutila, Dystrophia retinae pigmentosa–dysacusis syndrome (DRD): a study of the Usher- or Hallgren syndrome, J. Genet. Hum. 18 (1970) 57–88.
[211] J. Dammeyer, Children with Usher syndrome: mental and behavioral disorders, Behav. Brain Funct. 8 (2012) 16.
[212] H. Chaib, J. Kaplan, S. Gerber, C. Vincent, H. Ayadi, R. Slim, A. Munnich, J. Weissenbach, C. Petit, A newly identified locus for Usher syndrome type I, USH1E, maps to chromosome 21q21, Hum. Mol. Genet. 6 (1997) 27–31.
[213] Z.M. Ahmed, S. Riazuddin, S.N. Khan, P.L. Friedman, T.B. Friedman, USH1H, a novel locus for type I Usher syndrome, maps to chromosome 15q22-23, Clin. Genet. 75 (2009) 86–91.
[214] T.J. Jaworek, R. Bhatti, N. Latief, S.N. Khan, S. Riazuddin, Z.M. Ahmed, USH1K, a novel locus for type I Usher syndrome, maps to chromosome 10p11.21-q21.1, J. Hum. Genet. 57 (2012) 633–637.
[215] E. Schneider, T. Marker, A. Daser, G. Frey-Mahn, V. Beyer, R. Farcas, B. Schneider-Ratzke, N. Kohlschmidt, B. Grossmann, K. Bauss, U. Napiontek, A. Keilmann, O. Bartsch, U. Zechner, U. Wolfrum, T. Haaf, Homozygous disruption of PDZD7 by reciprocal translocation in a consanguineous family: a new member of the Usher syndrome protein interactome causing congenital hearing impairment, Hum. Mol. Genet. 18 (2009) 655–666.
[216] C.J. Kros, W. Marcotti, S.M. van Netten, T.J. Self, R.T. Libby, S.D. Brown, G.P. Richardson, K.P. Steel, Reduced climbing and increased slipping adaptation in cochlear hair cells of mice with Myo7a mutations, Nat. Neurosci. 5 (2002) 41–47.

CHAPTER 3

DISTINCT EXPRESSION AND FUNCTION OF WHIRLIN ISOFORMS IN THE INNER EAR AND RETINA: AN INSIGHT INTO PATHOGENESIS OF USH2D AND DFNB31

Jun Yang designed the original study. My role was to take over this project when I joined the lab. I did a majority of the experiments in the manuscript. I analyzed the data, generated figures and wrote the methods section for my experiments. Jun Yang wrote the manuscript and I helped revise each version of the manuscript.

This is a PDF of an article accepted for publication in Human Molecular Genetics following peer review. Reprinted from Pranav Dinesh Mathur, Junhuang Zou, Tihua Zheng, Ali Almishaal, Yong Wang, Qian Chen, Le Wang, Deepti Vashist, Steve Brown, Albert Park, Jun Yang. (2015) Distinct Expressions and Functions of Whirlin Isoforms in the Inner Ear and Retina: an Insight into Pathogenesis of USH2D and DFNB31. *Human Mol Gen.* 24(21):6213-28., with permission from Oxford University Press and Elsevier. License obtained through RightsLink. The version of this record mentioned above is available online at: http://hmg.oxfordjournals.org/content/24/21/6213.long

Human Molecular Genetics, 2015, Vol. 24, No. 21 6213–6228

doi: 10.1093/hmg/ddv339
Advance Access Publication Date: 24 August 2015
Original Article

ORIGINAL ARTICLE

Distinct expression and function of whirlin isoforms in the inner ear and retina: an insight into pathogenesis of USH2D and *DFNB31*

Pranav Dinesh Mathur[1,2], Junhuang Zou[1], Tihua Zheng[1], Ali Almishaal[3], Yong Wang[4], Qian Chen[1], Le Wang[1,5], Deepti Vashist[1], Steve Brown[6], Albert Park[4] and Jun Yang[1,2,4,*]

[1]Department of Ophthalmology and Visual Sciences, Moran Eye Center, University of Utah, 65 Mario Capecchi Drive, Salt Lake City, UT 84132, USA, [2]Department of Neurobiology and Anatomy, University of Utah, 20 North 1900 East, Salt Lake City, UT 84132, USA, [3]Department of Communication Sciences and Disorders, University of Utah, 390 South 1530 East, Salt Lake City, UT 84112, USA, [4]Division of Otolaryngology, Department of Surgery, University of Utah, 50 North Medical Drive, Salt Lake City, UT 84132, USA, [5]The First Affiliated Hospital, Jilin University, Changchun, Jilin 130061, China and [6]Mammalian Genetics Unit, Medical Research Council, Harwell, Oxfordshire OX11 ORD, UK

*To whom correspondence should be addressed at: John A Moran Eye Center, University of Utah, 65 Mario Capecchi Drive, Bldg 523, Salt Lake City, UT 84132, USA. Tel: +1 8012132591; Email: jun.yang@hsc.utah.edu

Abstract

Usher syndrome (USH) is the most common inherited deaf-blindness with the majority of USH causative genes also involved in nonsyndromic recessive deafness (DFNB). The mechanism underlying this disease variation of USH genes is unclear. Here, we addressed this issue by investigating the *DFNB31* gene, whose mutations cause USH2D or *DFNB31* depending on their position. We found that the mouse *DFNB31* ortholog (*Dfnb31*) expressed different mRNA variants and whirlin protein isoforms in the cochlea and retina, where these isoforms played different roles spatially and temporally. Full-length (FL-) whirlin in photoreceptors and hair cell stereociliary bases is important for the USH type 2 protein complex, while FL- and C-terminal (C-) whirlins in hair cell stereociliary tips participate in stereociliary elongation. Mutations in the whirlin N-terminal region disrupted FL-whirlin isoform in the inner ear and retina but not C-whirlin in the inner ear, and led to retinal degeneration as well as moderate to severe hearing loss. By contrast, a mutation in the whirlin C-terminal region eliminated all normal whirlin isoforms but generated a truncated N-terminal whirlin protein fragment, which was partially functional in the retina and thus prevented retinal degeneration. Mice with this mutation had profound hearing loss. In summary, disruption of distinct whirlin isoforms by *Dfnb31* mutations leads to a variety of phenotype configurations and may explain the mechanism underlying the different disease manifestations of human *DFNB31* mutations. Our findings have a potential to improve diagnosis and treatment of USH disease and quality of life in USH patients.

Introduction

Usher syndrome (USH) is an incurable autosomal recessive genetic disease. It is manifested as combined congenital or progressive hearing loss and progressive retinal degeneration. Some patients also have balance dysfunction. This disease accounts for the majority of deaf-blindness cases, with a prevalence of 1 in 6000 people in the world (1). Currently, approximately 10 USH causative and modifier genes have been identified (2). Among these genes,

Received: June 22, 2015. **Revised and Accepted:** August 17, 2015

nine are also associated with other diseases with the most common one being nonsyndromic recessive deafness (DFNB) (2). The involvement of USH genes in multiple diseases yields uncertainty for early accurate diagnosis, which is crucial for timely treatment and education of patients in preparation for the onset of symptoms at a later age, such as retinal degeneration. However, the molecular mechanisms underlying these distinct disease manifestations caused by mutant USH genes are poorly understood. Genotype–phenotype correlations are proposed, although non-genetic factors and/or unknown modifier genes may also be involved. For example, nonsense, frameshift, and some splice site mutations of harmonin, cadherin 23, and protocadherin 15 genes have been found to cause USH. Conversely, missense and some other splice site mutations of these genes are associated with DFNB, probably due to their residual functions (3–5). Additionally, most USH genes express multiple alternatively spliced protein isoforms, which may have different functions in the inner ear and retina (6–13). Disruption of the different isoforms of the same genes may also contribute to the genotype–phenotype correlations found in USH patients (14,15).

DFNB31 is the causative gene of USH2D (OMIM: 611383) (14,16,17) and *DFNB31* subtypes (OMIM: 607084) (18,19) (Fig. 1A). There appears to be a correlation between the mutation position and disease manifestation. Mutations leading to premature translation termination at whirlin protein N- and C-terminal regions tend to cause USH2D and *DFNB31*, respectively. This genotype–phenotype correlation was also observed in mice (Fig. 1A). Two *Dfnb31* (also known as *Whrn* in mice) mutant mouse lines have been phenotypically characterized in detail (18,20,21). *Dfnb31*$^{neo/neo}$ mice, generated by replacing 3′ part of *Dfnb31* first exon with a *Neo*^{r} cassette, exhibit hearing loss and late-onset retinal degeneration. On the other hand, *Dfnb31*$^{wi/wi}$ mice with a spontaneous deletion between *Dfnb31* exons 6–9 are deaf but do not develop retinal degeneration. Up to now, the exact underlying molecular mechanism is unclear. *Dfnb31* encodes multiple whirlin isoforms derived from alternative splicing and usage of promoters in the inner ear and retina (11,22). It has been postulated that disruption of distinct isoforms by *DFNB31* mutations is the cause of USH2D and *DFNB31* manifestations (14,20). However, direct experimental evidence supporting this mechanism is still missing.

In inner ear hair cells, whirlin isoforms are localized to the stereociliary tips of mechanosensitive hair bundles and are required for normal stereociliary elongation (11). Whirlin isoforms are also present at the base of stereocilia as a component of the ankle link complex (23). In retinal photoreceptors, whirlin isoforms participate in organizing the periciliary membrane complex at the inner segment apex just beneath the outer segment, the organelle for phototransduction (20,24). However, it is unclear which exact whirlin protein isoforms are expressed in these tissues and what the specific subcellular localizations and functions of these isoforms are. The lack of this important information hinders development of therapies for USH2D and *DFNB31*, especially the viral-mediated gene replacement therapy. Additionally, understanding the functions of individual whirlin isoforms will provide novel insights into the molecular mechanisms underlying stereociliary bundle development, which is essential for stem cell-based regeneration of hair cells with functional stereociliary bundles.

In this study, we utilized the two well-characterized (*Dfnb31*$^{neo/neo}$ and *Dfnb31*$^{wi/wi}$ mice) and two additional (*Dfnb31*$^{tm1a/tm1a}$ and *Dfnb31*$^{wi/wi}$-BAC mice) *Dfnb31* mouse models. We show for the first time that the expression and localization of whirlin isoforms are different in the cochlea and the retina. These different whirlin isoforms have distinct functions in the respective tissues. We further present evidence that whirlin mutations at different gene positions disrupt the expression of whirlin isoforms differentially and thus lead to different combinations of inner ear and retinal phenotypes.

Results

Expression of *Dfnb31* mRNA variants in the inner ear and retina of wild-type, *Dfnb31*$^{neo/neo}$ and *Dfnb31*$^{wi/wi}$ mice

We studied the eleven *Dfnb31* mRNA variants that have so far been identified from the mouse inner ear and retina (Fig. 1B) (11,22). These *Dfnb31* mRNA variants are categorized into four groups with minor amino acid differences among variants within each group. Group 1 including variants 1–4 is translated into full-length whirlin isoforms (FL-whirlin) carrying three PDZ domains and one proline-rich region. Variants 5–7 in Group 2 share the same promoter region with Group 1, but are alternatively spliced to skip 3′ part of exon 1 and either exons 2–5 or exons 2–6. This group of variants is predicted to be translated into proteins with only the proline-rich region and third PDZ domain (C-whirlin). Variants 8–9 in Group 3 utilize alternative promoters in intron 5 and can be translated into proteins similar to Group 2 proteins (C-whirlin). Groups 1–3 of *Dfnb31* mRNA variants were identified from the mouse vestibular system (11). The fourth group of *Dfnb31* mRNA variants (10–11) was found in mouse retinas (22). Alternative splicing after exon 4 or 7 in this group leads to short *Dfnb31* transcripts, which are thought to be translated into protein isoforms with only N-terminal one or two PDZ domains (N-whirlin).

We designed primers specific to each group of *Dfnb31* mRNA variants (Fig. 1B and Supplementary Material, Table S1) and characterized the expression of these variants by RT–PCR using total RNA isolated from the adult mouse retina and P4 mouse cochlea. In the wild-type retina, groups 1, 3 and 4 of *Dfnb31* mRNA variants were detected but not group 2 (Fig. 1C). Groups 1 and 3 of *Dfnb31* variants were truncated between exons 6-9 in *Dfnb31*$^{wi/wi}$ retinas, while all other *Dfnb31* variants were absent in *Dfnb31*$^{neo/neo}$ and *Dfnb31*$^{wi/wi}$ retinas (Fig. 1C). The truncated group 1 *Dfnb31* variants in *Dfnb31*$^{wi/wi}$ mice can be translated into N-whirlin fragments (hereafter referred to as truncated N-whirlin) with amino acid sequences similar but not identical to those of the normal N-whirlin isoforms translated from group 4 variants (Fig. 1D), while the truncated group 3 variant is probably unable to be translated into a functional protein (Fig. 1D). The reason underlying the difference between the RT–PCR results using primer pairs a/d and c/d for group 1 whirlin variants in *Dfnb31*$^{wi/wi}$ mice is unclear (Fig. 1C). Probably, an alternative 5′ sequence exists in the group 1 *Dfnb31* variants of *Dfnb31*$^{wi/wi}$ mice. In the wild-type cochlea, variants in group 1 as well as variant 8 were expressed (Fig. 1C). In the *Dfnb31*$^{neo/neo}$ cochlea, variant 8 was intact, while others were undetectable (Fig. 1C and D). In the case that an aberrant *Dfnb31* transcript lacking only exon 1 was expressed in *Dfnb31*$^{neo/neo}$ inner ears, we analyzed the nucleotide sequence of this potential aberrant transcript and could not find an inframe translation start codon except the one used in variant 8. Therefore, if this aberrant transcript existed in *Dfnb31*$^{neo/neo}$ inner ears, it could only be translated into a protein identical to C-whirlin. The *Dfnb31*$^{wi/wi}$ mutation truncated variants 1–4 and 8 in the cochlea (Fig. 1C and D), which is the same as in the retina.

Localization of whirlin protein isoforms in the cochlear hair cells of wild-type, *Dfnb31*$^{neo/neo}$ and *Dfnb31*$^{wi/wi}$ mice

Based on the RT–PCR results, we predicted that FL- and C-whirlin proteins could exist in the wild-type cochlea, C-whirlin protein in

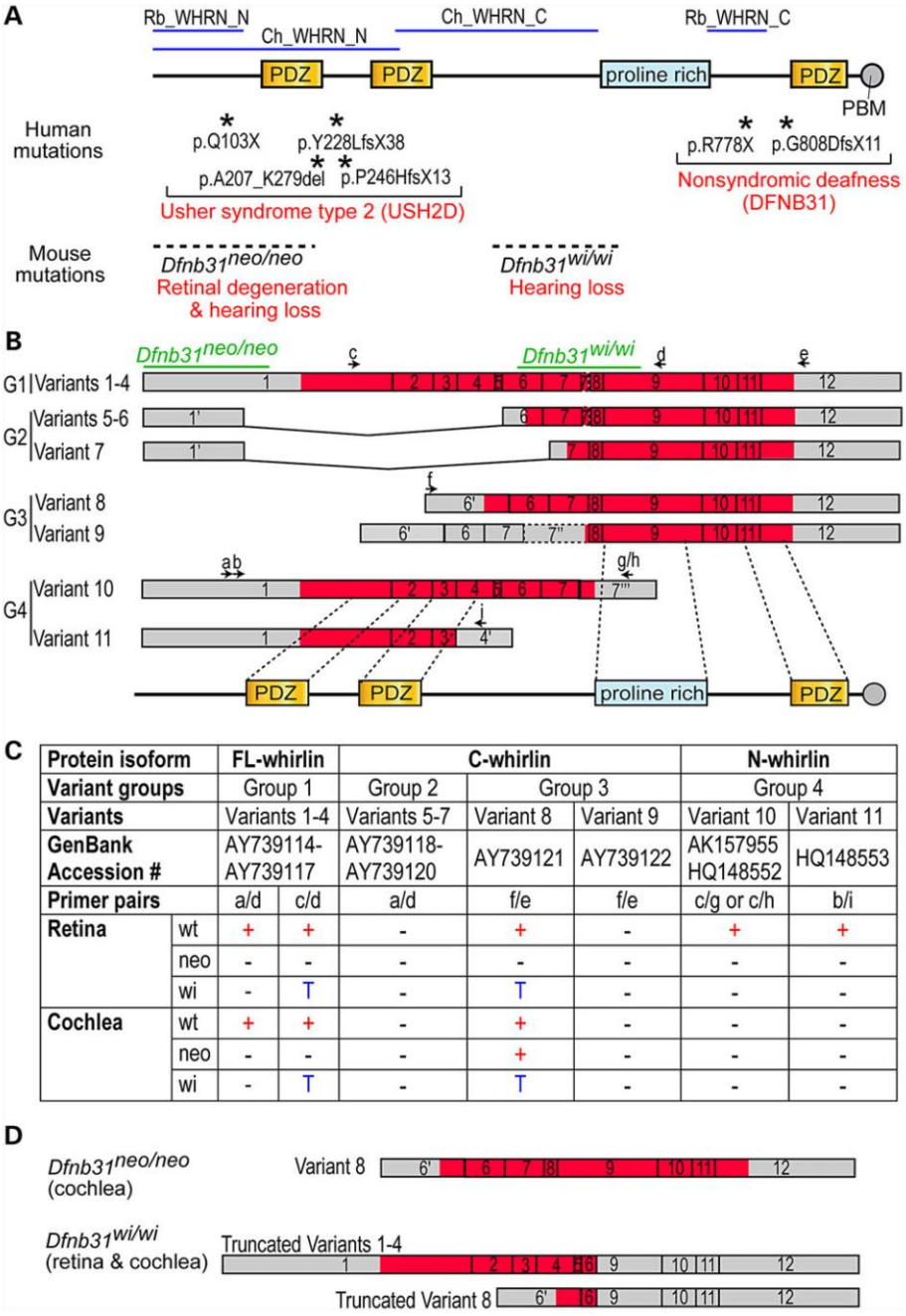

Protein isoform		FL-whirlin		C-whirlin			N-whirlin	
Variant groups		Group 1		Group 2	Group 3		Group 4	
Variants		Variants 1-4		Variants 5-7	Variant 8	Variant 9	Variant 10	Variant 11
GenBank Accession #		AY739114-AY739117		AY739118-AY739120	AY739121	AY739122	AK157955 HQ148552	HQ148553
Primer pairs		a/d	c/d	a/d	f/e	f/e	c/g or c/h	b/i
Retina	wt	+	+	-	+	-	+	+
	neo	-	-	-	-	-	-	-
	wi	-	T	-	T	-	-	-
Cochlea	wt	+	+	-	+	-	-	-
	neo	-	-	-	+	-	-	-
	wi	-	T	-	T	-	-	-

Figure 1. *DFNB31/Dfnb31* genotype–phenotype correlation and disruption of *Dfnb31* mRNA variants in *Dfnb31* mutant mice. (**A**) Mutations in the N- and C-terminal whirlin regions cause different diseases in humans (asterisks and upper red text) and phenotypes in mice (dashed lines and lower red text). Blue lines on the top mark the antigen regions of various whirlin antibodies used in this study. (**B**) Schematic diagram of various *Dfnb31* mRNA variants reported in the mouse inner ear and retina (11,22). Arabic numerals are exon numbers. Gray and red colors indicate untranslated and protein coding regions, respectively. Arrows and lower case letters show the position, direction, and name of primers used for RT–PCR experiments. The primer sequences are listed in Supplementary Material, Table S1. The exon regions corresponding to *Dfnb31* mutations and whirlin protein functional domains are shown at the top and bottom, respectively. (**C**) Summary of RT–PCR results showing disruption of *Dfnb31* mRNA variant expressions in $Dfnb31^{neo/neo}$ (neo) and $Dfnb31^{wi/wi}$ (wi) mice. *Dfnb31* mRNA variant expressions were complex and different in the wild-type (wt) retina and cochlea, and they were differentially disrupted in $Dfnb31^{neo/neo}$ and $Dfnb31^{wi/wi}$ mice. +, presence; –, absence; T, truncated. (**D**) *Dfnb31* variant 8 was intact in the $Dfnb31^{neo/neo}$ cochlea, and *Dfnb31* variants 1–4 and 8 were truncated in all tested tissues of $Dfnb31^{wi/wi}$ mice. Other *Dfnb31* variants were all disrupted in $Dfnb31^{neo/neo}$ and $Dfnb31^{wi/wi}$ mice.

the *Dfnb31*$^{neo/neo}$ cochlea (Fig. 1D), and truncated N-whirlin protein in the *Dfnb31*$^{wi/wi}$ cochlea (Fig. 1D). Although whirlin was previously localized to the ankle link complex (the base) and the tip of stereocilia in both cochlear hair cells (11,13,23,25–27), it was unclear which whirlin isoforms were located in these two subcellular regions and how *Dfnb31* mutations affect their localizations.

To address these, we generated and validated polyclonal antibodies from rabbit, Rb_WHRN_N and Rb_WHRN_C antibodies, which specifically detected whirlin N- and C-terminal regions, respectively (Fig. 1A and Supplementary Material, Fig. S1). By immunofluorescence of P4 cochlear whole-mounts, we found that the immunoreactivity of Rb_WHRN_N was at both stereociliary tips and bases in inner hair cell (IHC) bundles and only at stereociliary bases in outer hair cell (OHC) bundles of wild-type mice (Fig. 2A and Supplementary Material, Fig. S2). The immunoreactivity of Rb_WHRN_N was absent in both *Dfnb31*$^{neo/neo}$ and *Dfnb31*$^{wi/wi}$ IHC and OHC stereocilia (Fig. 2A and Supplementary Material, Fig. S2). Notably, some Rb_WHRN_N signals were found along the kinocilium in IHC and OHC bundles of wild-type and *Dfnb31*$^{wi/wi}$ but not *Dfnb31*$^{neo/neo}$ mice (Fig. 2A and Supplementary Material, Fig. S2), which could be non-specific in the wild-type and truncated N-whirlin fragments in *Dfnb31*$^{wi/wi}$ mutants. The immunoreactivity of Rb_WHRN_C was detected at both stereociliary tips and bases in wild-type IHCs and OHCs (Fig. 2B and Supplementary Material, Fig. S3), and was also localized at the stereociliary tips in *Dfnb31*$^{neo/neo}$ IHCs and OHCs (Fig. 2B and Supplementary Material, Fig. S3). No Rb_WHRN_C signals were detected in *Dfnb31*$^{wi/wi}$ IHCs and OHCs (Fig. 2B and Supplementary Material, Fig. S3). These findings of WHRN_N and WHRN_C immunostaining were consistently observed across the entire cochleas. Careful examination of whirlin immunostaining images also revealed that whirlin appeared to be present at the tip of only the tallest row of stereocilia and at the ankle link complex of several rows of stereocilia in the bundle (Fig. 2). In summary, during development, FL-whirlin is present at stereociliary tips and ankle link complexes of IHCs and only at stereociliary ankle link complexes of OHCs, while C-whirlin is at stereociliary tips of both IHCs and OHCs (Fig. 10C). In *Dfnb31*$^{neo/neo}$ cochleas, C-whirlin is intact at stereociliary tips, while FL-whirlin is disrupted (Fig. 10C). In *Dfnb31*$^{wi/wi}$ cochleas, truncated N-whirlin may be localized along the kinocilium.

Immunofluorescence of cochlear whole-mounts was also conducted at P60 to localize whirlin isoforms in mature hair cells (Fig. 3). At this time point, most stereociliary bundles of *Dfnb31*$^{wi/wi}$ IHCs and OHCs were severely degenerated. Thus, we did not include *Dfnb31*$^{wi/wi}$ mice in this experiment. Rb_WHRN_C antibody detected immunoreactivities only at stereociliary tips in wild-type and *Dfnb31*$^{neo/neo}$ IHCs but not OHCs (Fig. 3A). Furthermore, Rb_WHRN_N antibody detected immunoreactivities at stereociliary tips of wild-type but not *Dfnb31*$^{neo/neo}$ IHCs (Fig. 3B). These findings indicate that whirlin protein localization in mature cochlear hair cells is different from that in developing cochlear hair cells. Both FL-whirlin and C-whirlin are present at IHC but not OHC stereociliary tips in adult wild-type cochleas (Fig. 10C), and C-whirlin is intact at IHC stereociliary tips of mature *Dfnb31*$^{neo/neo}$ cochleas (Fig. 10C).

Morphological, molecular and functional defects of *Dfnb31*$^{neo/neo}$ and *Dfnb31*$^{wi/wi}$ cochlear stereociliary bundles

With the knowledge of differential disruptions of whirlin protein isoforms in *Dfnb31*$^{neo/neo}$ and *Dfnb31*$^{wi/wi}$ mice, we decided to decipher the functions of various whirlin isoforms in the cochlea and understand the pathology of *Dfnb31*$^{neo/neo}$ and *Dfnb31*$^{wi/wi}$ mice by analyzing and comparing their cochlear stereociliary bundle morphology, expression of whirlin-interacting proteins, and hearing function. We examined the stereociliary bundle morphology of *Dfnb31*$^{neo/neo}$ and *Dfnb31*$^{wi/wi}$ cochleas at P4 using scanning electron microscopy (SEM). At a low magnification (Fig. 4A), the stereociliary bundles of OHCs were observed to change from a sharp V- or W-shape to a U-shape in both mutants. Because only FL-whirlin was the isoform disrupted in both *Dfnb31*$^{neo/neo}$ and *Dfnb31*$^{wi/wi}$ cochleas, the similar changes in the OHC bundle shape of the two mutant mice suggest that FL-whirlin at the OHC ankle link complex is involved in maintaining the sharp V- or W-shape of bundles. Due to the normal shallow U-shape of wild-type IHC bundles at this age, we could not tell obvious changes in the shape of two mutant IHC bundles except the frequently observed ectopic stereocilia at the neural side of *Dfnb31*$^{wi/wi}$ IHC stereociliary bundles (Fig. 4C, arrows). We observed more than three rows of stereocilia in both *Dfnb31*$^{neo/neo}$ and *Dfnb31*$^{wi/wi}$ IHCs (Fig. 4C), which could result from loss of FL-whirlin at stereociliary tips and/or ankle link complexes. At a high magnification which permitted visualization of individual stereocilia, we found short and thick stereocilia in *Dfnb31*$^{wi/wi}$ IHCs and OHCs as reported previously (Fig. 4B and C) (21,28,29). However, *Dfnb31*$^{neo/neo}$ stereocilia appeared to have normal length in both IHCs and OHCs and looked thicker in IHCs and normal in OHCs (Fig. 4B and C). Measurement and quantification of stereociliary length (Fig. 5A and B) and thickness (data prepared in another manuscript) in the middle turn of P4 wild-type, *Dfnb31*$^{neo/neo}$ and *Dfnb31*$^{wi/wi}$ cochleas confirmed this impression. We also examined cochlear stereociliary length of P45 *Dfnb31*$^{neo/neo}$ and *Dfnb31*$^{wi/wi}$ mice using the same approach (Fig. 5C and D). We found that both *Dfnb31*$^{wi/wi}$ and *Dfnb31*$^{neo/neo}$ stereocilia were shorter than wild-type stereocilia in IHCs. The *Dfnb31*$^{wi/wi}$ IHC stereocilia became even shorter at this age, compared with those at P4, suggesting that the *Dfnb31*$^{wi/wi}$ IHC stereocilia are unable to maintain their length. In OHCs, the *Dfnb31*$^{wi/wi}$ stereociliary length was shorter, while the *Dfnb31*$^{neo/neo}$ stereociliary length was normal. These findings indicate that C-whirlin at stereociliary tips is sufficient for normal stereociliary length of developing hair cells and mature OHCs, while both FL- and C-whirlins at stereociliary tips are required for normal stereociliary length of mature IHCs.

Whirlin was previously shown to be transported by myosin XVa to the stereociliary tip, where whirlin is proposed to participate in stereociliary elongation by interacting with EPS8 and myosin XVa (11,30). We first confirmed the colocalization of whirlin and EPS8 at stereociliary tips of IHCs and OHCs by double immunofluorescence (Supplementary Material, Fig. S4B). We then analyzed the amounts of EPS8 and myosin XVa proteins at stereociliary tips in the middle turn of P4 *Dfnb31*$^{neo/neo}$ and *Dfnb31*$^{wi/wi}$ cochleas by measuring the intensities of their immunofluorescent signals (Fig. 6A). EPS8 protein of IHCs/OHCs and myosin XVa protein of OHCs were decreased in both whirlin mutant mice with *Dfnb31*$^{wi/wi}$ mice having the lowest levels, whereas myosin XVa protein of IHCs was increased in *Dfnb31*$^{neo/neo}$ and decreased in *Dfnb31*$^{wi/wi}$ mice. This result suggests that both FL-whirlin and C-whirlin are required to maintain the normal amount of EPS8 and myosin XVa at the stereociliary tip of cochlea hair cells. Because of the normal stereociliary length of *Dfnb31*$^{neo/neo}$ cochlear hair cells and the short stereociliary length of *Dfnb31*$^{wi/wi}$ cochlear hair cells observed by SEM at P4, our result also suggests that the amounts of EPS8 and myosin XVa at stereociliary tips may not strictly correlate with stereociliary length. We next studied the interactions of FL-whirlin

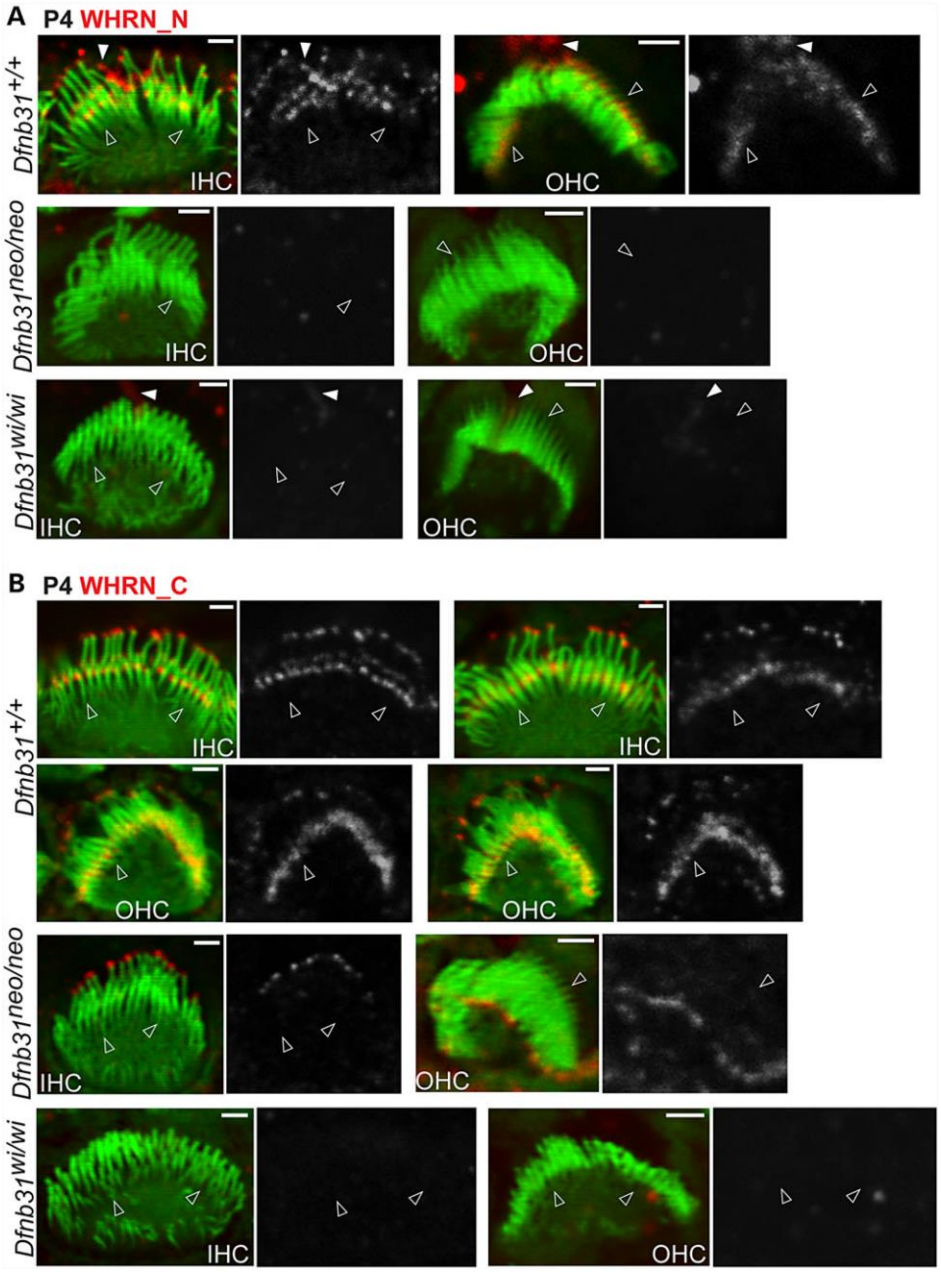

Figure 2. Whirlin protein localization in developing wild-type, *Dfnb31*$^{neo/neo}$ and *Dfnb31*$^{wi/wi}$ cochlear hair cells. (**A**) Immunostaining using rabbit WHRN_N antibody shows signals at the tip and base of IHC stereocilia and only at the base of OHC stereocilia in P4 wild type mice. The same experimental procedure detected no signals in P4 *Dfnb31*$^{neo/neo}$ and *Dfnb31*$^{wi/wi}$ cochlear stereocilia. Note that rabbit WHRN-N antibody also detected signals along the kinocilium in P4 wild-type and *Dfnb31*$^{wi/wi}$ cochlear hair cells (white filled arrows). (**B**) Immunofluorescence using rabbit WHRN_C antibody shows signals at the tip and base of both IHC and OHC stereocilia in P4 wild-type mice. In P4 *Dfnb31*$^{neo/neo}$ IHCs and OHCs, immunoreactivity of rabbit WHRN_C antibody was found at the stereociliary tip. No immunoreactivity of WHRN_C antibody was detected in P4 *Dfnb31*$^{wi/wi}$ cochlear stereociliary bundles. Empty arrows point to stereociliary bases. The red signals of whirlin proteins are shown in grayscale on the right of each overlay panel with the matched position of arrows. Red signals outside stereociliary bundles are non-specific. Scale bars, 1 μm.

(variant 2), C-whirlin (variant 8), and truncated N-whirlin (truncated variant 2 in *Dfnb31*$^{wi/wi}$) proteins with EPS8 and myosin XVa using their recombinant proteins expressed in mammalian cultured cells (Fig. 6B–D). We found that EPS8 was able to be coimmunoprecipitated with FL-whirlin, C-whirlin and truncated N-whirlin at a similar level (Fig. 6C) and that myosin XVa was able

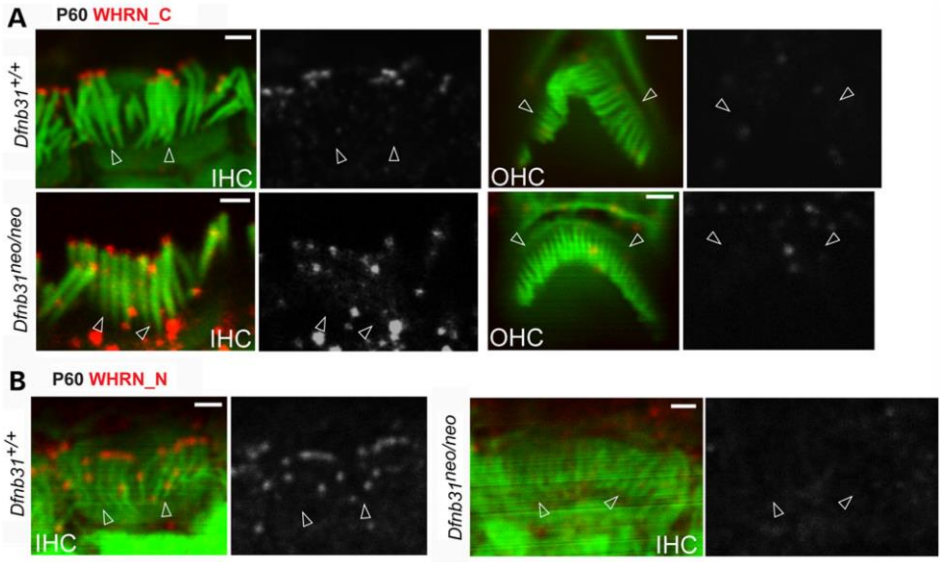

Figure 3. Whirlin protein localization in mature wild-type and *Dfnb31*$^{neo/neo}$ cochlear hair cells. (**A**) The rabbit WHRN_C antibody detected immunoreactivities at IHC but not OHC stereociliary tips of both wild-type and *Dfnb31*$^{neo/neo}$ mice at P60. (**B**) Immunostaining using rabbit WHRN_N antibody revealed immunoreactivities at IHC stereociliary tips of wild-type but not *Dfnb31*$^{neo/neo}$ mice at P60. Empty arrows point to stereociliary bases. The red signals of whirlin proteins are shown in grayscale on the right of each overlay panel with the matched position of arrows. Red signals outside stereociliary bundles are non-specific. Scale bars, 1 μm.

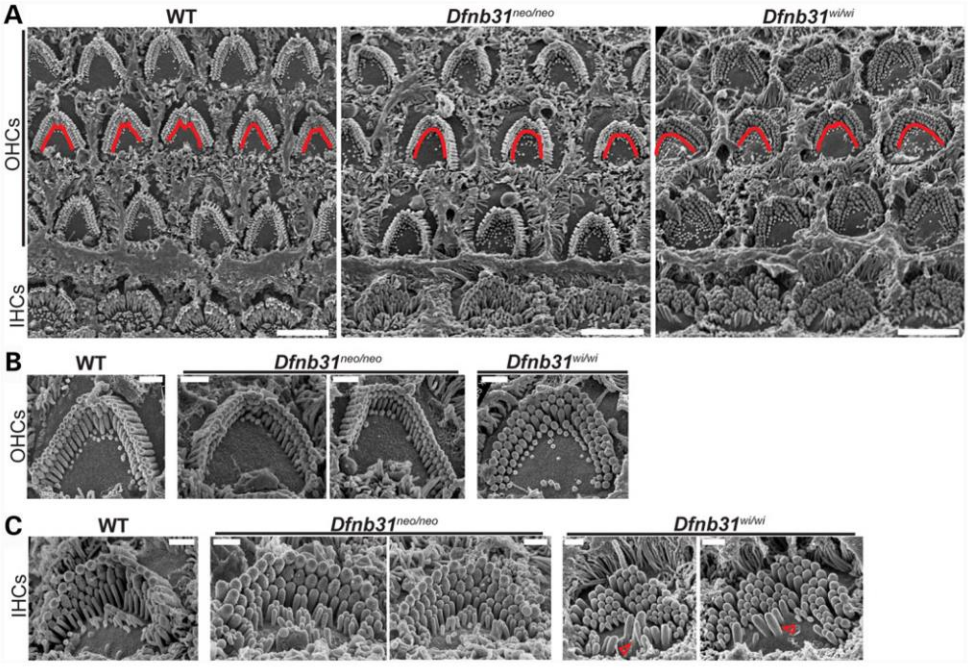

Figure 4. *Dfnb31*$^{wi/wi}$ cochlear stereociliary bundles have more severe morphological defects than *Dfnb31*$^{neo/neo}$ cochlear stereociliary bundles. (**A**) Low-magnification SEM images of wild-type, *Dfnb31*$^{neo/neo}$ and *Dfnb31*$^{wi/wi}$ cochlear stereociliary bundles. *Dfnb31*$^{neo/neo}$ and *Dfnb31*$^{wi/wi}$ OHC stereociliary bundles (traced by red lines) were altered to the U-shape from the V- or W-shape in wild-types. (**B**) Images of individual OHC stereociliary bundles from the cochlear middle turn. In addition to the bundle shape change, stereocilia in *Dfnb31*$^{wi/wi}$ mice were short and thick. (**C**) Images of individual IHC stereociliary bundles from the cochlear middle turn. Compared with wild-type mice, the IHC stereocilia of *Dfnb31*$^{neo/neo}$ and *Dfnb31*$^{wi/wi}$ mice were thick and frequently had more than three rows. Furthermore, *Dfnb31*$^{wi/wi}$ stereocilia were short, and ectopic stereocilia outside *Dfnb31*$^{wi/wi}$ stereociliary bundles (red arrows) were often seen. All images are from P4 animals. Scale bars, 5 μm in (A) and 1 μm in (B) and (C).

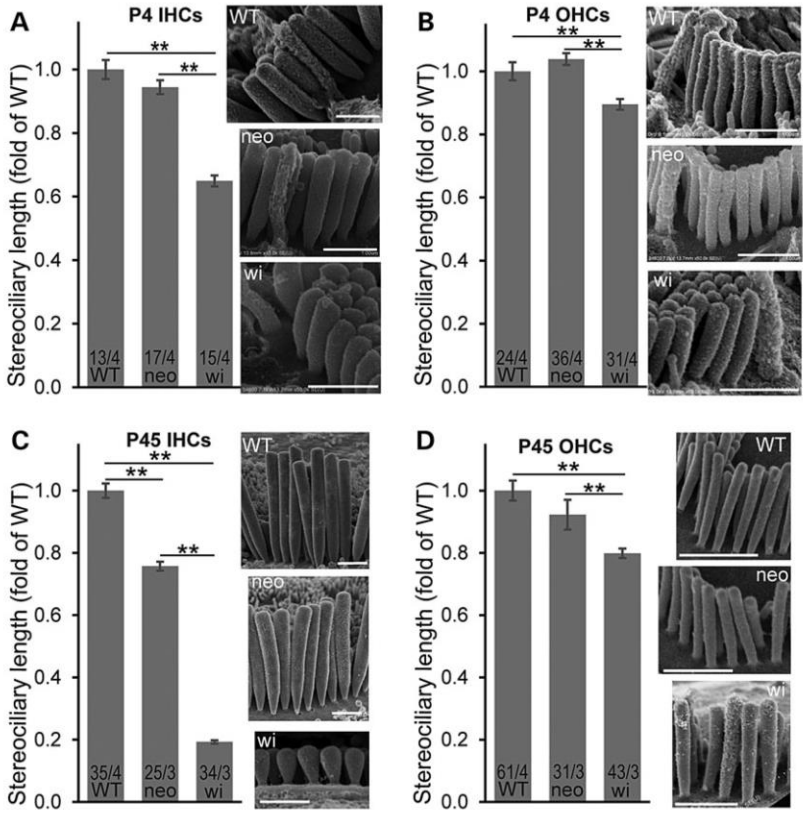

Figure 5. Measurement of stereociliary lengths in *Dfnb31*$^{neo/neo}$ and *Dfnb31*$^{wi/wi}$ cochlear hair cells. (**A** and **B**) *Dfnb31*$^{wi/wi}$ (wi) but not *Dfnb31*$^{neo/neo}$ (neo) mice at P4 had short stereocilia in IHCs (**A**) and OHCs (B). (**C**) Both *Dfnb31*$^{wi/wi}$ and *Dfnb31*$^{neo/neo}$ mice at P45 had short stereocilia in IHCs, although *Dfnb31*$^{neo/neo}$ IHC stereocilia were longer than *Dfnb31*$^{wi/wi}$ IHC stereocilia. (**D**) *Dfnb31*$^{wi/wi}$ but not *Dfnb31*$^{neo/neo}$ mice at P45 had short stereocilia in OHCs. Representative SEM images of stereocilia from each genotype at P4 and P45 are shown on the right of bar charts. Stereocilia in the longest row next to the kinocilium at P4 or in the middle of the row at P45 were measured. Numbers of cells and mice analyzed are listed in the bottom of bars before and after slashes, respectively. Student's *t*-tests (two-tail) were performed. Error bars, standard error of the mean. $^{**}P < 0.01$.

to be coimmunoprecipitated only with FL-whirlin and C-whirlin but not truncated N-whirlin (Fig. 6D). These results demonstrate that both N- and C-whirlin regions are involved in binding to EPS8, while only C-whirlin region associates with myosin XVa.

In addition, we assessed OHC function by measuring distortion product otoacoustic emissions (DPOAEs) and determined audibility curves using the auditory brainstem responses (ABRs) in *Dfnb31* mutant mice at P45-P60. In these experiments, we included *Dfnb31*$^{wi/neo}$ mice by crossing *Dfnb31*$^{neo/neo}$ and *Dfnb31*$^{wi/wi}$ mice, which presumably express C-whirlin from the *Dfnb31*^{neo} allele and truncated N-whirlin from the *Dfnb31*^{wi} allele, but not FL-whirlin. DPOAE thresholds were significantly elevated by at least 30 dB SPL above control animals for *Dfnb31*$^{wi/neo}$, *Dfnb31*$^{neo/neo}$ and *Dfnb31*$^{wi/wi}$ mice across all frequencies (8–32 kHz), but there was no significant difference in the DPOAE thresholds among the three whirlin mutants (Fig. 7A). These results indicate that OHCs of these mutants had similar functional deficits despite varying stereociliary lengths (Fig. 5B and D) and thicknesses (28,31) across genotypes. These OHC functional deficits probably resulted from abnormal stereociliary bundle shapes (Fig. 4A) caused by FL-whirlin loss, which is shared among the three whirlin mutant mice. However, the three whirlin mutant mice displayed different ABR threshold increases (Fig. 7B). *Dfnb31*$^{wi/wi}$ mice exhibited the most severe hearing loss, while *Dfnb31*$^{wi/neo}$ and *Dfnb31*$^{neo/neo}$ mice showed similar degrees of moderate hearing loss with *Dfnb31*$^{wi/neo}$ mice slightly better at the frequency of 5.6 kHz. The better hearing function of *Dfnb31*$^{neo/neo}$ mice than *Dfnb31*$^{wi/wi}$ mice is similar to that reported in USH2D and *DFNB31* patients (14,19). Because both IHCs and OHCs contribute to ABR measures, we believe that the difference in ABR threshold increases between *Dfnb31*$^{wi/wi}$ and *Dfnb31*$^{wi/neo}$/*Dfnb31*$^{neo/neo}$ mice resulted from differential IHC dysfunctions due to differences in C-whirlin expression. The moderate to severe hearing loss in *Dfnb31*$^{neo/neo}$ and *Dfnb31*$^{wi/neo}$ mice indicates a partial role of C-whirlin and the importance of FL-whirlin in hearing, respectively. Furthermore, the similarity of hearing loss between *Dfnb31*$^{wi/neo}$ and *Dfnb31*$^{neo/neo}$ mice indicates that the truncated N-whirlin present in *Dfnb31*$^{wi/neo}$ mice probably plays a minor role in hearing. In summary, it is the stereociliary bundle shape controlled by FL-whirlin but not the stereociliary length controlled by C-whirlin that is essential for normal OHC-mediated DPOAE; and it is the stereociliary length and three-row stereociliary arrangement controlled by both FL-whirlin and C-whirlin that is critical for the IHC function.

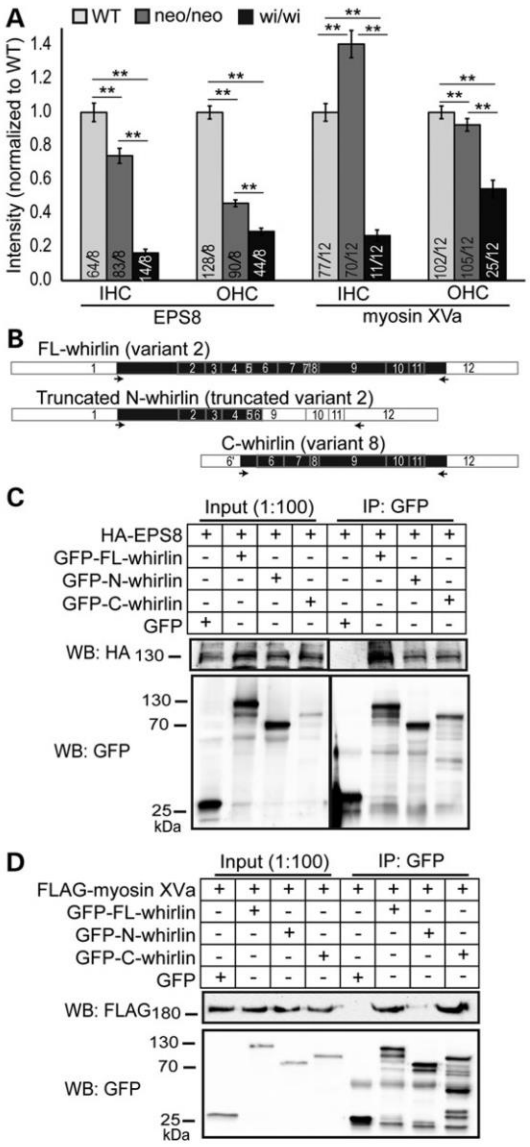

Figure 6. EPS8 and myosin XVa expressions in *Dfnb31*$^{neo/neo}$ and *Dfnb31*$^{wi/wi}$ cochlear hair cells and their interactions with whirlin fragments. (**A**) Quantification of EPS8 and myosin XVa expressions in wild-type (WT), *Dfnb31*$^{neo/neo}$ (neo/neo) and *Dfnb31*$^{wi/wi}$ (wi/wi) mice. EPS8 expression was reduced at the IHC and OHC stereociliary tip of both *Dfnb31*$^{neo/neo}$ and *Dfnb31*$^{wi/wi}$ mice. EPS8 expression was less in *Dfnb31*$^{wi/wi}$ hair cells than in *Dfnb31*$^{neo/neo}$ hair cells. Myosin XVa expression was increased in IHC stereocilia but decreased in OHC stereocilia of *Dfnb31*$^{neo/neo}$ mice, while myosin XVa expression was reduced in both IHC and OHC stereocilia of *Dfnb31*$^{wi/wi}$ mice. Numbers of cells and mice analyzed are shown in the bottom of each bar before and after slashes, respectively. Error bars represent standard error of the mean. Student's t-tests (two-tail) were performed. **$P < 0.01$. (**B**) Schematic diagram of whirlin protein fragments used in the coimmunoprecipitation experiments shown in (C) and (D). Arabic numerals are exon numbers. White and black colors indicate untranslated and protein coding regions, respectively. cDNA fragments flanked by arrows were cloned into the GFP-tagged expression vectors. (**C**) HA-tagged EPS8 protein was able to be coimmunoprecipitated with GFP-tagged FL-whirlin, truncated N-whirlin and C-whirlin. (**D**) FLAG-tagged myosin XVa tail fragment was able to be coimmunoprecipitated with GFP-tagged FL-whirlin and C-whirlin but not the truncated N-whirlin. GFP protein from the empty pEGFP-C vector was used as a negative control. The anti-GFP blots demonstrate the success of immunoprecipitations and the amounts of GFP-tagged proteins pulled down in the experiments.

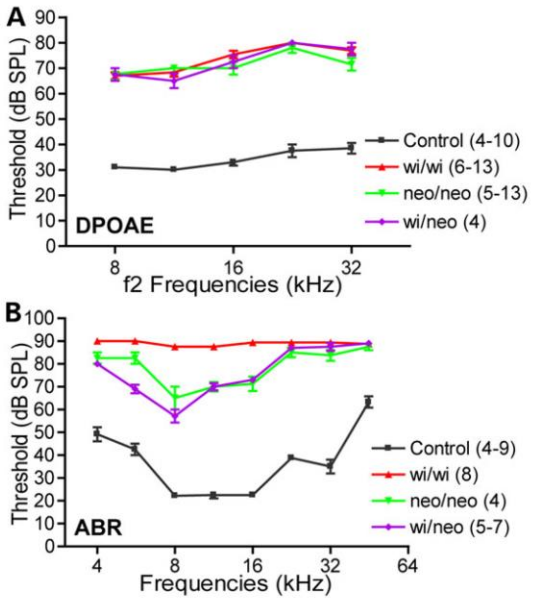

Figure 7. Hearing tests in *Dfnb31*$^{neo/neo}$, *Dfnb31*$^{wi/wi}$ and *Dfnb31*$^{wi/neo}$ mice. (**A**) *Dfnb31*$^{neo/neo}$ (green), *Dfnb31*$^{wi/wi}$ (red) and *Dfnb31*$^{wi/neo}$ (purple) mice exhibited similar DPOAE thresholds in the frequency range of 8–32 kHz at P45-P60. There was no statistically significant difference among the three *Dfnb31* mutant mice ($P > 0.05$). Compared with control mice (black), the thresholds in these three mutant mouse lines were all significantly elevated throughout the tested frequency range ($P < 0.01$). (**B**) *Dfnb31*$^{neo/neo}$, *Dfnb31*$^{wi/wi}$ and *Dfnb31*$^{wi/neo}$ mice displayed different levels of ABR threshold elevation in the frequency range of 4–45 kHz at P45-P60. The thresholds of *Dfnb31*$^{wi/wi}$ mice reached the test ceiling of our ABR system at most tested frequencies. The thresholds of *Dfnb31*$^{neo/neo}$ and *Dfnb31*$^{wi/neo}$ mice were similar to each other except at the frequency of 5.6 kHz. All differences among *Dfnb31*$^{neo/neo}$, *Dfnb31*$^{wi/wi}$ and *Dfnb31*$^{wi/neo}$ mice were statistically significant ($P < 0.01$) except the differences between *Dfnb31*$^{neo/neo}$ and *Dfnb31*$^{wi/neo}$ mice at frequencies of 4, 8, 11.3, 16, 22.6, 32 and 45 kHz. Error bars represent standard error of the mean. Numbers in the legend are the numbers of mice tested in each genotype group. Note that various numbers of mice were tested at different frequencies within the same genotype groups. Two-way ANOVA with Bonferroni correction for multiple comparisons and Student's t-tests (two-tail) were performed.

Verification of C-whirlin localization and function in the cochlea of *Dfnb31*$^{tm1a/tm1a}$ and *Dfnb31*$^{wi/wi}$-BAC mice

To verify our findings about the localization and function of whirlin isoforms, we decided to use two more *Dfnb31* mutant mouse lines that were readily available (Fig. 8A and B). *Dfnb31*$^{tm1a/tm1a}$ mice, generated by the European Conditional Mouse Mutagenesis Program (EUCOMM), have a gene trapping cassette in intron 3 (Fig. 8B). The *tm1a* allele was predicted to trap and truncate groups 1 and 4 of *Dfnb31* mRNA variants after exon 3 and to affect expression of these *Dfnb31* variants but not variant 8. Thus, *Dfnb31*$^{tm1a/tm1a}$ mice could be an independent mouse line to verify our findings of *Dfnb31*$^{neo/neo}$ mice. *Dfnb31*$^{wi/wi}$-BAC mice, published previously (18), are *Dfnb31*$^{wi/wi}$ mice carrying a transgenic bacterial artificial chromosome clone, BAC279, which contains

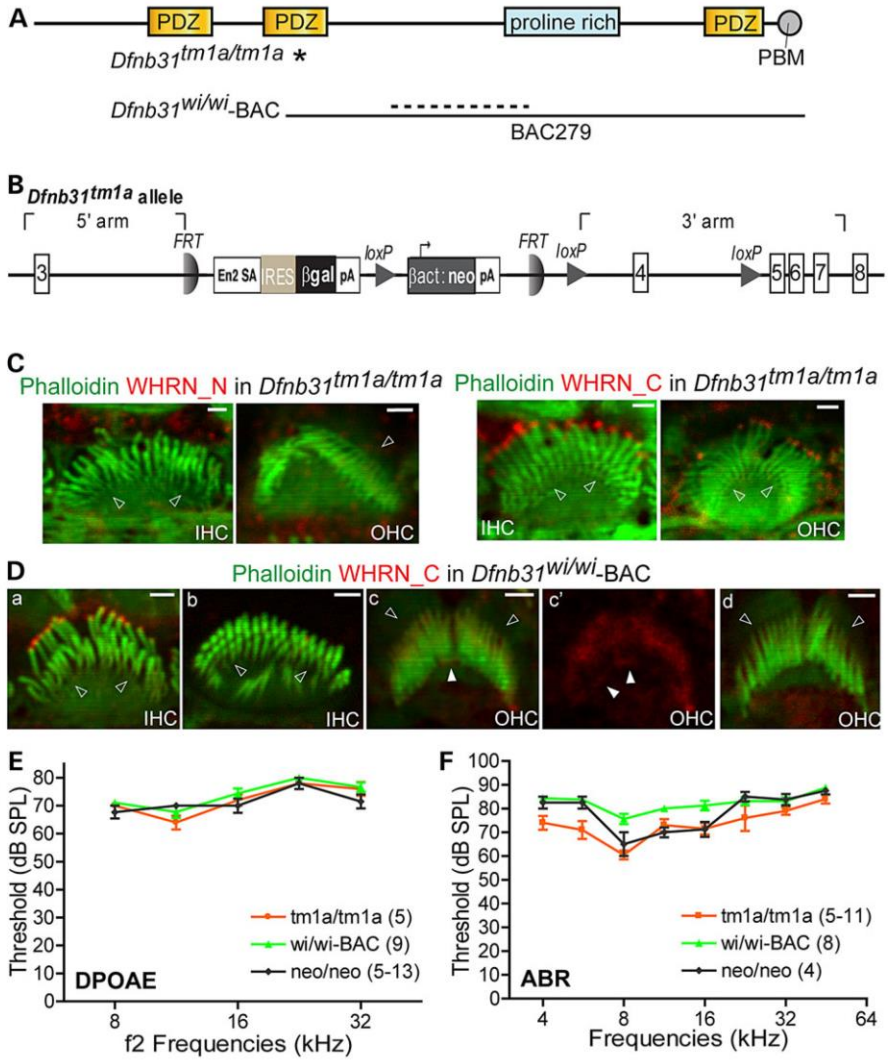

Figure 8. Cochlear phenotypes of *Dfnb31*$^{tm1a/tm1a}$ and *Dfnb31*$^{wi/wi}$-BAC mice are similar to those of *Dfnb31*$^{neo/neo}$ mice. (**A**) Positions of *Dfnb31*$^{tm1a/tm1a}$ (asterisk) and *Dfnb31*$^{wi/wi}$ (dashed line) mutations and the region covered by BAC279 clone (black line) in *Dfnb31*$^{wi/wi}$-BAC mice. (**B**) Detailed scheme of the *Dfnb31*^{tm1a} allele. (**C**) Immunostaining of P4 *Dfnb31*$^{tm1a/tm1a}$ IHCs and OHCs demonstrated no immunoreactivities from rabbit WHRN_N antibody (left) and specific immunoreactivities at stereociliary tips from rabbit WHRN_C antibody (right). (**D**) Immunostaining of P4 *Dfnb31*$^{wi/wi}$-BAC IHCs and OHCs. Whirlin C-terminal signal was detected at stereociliary tips in most (a) but not the rest (b) of IHCs. Some OHCs exhibited whirlin C-terminal signal at the stereociliary base and tip (white arrows in c and c′, c′ is the red channel image of c), while other OHCs showed weak whirlin C-terminal signal only around stereociliary bases (d). Empty arrows in (C) and (D), stereociliary bases; scale bars in (C) and (D), 1 µm. (**E**) DPOAE thresholds of *Dfnb31*$^{tm1a/tm1a}$ and *Dfnb31*$^{wi/wi}$-BAC mice were similar to those of *Dfnb31*$^{neo/neo}$ at P45-P60 ($P > 0.05$). (**F**) ABR thresholds of *Dfnb31*$^{tm1a/tm1a}$ (tm1a/tm1a) and *Dfnb31*$^{wi/wi}$-BAC (wi/wi-BAC) mice were close to those of *Dfnb31*$^{neo/neo}$ (neo/neo) at P45-P60 ($P > 0.05$) except slightly lower ABR thresholds at 5.6 kHz in *Dfnb31*$^{tm1a/tm1a}$ mice ($P < 0.05$) and slightly higher ABR thresholds at 8–16 kHz in *Dfnb31*$^{wi/wi}$-BAC mice ($P < 0.01$). Error bars, SE; numbers in the legend, numbers of mice tested. Two-way ANOVA with Bonferroni correction for multiple comparisons and Student's *t*-tests (two-tail) were performed.

a *Dfnb31* 3′-terminal genomic sequence starting at exon 4 (Fig. 8A). *Dfnb31*$^{wi/wi}$-BAC mice were considered as *Dfnb31*$^{wi/wi}$ mice expressing a C-whirlin fragment (18). To test C-whirlin expression in these two new whirlin mutant mice, we did immunofluorescence of P4 *Dfnb31*$^{tm1a/tm1a}$ and *Dfnb31*$^{wi/wi}$-BAC cochleas. Similar to *Dfnb31*$^{neo/neo}$ mice (Fig. 2), we observed immunoreactivities of Rb_WHRN_C but not Rb_WHRN_N at stereociliary tips of *Dfnb31*$^{tm1a/tm1a}$ IHCs and OHCs (Fig. 8C). In *Dfnb31*$^{wi/wi}$-BAC mice, Rb_WHRN_C immunofluorescent signals were seen in the vast majority of IHCs (Fig. 8Da), while they were absent in ∼4% of IHCs. The latter IHCs were mostly distributed in the apical cochlear turn and showed short stereocilia (Fig. 8Db). However, only about 33% of *Dfnb31*$^{wi/wi}$-BAC OHCs displayed Rb_WHRN_C signals at stereociliary tips (Fig. 8Dc and Dc′), and most of these cells were in the apical turn. DPOAE thresholds of *Dfnb31*$^{tm1a/tm1a}$ and *Dfnb31*$^{wi/wi}$-BAC mice were the same as those of *Dfnb31*$^{neo/neo}$ mice at frequencies of 8–32 kHz (Fig. 8E), although most *Dfnb31*$^{wi/wi}$-BAC OHCs did not have C-whirlin at stereociliary tips (Fig. 8Dd). In

general, ABR thresholds were similar among *Dfnb31*$^{tm1a/tm1a}$, *Dfnb31*$^{wi/wi}$-BAC and *Dfnb31*$^{neo/neo}$ mice in the frequency range of 4–45 kHz (Fig. 8F). *Dfnb31*$^{wi/wi}$-BAC mice had slightly worse hearing than the other two mutants at frequencies of 8, 11.3 and 16 kHz, which was probably due to the incomplete expression and localization of C-whirlin at IHC stereociliary tips. *Dfnb31*$^{tm1a/tm1a}$ mice exhibited hearing function slightly better than *Dfnb31*$^{neo/neo}$ mice at the frequency of 5.6 kHz, which could result from their genetic background differences (*Dfnb31*$^{tm1a/tm1a}$: C57BL/6N and *Dfnb31*$^{neo/neo}$: C57BL/6J*129/Sv). Therefore, the findings in *Dfnb31*$^{tm1a/tm1a}$ and *Dfnb31*$^{wi/wi}$-BAC mice are consistent with what we discovered in *Dfnb31*$^{neo/neo}$ mice that C-whirlin in IHC stereociliary tips plays a role in stereociliary elongation and hearing function, while C-whirlin in OHC stereociliary tips may be dispensable for hearing.

Differential disruptions of whirlin expression and function in *Dfnb31*$^{neo/neo}$ and *Dfnb31*$^{wi/wi}$ retinas

Our RT–PCR results (Fig. 1C and D) allowed us to predict that FL-, N- and C-whirlin proteins may exist in wild-type retinas; FL-whirlins may be truncated as truncated N-whirlin fragments in *Dfnb31*$^{wi/wi}$ retinas; and no whirlin proteins exist in *Dfnb31*$^{neo/neo}$ retinas. To verify this, we performed immunoblotting analysis of retinal lysates from wild-type, *Dfnb31*$^{neo/neo}$ and *Dfnb31*$^{wi/wi}$ retinas using Rb_WHRN_N and Rb_WHRN_C antibodies. However, we could not draw any clear conclusions from this experiment because of non-specific bands detected by these two antibodies. Accordingly, we adopted a new approach. We first did immunoprecipitation experiments from retinal lysates of these mice using Rb_WHRN_N and Rb_WHRN_C antibodies and then performed immunoblotting analyses of the immunoprecipitates using chicken WHRN_N and WHRN_C antibodies, respectively (Fig. 9A). In the Rb_WHRN_C immunoprecipitates, no whirlin-specific band was detected except the FL-whirlin in the wild-type retina, suggesting that no C-whirlin is expressed in the wild-type, *Dfnb31*$^{neo/neo}$ or *Dfnb31*$^{wi/wi}$ retinas and no FL-whirlin in the *Dfnb31*$^{neo/neo}$ or *Dfnb31*$^{wi/wi}$ retinas at the protein level. In the Rb_WHRN_N immunoprecipitates, a strong FL-whirlin band was revealed at about 110 kDa in wild-type retinas; a 37-kDa whirlin-specific band was seen in *Dfnb31*$^{wi/wi}$ retinas; and no whirlin-specific band was present in *Dfnb31*$^{neo/neo}$ retinas. To identify the 37-kDa whirlin-specific band in *Dfnb31*$^{wi/wi}$ retinas, gel slices at the 37-kDa position in the wild-type and *Dfnb31*$^{wi/wi}$ lanes were cut and subjected to mass spectrometry. While no whirlin peptides were found in the wild-type sample, 10 whirlin peptides distributed in the N-terminal region of FL-whirlin were identified in the *Dfnb31*$^{wi/wi}$ sample, indicating that the truncated *Dfnb31* variants 1–4 are not subjected to nonsense-mediated mRNA decay and are able to be translated into truncated N-whirlin protein fragments in *Dfnb31*$^{wi/wi}$ retinas (Fig. 9A). Furthermore, an extremely weak whirlin-specific band was observed at about 35 kDa in wild-type but not *Dfnb31*$^{neo/neo}$ or *Dfnb31*$^{wi/wi}$ retinas. Although we did not sequence this band using mass spectrometry, it could be the normal N-whirlin band. Notably, the truncated N-whirlin in *Dfnb31*$^{wi/wi}$ retinas and weak 35-kDa band in wild-type retinas were not observed in our previous study (20), which could be due to the relatively high quality of Rb_WHRN_N antibody generated and used in this study.

To examine the localization of the truncated N-whirlin in *Dfnb31*$^{wi/wi}$ retinas, we conducted immunofluorescence (Fig. 9B). WHRN_N and WHRN_C antibodies were able to detect punctate signals of FL-whirlin and perhaps the low level of N-whirlin at the periciliary membrane complex above the ciliary rootlet in wild-type but not *Dfnb31*$^{neo/neo}$ photoreceptors. In *Dfnb31*$^{wi/wi}$ photoreceptors, we did observe weak WHRN_N but not WHRN_C immunoreactivities above the ciliary rootlet, indicating the truncated N-whirlin fragment was localized normally.

Whirlin was demonstrated to interact with usherin and GPR98, components of the periciliary membrane complex, in photoreceptors (20,24). These interactions are mediated mainly by whirlin N-terminal region (32). Interestingly, immunostaining for GPR98 detected weak signals localized correctly at the periciliary membrane complex in *Dfnb31*$^{wi/wi}$ retinas (Fig. 9C). Considering the previous finding (20) that residual usherin is present in *Dfnb31*$^{wi/wi}$ but not *Dfnb31*$^{neo/neo}$ photoreceptors, we conclude that the truncated N-whirlin fragment is functional in recruiting GPR98 and usherin to the periciliary membrane complex in *Dfnb31*$^{wi/wi}$ retinas, which spares the retina from degeneration. As mentioned above, EPS8 interacts with whirlin at the stereociliary tip of hair cells, and EPS8 expression was reduced in both *Dfnb31*$^{wi/wi}$ and *Dfnb31*$^{neo/neo}$ cochlear hair cells. Therefore, we examined the EPS8 protein expression level in *Dfnb31*$^{neo/neo}$ retinas by immunoblotting and found no significant change in the mutants (Supplementary Material, Fig. S4A).

Discussion

This study presents the first definitive evidence linking differential disruptions of whirlin isoforms to various *Dfnb31* mutations and phenotype manifestations, and suggests an explanation for the genotype–phenotype correlation observed in humans and mice carrying *DFNB31*/*Dfnb31* mutations. We show that *Dfnb31* expression is complex and different in the cochlea and the retina. In these tissues, whirlin isoforms are localized in distinct subcellular compartments and play specific roles. Mutations in different regions of the *Dfnb31* gene disrupt the expression of different whirlin isoforms and lead to hearing loss with or without retinal degeneration in mice, similar to USH2D and *DFNB31* in humans.

Four groups of *Dfnb31* mRNA variants were reported previously in mouse P5 vestibular organs and adult retinas (11,22) with similar *DFNB31* mRNA variants identified in humans (18). Groups 1, 2 and 4 share the same promoter region, but are spliced differently, which results in alternative translation initiation and termination sites. Variants in group 3 have their unique promoter regions. Therefore, the alternative usage of promoters and exons at the transcriptional level as well as the alternative usage of start and stop sites at the translational level provides multiple potential spatial and temporal controls for *Dfnb31* gene expression. For example, the alternative splice sites and promoter used in *Dfnb31* variant 9 could be very weak so that the expression level of this variant is too low to be detected in our experiments (Fig. 1C). Mutations in *Dfnb31*$^{neo/neo}$ and *Dfnb31*$^{tm1a/tm1a}$ mice are positioned in exon 1 and intron 3, respectively. These locations are similar to those of p.Q103X, p.Y228LfsX38, p.A207_K279del, and p.P246HfsX13 mutations in USH2D patients (14,16,17). Our findings from *Dfnb31*$^{neo/neo}$ and *Dfnb31*$^{tm1a/tm1a}$ mice suggest that *DFNB31* variants of groups 1 and 4 but not variant 8 are affected by these mutations in USH2D patients. The affected *DFNB31* variants are probably degraded through nonsense-mediated mRNA decay and cannot be translated into protein fragments with functional domains. By contrast, the *Dfnb31*$^{wi/wi}$ mutation is between exons 6 and 9 at the C-terminal half of whirlin, similar to the mutations of p.R778X and p.G808DfsX11 found in *DFNB31* patients (18,19). Thus, the mutations in *DFNB31* patients could disrupt the same

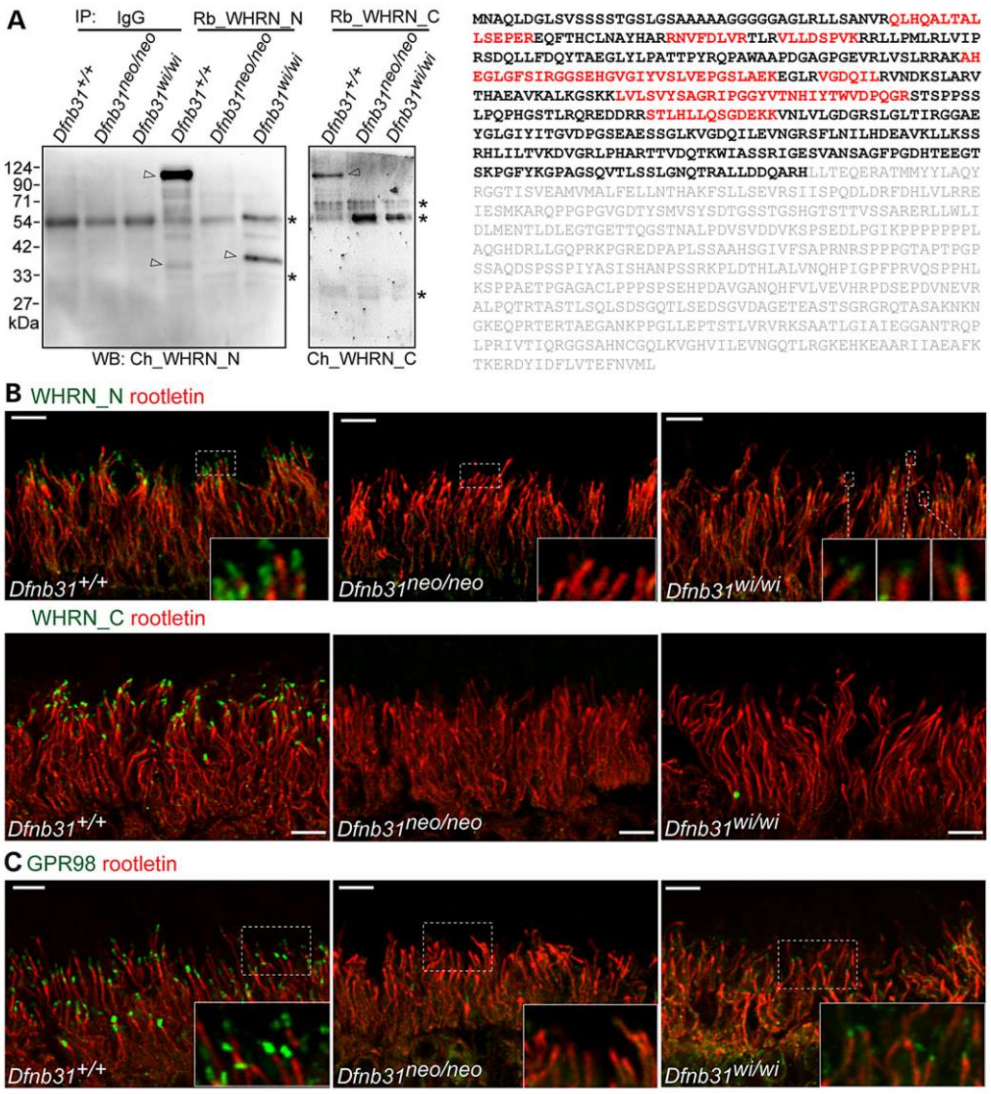

Figure 9. Whirlin protein expression, localization and function in *Dfnb31*$^{neo/neo}$ and *Dfnb31*$^{wi/wi}$ photoreceptors. (**A**) Left, immunoblotting of whirlin immunoprecipitates from adult wild-type, *Dfnb31*$^{neo/neo}$ and *Dfnb31*$^{wi/wi}$ retinas. Arrows point to whirlin-specific bands, and asterisks label the antibody or non-specific bands. IP, immunoprecipitation; WB, immunoblotting; IgG, rabbit immunoglobulin, a negative control; Rb_WHRN_N and Rb_WHRN_C, rabbit antibodies against whirlin N- and C-terminal regions, respectively (Fig. 1A); Ch_WHRN_N and Ch_WHRN_C, chicken antibodies against whirlin N- and C-terminal regions, respectively (Fig. 1A). Right, peptides identified by mass spectrometry are labeled in red in the amino acid sequence of whirlin isoform 2 (NP_001008791). Amino acids labeled in gray are after the *Dfnb31*^{wi} mutation. (**B**) Immunostaining of wild-type, *Dfnb31*$^{neo/neo}$ and *Dfnb31*$^{wi/wi}$ retinas using rabbit WHRN_N (upper row) and WHRN_C (lower row) antibodies. Residual whirlin signals (green) were detected above the ciliary rootlet (rootletin, red) at the periciliary membrane complex in *Dfnb31*$^{wi/wi}$ but not *Dfnb31*$^{neo/neo}$ photoreceptors using the WHRN_N antibody, while no whirlin signals were found in *Dfnb31*$^{neo/neo}$ or *Dfnb31*$^{wi/wi}$ photoreceptors using the WHRN_C antibody. Insets are the amplified view of regions framed by white dashed lines. (**C**) Residual GPR98 signals (green) were detected above the ciliary rootlet (rootletin, red) at the periciliary membrane complex in *Dfnb31*$^{wi/wi}$ but not *Dfnb31*$^{neo/neo}$ photoreceptors. Insets are the enlarged view of GPR98 signals in white boxes. Scale bars, 5 μm.

groups of *DFNB31* mRNA variants as the *Dfnb31*$^{wi/wi}$ mutation and thus generate similar truncated whirlin protein fragments.

Our results demonstrate that *Dfnb31* expresses three main protein isoforms, FL-, C- and N-whirlins, despite the existence of many mRNA variants. In the retina, FL-whirlin and perhaps a low level of N-whirlin are localized to the periciliary membrane complex of photoreceptors, where they were previously shown to interact with usherin and GPR98, the two proteins also associated with USH, in a multiprotein complex (Fig. 10A) (20,24,33). C-whirlin was not observed to be expressed in photoreceptors using immunostaining and pull-down assays. In the inner ear, the localization of whirlin isoforms is hair cell- and time-dependent (Fig. 10C). FL- and C-whirlins are located at stereociliary tips of IHCs, while only C-whirlin is at the OHC stereociliary tips during development. At the stereociliary tip, whirlin isoforms interact with EPS8 and myosin XVa, and contribute to the normal

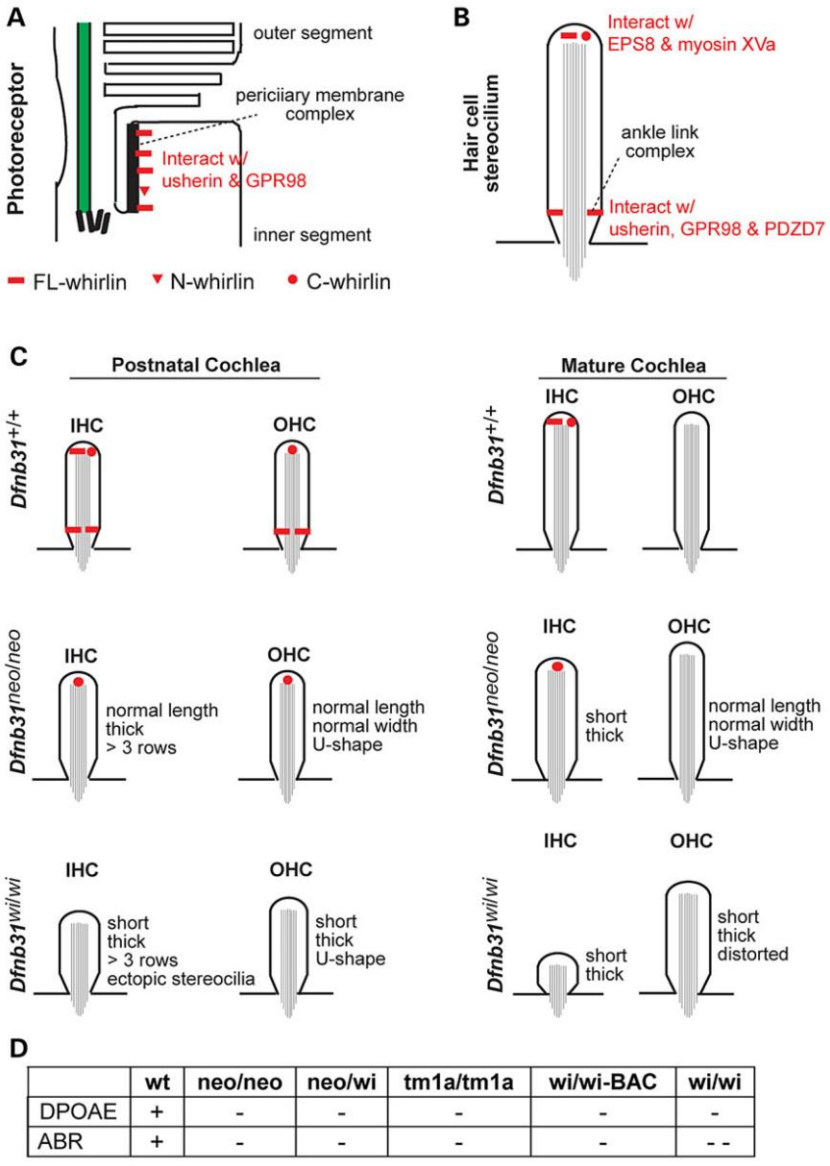

	wt	neo/neo	neo/wi	tm1a/tm1a	wi/wi-BAC	wi/wi
DPOAE	+	-	-	-	-	-
ABR	+	-	-	-	-	- -

Figure 10. Summary of localization and function of various whirlin isoforms in photoreceptors and cochlear hair cells. (**A**) FL- and N-whirlins are components of the periciliary membrane complex in photoreceptors. (**B**) In hair cells, FL- and C-whirlins at stereociliary tips interact with EPS8 and myosin XVa for stereociliary elongation, and FL-whirlin at stereociliary bases is a component of the ankle link complex. (**C**) Localization of various whirlin isoforms in the developing and mature cochlear hair cells of wild-type, *Dfnb31*$^{neo/neo}$ and *Dfnb31*$^{wi/wi}$ mice. The changes of stereociliary length and thickness in *Dfnb31*$^{neo/neo}$ and *Dfnb31*$^{wi/wi}$ mice are also shown. (**D**) Results of hearing tests in various whirlin mutant mice. +, normal; –, mildly abnormal; – –, severely abnormal.

stereociliary length in cochlear hair cells (Fig. 10B) (11,30). Only FL-whirlin is present in the ankle link complex at stereociliary bases of cochlear hair cells, where it interacts with usherin, GPR98, and PDZD7 (Fig. 10B) (23,32). Notably, the ankle link complex is a transient structure in cochlear hair cells during development and thus FL-whirlin transiently exists at cochlear stereociliary bases. N-whirlin from group 4 variants probably does not exist in the inner ear. The differential localizations of whirlin isoforms could result from differential localizations of their interacting proteins. For example, the absence of C-whirlin in the ankle link complex is probably due to its lack of N-terminal two PDZ domains, which are known to mediate the interactions between whirlin and ankle link complex components (32).

Previous (20,21,28) and current thorough phenotypical characterizations of various whirlin mutant mice (Fig. 10C) allow us to deduce the functions of various whirlin isoforms in the retina

and cochlea. The absence of retinal degeneration and existence of truncated N-whirlin, usherin, and GPR98 at the correct photoreceptor subcellular compartment in *Dfnb31*$^{wi/wi}$ mice as well as the sequence similarity between the truncated N-whirlin and the normal N-whirlin from group 4 variants indicate that normal N-whirlin may function as FL-whirlin in organizing the periciliary membrane complex of photoreceptors. In the inner ear, the longer stereociliary length in *Dfnb31*$^{neo/neo}$ than in *Dfnb31*$^{wi/wi}$ cochlear hair cells and the presence of C-whirlin at *Dfnb31*$^{neo/neo}$ but not *Dfnb31*$^{wi/wi}$ cochlear stereociliary tips indicate that C-whirlin is indispensable for normal stereociliary length (Fig. 10C). However, the shortening of stereocilia in *Dfnb31*$^{neo/neo}$ mature IHCs indicates that FL-whirlin at stereociliary tips is also required for normal stereociliary length in these cells (Fig. 10C). The shared U-shape phenotypes of *Dfnb31*$^{neo/neo}$ and *Dfnb31*$^{wi/wi}$ OHC bundles imply that the FL-whirlin at the ankle link complex plays a role in the sharp V- or W-shape stereociliary organization of OHCs (Fig. 10C). Furthermore, the stereociliary thickness could be controlled by FL-whirlin at both stereociliary tips and bases of IHCs and by C-whirlin at stereociliary tips of OHCs (Fig. 10C). The three-row stereociliary arrangement of IHC bundles could be related with functions of both FL- and C-whirlins (Fig. 10C).

Surprisingly, our study demonstrates that expression levels of EPS8 and myosin XVa at hair cell stereociliary tips are not closely correlated with stereociliary length, as proposed previously (11,30). Although we observed decreased EPS8 and myosin XVa expressions and short stereocilia in *Dfnb31*$^{wi/wi}$ cochleas as shown in the previous report (30), the changes of EPS8 and myosin XVa expressions at stereociliary tips of *Dfnb31*$^{neo/neo}$ cochleas did not affect stereociliary length at P4. This finding suggests that other proteins may take part in stereociliary elongation and be able to compensate for small changes of EPS8 and myosin XVa expressions. The changes of myosin XVa expression could be compensated by myosin IIIa expression and the emergence of myosin VIIa at stereociliary tips in *Dfnb31*$^{neo/neo}$ mice. Myosin IIIa is known to be able to elongate stereocilia probably through a direct interaction with espin1 at stereociliary tips (34). Myosin VIIa was shown to be present at *Dfnb31*$^{wi/wi}$ stereociliary tips (35) and thus may also localize at *Dfnb31*$^{neo/neo}$ stereociliary tips. The elongation of stereocilia in myosin VIIa mutant mice indicates that myosin VIIa could function in regulation of stereociliary length under some specific circumstances. EPS8L2 belongs to the EPS8 protein family. Its expression complements EPS8 expression spatiotemporally in cochlear hair cells (36) and thus could compensate the small decrease of EPS8 expression in *Dfnb31*$^{neo/neo}$ mice during development.

In addition to understanding the basic scientific question on the roles of whirlin isoforms in hair cell stereociliary development/maintenance and photoreceptor structural maintenance, our study has significant clinical impacts on diagnosis, prognosis, and treatments of hearing loss and vision problems caused by *DFNB31* mutations. Our molecular and cellular investigations of various *Dfnb31* mutations in the mouse cochlea and retina provide convincing evidence for an existence of genotype–phenotype correlation in patients carrying *DFNB31* mutations. This finding allows early accurate diagnosis and prognosis, so that patients are able to be well prepared for their later vision problems and, if available, to receive treatments before the occurrence of vision problems. One patient with a p.Q54X mutation in N-terminal region of *DFNB31* was recently reported to show nonsyndromic retinitis pigmentosa (37). However, this patient self-reported normal hearing and was unavailable for auditory examination in the study. It is possible that the patient may have some level of hearing loss according to another study (16). In that study, a patient with a p.P246HfsX13 mutation in N-terminal region of *DFNB31* had normal hearing by self-report but upon auditory examination displayed a moderate hearing loss. If our prediction is true, the hearing symptom of p.Q54X mutation is consistent with the less severe hearing loss found in *Dfnb31*$^{neo/neo}$ mice (Figs 7B, 8F and 10D). The knowledge of whirlin expression complexity will also help develop effective therapies. For example, AAV-mediated whirlin replacement therapy has been explored in the mouse retina and inner ear (24,38). In these studies, only FL-whirlin was delivered into photoreceptors and hair cells. Although the periciliary membrane complex in photoreceptors and stereociliary morphology in hair cells have been rescued, ABR thresholds are not restored. Our study suggests that delivery of multiple whirlin isoforms may be required to solve this problem. Furthermore, our thorough phenotypical characterizations of various *Dfnb31* mutant mouse models provide valuable information for these models to be used for testing new therapies. Finally, expression of multiple isoforms and causal association with various diseases (e.g. USH versus. DFNB) are two features shared by many USH genes (2). Therefore, disruption of different isoform expressions could be one of the common mechanisms underlying various disease manifestations caused by USH gene mutations.

Materials and Methods

Animals

Dfnb31 targeted mutant (*Dfnb31*$^{neo/neo}$ also known as *Dfnb31*^{tm1Tili}, MGI:4462398), whirler (*Dfnb31*$^{wi/wi}$, MGI:1857090), and *Dfnb31*$^{wi/wi}$ carrying BAC279 (*Dfnb31*$^{wi/wi}$-BAC also known as Tg(Dfnb31)#Ptt, MGI:5616436) mice were described previously (18,20). *Dfnb31*$^{tm1a(EUCOMM)wtsi}$ (MGI:4432119) mice were purchased as frozen sperms from EUCOMM and revived at the University of Utah Transgenic and Gene Targeting mouse core. All experiments involving animals were performed in compliance with the Institutional Animal Care and Use Committee at the University of Utah.

Antibodies and reagents

Two whirlin fragments (1-124 aa and 375-800 aa, NP_082916) were cloned into pET28 vectors, expressed with His tag in BL21-CodonPlus (DE3)-RIPL cells (Agilent Technologies, Santa Clara, CA, USA), and purified by chromatography using Ni^{2+}-charged His•Bind resin (EMD Millipore, Billerica, MA, USA). The other two whirlin fragments (1-472 aa and 721-907 aa, NP_082916) were cloned into pGEX-4T-1 vector, expressed with GST tag in BL21-CodonPlus (DE3)-RIPL cells, and purified by chromatography using glutathione sepharose™ 4 Fast Flow resin (GE Healthcare Life Sciences, Pittsburgh, PA, USA). Purified His-tagged whirlin proteins were applied to immunize rabbits. Antibodies against whirlin were then affinity-purified against the corresponding GST-tagged whirlin fragments. Therefore, the antigen regions of rabbit WHRN_N and WHRN_C antibodies are 1-124 aa and 721-800 aa, respectively. The specificity of purified antibodies was confirmed by immunoblotting of whirlin N- and C-terminal fragments expressed in HEK293 cells (Supplementary Material, Fig. S1). Rabbit GPR98, myosin XVa, and GRP antibodies and chicken whirlin antibodies (WHRN_N aka PDZ350 and WHRN_C aka PDZIE) were described previously (13,20). Antibodies against HA, FLAG, actin, and γ-tubulin (Sigma-Aldrich, St. Louis, MO, USA) and antibody against EPS8 (Santa Cruz Biotechnology, Dallas, TX, USA) were purchased. Alexa fluorochrome-conjugated phalloidin and secondary antibodies were obtained from Life

Technologies (Grand Island, NY, USA). Rabbit immunoglobulin and horseradish peroxidase-conjugated secondary antibodies were from Jackson ImmunoResearch (West Grove, PA, USA).

RNA isolation, RT–PCR, immunoprecipitation, immunoblotting and mass spectrometry

Total RNA was extracted from mouse retinas and cochleas using SurePrep™ RNA Purification Kit (Fisher BioReagents®, Fair Lawn, NJ, USA). RT–PCR was conducted from total RNA using Thermoscript RT–PCR kit (Life Technologies). Manufacturer's instructions were followed exactly during RNA isolation and RT–PCR. EPS8 cDNA fragment (330-2795 bp, NM_001271595) was generated from mouse retinal total RNAs by RT–PCR and inserted into pCMV-HA vector (Clontech Laboratories, Mountain View, CA, USA). Myosin XVa cDNA fragment (2603-7009 bp, NM_182698) was subcloned from a full-length construct (Thomas B. Friedman, NIDCD) into p3XFLAG-Myc-CMV vector (Sigma-Aldrich). Whirlin variant 8 cDNA (311-1963bp, AY739121) was amplified from mouse cochleas by RT–PCR and cloned into pEGFP-C vector (Clontech Laboratories). Truncated N-whirlin fragment was cloned by replacing wild-type whirlin fragment between ppuM1 and BstZ7i sites in FL-whirlin/pEGFP-C vector (31) with the cDNA fragment between the same two sites amplified from *Dfnb31*$^{wi/wi}$ retinas. To study the interactions of EPS8 and myosin XVa with whirlin fragments, HEK293 cells were cotransfected with GFP-tagged whirlin plasmids and either HA-tagged EPS8 plasmid or FLAG-tagged myosin XVa plasmid. Immunoprecipitations of GFP-tagged whirlin fragments were performed from the transfected cell lysates. The presence of EPS8 and myosin XVa in the immunoprecipitates was examined by immunoblotting using antibodies against HA and FLAG, respectively. Immunoprecipitation and immunoblotting were carried out according to our previous descriptions (13,32). For mass spectrometry, immunoprecipitated samples from wild-type and *Dfnb31*$^{wi/wi}$ retinas were run on SDS-PAGE side by side in duplicate. One pair of the samples were subjected to immunoblotting. The gel slices of the other pair of samples were cut on the gel according to the immunoblotting signals and submitted to the Taplin Mass Spectrometry Facility, Harvard Medical School, for protein identification.

Immunofluorescence and SEM

Procedures for immunofluorescence of retinal sections and whole-mount cochlear tissues were the same as previously described (13). Double immunostaining of mouse cochleas for whirlin and EPS8 was first conducted by standard immunofluorescence procedures with rabbit EPS8 antibody and Alexa Fluor® 594 goat anti-rabbit secondary antibody. Subsequently, the cochleas were incubated with 0.45 mg/ml rabbit immunoglobulin for 2 h, washed with PBS, incubated with the biotin-labeled rabbit whirlin antibody in 5% goat serum/PBS overnight, washed with PBS and finally incubated with Alexa Fluor®488-streptavidin for 1 h. Fluorescent images were taken using a confocal laser scanning microscope (Model FV1000, Olympus, Tokyo, Japan). SEM procedures were described previously (13).

Quantification of EPS8 and myosin XVa expressions

In the retina, EPS8 expressions from different genotypes were quantified by measuring EPS8 immunoblotting signal intensities using ImageJ (NIH). The EPS8 signals were normalized using loading control, actin signals, from the same samples. To quantify EPS8 and myosin XVa expressions in the cochlea, tissues from different genotypes were immunostained simultaneously with exactly the same condition to reduce variations. Fluorescent signals were subsequently captured using the same confocal imaging settings. Intensities of EPS8 and myosin XVa immunofluorescence signals were measured at the tip of stereocilia in OHCs and IHCs using ImageJ and subtracted from the background signals at regions next to stereociliary bundles. The EPS8 and myosin XVa expressions in *Dfnb31* mutant mice were normalized by their corresponding expressions in wild-type mice. Quantification of EPS8 and myosin XVa expressions was performed by a person unaware of the genotypes.

Measurement of stereociliary length, ABR and DPOAE

Measurements of cochlear stereociliary lengths were conducted blind to genotype using ImageJ. To measure cochlear stereociliary length, longest stereocilia next to the kinocilium in the stereociliary bundle were chosen in SEM graphs captured from the cochlear middle turn. ABR and DPOAE were tested in mice as previously reported (13).

Statistics

Two-way ANOVA with Bonferroni correction for multiple comparisons was performed using GraphPad Prism 4, to analyze the significance of differences in ABR and DPOAE thresholds among genotypes at various sound frequencies. Student's *t*-tests were conducted using Microsoft Office Excel to compare values, such as stereociliary length and expression level, between two different genotype groups. A *P*-value of <0.05 was considered to indicate a statistically significant difference between groups.

Supplementary Material

Supplementary Material is available at *HMG* online.

Acknowledgements

We thank Masaaki Yoshigi (University of Utah) and Ross Tomaino (Harvard Medical School) for mass spectrometry assistance, Thomas Friedman (NIDCD) for myosin XVa full-length cDNA, and the Wellcome Trust Sanger Institute Mouse Genetics Project (Sanger MGP) and its funders for providing the mutant mice line (Allele: *Dfnb31*$^{tm1a(EUCOMM)wtsi}$).

Conflict of Interest statement. None declared.

Funding

This work was supported by the National Institutes of Health (EY020853 to J.Y., EY014800 to the Department of Ophthalmology &Visual Sciences, University of Utah); Foundation Fighting Blindness (to J.Y.); E. Matilda Ziegler Foundation for the Blind, Inc. (to J.Y.); Research to Prevent Blindness, Inc. (to J.Y. and the Department of Ophthalmology & Visual Sciences, University of Utah); Hearing Health Foundation (to J.Z.); National Organization for Hearing Research Foundation (to J.Z.); and a startup package from the Moran Eye Center, University of Utah (to J.Y.).

References

1. Kimberling, W.J., Hildebrand, M.S., Shearer, A.E., Jensen, M.L., Halder, J.A., Trzupek, K., Cohn, E.S., Weleber, R.G., Stone, E.M. and Smith, R.J. (2010) Frequency of Usher syndrome in two

pediatric populations: implications for genetic screening of deaf and hard of hearing children. *Genet. Med.*, **12**, 512–516.
2. Mathur, P. and Yang, J. (2015) Usher syndrome: hearing loss, retinal degeneration and associated abnormalities. *Biochim. Biophys. Acta.*, **1852**, 406–420.
3. Riazuddin, S., Nazli, S., Ahmed, Z.M., Yang, Y., Zulfiqar, F., Shaikh, R.S., Zafar, A.U., Khan, S.N., Sabar, F., Javid, F.T. *et al.* (2008) Mutation spectrum of MYO7A and evaluation of a novel nonsyndromic deafness DFNB2 allele with residual function. *Hum. Mutat.*, **29**, 502–511.
4. Schultz, J.M., Bhatti, R., Madeo, A.C., Turriff, A., Muskett, J.A., Zalewski, C.K., King, K.A., Ahmed, Z.M., Riazuddin, S., Ahmad, N. *et al.* (2011) Allelic hierarchy of CDH23 mutations causing non-syndromic deafness DFNB12 or Usher syndrome USH1D in compound heterozygotes. *J. Med. Genet.*, **48**, 767–775.
5. Miyasaka, Y., Suzuki, S., Ohshiba, Y., Watanabe, K., Sagara, Y., Yasuda, S.P., Matsuoka, K., Shitara, H., Yonekawa, H., Kominami, R. *et al.* (2013) Compound heterozygosity of the functionally null Cdh23(v-ngt) and hypomorphic Cdh23(ahl) alleles leads to early-onset progressive hearing loss in mice. *Exp. Anim.*, **62**, 333–346.
6. Chen, Z.Y., Hasson, T., Kelley, P.M., Schwender, B.J., Schwartz, M.F., Ramakrishnan, M., Kimberling, W.J., Mooseker, M.S. and Corey, D.P. (1996) Molecular cloning and domain structure of human myosin-VIIa, the gene product defective in Usher syndrome 1B. *Genomics*, **36**, 440–448.
7. Verpy, E., Leibovici, M., Zwaenepoel, I., Liu, X.Z., Gal, A., Salem, N., Mansour, A., Blanchard, S., Kobayashi, I., Keats, B.J. *et al.* (2000) A defect in harmonin, a PDZ domain-containing protein expressed in the inner ear sensory hair cells, underlies Usher syndrome type 1C. *Nat. Genet.*, **26**, 51–55.
8. Ahmed, Z.M., Goodyear, R., Riazuddin, S., Lagziel, A., Legan, P. K., Behra, M., Burgess, S.M., Lilley, K.S., Wilcox, E.R., Griffith, A. J. *et al.* (2006) The tip-link antigen, a protein associated with the transduction complex of sensory hair cells, is protocadherin-15. *J. Neurosci.*, **26**, 7022–7034.
9. Di Palma, F., Pellegrino, R. and Noben-Trauth, K. (2001) Genomic structure, alternative splice forms and normal and mutant alleles of cadherin 23 (Cdh23). *Gene*, **281**, 31–41.
10. Adato, A., Lefevre, G., Delprat, B., Michel, V., Michalski, N., Chardenoux, S., Weil, D., El-Amraoui, A. and Petit, C. (2005) Usherin, the defective protein in Usher syndrome type IIA, is likely to be a component of interstereocilia ankle links in the inner ear sensory cells. *Hum. Mol. Genet.*, **14**, 3921–3932.
11. Belyantseva, I.A., Boger, E.T., Naz, S., Frolenkov, G.I., Sellers, J. R., Ahmed, Z.M., Griffith, A.J. and Friedman, T.B. (2005) Myosin-XVa is required for tip localization of whirlin and differential elongation of hair-cell stereocilia. *Nat. Cell Biol.*, **7**, 148–156.
12. McMillan, D.R., Kayes-Wandover, K.M., Richardson, J.A. and White, P.C. (2002) Very large G protein-coupled receptor-1, the largest known cell surface protein, is highly expressed in the developing central nervous system. *J. Biol. Chem.*, **277**, 785–792.
13. Zou, J., Zheng, T., Ren, C., Askew, C., Liu, X.P., Pan, B., Holt, J.R., Wang, Y. and Yang, J. (2014) Deletion of PDZD7 disrupts the Usher syndrome type 2 protein complex in cochlear hair cells and causes hearing loss in mice. *Hum. Mol. Genet.*, **23**, 2374–2390.
14. Ebermann, I., Scholl, H.P., Charbel Issa, P., Becirovic, E., Lamprecht, J., Jurklies, B., Millan, J.M., Aller, E., Mitter, D. and Bolz, H. (2007) A novel gene for Usher syndrome type 2: mutations in the long isoform of whirlin are associated with retinitis pigmentosa and sensorineural hearing loss. *Hum. Genet.*, **121**, 203–211.
15. Ouyang, X.M., Xia, X.J., Verpy, E., Du, L.L., Pandya, A., Petit, C., Balkany, T., Nance, W.E. and Liu, X.Z. (2002) Mutations in the alternatively spliced exons of USH1C cause non-syndromic recessive deafness. *Hum. Genet.*, **111**, 26–30.
16. Audo, I., Bujakowska, K., Mohand-Said, S., Tronche, S., Lancelot, M.E., Antonio, A., Germain, A., Lonjou, C., Carpentier, W., Sahel, J.A. *et al.* (2011) A novel DFNB31 mutation associated with Usher type 2 syndrome showing variable degrees of auditory loss in a consanguineous Portuguese family. *Mol. Vis.*, **17**, 1598–1606.
17. Besnard, T., Vache, C., Baux, D., Larrieu, L., Abadie, C., Blanchet, C., Odent, S., Blanchet, P., Calvas, P., Hamel, C. *et al.* (2012) Non-USH2A mutations in USH2 patients. *Hum. Mutat.*, **33**, 504–510.
18. Mburu, P., Mustapha, M., Varela, A., Weil, D., El-Amraoui, A., Holme, R.H., Rump, A., Hardisty, R.E., Blanchard, S., Coimbra, R.S. *et al.* (2003) Defects in whirlin, a PDZ domain molecule involved in stereocilia elongation, cause deafness in the whirler mouse and families with DFNB31. *Nat. Genet.*, **34**, 421–428.
19. Tlili, A., Charfedine, I., Lahmar, I., Benzina, Z., Mohamed, B. A., Weil, D., Idriss, N., Drira, M., Masmoudi, S. and Ayadi, H. (2005) Identification of a novel frameshift mutation in the DFNB31/WHRN gene in a Tunisian consanguineous family with hereditary non-syndromic recessive hearing loss. *Hum. Mutat.*, **25**, 503.
20. Yang, J., Liu, X., Zhao, Y., Adamian, M., Pawlyk, B., Sun, X., McMillan, D.R., Liberman, M.C. and Li, T. (2010) Ablation of whirlin long isoform disrupts the USH2 protein complex and causes vision and hearing loss. *PLoS Genet.*, **6**, e1000955.
21. Holme, R.H., Kiernan, B.W., Brown, S.D. and Steel, K.P. (2002) Elongation of hair cell stereocilia is defective in the mouse mutant whirler. *J. Comp. Neurol.*, **450**, 94–102.
22. Wright, R.N., Hong, D.H. and Perkins, B. (2012) RpgrORF15 connects to the usher protein network through direct interactions with multiple whirlin isoforms. *Invest. Ophthalmol. Vis. Sci.*, **53**, 1519–1529.
23. Michalski, N., Michel, V., Bahloul, A., Lefevre, G., Barral, J., Yagi, H., Chardenoux, S., Weil, D., Martin, P., Hardelin, J.P. *et al.* (2007) Molecular characterization of the ankle-link complex in cochlear hair cells and its role in the hair bundle functioning. *J. Neurosci.*, **27**, 6478–6488.
24. Zou, J., Luo, L., Shen, Z., Chiodo, V.A., Ambati, B.K., Hauswirth, W.W. and Yang, J. (2011) Whirlin replacement restores the formation of the USH2 protein complex in whirlin knockout photoreceptors. *Invest. Ophthalmol. Vis. Sci.*, **52**, 2343–2351.
25. Delprat, B., Michel, V., Goodyear, R., Yamasaki, Y., Michalski, N., El-Amraoui, A., Perfettini, I., Legrain, P., Richardson, G., Hardelin, J.P. *et al.* (2005) Myosin XVa and whirlin, two deafness gene products required for hair bundle growth, are located at the stereocilia tips and interact directly. *Hum. Mol. Genet.*, **14**, 401–410.
26. Kikkawa, Y., Mburu, P., Morse, S., Kominami, R., Townsend, S. and Brown, S.D. (2005) Mutant analysis reveals whirlin as a dynamic organizer in the growing hair cell stereocilium. *Hum. Mol. Genet.*, **14**, 391–400.
27. Grati, M., Shin, J.B., Weston, M.D., Green, J., Bhat, M.A., Gillespie, P.G. and Kachar, B. (2012) Localization of PDZD7 to the stereocilia ankle-link associates this scaffolding protein with the Usher syndrome protein network. *J. Neurosci.*, **32**, 14288–14293.
28. Mogensen, M.M., Rzadzinska, A. and Steel, K.P. (2007) The deaf mouse mutant whirler suggests a role for whirlin in actin filament dynamics and stereocilia development. *Cell Motil. Cytoskeleton*, **64**, 496–508.

29. Mustapha, M., Beyer, L.A., Izumikawa, M., Swiderski, D.L., Dolan, D.F., Raphael, Y. and Camper, S.A. (2007) Whirler mutant hair cells have less severe pathology than shaker 2 or double mutants. *J. Assoc. Res. Otolaryngol.*, **8**, 329–337.
30. Manor, U., Disanza, A., Grati, M., Andrade, L., Lin, H., Di Fiore, P.P., Scita, G. and Kachar, B. (2011) Regulation of stereocilia length by myosin XVa and whirlin depends on the actin-regulatory protein Eps8. *Curr. Biol.*, **21**, 167–172.
31. Wang, L., Zou, J., Shen, Z., Song, E. and Yang, J. (2012) Whirlin interacts with espin and modulates its actin-regulatory function: an insight into the mechanism of Usher syndrome type II. *Hum. Mol. Genet.*, **21**, 692–710.
32. Chen, Q., Zou, J., Shen, Z., Zhang, W. and Yang, J. (2014) Whirlin and PDZ Domain Containing 7 (PDZD7) Proteins are Both Required to Form the Quaternary Protein Complex Associated with Usher Syndrome Type 2. *J. Biol. Chem.*, **289**, 36070–36088.
33. van Wijk, E., van der Zwaag, B., Peters, T., Zimmermann, U., Te Brinke, H., Kersten, F.F., Marker, T., Aller, E., Hoefsloot, L. H., Cremers, C.W. *et al.* (2006) The DFNB31 gene product whirlin connects to the Usher protein network in the cochlea and retina by direct association with USH2A and VLGR1. *Hum. Mol. Genet.*, **15**, 751–765.
34. Salles, F.T., Merritt, R.C. Jr, Manor, U., Dougherty, G.W., Sousa, A.D., Moore, J.E., Yengo, C.M., Dose, A.C. and Kachar, B. (2009) Myosin IIIa boosts elongation of stereocilia by transporting espin 1 to the plus ends of actin filaments. *Nat. Cell Biol.*, **11**, 443–450.
35. Prosser, H.M., Rzadzinska, A.K., Steel, K.P. and Bradley, A. (2008) Mosaic complementation demonstrates a regulatory role for myosin VIIa in actin dynamics of stereocilia. *Mol. Cell. Biol.*, **28**, 1702–1712.
36. Furness, D.N., Johnson, S.L., Manor, U., Ruttiger, L., Tocchetti, A., Offenhauser, N., Olt, J., Goodyear, R.J., Vijayakumar, S., Dai, Y. *et al.* (2013) Progressive hearing loss and gradual deterioration of sensory hair bundles in the ears of mice lacking the actin-binding protein Eps8L2. *Proc. Natl. Acad. Sci. USA*, **110**, 13898–13903.
37. Nishiguchi, K.M., Tearle, R.G., Liu, Y.P., Oh, E.C., Miyake, N., Benaglio, P., Harper, S., Koskiniemi-Kuendig, H., Venturini, G., Sharon, D. *et al.* (2013) Whole genome sequencing in patients with retinitis pigmentosa reveals pathogenic DNA structural changes and NEK2 as a new disease gene. *Proc. Natl. Acad. Sci. USA*, **110**, 16139–16144.
38. Chien, W., Isgrig, K., Roy, S., Belyantseva, I.A., Drummond, M., May, L., Fitzgerald, T., Friedman, T.B. and Cunningham, L. (2015) Gene Therapy Restores Hair Cell Stereocilia Morphology in the Whirler Mouse Cochlea. *ARO 38th Annual MidWinter Meeting Abstract Book*, **38**, 268.

CHAPTER 4

A STUDY OF WHIRLIN ISOFORMS IN THE MOUSE VESTIBULAR SYSTEM SUGGESTS POTENTIAL VESTIBULAR DYSFUNCTION IN DFNB31-DEFICIENT PATIENTS

Jun Yang and I designed the study. I did all the experiments and analyzed the data, except vestibular recordings part of the manuscript. I generated figures and wrote the methods section for my experiments. Jun Yang wrote the manuscript. Timothy Jones wrote the vestibular recordings part of the manuscript. I helped revise each version of the manuscript.

This is a precopyedited, author-produced PDF of an article accepted for publication in Human Molecular Genetics following peer review. Reprinted from Pranav Dinesh Mathur, Sarath Vijayakumar, Deepti Vashist, Sherri M. Jones, Timothy A. Jones, Jun Yang. (2015) A Study of Whirlin Isoforms in the Mouse Vestibular System Suggests Potential Vestibular Dysfunction in DFNB31-Defecient Patients. *Human Mol Gen* 24 (24): 7017-30, with permission from Oxford University Press and Elsevier. License obtained through RightsLink. The version of this record mentioned above is available online at: http://hmg.oxfordjournals.org/content/24/24/7017.long

HMG Advance Access published October 11, 2015

OXFORD

Human Molecular Genetics, 2015, 1–14

doi: 10.1093/hmg/ddv403
Advance Access Publication Date: 29 September 2015
Original Article

ORIGINAL ARTICLE

A study of whirlin isoforms in the mouse vestibular system suggests potential vestibular dysfunction in *DFNB31*-deficient patients

Pranav Dinesh Mathur[1,2], Sarath Vijayakumar[3], Deepti Vashist[1], Sherri M. Jones[3], Timothy A. Jones[3] and Jun Yang[1,2,4,*]

[1]Department of Ophthalmology and Visual Sciences, Moran Eye Center, University of Utah, 65 Mario Capecchi Drive, Salt Lake City, UT 84132, USA, [2]Department of Neurobiology and Anatomy, University of Utah, 20 North 1900 East, Salt Lake City, UT 84132, USA, [3]Department of Special Education and Communication Disorders, University of Nebraska-Lincoln, 304 Barkley Memorial Center, Lincoln, NE 68583, USA and [4]Division of Otolaryngology, Department of Surgery, University of Utah, 50 North Medical Drive, Salt Lake City, UT 84132, USA

*To whom correspondence should be addressed at: John A Moran Eye Center, University of Utah, 65 Mario Capecchi Drive, Bldg 523, Salt Lake City, UT 84132, USA. Tel: +1 801 213 2591; Email: jun.yang@hsc.utah.edu

Abstract

The *DFNB31* gene plays an indispensable role in the cochlea and retina. Mutations in this gene disrupt its various isoforms and lead to non-syndromic deafness, blindness and deaf-blindness. However, the known expression of *Dfnb31*, the mouse ortholog of *DFNB31*, in vestibular organs and the potential vestibular-deficient phenotype observed in one *Dfnb31* mutant mouse (*Dfnb31*$^{wi/wi}$) suggest that *DFNB31* may also be important for vestibular function. In this study, we find that full-length (FL-) and C-terminal (C-) whirlin isoforms are expressed in the vestibular organs, where their stereociliary localizations are similar to those of developing cochlear inner hair cells. No whirlin is detected in *Dfnb31*$^{wi/wi}$ vestibular organs, while only C-whirlin is expressed in *Dfnb31*$^{neo/neo}$ vestibular organs. Both FL- and C-whirlin isoforms are required for normal vestibular stereociliary growth, although they may play slightly different roles in the central and peripheral zones of the crista ampullaris. Vestibular sensory-evoked potentials demonstrate severe to profound vestibular deficits in *Dfnb31*$^{neo/neo}$ and *Dfnb31*$^{wi/wi}$ mice. Swimming and rotarod tests demonstrate that the two *Dfnb31* mutants have balance problems, with *Dfnb31*$^{wi/wi}$ mice being more affected than *Dfnb31*$^{neo/neo}$ mice. Because *Dfnb31*$^{wi/wi}$ and *Dfnb31*$^{neo/neo}$ mice faithfully recapitulate hearing and vision symptoms in patients, our findings of vestibular dysfunction in these *Dfnb31* mutants raise the question of whether *DFNB31*-deficient patients may acquire vestibular as well as hearing and vision loss.

Introduction

DFNB31 is the causative gene for Usher syndrome type 2 USH2D (OMIM; 611383) (1–3) and non-syndromic deafness DFNB31 (OMIM; 607084) (4,5) with USH2D being characterized by moderate to severe hearing loss and progressive retinal degeneration. A recent study also identified a *DFNB31* mutation in patients with only progressive retinal degeneration (6). These phenotypes of hearing loss and retinal degeneration are recapitulated in mice carrying a mutant *Dfnb31* gene, the ortholog of *DFNB31* and also known as *Whrn* (7). Therefore, *DFNB31*/*Dfnb31* is essential for both hearing and vision. *Dfnb31* expresses multiple whirlin isoforms in cochlear hair cells and retinal photoreceptors (8–10). In the cochlea, full-length (FL-) whirlin isoform is localized at stereociliary tips and ankle link complexes in inner hair cells

Received: July 22, 2015. **Revised:** September 10, 2015. **Accepted:** September 21, 2015

and stereociliary ankle link complexes in outer hair cells; C-terminal (C-) whirlin isoform is present at stereociliary tips in both inner and outer hair cells. The FL- and C-whirlin isoforms at hair cell stereociliary tips are required for normal stereociliary elongation (4,10,11), while FL-whirlin isoform also participates in the formation of the ankle link complex (12,13), which is a transient subcellular structure during cochlear stereociliary bundle development (14–16). Defects in the ankle link complex are associated with Usher syndrome type 2 (USH2) (13,16) (manuscript submitted). In photoreceptors, FL- and probably N-terminal (N-) whirlin isoforms organize the formation of the periciliary membrane complex between the outer and inner segment (10). Although the function of the periciliary membrane complex is currently unclear, defects in this structure are known to cause retinal degeneration (7). Our previous study demonstrates that the differential expression, localization and function of various whirlin isoforms underlie the distinct phenotypical combinations in mice carrying different *Dfnb31* mutations (10) and are highly likely the cause of variable disease manifestations of *DFNB31* mutations in humans.

In addition to its cochlear and retinal expressions, *Dfnb31* has been reported to have nine mRNA variants and its protein isoforms were localized at hair cell stereociliary tips and ankle link complexes in mouse and rat vestibular systems (9,15,17,18). Furthermore, *Dfnb31*$^{wi/wi}$ mice with a deletion between *Dfnb31* exons 6 and 9 (Fig. 1A) exhibit circling and head-bobbing behaviors (4,19), suggestive of vestibular dysfunction. In contrast, *Dfnb31*$^{neo/neo}$ mice with a mutation in *Dfnb31* exon 1 show no overt balance disorder phenotype. Therefore, it is important to understand the role of whirlin isoforms in the vestibular system. In this study, we thoroughly investigated whirlin isoforms in mouse vestibular end organs. We found that the expression, localization and function of whirlin isoforms in vestibular hair cells (VHCs) are similar to those of developing cochlear inner hair cells. Examinations of stereociliary morphology, vestibular function and balance behaviors clearly demonstrated the existence of peripheral vestibular dysfunction in *Dfnb31*$^{neo/neo}$ and *Dfnb31*$^{wi/wi}$ mice, which are USH2D and DFNB31 animal models, respectively. Therefore, our findings prompt the question of whether *DFNB31*-deficient patients harbor occult peripheral vestibulopathy.

Results

Expression and localization of whirlin isoforms in the wild-type, *Dfnb31*$^{neo/neo}$ and *Dfnb31*$^{wi/wi}$ vestibular systems

Eleven *Dfnb31* mRNA variants identified previously from the mouse inner ear and retina (8,17) were investigated in the

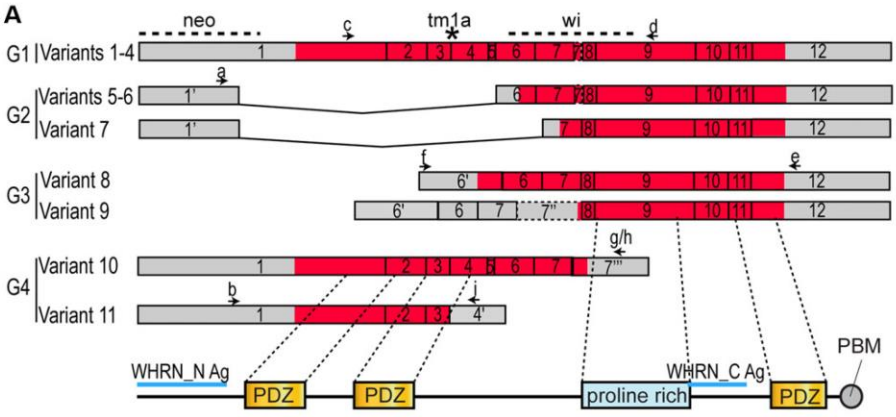

B

Protein isoform		FL-whirlin	C-whirlin			N-whirlin	
Variant groups		Group 1	Group 2	Group 3		Group 4	
Variants		Variants 1-4	Variants 5-7	Variant 8	Variant 9	Variant 10	Variant 11
GenBank Accession #		AY739114-AY739117	AY739118-AY739120	AY739121	AY739122	AK157955 HQ148552	HQ148553
Primer pairs		c/d	a/d	f/e	f/e	c/g or c/h	b/i
Vestibular System	wt	+	-	+	-	-	-
	neo	-	-	+	-	-	-
	wi	T	-	T	-	-	-

Figure 1. Expression of *Dfnb31* mRNA variants in wild-type and *Dfnb31* mutant vestibular systems. (**A**) Schematic diagram of various *Dfnb31* mRNA variants identified previously from the mouse inner ear and retina (8,17). Arabic numerals are exon numbers. Gray and red colors indicate untranslated and protein coding regions, respectively. Arrows and lower case letters show the position and direction of primers used for RT–PCR experiments in (**B**). Positions of *Dfnb31*$^{neo/neo}$, *Dfnb31*$^{wi/wi}$ and *Dfnb31*$^{tm1a/tm1a}$ mutations are labeled by dashed lines and an asterisk at the top. The exon regions corresponding to whirlin protein functional domains are shown at the bottom. Blue lines indicate the antigen regions of whirlin antibodies. (B) Summary of RT–PCR results showing differential disruption of *Dfnb31* mRNA variants in *Dfnb31*$^{neo/neo}$ (neo) and *Dfnb31*$^{wi/wi}$ (wi) vestibular systems. In general, variant 8 was intact, while variants 1–4 were disrupted in the *Dfnb31*$^{neo/neo}$ vestibular system; variants 1–4 and 8 were all truncated in the *Dfnb31*$^{wi/wi}$ vestibular system. +, presence; –, absence; T, truncated.

mouse vestibular system in this study. These *Dfnb31* mRNA variants were categorized into four groups according to their alternative use of promoters and alternative splicing of exons (Fig. 1A). Variants of Group 1 can be translated into FL-whirlin possessing three PDZ domains and one proline-rich region. Group 2 variants share the same promoter region with Group 1, but are alternatively spliced to skip regions between exons 1–5 and exons 1–6, while Group 3 variants utilize alternative promoters in intron 5. The variants in Groups 2 and 3 are predicted to be translated into proteins with only the proline-rich region and the third PDZ domain (C-whirlin). Variants in Group 4 undergo alternative splicing after exon 4 or 7, which leads to protein isoforms with only N-terminal one or two PDZ domains (N-whirlin). We designed primers specific to each group of *Dfnb31* mRNA variants (Fig. 1A and Supplementary Material, Table S1) and characterized the expression of these *Dfnb31* variants by RT–PCR using total RNA isolated from combined P4 mouse saccules, utricles and cristae. In the wild-type vestibular system, variants in Group 1 as well as variant 8 in Group 3 were expressed (Fig. 1B). In the *Dfnb31*$^{neo/neo}$ vestibular system, which carries the *Dfnb31* mutation in the 5′ region of exon 1 (Fig. 1A), variant 8 was intact, while others were undetectable (Fig. 1B). Finally, the *Dfnb31*$^{wi/wi}$ mutation (Fig. 1A) produced truncated Group 1 variants and variant 8 in the vestibular system (Fig. 1B), which results in frameshift and premature termination of their protein translation. The truncated Group 1 protein products have amino acid sequences similar to N-whirlin followed by 58 aberrant amino acids from the out-of-frame sequence, while the truncated variant 8 protein product has 76 whirlin amino acids with no known functional domains as well as the 58 aberrant amino acids.

The above RT–PCR results suggested that FL- and C-whirlins existed in the wild-type vestibular system, C-whirlin in the *Dfnb31*$^{neo/neo}$ vestibular system, and truncated N-whirlin in the *Dfnb31*$^{wi/wi}$ vestibular system. To reveal the subcellular locations of these whirlin isoforms in VHCs, we performed immunostaining of mouse vestibular whole-mounts at P4 using rabbit WHRN_N and WHRN_C antibodies, which specifically detect against the whirlin N- and C-terminal regions, respectively (Fig. 1A and data not shown). Immunoreactivities of WHRN_C were found at the tips of the tallest stereocilia and bases of probably all stereocilia in wild-type VHCs (Fig. 2Aa–Ab), at only the tips of the tallest stereocilia in *Dfnb31*$^{neo/neo}$ VHCs (Fig. 2Ac–Ae), and absent in *Dfnb31*$^{wi/wi}$ VHCs (Fig. 2Ae). Additionally, immunoreactivities of WHRN_N were found in regions similar to those of WHRN_C in wild-type VHCs (Fig. 2B) and absent in *Dfnb31*$^{neo/neo}$ and *Dfnb31*$^{wi/wi}$ VHCs (data not shown). Therefore, FL-whirlin is present at both stereociliary tips and ankle link complexes, and C-whirlin is only at stereociliary tips in wild-type VHCs. In *Dfnb31*$^{neo/neo}$ VHCs, C-whirlin is at stereociliary tips. The truncated N-whirlin may not exist in *Dfnb31*$^{wi/wi}$ VHCs due to nonsense-mediated mRNA decay.

Stereociliary morphology, cytocauds and hair cell density in *Dfnb31*$^{neo/neo}$ and *Dfnb31*$^{wi/wi}$ vestibular systems

The vestibular system consists of the otolith organs (saccule and utricle) and semicircular canals (crista ampullaris). We examined the VHC stereociliary morphology of *Dfnb31*$^{neo/neo}$ and *Dfnb31*$^{wi/wi}$ mice by phalloidin staining of saccules, utricles and cristae at P4. We utilized oncomodulin, calretinin and β-III tubulin as markers

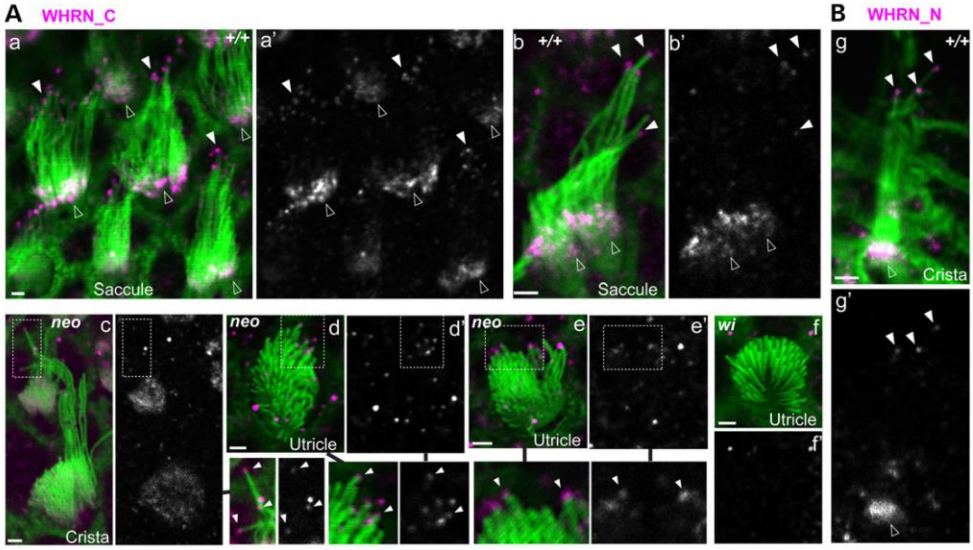

Figure 2. Whirlin protein localization in wild-type, *Dfnb31*$^{neo/neo}$ and *Dfnb31*$^{wi/wi}$ VHCs. (**A**) Immunostaining using rabbit WHRN_C antibody showed signals at stereociliary bases and tips in wild-type VHCs (+/+, **a** and **b**), signals at stereociliary tips in *Dfnb31*$^{neo/neo}$ VHCs (*neo*, **c–e**) and no stereociliary signals in *Dfnb31*$^{wi/wi}$ VHCs (*wi*, **f**) at P4. Note weak diffuse whirlin signals were also found in the cuticular plate of VHCs in the *Dfnb31*$^{neo/neo}$ peripheral crista (**c**). Signals from the magenta channel are shown in grayscale (**a′–f′**) on the right of the merged images (a–f). Regions in the dashed frames are enlarged either on the right of (c, and c′) or below (d, d′, c and c′) the original images and are linked by black lines. (**B**) Immunostaining using rabbit WHRN_N antibody showed signals at stereociliary bases and tips in P4 wild-type VHCs. Signals from the magenta channel are shown in grayscale (g′) below the merged image (g). Green, phalloidin; magenta, whirlin signals. Some magenta signals on or outside stereociliary bundles are non-specific. Scale bars, 1 μm.

to distinguish VHCs of the macular striola and extrastriola, VHCs of the crista central and peripheral regions as well as type I and type II VHCs. Oncomodulin is expressed in type I hair cells of the macular striola and the crista central region, which accounts for the majority of VHCs in these regions (20). Calretinin mainly labels the calyceal afferent of type I cells (21,22) and the soma of type II cells (22,23) and thus gives empty circular and filled spot signal patterns, respectively. Additionally, β-III tubulin is a marker for type I calyceal afferents (22). Therefore, combined staining for calretinin and β-III tubulin gives circular signals surrounding phalloidin signals for type I cells mainly in the macular striola and the crista central region and filled spot signals for type II cells mainly in the macular extrastriola and the crista peripheral region. We found shortening of stereocilia throughout the entire saccule and utricle of both *Dfnb31*$^{neo/neo}$ and *Dfnb31*$^{wi/wi}$ mice (data not shown). However, stereocilia were short throughout the *Dfnb31*$^{wi/wi}$ crista, but only restricted to the central region of *Dfnb31*$^{neo/neo}$ cristae (Figs 2Ac, 3A and B and 4). Measurement of type I stereociliary length in the whole saccule and central crista stained by phalloidin at P4 and P30–40 demonstrated that *Dfnb31*$^{neo/neo}$ stereocilia were longer than *Dfnb31*$^{wi/wi}$ stereocilia, although both mutants were much shorter than wild-type stereocilia (Fig. 4). A careful examination revealed that *Dfnb31*$^{neo/neo}$ vestibular stereociliary bundles had a greater staircase spacing than *Dfnb31*$^{wi/wi}$ vestibular stereociliary bundles. We also compared the stereociliary length between type I and type II hair cells in the two whirlin mutant mice (Fig. 3C). We observed shorter type II stereocilia than type I stereocilia in both whirlin mutants. For example, in *Dfnb31*$^{neo/neo}$ central cristae, the stereociliary length of type I cells is 4.05 ± 0.24 μm (mean ± SE, $n = 36$ type I cells, 4 mice), and the stereociliary length of type II cells is 3.09 ± 0.15 μm (mean ± SE, $n = 34$ type II cells, 4 mice). Considering that type II stereocilia are ∼50% of type I stereocilia in length in the wild-type mouse utricle (22), the mutations in the two *Dfnb31* mutant mice probably affected both types of hair cells similarly.

To corroborate our observations from the phalloidin-stained vestibular whole mounts, we performed scanning electron microscopy (SEM) on wild-type, *Dfnb31*$^{neo/neo}$ and *Dfnb31*$^{wi/wi}$ otolith organs at P40–P45. Consistently, we observed shortened stereocilia throughout the entire utricle and saccule of the two *Dfnb31* mutants with *Dfnb31*$^{wi/wi}$ stereocilia being the shortest (Fig. 5A). Additionally, the stereocilia in both *Dfnb31*$^{neo/neo}$ and *Dfnb31*$^{wi/wi}$ VHCs were thicker relative to wild-type stereocilia, while the difference in thicknesses between *Dfnb31*$^{neo/neo}$ and *Dfnb31*$^{wi/wi}$ stereocilia was not statistically significant (Fig. 5B). This thick stereocilia phenotype was also reported previously in *Dfnb31*$^{neo/neo}$ and *Dfnb31*$^{wi/wi}$ cochlear hair cells (24,25). The high-magnification SEM images further allowed us to examine the staircase arrangement of *Dfnb31* mutant vestibular bundles by measuring the length difference (the spacing) between different stereociliary rows. In *Dfnb31*$^{neo/neo}$ vestibular bundles, we found that the spacing between the tallest and the second tallest stereociliary rows and the spacing between the second and third tallest stereociliary rows were significantly reduced by 47.75 and 61.30%, respectively (Fig. 5B). Because the longest stereocilia were shortened by 48.44%, as shown in P30–P40 *Dfnb31*$^{neo/neo}$ saccules (Fig. 4), this finding indicated that the tallest and second tallest stereociliary rows were shortened to a similar extent, while the third tallest stereociliary row was shortened more severely. Therefore, the staircase stereociliary arrangement in *Dfnb31*$^{neo/neo}$ VHCs was not affected significantly. In *Dfnb31*$^{wi/wi}$ otolith organs, hair bundles with two different abnormal morphologies were observed, wi1 and wi2 (labeled 1 and 2 in Fig. 5A, respectively). While both wi1 and wi2 bundles showed short stereocilia with similar length, wi1 bundles also had several taller stereocilia (arrows in Fig. 5A). Compared with wild-type vestibular bundles, the spacing between the tallest and second tallest rows and the spacing between the second and third tallest rows were reduced by 48.88 and 74.00% for wi1 bundles, respectively, and by 82.85 and 82.37% for wi2 bundles, respectively (Fig. 5B). Although not measured, the spacing between the third and the rest rows in wi1 bundles seemed similar to the spacing between rows in wi2 bundles (Fig. 5A). Therefore, both wi1 and wi2 bundles lacked the evident staircase stereociliary arrangement (Fig. 5A and B), although the remnant staircase pattern existed in wi1 bundles. These two *Dfnb31*$^{wi/wi}$ bundle morphologies might result from the difference between vestibular type I and type II cells, but further studies were needed to confirm this notion.

Cytocauds are a pathological structure of actin bundles commonly found in hair cells with abnormal stereociliary dimensions, such as *Dfnb31*$^{wi/wi}$ VHCs (26–31). Consistently, we found a large number of cytocauds in P4 *Dfnb31*$^{wi/wi}$ vestibular organs by phalloidin staining (Fig. 6A). This phenotype was also seen in P4 *Dfnb31*$^{neo/neo}$ vestibular organs (Fig. 6A). Three-dimensional (3D) reconstruction of z-stacked phalloidin-stained images clearly showed that cytocauds originated at the cuticular plate level and extended toward the cell body (Fig. 6B). From the top view, cytocauds appeared to originate from actin filaments close to the plasma membrane (magenta arrows in Fig. 6A). Additionally, measurement of hair cell numbers in the saccular striola showed that hair cell densities in the vestibular organs of the two whirlin mutants were comparable with those of wild-types at P30 (Fig. 6C).

Vestibular function of *Dfnb31*$^{neo/neo}$ and *Dfnb31*$^{wi/wi}$ mice

Vestibular function was directly assessed in adult mice (P30–P60) by linear vestibular sensory-evoked potential (VsEP) tests. Figure 7A illustrates vestibular response waveforms from representative wild-type, *Dfnb31*$^{neo/neo}$ and *Dfnb31*$^{wi/wi}$ mice. The VsEP waveforms reflect the vestibular macular response to the maximum stimulus level used in the present study (+6dB$_{re:1g/ms}$). Wild-type animals demonstrated typical VsEP responses comparable with standard control C57Bl/6J mice. In contrast, VsEP responses for the two whirlin mutant groups (*Dfnb31*$^{neo/neo}$ and *Dfnb31*$^{wi/wi}$) were either absent or they reflected mere remnants of a response. In both whirlin mutant groups, the results indicated a severe to profound loss of saccular and utricular function. VsEP was also examined in a third *Dfnb31* mutant mouse line, *Dfnb31*$^{tm1a/tm1a}$ (EUCOMM), which has a gene trap cassette after exon 3 (Fig. 1A) and has a disrupted whirlin isoform expression in the cochlea similar to that in the *Dfnb31*$^{neo/neo}$ cochlea (10). VsEP results in *Dfnb31*$^{tm1a/tm1a}$ mutants were comparable with those of *Dfnb31*$^{neo/neo}$ (data not shown).

Nine of the 14 *Dfnb31*$^{neo/neo}$ mice had no response at the highest stimulus levels (e.g. Fig. 7A), whereas responses were absent in 6 of the 12 *Dfnb31*$^{wi/wi}$ mice. The distributions were not significantly different. When present, vestibular responses of *Dfnb31*$^{neo/neo}$ and *Dfnb31*$^{wi/wi}$ mice were comparable. Among the 11 of 26 animals that had responses, VsEP thresholds (Fig. 7B), amplitudes (Fig. 7C, p1–n1, +6dB$_{re:1g/ms}$) and onset latencies (Fig. 7D, p1 latency, +6dBr:1g/ms) were not significantly different for the two mutant strains. One exception was that n1 latencies for *Dfnb31*$^{neo/neo}$ were slightly longer than those for *Dfnb31*$^{wi/wi}$ [Fig. 7D, multivariate analysis of variance (MANOVA), n1, least significant difference (LSD): $P = 0.05$, +6dB$_{re:1g/ms}$].

Of those mutant mice that had responses, thresholds for vestibular responses were significantly higher than wild-type

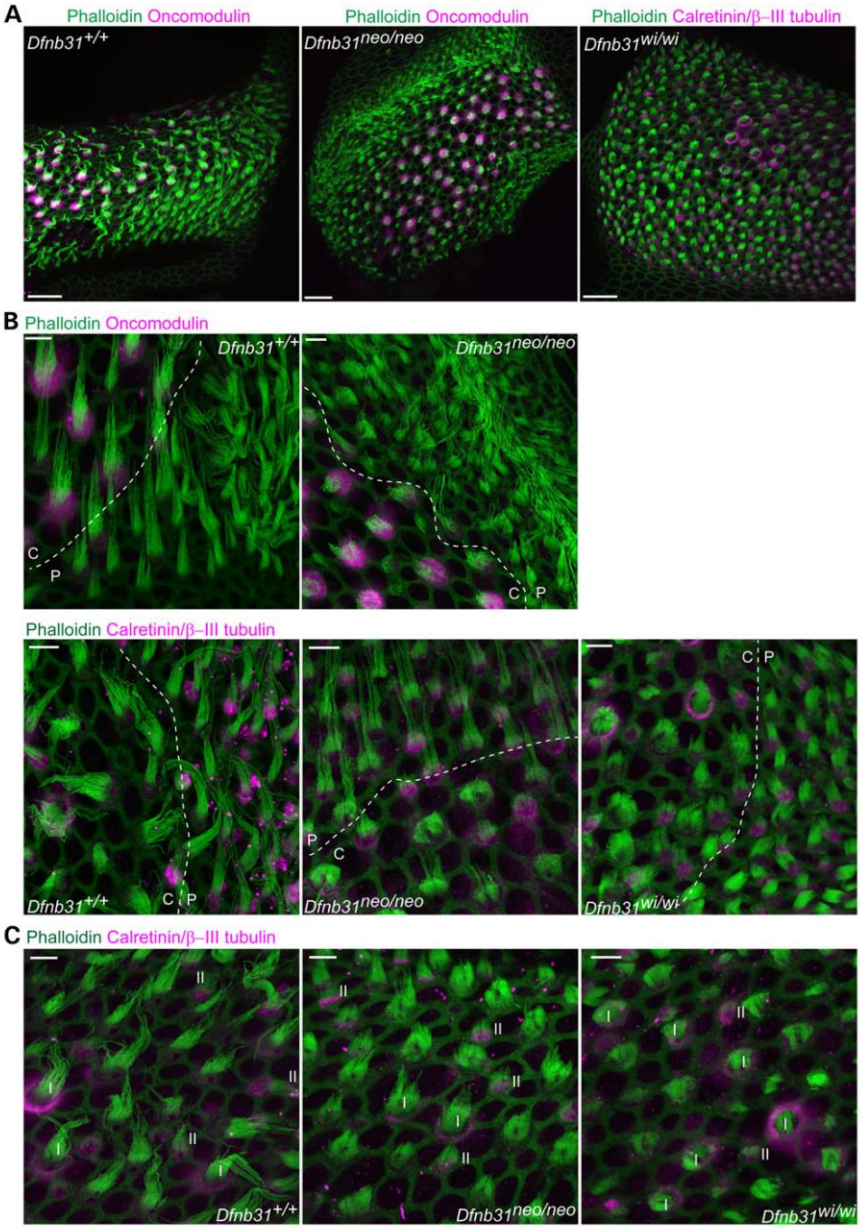

Figure 3. Stereociliary length is differentially affected in the central and peripheral regions of *Dfnb31*$^{neo/neo}$ but not *Dfnb31*$^{wi/wi}$ cristae. (**A**) Compared with stereociliary bundles of wild-type cristae (phalloidin, green), *Dfnb31*$^{neo/neo}$ stereociliary bundles were short in the central (oncomodulin positive, magenta) but not peripheral (oncomodulin negative) crista and *Dfnb31*$^{wi/wi}$ stereociliary bundles were short throughout the entire crista. Note that the central and peripheral region of *Dfnb31*$^{wi/wi}$ cristae were determined using the combined calretinin and β-III tubulin signals (magenta). Calyceal afferents (magenta circles) around stereociliary bundles are characteristic of type I hair cells in the central region. The images were taken at P4. (**B**) High-magnification images showing hair cell stereociliary bundles around the boundary (dashed lines) between the central (C) and peripheral (P) regions of P4 cristae. Upper row: central regions were labeled by oncomodulin staining. Lower row: central regions were determined by having type I hair cells (labeled as magenta circles) and wide shape of stereociliary bundles. (**C**) Both type I and type II stereociliary bundles were shortened in P4 *Dfnb31*$^{neo/neo}$ and *Dfnb31*$^{wi/wi}$ cristae. Type I (white Is) and type II (white IIs) hair cells were distinguished by combined calretinin and β-III tubulin signals (magenta circles, type I; magenta spots, type II). Scale bars, 20 μm in A and 5 μm in B and C.

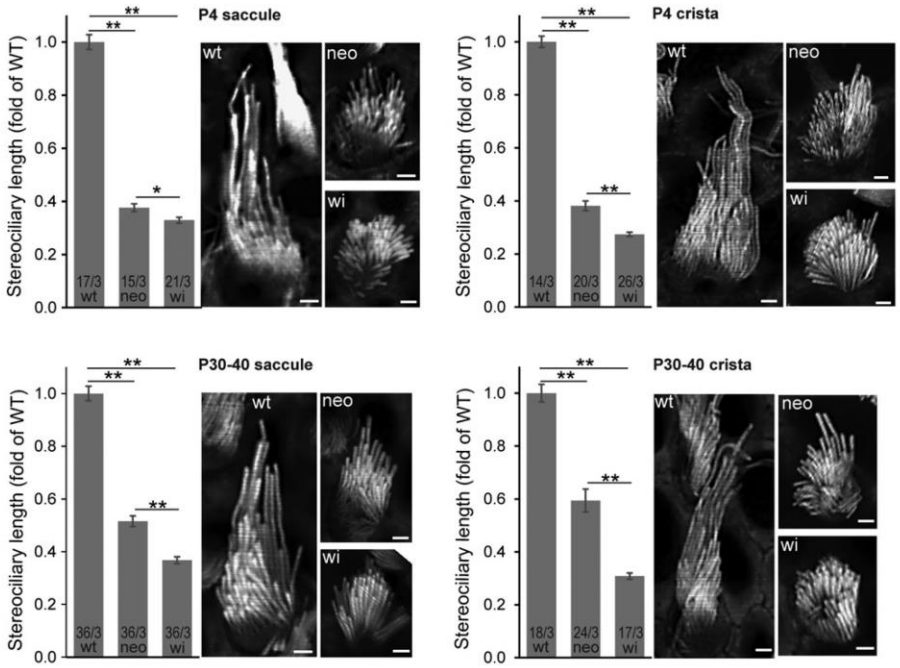

Figure 4. Stereociliary length and staircase arrangement in *Dfnb31*$^{neo/neo}$ and *Dfnb31*$^{wi/wi}$ vestibular hair bundles. Stereociliary length was measured in images captured from phalloidin-stained saccules (left) and cristae (right) at P4 (upper) and P30–40 (low). The stereocilia in both *Dfnb31*$^{neo/neo}$ (neo) and *Dfnb31*$^{wi/wi}$ (wi) vestibular systems were significantly shorter than those in wild-type vestibular system (wt). *Dfnb31*$^{wi/wi}$ vestibular stereocilia were even shorter than *Dfnb31*$^{neo/neo}$ vestibular stereocilia. Student's *t*-tests (two-tail) were performed. Numbers before and after slashes at the bottom of bar charts are the numbers of cells and animals analyzed, respectively. Compared with wild-type and *Dfnb31*$^{neo/neo}$ vestibular hair bundles, *Dfnb31*$^{wi/wi}$ vestibular hair bundles had less obvious staircase arrangement of stereocilia. Error bars, standard error of the mean; $^{**}P < 0.01$; scale bars, 1 μm.

(Fig. 7B; ANOVA, LSD; *Dfnb31*$^{neo/neo}$: $P = 1.0 \times 10^{-5}$; *Dfnb31*$^{wi/wi}$: $P = 4.3 \times 10^{-5}$, Table 1). Similarly, amplitudes were significantly lower (Fig. 7C, p1–n1, $+6dB_{re:1g/ms}$; ANOVA, *Dfnb31*$^{neo/neo}$: $P = 0.01$; *Dfnb31*$^{wi/wi}$: $P = 0.01$) and latencies significantly prolonged in mutant mice compared with wild-type animals (Fig. 7D; $+6dB_{re:1g/ms}$, MANOVA, p1: *Dfnb31*$^{neo/neo}$: $P = 1.0 \times 10^{-7}$; *Dfnb31*$^{wi/wi}$: $P = 5.6 \times 10^{-7}$; n1: *Dfnb31*$^{neo/neo}$: $P = 2.0 \times 10^{-8}$; *Dfnb31*$^{wi/wi}$: $P = 2.2 \times 10^{-7}$; Table 1).

Despite the presence of responses in some mutant animals, the features of the responses reflected highly unusual characteristics (quantitative metrics are summarized in Table 1). Responses bore little resemblance to normal VsEPs. As noted above, response onset latencies were substantially delayed (>2 ms), amplitudes were considerably reduced. In addition, the relationship between latency and stimulus level was, depending on the animal, flat, degraded or, surprisingly, inverted (e.g. latency decreased with decreasing stimulus level). Figure 7C and D illustrates the mean amplitudes and latencies as a function of stimulus level for wild-type, *Dfnb31*$^{neo/neo}$ and *Dfnb31*$^{wi/wi}$ mice. The results for wild-type animals demonstrated the normal systematic increase in amplitudes and decrease in latencies as stimulus level is increased over a wide dynamic range. In contrast, the dynamic range for the responses of the *Dfnb31*$^{neo/neo}$ and *Dfnb31*$^{wi/wi}$ mice was very narrow (reflecting the high thresholds), and on average, latencies and amplitudes changed relatively little with increases in stimulus level (Fig. 7C and D).

Balance behaviors of *Dfnb31*$^{neo/neo}$, *Dfnb31*$^{wi/wi}$ and *Dfnb31*$^{wi/neo}$ mice

We evaluated balance behaviors of *Dfnb31*$^{neo/neo}$, *Dfnb31*$^{wi/wi}$ and *Dfnb31*$^{wi/neo}$ mice using swimming and rotarod tests. Although *Dfnb31*$^{neo/neo}$ and *Dfnb31*$^{wi/neo}$ mice did not show a circling behavior in the cage, they did exhibit irregular swimming behaviors including swimming in a circle and occasional immobile floating. However, *Dfnb31*$^{neo/neo}$ and *Dfnb31*$^{wi/neo}$ mice swam better than *Dfnb31*$^{wi/wi}$ mice, which mostly displayed underwater tumbling (Fig. 8A). A swimming test was also conducted for *Dfnb31*$^{tm1a/tm1a}$ mice, which did not exhibit circling and head-bobbing behaviors. Swimming results of *Dfnb31*$^{tm1a/tm1a}$ mutants were comparable with those of *Dfnb31*$^{neo/neo}$ mutants (data not shown). In the rotarod test, *Dfnb31*$^{neo/neo}$ and *Dfnb31*$^{wi/neo}$ mice were able to stay on the rotating rod longer than *Dfnb31*$^{wi/wi}$ mice but shorter than wild-type mice (Fig. 8B). Additionally, the performance of *Dfnb31*$^{wi/neo}$ mice in the swimming and rotarod tests was similar to *Dfnb31*$^{neo/neo}$ mice (Fig. 8A and B), indicating that the truncated N-whirlin from the *Dfnb31*^{wi} allele plays a negligible role in balance maintenance, consistent with our immunostaining finding that truncated N-whirlin may not exist at the protein level in *Dfnb31*$^{wi/wi}$ VHCs. In summary, the swimming and rotarod tests demonstrate that all tested *Dfnb31* mutant mice have some level of balance problems with the *Dfnb31*$^{wi/wi}$ mice having the worst balance performance.

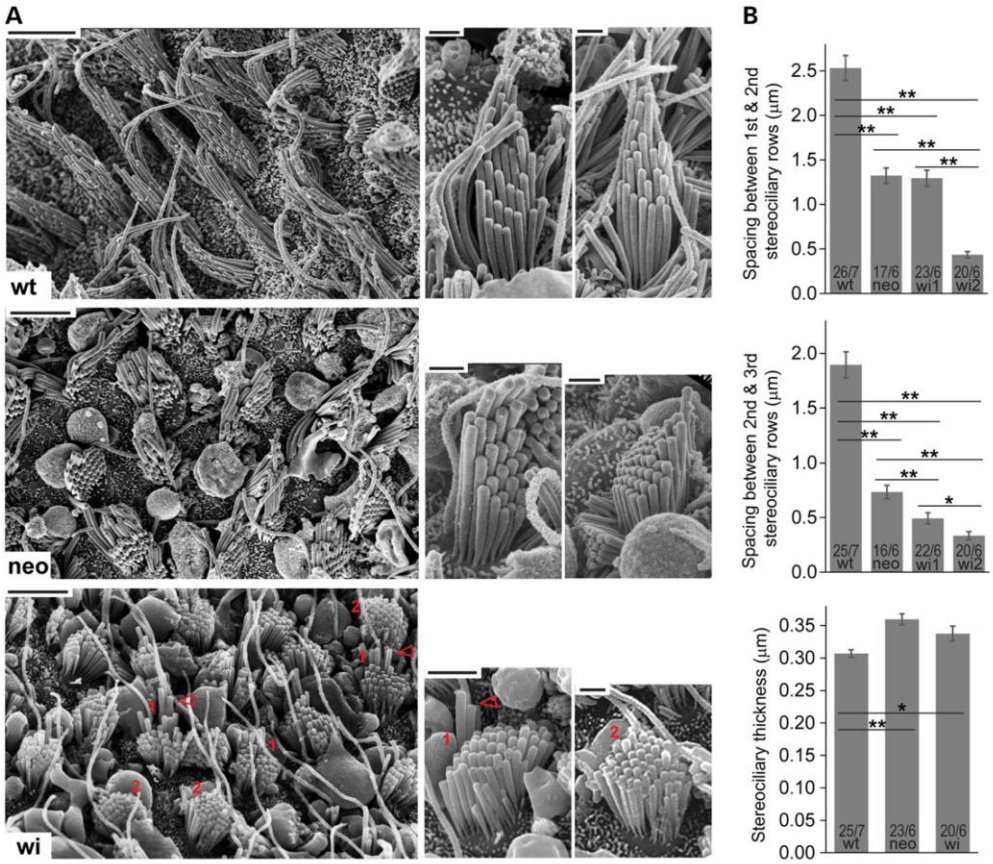

Figure 5. SEM observation of *Dfnb31*$^{neo/neo}$ and *Dfnb31*$^{wi/wi}$ vestibular stereociliary bundles. (**A**) Left, low-magnification images of the sensory epithelium from P45 wild-type (wt), *Dfnb31*$^{neo/neo}$ (neo) and *Dfnb31*$^{wi/wi}$ (wi) otolith organs. Stereociliary length is significantly reduced in *Dfnb31*$^{neo/neo}$ and *Dfnb31*$^{wi/wi}$ vestibular hair bundles, with *Dfnb31*$^{neo/neo}$ hair bundles being longer than *Dfnb31*$^{wi/wi}$ hair bundles. In general, *Dfnb31*$^{neo/neo}$ hair bundles have more obvious staircase arrangement of stereocilia than *Dfnb31*$^{wi/wi}$ hair bundles. However, there appears to be two types of *Dfnb31*$^{wi/wi}$ hair bundles. The *Dfnb31*$^{wi/wi}$ hair bundles labeled by '1' in red have relatively longer tallest stereocilia (red arrows) than the *Dfnb31*$^{wi/wi}$ hair bundles labeled by '2'. Scale bars, 5 μm. Right, representative single stereociliary bundles from wild-type, *Dfnb31*$^{neo/neo}$ and *Dfnb31*$^{wi/wi}$ otolith organs at P40–P45. Besides shorter stereocilia, the *Dfnb31*$^{neo/neo}$ and *Dfnb31*$^{wi/wi}$ vestibular hair bundles have thicker stereocilia. Scale bars, 1 μm. (**B**) Quantification of distance between stereociliary rows and stereociliary thickness. Top, the distances between the tallest and the second tallest stereociliary rows in *Dfnb31*$^{neo/neo}$ and *Dfnb31*$^{wi/wi}$ vestibular bundles are shorter than that in wild-types. Compared with *Dfnb31*$^{neo/neo}$ bundles, wi2 *Dfnb31*$^{wi/wi}$ bundles have a shorter distance and wi1 *Dfnb31*$^{wi/wi}$ bundles have a similar distance. Middle, the distances between the second and third tallest stereociliary rows in *Dfnb31*$^{neo/neo}$ and *Dfnb31*$^{wi/wi}$ vestibular bundles are shorter than that in wild-types, with *Dfnb31*$^{wi/wi}$ bundles having the shortest distance. Bottom, both *Dfnb31*$^{neo/neo}$ and *Dfnb31*$^{wi/wi}$ vestibular bundles have thicker stereocilia than wild-type bundles. Error bars, standard error of the mean; $^{**}P < 0.01$; $^{*}P < 0.05$.

Discussion

This study presents the first definitive evidence that various *Dfnb31* mutations are able to lead to vestibular dysfunction in mice, no matter whether these mutations cause hearing loss with or without retinal degeneration. This finding suggests the possibility that *DFNB31*-deficient patients may have some degree of bilateral vestibulopathy with DFNB31 patients being more severe than USH2D patients. Our study also demonstrates that FL- and C-whirlin deficiencies lead to significant shortening and widening of VHC stereocilia in mice, which may represent an underlying cause of the observed vestibular dysfunction.

Although both FL- and C-whirlins are essential for normal vestibular stereociliary length, our findings demonstrate that they may have slightly different roles. We show that both *Dfnb31*$^{neo/neo}$ and *Dfnb31*$^{wi/wi}$ VHCs have significantly shorter stereocilia than wild-types with *Dfnb31*$^{neo/neo}$ stereocilia being just slightly longer than *Dfnb31*$^{wi/wi}$ stereocilia in most sensory epithelia of the vestibular system, including the entire saccule, utricle and central zone of the crista (Fig. 4 and data not shown). Considering the disruption of FL-whirlin expression in both *Dfnb31*$^{neo/neo}$ and *Dfnb31*$^{wi/wi}$ VHCs and the expression of an intact C-whirlin in *Dfnb31*$^{neo/neo}$ VHCs (Figs 1B, C and 2), the above finding indicates that FL-whirlin but not C-whirlin plays a predominant role in stereociliary elongation in the majority of VHCs. On the other hand, C-whirlin appears more important for stereociliary elongation in the VHCs of the crista peripheral region, because the stereocilia in this region of *Dfnb31*$^{neo/neo}$ mice

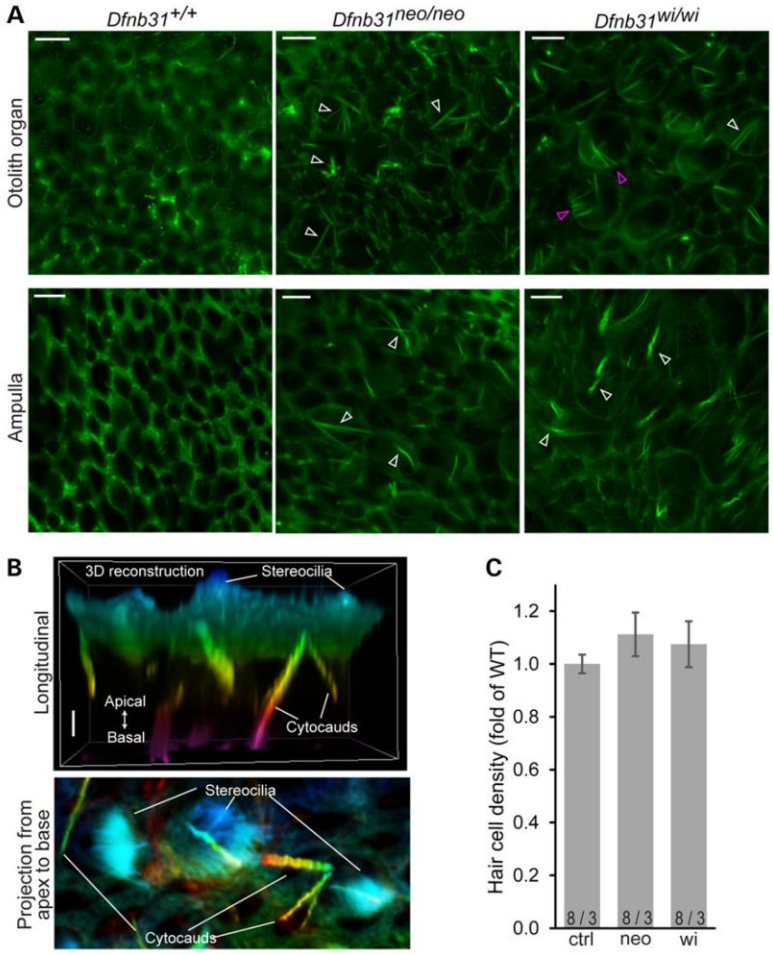

Figure 6. Cytocauds and hair cell densities in *Dfnb31*$^{neo/neo}$ and *Dfnb31*$^{wi/wi}$ vestibular organs. (**A**) Cytocauds (arrows) were revealed in *Dfnb31*$^{neo/neo}$ and *Dfnb31*$^{wi/wi}$ mice by staining otolith organs (upper row) and ampullae (lower row) for phalloidin at P4. Magenta arrows point to cytocauds originating from actin filaments at hair cell lateral surfaces. Images were taken at the level below the cuticular plate of hair cells. (**B**) Three-dimensional reconstruction of phalloidin signals from P4 *Dfnb31*$^{wi/wi}$ utricular hair cells. Upper, longitudinal view of phalloidin signals in the apical portion of hair cells. Lower, projection view of phalloidin signals along the apical–basal axis of hair cells. Phalloidin signals are pseudo-colored using a rainbow scale according to depth along hair cell apical–basal axis. Blue, apical; purple, basal. (**C**) Hair cell densities were analyzed in the striolar region of saccules from control (ctrl), *Dfnb31*$^{neo/neo}$ (neo) and *Dfnb31*$^{wi/wi}$ (wi) mice at P30. There was no significant difference among these genotype groups. Error bars are shown as standard error of the mean. Numbers before and after slashes are the numbers of saccular regions and mice examined, respectively. Student's *t* tests (two-tail) were performed. Scale bars, 5 μm in A and 1 μm in B.

are much longer than those of *Dfnb31*$^{wi/wi}$ mice (Figs. 2Ac and 3A and B). Additionally, C-whirlin may contribute to the formation of different lengths of stereociliary rows in the bundle, which is suggested by the existence of staircase-like stereociliary arrangement in *Dfnb31*$^{neo/neo}$ but not *Dfnb31*$^{wi/wi}$ VHCs (Figs. 2A, 4 and 5). Therefore, although the localization of whirlin isoforms in VHCs is similar to that of developing cochlear inner hair cells, the functional roles of the two whirlin isoforms appear not exactly the same in the two different types of hair cells. In the developing cochlear inner hair cells, C-whirlin is more important than FL-whirlin for normal stereociliary length (10). Furthermore, like in the cochlea (24,25), the change of stereociliary thickness occurs in *Dfnb31*$^{neo/neo}$ and *Dfnb31*$^{wi/wi}$ VHCs, suggesting that whirlin isoforms, especially FL-whirlin, also play a role in vestibular stereociliary thickness. This function could be contributed to by whirlin isoforms at both the stereociliary tip and the ankle link complex in VHCs.

To our knowledge, linear VsEP measurements of the present study represent the first direct testing of peripheral vestibular function in whirlin animal models. Our findings of severe to profound vestibular deficits from otolith organs of both *Dfnb31*$^{neo/neo}$ and *Dfnb31*$^{wi/wi}$ mice may be surprising, given the better performance of *Dfnb31*$^{neo/neo}$ mice in balance behavioral tests, especially

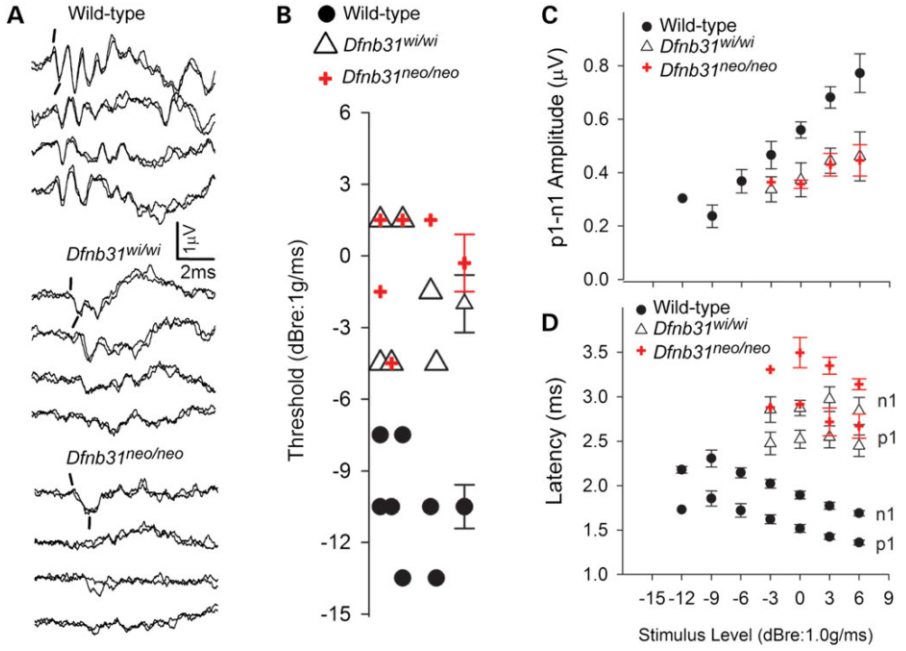

Figure 7. VsEP responses of *Dfnb31*$^{neo/neo}$ and *Dfnb31*$^{wi/wi}$ mice. (**A**) Representative VsEP responses from wild-type, *Dfnb31*$^{wi/wi}$ and *Dfnb31*$^{neo/neo}$ mutant mice. Prominent normal responses are present in wild-type animals, whereas responses are absent or appear as mere remnants of responses in the two mutant mouse groups. Positive peak p1 and negative peak n1 are marked for the first response pairs of each group. (**B**) VsEP threshold distributions are represented for all wild-type (filled circles) mice and for those mutant animals having responses (*Dfnb31*$^{wi/wi}$, open triangle, *Dfnb31*$^{neo/neo}$, plus sign). Mean and standard errors are shown to the right for each group. As can be seen there is no overlap between the distribution of wild-type and mutant genotypes, whereas the whirlin mutants have the same distribution. Mean thresholds for mutant mice were significantly higher than wild-types ($P < 5.0 \times 10^{-5}$). (**C** and **D**) VsEP response amplitudes (C, p1–n1) and latencies (D, p1, n1) as a function of stimulus level for wild-type (filled circles) and mutant mice (*Dfnb31*$^{wi/wi}$, open triangle, *Dfnb31*$^{neo/neo}$, plus sign). There was no overlap of the wild-type and mutant curves. Latencies were significantly prolonged for mutant animals (e.g. p1: $P < 6.0 \times 10^{-7}$) and amplitudes were significantly reduced (p1–n1, $P = 0.01$). Univariate ANOVA or MANOVA and *post hoc* tests with LSD were performed.

Table 1. Summary findings for VsEPs

	Threshold	p1	p1–n1
WT	−10.5 ± 2.45 (7)	1359 ± 72 (7)	0.77 ± 0.19 (7)
Dfnb31$^{wi/wi}$	−2.0 ± 2.9 (6)**	2448 ± 294 (6)***	0.46 ± 0.22 (6)*
Dfnb31$^{neo/neo}$	−0.3 ± 2.7 (5)**	2669 ± 304 (5)***	0.45 ± 0.13 (5)*

Threshold in dB re:1g/ms. p1 latency in μs and p1–n1 amplitude in μV at stimulus level of + 6 $dB_{re:1g/ms}$.
Comparisons made to wild-type (WT) animals: *$P = 0.01$, **$P < 5.0 \times 10^{-5}$, ***$P < 6.0 \times 10^{-7}$. *Post hoc* LSDs.

the swimming test, which significantly reduces proprioceptive compensation. Indeed, the balance behaviors tested in this study require some gravity receptor input to the central nervous system (CNS). The ability of the CNS to compensate for loss of vestibular function is remarkable and even the smallest residual function in many cases provides sufficient information to achieve relatively normal balance behaviors (33). The absence of the VsEP in a majority of *Dfnb31*$^{neo/neo}$ mice (64%) demonstrates that the level of synchronous neural input was exceedingly small, so small that the number of neurons firing synchronously in response to the stimulus was simply too few to be resolved by VsEP measurement. We have reported similar results in other mutants with profound vestibular loss (i.e. absent VsEP with absent or subtle defects in behavior and swimming tests, e.g. in 31). In contrast to the *Dfnb31*$^{neo/neo}$ mice, *Dfnb31*$^{wi/wi}$ animals circled, oriented abnormally in water and remained on the rotating rod for less time. This was true despite evidence of remnant gravity receptor responses in 50% of the *Dfnb31*$^{wi/wi}$ animals. Thus, in *Dfnb31*$^{wi/wi}$ mice, their behaviors indicated that the CNS was probably unable to compensate adequately for the incomplete peripheral loss, and that the dysfunction may extend to central motor control systems and/or to somatomotor reflex circuitry itself.

Evidence supporting a wider influence of whirlin on neural function outside of the inner ear and retina has been provided recently. Whirlin is expressed widely in the central and peripheral nervous system, including somatomotor reflex circuits and has been shown to be absent in these tissues of *Dfnb31*$^{wi/wi}$ mice (25,34,35). It is possible therefore that the complex circuitry supporting behaviors such as swimming is sufficiently compromised to contribute to the severe swimming and locomotor phenotype of the *Dfnb31*$^{wi/wi}$ mouse. A corollary to this hypothesis is that much of the central deficit must be rescued to some extent in the *Dfnb31*$^{neo/neo}$ mouse, since it can successfully orient in the water. This hypothesis requires that C-whirlin serves as a

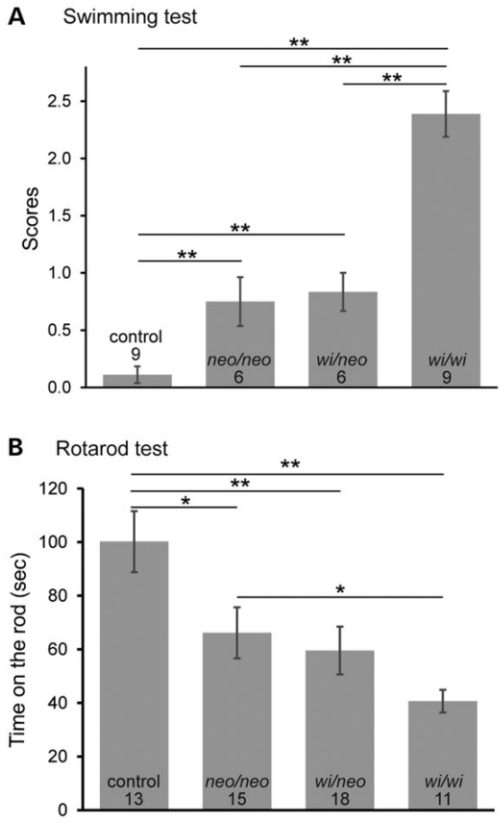

Figure 8. Balance behavioral tests on *Dfnb31*$^{neo/neo}$, *Dfnb31*$^{wi/neo}$ and *Dfnb31*$^{wi/wi}$ mice. (**A**) Swimming test scores of control, *Dfnb31*$^{neo/neo}$ (*neo/neo*), *Dfnb31*$^{wi/neo}$ (*wi/neo*) and *Dfnb31*$^{wi/wi}$ (*wi/wi*) mice at P60. *Dfnb31*$^{neo/neo}$ and *Dfnb31*$^{wi/neo}$ mice were able to swim better than *Dfnb31*$^{wi/wi}$ mice, while the *Dfnb31*$^{neo/neo}$ and *Dfnb31*$^{wi/neo}$ mice had similar swimming behaviors. All *Dfnb31* mutant mice had abnormal swimming behaviors, compared with control mice. Swimming test scores were defined as follows (32): 0, normal swimming; 1, irregular swimming; 2, immobile floating; and 3, underwater tumbling. (**B**) Rotarod test results of control, *Dfnb31*$^{neo/neo}$, *Dfnb31*$^{neo/wi}$ and *Dfnb31*$^{wi/wi}$ mice at P35–45. *Dfnb31*$^{neo/neo}$, *Dfnb31*$^{wi/neo}$ and *Dfnb31*$^{wi/wi}$ mice could not stay on the rotating rod as long as control mice. *Dfnb31*$^{neo/neo}$ and *Dfnb31*$^{wi/neo}$ mice performed better than *Dfnb31*$^{wi/wi}$ mice, while *Dfnb31*$^{neo/neo}$ and *Dfnb31*$^{neo/wi}$ mice had similar levels of performance. Error bars are shown as standard error of the mean. Numbers at the bottom of each bar are numbers of mice tested. Student's *t*-tests (two-tail) were performed. $^{**}P < 0.01$; $^{*}P < 0.05$.

functional replacement for FL-whirlin and partially restores function in neural elements outside of the inner ear and retina.

Another factor that may contribute to better balance behaviors of *Dfnb31*$^{neo/neo}$ mice despite their linear VsEP abnormality similar to *Dfnb31*$^{wi/wi}$ mice is the potential better semicircular canal function of *Dfnb31*$^{neo/neo}$ mice. In the vestibular system, otolith organs are responsible for linear acceleration and gravity sensation, and semicircular canals sense angular acceleration. It has been shown that mice with defective otolith organs, such as *Nox3*, *Otop1*, *Muted* and *Cyba* mice with absent otoconia, do not exhibit circling behaviors (36–39), whereas mice with horizontal semicircular canal problems tend to circle (40,41). We found *Dfnb31*$^{neo/neo}$ mice have much longer VHC stereocilia in the peripheral zone of the crista than *Dfnb31*$^{wi/wi}$ mice, suggesting the possibility that *Dfnb31*$^{neo/neo}$ mice have better semicircular canal function. This could explain the absence and presence of a circling behavior of *Dfnb31*$^{neo/neo}$ and *Dfnb31*$^{wi/wi}$ mice, respectively, despite these two mutants having similar levels of macular dysfunction. The better stereociliary morphology in *Dfnb31*$^{neo/neo}$ cristae may also explain the better rotarod performance of this *Dfnb31* mutant mouse. On the other hand, better semicircular canal function is not likely to explain the improved swimming behavior (i.e. ability to orient and consistently reach the water surface) in *Dfnb31*$^{neo/neo}$ mice, inasmuch as normal semicircular canal function in otoconia-deficient mice does not rescue abnormal swimming behaviors (36–39,42).

DFNB31 mutations have been shown to cause USH2D (1–3), non-syndromic deafness DFNB31 (4,5) and non-syndromic retinal degeneration (6). All of these diseases are characterized by normal vestibular function in human patients. This raises the question of whether the absence of evidence for vestibular dysfunction in the human reflects a real species difference in the consequences of *DFNB31*/*Dfnb31* mutations? Or is there an occult macular deficit in the human that is masked as a result of CNS compensation to peripheral sensory weakness or alternatively a deficit unseen due to a limitation of the assessment methods available for testing human macular function; or perhaps both?

USH2D patients are thought to represent a small fraction of the USH2 patient population as a whole (43). Investigations providing in-depth vestibular, balance and posturography testing of USH2 patients to date have evaluated a relatively small number of subjects [e.g. $n = 9$, (44)]. Although they reported no vestibular deficits in USH2 patients, it is possible that the small sample did not include USH2D patients since genotyping was not possible at that time. Overall, only a limited number of confirmed USH2D patients have been studied (1–3). In most of these cases, no direct measurements of vestibular function were made. Objective vestibular testing was reported in the study of one family which defined USH2D for the first time (3). Testing consisted of recording the medical history of motor development and measuring the response to caloric stimulation. The findings consistently indicated normal vestibular function in USH2D patients. Similarly, only one study examined DFNB31 patients from one family for vestibular dysfunction and concluded normal vestibular function (5), although the details of vestibular function measurement were not given. In fact, a recent survey-based study on patients with non-syndromic deafness DFNB1 shows that 54% of 235 patients may have vestibular dysfunction (45). Therefore, it is possible that in *DFNB31*-deficient patients, a more moderate vestibular macular deficit existed and hypothetically was not apparent as a result of CNS compensation and/or because the tests used were insensitive to macular deficits (e.g. caloric tests). This is a question that may be addressed in the future using more sensitive clinical tests now available including cervical and ocular vestibular-evoked myogenic potentials or off-axis rotational tests. Clarifying these issues will be important if we are to fully understand the mechanisms at work in the development of *DFNB31*/*Dfnb31*-related diseases in both humans and mice.

In summary, our molecular, morphological, direct functional and behavioral studies on the vestibular system of whirlin mutant mice demonstrate that the expression and localization of FL- and C-whirlins in VHCs are similar to those found in developing cochlear inner hair cells with both whirlins at stereociliary tips and only FL-whirlin at the ankle link complex. Both FL- and C-whirlin proteins are indispensable for normal vestibular

stereociliary dimensions, macular neuroepithelial function and balance behaviors.

Materials and Methods

Animals

Dfnb31 targeted mutant (*Dfnb31*$^{neo/neo}$ also known as *Dfnb31*^{tm1Tili}, MGI:4462398) and whirler (*Dfnb31*$^{wi/wi}$, MGI:1857090) mice were described previously (4,7). *Dfnb31*$^{wi/neo}$ mice were generated by crossing *Dfnb31*$^{neo/neo}$ and *Dfnb31*$^{wi/wi}$ mice. *Dfnb31*$^{tm1a(EUCOMM)wtsi}$ mice (MGI:4432119) were purchased as frozen sperms from EUCOMM and revived at the University of Utah Transgenic and Gene Targeting mouse core. All experiments involving animals were performed in compliance with the Institutional Animal Care and Use Committees at the University of Utah and the University of Nebraska-Lincoln.

Antibodies and reagents

Two His tag-fused whirlin fragments (1–124 aa and 375–800 aa, NP_082916, in pET28 vector) were expressed in BL21-CodonPlus (DE3)-RIPL cells (Agilent Technologies, Santa Clara, CA, USA), and purified by chromatography using Ni^{2+}-charged His•Bind resin (EMD Millipore, Billerica, MA, USA). Two GST-fused whirlin fragments (1–472 aa and 721–907 aa, NP_082916, in pGEX-4T-1 vector) were expressed in the same BL21 cells as above, and purified by chromatography using glutathione sepharose™ 4 Fast Flow resin (GE Healthcare Life Sciences, Pittsburgh, PA, USA). The purified His-tagged whirlin proteins were used to immunize rabbits, and antibodies against whirlin were affinity-purified against the corresponding GST-tagged whirlin fragments. The specificity of the purified antibodies was confirmed by immunoblotting of recombinant whirlin N- and C-terminal fragments expressed in HEK293 cells (data not shown). Antibodies against calretinin, β-III tubulin (TUJ1) and oncomodulin were purchased from Millipore (Temecula, CA, USA), Covance (Princeton, NJ, USA) and Santa Cruz Biotechnology (Dallas, TX, USA), respectively. Alexa fluorochrome-conjugated phalloidin and secondary antibodies were obtained from Life Technologies (Grand Island, NY, USA).

RNA isolation and RT–PCR

Total RNA was extracted from P4 mouse vestibular organs using SurePrep™ RNA Purification Kit (Fisher BioReagents®, Fair Lawn, NJ, USA). RT–PCR was conducted from total RNA using Thermoscript RT–PCR kit (Life Technologies) and Expand Long Template PCR System (Roche Life Science, Indianapolis, IN, USA). Manufacturer's instructions were followed exactly during RNA isolation and RT–PCR.

Immunofluorescence, 3D reconstruction and SEM

Procedures for immunofluorescence of mouse vestibular tissues were the same as previously reported (16). Fluorescent images were taken using a confocal laser scanning microscope (Model FV1000, Olympus, Tokyo, Japan). To build the 3D reconstruction of confocal images, a series of images taken at a 0.2-μm step along the z-axis were first deconvoluted using Autoquant ×3 (Bitplane, South Windsor, CT, USA) and then reconstructed using Elements software from Nikon (Melville, NY, USA). Z-dimensional data were converted to lambda and coded by pseudocolor. First and last stacks were assigned to the two end wavelengths of rainbow, while middle stacks obtained wavelength values in between. SEM procedures were described previously (16).

Measurements of vestibular stereociliary length, thickness, distance between stereociliary rows and hair cell density

All measurements were performed blind to genotype using ImageJ. Stereociliary length of the vestibular system was measured in confocal images of phalloidin-stained whole-mounts. Measurements were performed on the longest stereocilia in the bundle exclusively in the central region of cristae and mostly in the extrastriolar region of saccules. Stereociliary thickness and distance between stereociliary rows were assessed using SEM images of mouse otolith organs. For the stereociliary thickness, two stereocilia in the tallest row of one bundle were measured and averaged. The distance between the tallest and the second tallest rows as well as the distance between the second and third tallest rows were measured in hair bundles with discernable stereociliary rows. To calculate the hair cell density, total numbers of hair bundles within an area of 1778 μm^2 were counted at the saccular striola. The hair cell densities of whirlin mutant mice were normalized by the hair cell density of wild-type mice.

Swimming and rotarod tests

For swimming tests, mice were placed in a large container filled with warm water. Their swimming behaviors were observed blind to genotype. Scores of 0–3 were assigned according to the criteria published previously (32). In short, a score of 0 denoted normal swimming behaviors, while scores of increasing numbers indicated an increasing severity of abnormal swimming behaviors with a score of 3 being underwater tumbling. Rotarod tests were performed on adult mice using a ROTO-ROD Series 8 machine (IITC Life Science, Woodland Hills, CA, USA) over a period of 3 consecutive days. Mice were trained the first 2 days and tested on the third day during the same time period of the day to eliminate a circadian behavioral difference. Before any trials each day, mice were maintained in the test room for at least 30 min to adapt to the environment. Five trials per day were conducted. During each trial, mice were kept on a rotating rod for a maximum period of 180 s or until they fell. The rotating rod started at a speed of 5 rpm, increased to 10 rpm in 120 s, and remained at 10 rpm on day 1. The rotating speed was then changed to 7 rpm at the beginning, accelerated to 15 rpm in 120 s and kept at 15 rpm on day 2. On day 3, the rotating rod was initiated at 15 rpm and accelerated to 25 rpm in 120 s. Between the five trials on the same day, mice were given a 5 min rest with free access to food and water. On day 3, the lengths of time mice were able to stay on the rotating rod were recorded and averaged from the five trials of the same mice.

Vestibular sensory-evoked potential

The linear VsEP is a compound action potential produced by eighth nerve neurons innervating gravity receptors (otolith organs) and their central relays in the brainstem (33,46–48). During VsEP testing, mice were deeply anesthetized by intraperitoneal injection of ketamine/xylazine (18:2 mg/ml; 5–7 μl/g body weight) followed by maintenance doses of 0.05 ml every 60 min as needed to maintain adequate anesthesia. Core body temperature was maintained at 37.0 ± 0.2°C using a homeothermic heating blanket system.

VsEP recordings were based on methods published previously (46,48,49). Briefly, vestibular stimuli (linear head translations) were delivered by securing the mouse head to a mechanical shaker (Model ET-132203, Labworks Inc., Costa Mesa, CA, USA) using a non-invasive head clip. Linear acceleration ramps (17 pulses/s, 2 ms duration) were used to generate rectangular (step) jerk stimuli specified in units of g/ms, where 1 g = 9.8 m/s^2, that were in turn applied to the head. Jerk stimuli ranged in amplitude from + 6 to −18dBre:1 g/ms and were adjusted in levels of 3 dB. Stimuli were presented to the head in the naso-occipital axis, thus stimulating both saccular and utricular receptors.

Subcutaneous needle electrodes were placed posterior to the right pinna and at the right hip for inverting and ground electrodes, respectively. Stainless-steel wire placed subcutaneously at the nuchal crest served as the non-inverting electrode. Electroencephalographic activity was amplified (×200 000), filtered (300–3000 Hz) and digitized (1024 points at 10 μs/point). Two hundred and fifty-six primary responses were averaged and replicated for each VsEP waveform. A VsEP intensity series was collected beginning at the maximum stimulus level (i.e. +6 dB re: 1.0 g/ms) with and without acoustic masking (50–50 000 Hz forward masker at 90 dB SPL), and then stimulus levels were increased from −18 dB to +6 dBre:1 g/ms in 3 dB steps to determine vestibular response threshold. Threshold was defined as the stimulus level halfway between the highest level failing to produce a response and the lowest level producing a response.

The first two VsEP positive (p1) and negative (n1) response peaks were scored. Latency was defined as the elapsed time from the stimulus onset to the scored response peak (μs). Response amplitudes were defined as the amplitude of the positive peak (in microvolts) minus the amplitude of the negative peak (p1–n1). These provided response measures for vestibular peripheral nerve response onset latencies and amplitudes (47). These response metrics as well as threshold were used to evaluate the effects of genotype.

Statistics

Student's *t*-tests were conducted using Microsoft Office Excel to compare the following values between two genotype groups: stereociliary lengths, stereociliary thicknesses, distances between stereociliary rows, cell densities, swimming scores and times remaining on Rotarod. A *P*-value of <0.05 was considered to indicate a statistically significant difference between groups. For VsEP data, univariate ANOVA or MANOVA (SPSS v.22, Chicago, IL, USA) was used to compare latencies, amplitudes and thresholds between genotypes and LSD was used for *post hoc* tests.

Supplementary Material

Supplementary Material is available at *HMG* online.

Acknowledgements

We thank the Wellcome Trust Sanger Institute Mouse Genetics Project (Sanger MGP) and its funders for providing the mutant mouse line (Allele: *Dfnb31*$^{tm1a(EUCOMM)wtsi}$).

Conflict of Interest statement. None declared.

Funding

This work was supported by the National Institutes of Health (EY020853 to J.Y., EY014800 to the Department of Ophthalmology and Visual Sciences, University of Utah); Research to Prevent Blindness, Inc. (to J.Y. and the Department of Ophthalmology and Visual Sciences, University of Utah); Hearing Health Foundation; the Nebraska Tobacco Settlement Biomedical Research Foundation (T.A.J, S.M.J.); Department of Special Education and Communication Disorders, UNL (T.A.J., S.V.) and a startup package from the Moran Eye Center, University of Utah (to J.Y.).

References

1. Audo, I., Bujakowska, K., Mohand-Said, S., Tronche, S., Lancelot, M.E., Antonio, A., Germain, A., Lonjou, C., Carpentier, W., Sahel, J.A. *et al.* (2011) A novel DFNB31 mutation associated with Usher type 2 syndrome showing variable degrees of auditory loss in a consanguineous Portuguese family. *Mol. Vis.*, **17**, 1598–1606.
2. Besnard, T., Vache, C., Baux, D., Larrieu, L., Abadie, C., Blanchet, C., Odent, S., Blanchet, P., Calvas, P., Hamel, C. *et al.* (2012) Non-USH2A mutations in USH2 patients. *Hum. Mutat.*, **33**, 504–510.
3. Ebermann, I., Scholl, H.P., Charbel Issa, P., Becirovic, E., Lamprecht, J., Jurklies, B., Millan, J.M., Aller, E., Mitter, D. and Bolz, H. (2007) A novel gene for Usher syndrome type 2: mutations in the long isoform of whirlin are associated with retinitis pigmentosa and sensorineural hearing loss. *Hum. Genet.*, **121**, 203–211.
4. Mburu, P., Mustapha, M., Varela, A., Weil, D., El-Amraoui, A., Holme, R.H., Rump, A., Hardisty, R.E., Blanchard, S., Coimbra, R.S. *et al.* (2003) Defects in whirlin, a PDZ domain molecule involved in stereocilia elongation, cause deafness in the whirler mouse and families with DFNB31. *Nat. Genet.*, **34**, 421–428.
5. Tlili, A., Charfedine, I., Lahmar, I., Benzina, Z., Mohamed, B.A., Weil, D., Idriss, N., Drira, M., Masmoudi, S. and Ayadi, H. (2005) Identification of a novel frameshift mutation in the DFNB31/WHRN gene in a Tunisian consanguineous family with hereditary non-syndromic recessive hearing loss. *Hum. Mutat.*, **25**, 503–507.
6. Nishiguchi, K.M., Tearle, R.G., Liu, Y.P., Oh, E.C., Miyake, N., Benaglio, P., Harper, S., Koskiniemi-Kuendig, H., Venturini, G., Sharon, D. *et al.* (2013) Whole genome sequencing in patients with retinitis pigmentosa reveals pathogenic DNA structural changes and NEK2 as a new disease gene. *Proc. Natl Acad. Sci. USA*, **110**, 16139–16144.
7. Yang, J., Liu, X., Zhao, Y., Adamian, M., Pawlyk, B., Sun, X., McMillan, D.R., Liberman, M.C. and Li, T. (2010) Ablation of whirlin long isoform disrupts the USH2 protein complex and causes vision and hearing loss. *PLoS Genet.*, **6**, e1000955.
8. Wright, R.N., Hong, D.H. and Perkins, B. (2012) RpgrORF15 connects to the usher protein network through direct interactions with multiple whirlin isoforms. *Invest. Ophthalmol. Vis. Sci.*, **53**, 1519–1529.
9. Kikkawa, Y., Mburu, P., Morse, S., Kominami, R., Townsend, S. and Brown, S.D. (2005) Mutant analysis reveals whirlin as a dynamic organizer in the growing hair cell stereocilium. *Hum. Mol. Genet.*, **14**, 391–400.
10. Mathur, P., Zou, J., Zheng, T., Almishaal, A., Wang, Y., Chen, Q., Wang, L., Vashist, D., Brown, S., Park, A. *et al.* (2015) Distinct expression and function of whirlin isoforms in the inner ear and retina: an insight into pathogenesis of USH2D and DFNB31. *Hum. Mol. Genet.*, doi: 10.1093/hmg/ddv339.
11. Holme, R.H., Kiernan, B.W., Brown, S.D. and Steel, K.P. (2002) Elongation of hair cell stereocilia is defective in the mouse mutant whirler. *J. Comp. Neurol.*, **450**, 94–102.

12. Chen, Q., Zou, J., Shen, Z., Zhang, W. and Yang, J. (2014) Whirlin and PDZ domain containing 7 (PDZD7) proteins are both required to form the quaternary protein complex associated with Usher syndrome type 2. *J. Biol. Chem.*, **289**, 36070–36088.
13. Michalski, N., Michel, V., Bahloul, A., Lefevre, G., Barral, J., Yagi, H., Chardenoux, S., Weil, D., Martin, P., Hardelin, J.P. *et al.* (2007) Molecular characterization of the ankle-link complex in cochlear hair cells and its role in the hair bundle functioning. *J. Neurosci.*, **27**, 6478–6488.
14. Goodyear, R.J., Marcotti, W., Kros, C.J. and Richardson, G.P. (2005) Development and properties of stereociliary link types in hair cells of the mouse cochlea. *J. Comp. Neurol.*, **485**, 75–85.
15. Grati, M., Shin, J.B., Weston, M.D., Green, J., Bhat, M.A., Gillespie, P.G. and Kachar, B. (2012) Localization of PDZD7 to the stereocilia ankle-link associates this scaffolding protein with the Usher syndrome protein network. *J. Neurosci.*, **32**, 14288–14293.
16. Zou, J., Zheng, T., Ren, C., Askew, C., Liu, X.P., Pan, B., Holt, J.R., Wang, Y. and Yang, J. (2014) Deletion of PDZD7 disrupts the Usher syndrome type 2 protein complex in cochlear hair cells and causes hearing loss in mice. *Hum. Mol. Genet.*, **23**, 2374–2390.
17. Belyantseva, I.A., Boger, E.T., Naz, S., Frolenkov, G.I., Sellers, J.R., Ahmed, Z.M., Griffith, A.J. and Friedman, T.B. (2005) Myosin-XVa is required for tip localization of whirlin and differential elongation of hair-cell stereocilia. *Nat. Cell Biol.*, **7**, 148–156.
18. Delprat, B., Michel, V., Goodyear, R., Yamasaki, Y., Michalski, N., El-Amraoui, A., Perfettini, I., Legrain, P., Richardson, G., Hardelin, J.P. *et al.* (2005) Myosin XVa and whirlin, two deafness gene products required for hair bundle growth, are located at the stereocilia tips and interact directly. *Hum. Mol. Genet.*, **14**, 401–410.
19. Fleming, J., Rogers, M.J., Brown, S.D. and Steel, K.P. (1994) Linkage analysis of the whirler deafness gene on mouse chromosome 4. *Genomics*, **21**, 42–48.
20. Simmons, D.D., Tong, B., Schrader, A.D. and Hornak, A.J. (2010) Oncomodulin identifies different hair cell types in the mammalian inner ear. *J. Comp. Neurol.*, **518**, 3785–3802.
21. Desai, S.S., Zeh, C. and Lysakowski, A. (2005) Comparative morphology of rodent vestibular periphery. I. Saccular and utricular maculae. *J. Neurophysiol.*, **93**, 251–266.
22. Li, A., Xue, J. and Peterson, E.H. (2008) Architecture of the mouse utricle: macular organization and hair bundle heights. *J. Neurophysiol.*, **99**, 718–733.
23. Pujol, R., Pickett, S.B., Nguyen, T.B. and Stone, J.S. (2014) Large basolateral processes on type II hair cells comprise a novel processing unit in mammalian vestibular organs. *J. Comp. Neurol.*, **522**, 3141–3159.
24. Mogensen, M.M., Rzadzinska, A. and Steel, K.P. (2007) The deaf mouse mutant whirler suggests a role for whirlin in actin filament dynamics and stereocilia development. *Cell Motil. Cytoskeleton*, **64**, 496–508.
25. Wang, L., Zou, J., Shen, Z., Song, E. and Yang, J. (2012) Whirlin interacts with espin and modulates its actin-regulatory function: an insight into the mechanism of Usher syndrome type II. *Hum. Mol. Genet.*, **21**, 692–710.
26. Anniko, M., Sobin, A. and Wersall, J. (1980) Vestibular hair cell pathology in the Shaker-2 mouse. *Arch. Otorhinolaryngol.*, **226**, 45–50.
27. Probst, F.J., Fridell, R.A., Raphael, Y., Saunders, T.L., Wang, A., Liang, Y., Morell, R.J., Touchman, J.W., Lyons, R.H., Noben-Trauth, K. *et al.* (1998) Correction of deafness in shaker-2 mice by an unconventional myosin in a BAC transgene. *Science*, **280**, 1444–1447.
28. Beyer, L.A., Odeh, H., Probst, F.J., Lambert, E.H., Dolan, D.F., Camper, S.A., Kohrman, D.C. and Raphael, Y. (2000) Hair cells in the inner ear of the pirouette and shaker 2 mutant mice. *J. Neurocytol.*, **29**, 227–240.
29. Kanzaki, S., Beyer, L.A., Canlon, B., Meixner, W.M. and Raphael, Y. (2002) The cytocaud: a hair cell pathology in the waltzing Guinea pig. *Audiol. Neurootol.*, **7**, 289–297.
30. Mustapha, M., Beyer, L.A., Izumikawa, M., Swiderski, D.L., Dolan, D.F., Raphael, Y. and Camper, S.A. (2007) Whirler mutant hair cells have less severe pathology than shaker 2 or double mutants. *J. Assoc. Res. Otolaryngol.*, **8**, 329–337.
31. Goodyear, R.J., Jones, S.M., Sharifi, L., Forge, A. and Richardson, G.P. (2012) Hair bundle defects and loss of function in the vestibular end organs of mice lacking the receptor-like inositol lipid phosphatase PTPRQ. *J. Neurosci.*, **32**, 2762–2772.
32. Hardisty-Hughes, R.E., Parker, A. and Brown, S.D. (2010) A hearing and vestibular phenotyping pipeline to identify mouse mutants with hearing impairment. *Nat. Protoc.*, **5**, 177–190.
33. Jones, S.M. and Jones, T.A. (2014) Genetics of peripheral vestibular dysfunction: lessons from mutant mouse strains. *J. Am. Acad. Audiol.*, **25**, 289–301.
34. Yap, C.C., Liang, F., Yamazaki, Y., Muto, Y., Kishida, H., Hayashida, T., Hashikawa, T. and Yano, R. (2003) CIP98, a novel PDZ domain protein, is expressed in the central nervous system and interacts with calmodulin-dependent serine kinase. *J. Neurochem.*, **85**, 123–134.
35. Green, J.A., Yang, J., Grati, M., Kachar, B. and Bhat, M.A. (2013) Whirlin, a cytoskeletal scaffolding protein, stabilizes the paranodal region and axonal cytoskeleton in myelinated axons. *BMC Neurosci.*, **14**, 96.
36. Nakano, Y., Longo-Guess, C.M., Bergstrom, D.E., Nauseef, W.M., Jones, S.M. and Banfi, B. (2008) Mutation of the Cyba gene encoding p22phox causes vestibular and immune defects in mice. *J. Clin. Invest.*, **118**, 1176–1185.
37. Lyon, M.F. (1951) Hereditary absence of otoliths in the house mouse. *J. Physiol.*, **114**, 410–418.
38. Paffenholz, R., Bergstrom, R.A., Pasutto, F., Wabnitz, P., Munroe, R.J., Jagla, W., Heinzmann, U., Marquardt, A., Bareiss, A., Laufs, J. *et al.* (2004) Vestibular defects in head-tilt mice result from mutations in Nox3, encoding an NADPH oxidase. *Genes Dev.*, **18**, 486–491.
39. Hurle, B., Ignatova, E., Massironi, S.M., Mashimo, T., Rios, X., Thalmann, I., Thalmann, R. and Ornitz, D.M. (2003) Non-syndromic vestibular disorder with otoconial agenesis in tilted/mergulhador mice caused by mutations in otopetrin 1. *Hum. Mol. Genet.*, **12**, 777–789.
40. Jen, J.C. (2009) Bilateral vestibulopathy: clinical, diagnostic, and genetic considerations. *Semin. Neurol.*, **29**, 528–533.
41. Cryns, K., van Alphen, A.M., van Spaendonck, M.P., van de Heyning, P.H., Timmermans, J.P., de Zeeuw, C.I. and van Camp, G. (2004) Circling behavior in the Ecl mouse is caused by lateral semicircular canal defects. *J. Comp. Neurol.*, **468**, 587–595.
42. Zhao, X., Jones, S.M., Yamoah, E.N. and Lundberg, Y.W. (2008) Otoconin-90 deletion leads to imbalance but normal hearing: a comparison with other otoconia mutants. *Neuroscience*, **153**, 289–299.
43. Mathur, P. and Yang, J. (2015) Usher syndrome: hearing loss, retinal degeneration and associated abnormalities. *Biochim. Biophys. Acta*, **1852**, 406–420.
44. Moller, C.G., Kimberling, W.J., Davenport, S.L., Priluck, I., White, V., Biscone-Halterman, K., Odkvist, L.M., Brookhouser,

P.E., Lund, G. and Grissom, T.J. (1989) Usher syndrome: an otoneurologic study. *Laryngoscope*, **99**, 73–79.
45. Dodson, K.M., Blanton, S.H., Welch, K.O., Norris, V.W., Nuzzo, R.L., Wegelin, J.A., Marin, R.S., Nance, W.E., Pandya, A. and Arnos, K.S. (2011) Vestibular dysfunction in DFNB1 deafness. *Am. J. Med. Genet. A*, **155A**, 993–1000.
46. Jones, T.A. and Jones, S.M. (1999) Short latency compound action potentials from mammalian gravity receptor organs. *Hear. Res.*, **136**, 75–85.
47. Nazareth, A.M. and Jones, T.A. (1998) Central and peripheral components of short latency vestibular responses in the chicken. *J. Vestib. Res.*, **8**, 233–252.
48. Jones, S.M., Erway, L.C., Johnson, K.R., Yu, H. and Jones, T.A. (2004) Gravity receptor function in mice with graded otoconial deficiencies. *Hear. Res.*, **191**, 34–40.
49. Mock, B., Jones, T.A. and Jones, S.M. (2011) Gravity receptor aging in the CBA/CaJ strain: a comparison to auditory aging. *J. Assoc. Res. Otolaryngol.*, **12**, 173–183.

CHAPTER 5

DISCUSSION

Introduction

Usher Syndrome (USH) is one of the major causes of deaf-blindness worldwide, with an estimated frequency of 1:6000 (Kimberling et al., 2010). USH is an autosomal recessive genetic disease and there is no cure to date. More than 16 loci have been associated with USH. In addition, it is predicted that there are several unidentified loci/genes associated with USH yet to be discovered (Vozzi et al., 2011). Based on the severity of the disease, USH has been subdivided into three categories. USH1 is the most severe, wherein patients have congenital hearing loss, early onset retinal degeneration, and vestibular disorder. USH2 is the most prevalent, wherein patients have moderate congenital hearing loss and retinal degeneration starting as early as adolescence. USH3 patients have progressive hearing loss, retinal degeneration, and variable vestibular deficits.

Sensorineural hearing loss and vestibular deficit in USH patients occur primarily due to defective hair cells in the inner ear. In the cochlea, the coil-shaped organ of Corti is positioned on top of the basilar membrane, which resonates in response to vibrations induced by sound waves. The organ of Corti has three rows of outer hair cells (OHCs) and one row of inner hair cells (IHCs). Each sensory hair cell contains a stereociliary bundle composed of actin-based stereocilia, derived from microvilli, and a transient microtubule-based kinocilium. OHC stereocilia tips are inserted into the overlying tectorial membrane. Therefore, vibration of the basilar membrane develops a shear that deflects and stimulates the OHC stereocilia. The resulting mechanotransduction response induces longitudinal oscillation of the OHC cell body and thus amplifies the vibration of the basilar membrane. The amplified signals subsequently deflect the stereociliary bundle

of inner hair cells (IHCs) that synapse with the afferent spiral ganglion auditory nerve fibers and send the signal to the brain. Stereocilia in the vestibular hair cells (VHCs) sense movement of the head and they function in a similar manner to those of cochlear hair cells. The specialized stereocilia in the hair cells receive sound/head-movement inputs, which makes the organization, arrangement and development of these stereocilia crucial for normal hearing and balance. A developing hair cell has several stereociliary links, including kinociliary links, shaft links, tip links, and ankle links, that connect one stereocilium to its neighboring stereocilia (Fig. 5.1A). Tip links connect the tips of shorter stereocilia to the lateral wall of its neighboring taller stereocilia and are essential for ion channel opening during mechanotransduction. Kinociliary links connect the kinocilium with its neighboring stereocilia, while shaft links connect adjacent stereocilia to each other. These links are thought to be required for bundle development and maintenance (Goodyear, Marcotti, Kros, & Richardson, 2005). Ankle links are present at the stereociliary base transiently (postnatal day (P) 2 – 12) in the organ of Corti hair cells, and permanently in the VHCs. Ankle links are required for the organization of a developing organ of Corti hair cell bundle and are also thought to have a signaling function (Michalski et al., 2007). USH proteins are localized at different regions in the hair cell stereocilia, and are required directly or indirectly for receiving and processing sound/balance inputs.

Retinal degeneration in USH patients occurs in the form of retinitis pigmentosa (RP), with night-blindness and tunnel vision as typical symptoms. These symptoms arise as a result of degeneration of rod photoreceptors in the retina. Cone photoreceptors degenerate in advanced RP stages and could lead to complete blindness. Photoreceptors

Figure 5.1: Structure of a rod photoreceptor and a developing inner ear hair cell.
(A) A developing inner ear hair cell (P2-12) has ankle links present at the base of stereocilia. Other shaft links are also present. Tip links connect neighboring short stereocilia in the adjacent row and are required for mechanotransduction. (B) A rod photoreceptor has an outer segment with discs that contain rhodopsin. Rhodopsin receives light in the form of photons. The photoreceptor inner segment contains mainly organelles required for metabolism. The periciliary membrane complex (in blue) is located above the basal body in the apical region of inner segment, close to the outer segment. The cell body contains the photoreceptor nucleus, while the synaptic region contains ribbon synapses.

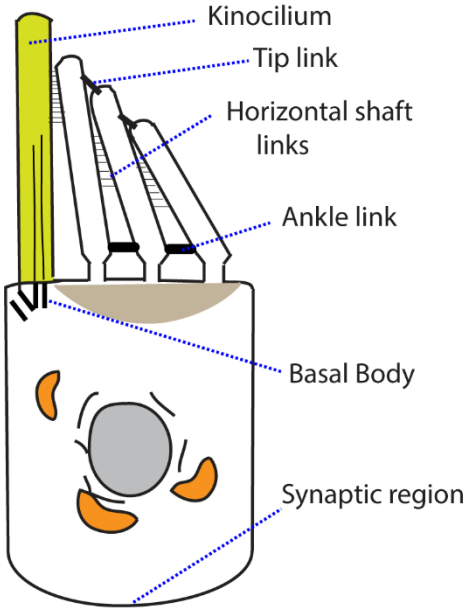
Kinocilium
Tip link
Horizontal shaft links
Ankle link
Basal Body
Synaptic region

A

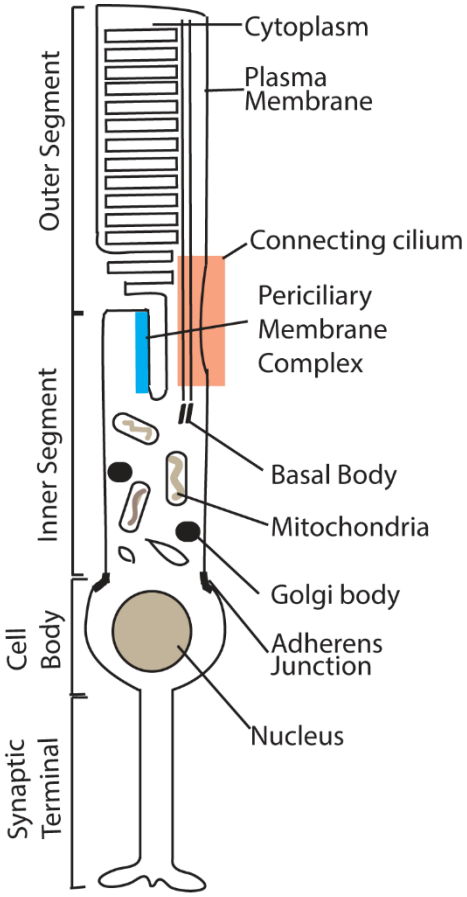
Outer Segment
Inner Segment
Cell Body
Synaptic Terminal
Cytoplasm
Plasma Membrane
Connecting cilium
Periciliary Membrane Complex
Basal Body
Mitochondria
Golgi body
Adherens Junction
Nucleus

B

are special sensory neurons that sense light. Photons are received by rhodopsin present on the outer segment photoreceptors discs. The outer segment lacks protein production machinery and relies on the inner segment for its supply of proteins. The periciliary membrane complex (PMC) is located at the apex of the inner segment above the basal body and is supposedly involved in transporting protein cargos from the inner to the outer segment (Fig. 5.1B) (Yang et al., 2010a). USH proteins are localized at different locations within photoreceptors and are likely required for photoreceptor maintenance and function.

Despite many years of research on USH genes, the molecular mechanisms by which their disruption causes hearing loss remains unexplained. Specifically, for most USH genes, mutations in different regions of the same genes can cause either USH or other discrete diseases (Table 5.1). For example, mutations in a recently identified USH1 gene, *CIB2*, may either lead to USH1J, a subtype of USH1, or DFNB48, a subtype of DFNB (nonsyndromic autosomal recessive deafness) (Riazuddin et al., 2012). Understanding molecular mechanisms underlying this variability will be essential for not only early and accurate diagnosis but also developing therapies. To address this issue, I studied an USH2 gene, *DFNB31,* that produces a protein called whirlin.

Mutations in *DFNB31* cause variable disease manifestations

Mutations in *DFNB31* lead to either USH2D, a subtype of USH2, or DFNB31, a subtype of DFNB. USH2D patients have a moderate level of hearing loss and retinitis pigmentosa (RP), while DFNB31 patients have profound sensorineural hearing loss and normal vision. The *DFNB31* gene was identified as one of the causes of DFNB in 2003,

Table 5.1: USH genes other than DFNB31 showing different disease manifestations.

Gene name	Diseases associated		Total number of protein isoforms found	References
	USH subtype	Other diseases		
MYO7A	USH1B	DFNB2, DFNA11, atypical USH	1	(Liu et al. 1998; Liu et al. 1999; Liu et al. 1997; Riazuddin et al. 2008)
USH1C	USH1C	DFNB18	3	(Zubair M. Ahmed et al., 2002; Ouyang et al., 2002; Reiners et al., 2003; Verpy et al., 2000)
CDH23	USH1D	DFNB12	3	(Bork et al., 2001; Lagziel et al., 2005, 2009; Schultz et al., 2005, 2011)
PCDH15	USH1F	DFNB23	4	(Z. M. Ahmed et al., 2006; Zubair M. Ahmed et al., 2003; Doucette et al., 2009)
CIB2	USH1J	DFNB48	3	(Riazuddin et al., 2012)
USH2A	USH2A	Nonsyndromic RP	2	(Eudy, 1998; Rivolta, Sweklo, Berson, & Dryja, 2000; van Wijk et al., 2004)
ADGRV1	USH2C	Febrile and afebrile seizures	1	(Nakayama et al., 2002; Randy McMillan, Kayes-Wandover, Richardson, & White, 2002; Skradski et al., 2001; Weston et al., 2004; Yagi et al., 2005)
PDZD7	Digenic USH	DFNB	3	(Ebermann et al., 2010; Schneider et al., 2009)

when the DFNB31 disease was studied in patients affected with prelingual sensorineural hearing impairment (Mburu et al., 2003; Mustapha et al., 2002). The affected individuals had a cysteine to threonine substitution in the 10th exon of *DFNB31*, changing the arginine codon to a stop codon (Arg778X) (Mburu et al., 2003). Another *DFNB31* mutation in the 11th exon (Gly808AspfsX11) also leads to profound deafness (Tlili et al., 2005). On the other hand, patients with compound heterozygous nonsense (Gln103X) and splice site (Val280Met) mutations in the 1st and 2nd exons of *DFNB31*, respectively, have USH2D, with moderate congenital hearing loss and RP that begins by the age of 20 years (Ebermann et al., 2007). Patients with either a homozygous one base-pair deletion (Pro246HisfsX13) or compound hetereozygous mutations (Pro246HisfsX13; Tyr228fs) in *DFNB31* also have USH2D symptoms (Audo et al., 2011; Besnard et al., 2012). Recently, a patient with a nonsense mutation (Gln54X) in *DFNB31* exon1 showed a relatively late onset of RP, but was unavailable for hearing tests (Nishiguchi et al., 2013). None of these aforementioned patients self-reported any vestibular deficits. In summary, the clinical reports suggest that mutations in the N-terminal region of DFNB31 lead to USH2D, while mutations toward the C-terminal end cause DFNB31 (Fig. 5.2).

***Dfnb31* mouse models recapitulate USH2D and DFNB31 diseases**

To understand the aforementioned genotype-phenotype correlation in *DFNB31*-deficient patients, I utilized mouse models with a series of mutations in the *DFNB31* ortholog, *Dfnb31*, to mimic various human *DFNB31*mutations that lead to USH2D and DFNB31. For example, a $Whrn^{tm1Tili}/Whrn^{tm1Tili}$ (MGI:4462398) mouse, hereafter referred to as $Dfnb31^{neo/neo}$, was generated by replacing the 5'-region of *Dfnb31* exon 1

Figure 5.2: Location and disease manifestation of human whirlin mutations.
FL-whirlin mRNA is translated into a protein with three PDZ domains, a proline rich (PR) domain and a PDZ binding motif (PBM). Asterisks in red denote mutations in the N-terminal region that cause USH2D. Asterisks in blue denote C-terminal mutations that cause DFNB31.

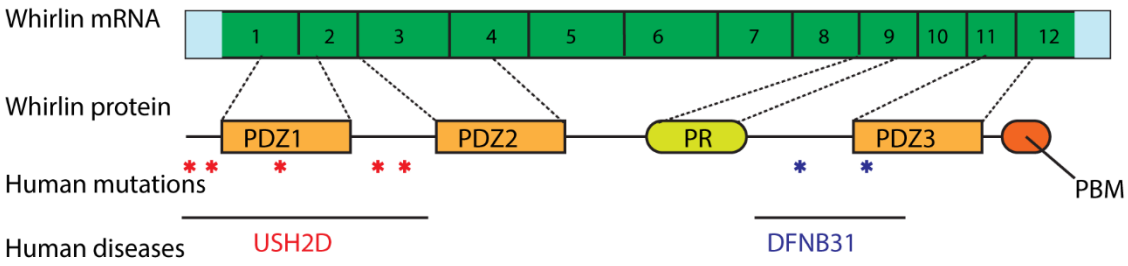
Whirlin mRNA
1
2
3
4
5
6
7
8
9
10
11
12
Whirlin protein
PDZ1
PDZ2
PR
PDZ3
PBM
Human mutations
Human diseases
USH2D
DFNB31

with a *Neo*^{r} cassette to mimic mutations found in USH2D patients (Yang et al., 2010b) (Fig 5.3B). This mouse shows moderate hearing loss and retinal degeneration similar to those observed in USH2D patients. Another *Dfnb31* mutant mouse *Whrn*$^{wi/wi}$ (MGI:1857090), hereafter referred to as *Dfnb31*$^{wi/wi}$, has a spontaneous deletion between exons 6-9 (Fig 5.3C). This 592bp deletion in the transcript creates a frameshift leading to a premature translation termination upstream of the 3rd PDZ domain. The *Dfnb31*$^{wi/wi}$ mice are profoundly deaf and show no retinal degeneration, resembling the symptoms found in DFNB31 patients (Holme, Kiernan, Brown, & Steel, 2002; Mburu et al., 2003; Yang et al., 2010a). Therefore, the *Dfnb31*$^{wi/wi}$ mutation represents C-terminal region mutations found in DFNB31 patients. In addition, I also studied the inner ear of *Dfnb31*$^{tm1a(EUCOMM)wtsi}$ (referred to as *Dfnb31*$^{tm1a/tm1a}$ hereafter) mice (MGI:4432119) for the first time. This mouse carries a gene trap insertion composed of a targeting cassette, placed between exon 3 and exon 4. Since this mouse has a mutation toward the 3' region of *Dfnb31*, it mimics the mutation region in USH2D patients. I also analyzed *Dfnb31*$^{wi/wi}$+BAC transgenic mice, generated by Mburu et al., (2003). To generate this mouse, a Bacterial Artificial Chromosome (BAC), containing the *Dfnb31* gDNA from exons 4-12, was inserted into the genome of *Dfnb31*$^{wi/wi}$ mice (Fig 5.3E). It was previously thought that this BAC insertion completely recued the hearing loss in *Dfnb31*$^{wi/wi}$ mice (Mburu et al., 2003). I utilized these *Dfnb31* mouse models to study whirlin expression in the inner ear and retina tissues, and to understand the pathogenesis of USH2D and DFNB31.

Figure 5.3: *Dfnb31* mRNA variants in WT, *Dfnb31*$^{neo/neo}$ and *Dfnb31*$^{wi/wi}$ mice.
(A) FL-, N-and C-terminal whirlin mRNA variants found in the WT mice. (B) Of these, only the C-terminal variant is found in the *Dfnb31*$^{neo/neo}$ mice, which has a *Neo*^{r} cassette (red box) in its exon1 3' region. (C) A deletion from exon 6 to 9 (red box) truncates both FL-whirlin mRNA and C-whirlin mRNA in *Dfnb31*$^{wi/wi}$ mice. Blue color denotes 3' and 5'-UTR; green color denotes CDS of whirlin mRNA; vertical yellow color line indicates a premature stop in truncated *Dfnb31*$^{wi/wi}$ mRNA fragments. (D) A targeting cassette (light blue box) in intron 3 of *Dfnb31*$^{tm1a/tm1a}$ gDNA disrupts the FL transcript. However, it is expected that C-terminal whirlin mRNA transcript will remain unaffected. L, loxP site. (E) *Dfnb31*$^{wi/wi}$+BAC mice is also expected to express C-terminal whirlin mRNA transcripts in addition to transcripts expressed by *Dfnb31*$^{wi/wi}$ mice.

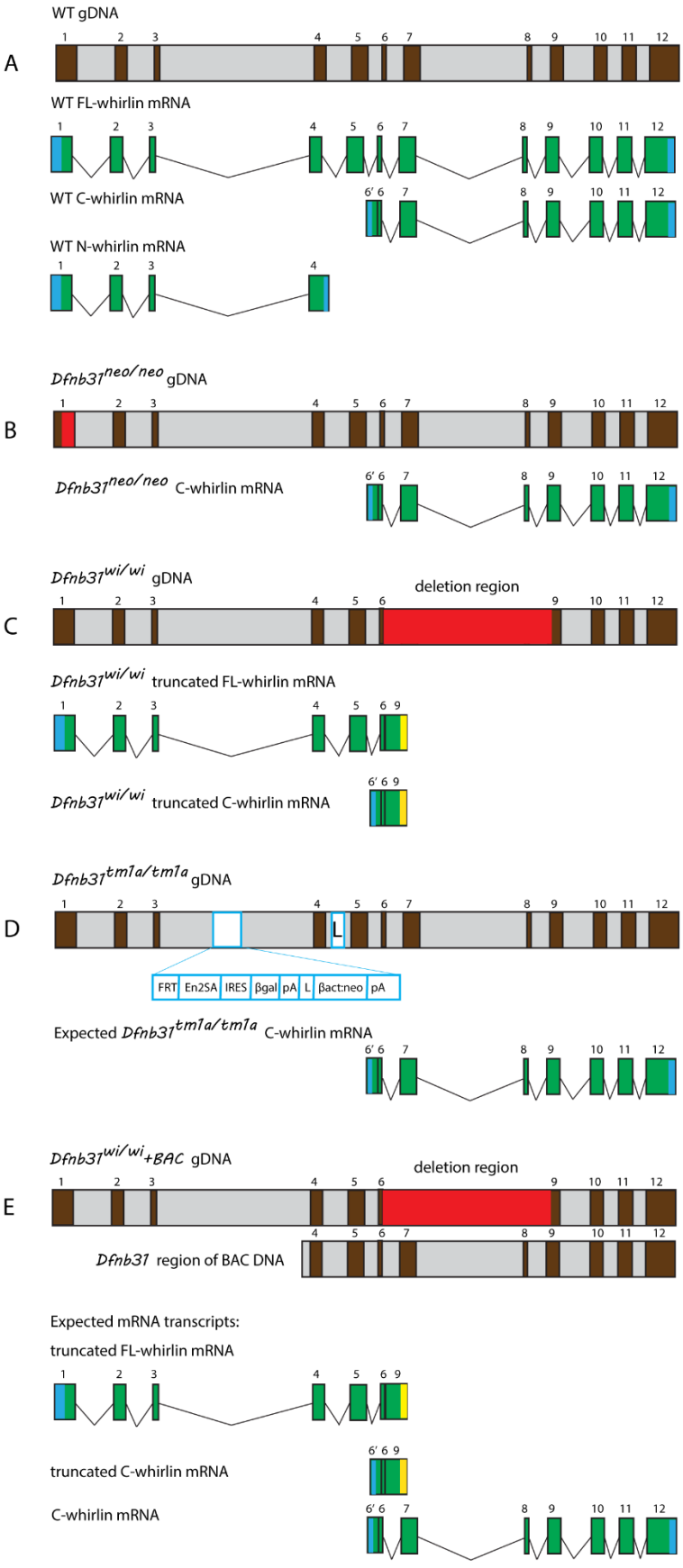
A
WT gDNA
WT FL-whirlin mRNA
WT C-whirlin mRNA
WT N-whirlin mRNA
B
Dfnb31neo/neo gDNA
Dfnb31neo/neo C-whirlin mRNA
C
Dfnb31wi/wi gDNA
deletion region
Dfnb31wi/wi truncated FL-whirlin mRNA
Dfnb31wi/wi truncated C-whirlin mRNA
D
Dfnb31tm1a/tm1a gDNA
FRT
En2SA
IRES
βgal
pA
L
βact:neo
pA
Expected Dfnb31tm1a/tm1a C-whirlin mRNA
E
Dfnb31wi/wi+BAC gDNA
deletion region
Dfnb31 region of BAC DNA
Expected mRNA transcripts:
truncated FL-whirlin mRNA
truncated C-whirlin mRNA
C-whirlin mRNA

Whirlin has different spatiotemporal expression patterns in the inner ear and retina

The presence of two different predicted promoter regions and alternative splicing in the *DFNB31*/*Dfnb31* gene yields several mRNA transcripts in humans and mice (Belyantseva et al., 2005; Mburu et al., 2003; Wright, Hong, & Perkins, 2012), and these mRNA transcripts encode whirlin protein splice isoforms. My research identified and compared the *Dfnb31* mRNA transcripts expressed in the organ of Corti, vestibular and retinal tissues of wildtype (WT), *Dfnb31*$^{neo/neo}$ and *Dfnb31*$^{wi/wi}$ mice. My results indicate that WT mice have transcripts encoding full-length (FL)-, N- and C-terminal whirlin proteins in the retina, but only transcripts encoding FL- and C-terminal proteins in the inner ear (Table 5.2). *Dfnb31*$^{neo/neo}$ mice lack all *Dfnb31* transcripts except the transcript encoding C-terminal whirlin protein in the inner ear. *Dfnb31*$^{wi/wi}$ mice have truncated FL- and C-whirlin mRNA transcripts in the inner ear and retina (Table 5.2; Fig. 5.3). FL-transcripts are expected to yield a FL-whirlin protein isoform having three PDZ domains, a PDZ binding motif (PBM) and a Proline Rich (PR) region. Transcripts encoding C-terminal whirlin have start sites in either exon 1 or exon 6, yet C-whirlin protein isoforms have only the PR, PDZ3, and PBM domains (Belyantseva et al., 2005; Mburu et al., 2003; Yang et al., 2010a). Finally, transcripts encoding N-terminal whirlin yield N-whirlin isoforms that contain either PDZ1 or both PDZ1 and PDZ2 domains (Wright et al., 2012).

Despite several studies on whirlin localization, a clear understanding of the localization of different whirlin isoforms was missing. For example, in one study, whirlin was shown to localize only at the stereociliary tips (Kikkawa et al., 2005). A different

Table 5.2: Different *Dfnb31* mRNA variants present in the retina and inner ear of WT, *Dfnb31*$^{neo/neo}$ and *Dfnb31*$^{wi/wi}$ mice.

Mouse models	Organs		
	Retina	Cochlea	Vestibular system
WT	Transcripts encoding FL- whirlin C- whirlin N- whirlin	Transcripts encoding FL- whirlin C- whirlin	Transcripts encoding FL- whirlin C- whirlin
Dfnb31$^{neo/neo}$	-	Transcript encoding C- whirlin	Transcript encoding C- whirlin
Dfnb31$^{wi/wi}$	Transcripts encoding truncated N- whirlin truncated C- whirlin.	Transcripts encoding truncated N- whirlin truncated C- whirlin	Transcripts encoding truncated N- whirlin truncated C- whirlin

study reported presence of whirlin at the stereociliary tips and bases (Delprat et al., 2005). A third study found whirlin localized at the OHC synaptic regions (van Wijk et al., 2006a). In my study, however, I could not see whirlin localization at the synapses. To confirm the presence of whirlin at the synapses, co-localization of whirlin with a known synaptic marker and use of the *Dfnb31* mutant mice as a negative control are essential. Moreover, this variation could be due to the use of different antibodies and sample fixation procedures. To decipher the localization of different whirlin isoforms in the inner ear and retina, I generated antibodies specific to the different whirlin regions and utilized *Dfnb31* mutants as controls in comparison to WT mice. I found that in the WT inner ear, both FL- and C-whirlin isoforms localize at the IHC and VHC stereociliary tips, whereas C-whirlin is the only isoform found in the OHC stereociliary tips. The only whirlin isoform found at the WT stereociliary base is FL-whirlin and it is present in all HC types (Fig. 5.4A,B) (Mathur, Vijayakumar, et al., 2015; Mathur, Zou, et al., 2015). In *Dfnb31*$^{neo/neo}$ mice, the FL-whirlin isoform at the stereociliary base is missing, but the C-whirlin isoform remains localized at the stereociliary tips of OHCs, IHCs and VHCs. (Fig. 5.4D,E). Localization of whirlin isoforms in *Dfnb31*$^{tm1a/tm1a}$ and majority of *Dfnb31*$^{wi/wi}$+BAC hair cells were similar to that of *Dfnb31*$^{neo/neo}$ hair cells (Fig 5.4D, E and J-L). *Dfnb31*$^{wi/wi}$ mice did not show any whirlin isoforms either at the stereociliary tips or at the stereociliary base of their inner ear hair cells (Fig 5.4G,H), suggesting that the truncated FL- and C-terminal whirlin *Dfnb31* transcripts are probably degraded by nonsense-mediated mRNA decay (Mathur, Vijayakumar, et al., 2015; Mathur, Zou, et al., 2015). In summary, my findings show that a 3'-region mutation in *Dfnb31*$^{neo/neo}$ and *Dfnb31*$^{tm1a/tm1a}$ mice spares the C-terminal whirlin isoform, while a 5'-region mutation in

Figure 5.4: Localization of whirlin isoforms (green) in the inner ear and retina.
(A) FL-whirlin is localized at the stereociliary base of developing (P2-P12) inner hair cells (IHCs) and outer hair cells (OHCs) in the organ of Corti. IHC stereociliary tips contain both FL- and C-whirlins, while OHC stereociliary tips contain only C-whirlin. (B) Localization of whirlin in vestibular hair cells (VHCs) is similar to that of IHCs as shown in A. (C) FL- and N-whirlins are localized at the periciliary membrane complex (PMC) of the WT photoreceptor cell. (D, E) Only C-whirlin is localized at the stereociliary tips of OHC, IHC and VHC in *Dfnb31*$^{neo/neo}$ mice. (F) No whirlin localizations were detected in *Dfnb31*$^{neo/neo}$ retinas. (G, H) *Dfnb31*$^{wi/wi}$ inner ear hair cells do not show any whirlin localizations. (I) Truncated N-whirlin fragment in *Dfnb31*$^{wi/wi}$ retinas localizes to the PMC. (J,K) 96% of *Dfnb31*$^{wi/wi}$ +BAC IHCs and only 33% of of *Dfnb31*$^{wi/wi}$ +BAC OHCs show localization of C-whirlin at their stereociliary tips. (L) Similar to *Dfnb31*$^{neo/neo}$ IHCs and OHCs, *Dfnb31*$^{tm1a/tm1a}$ show localization of only C-whirlin at their IHC and OHC stereociliary tips.

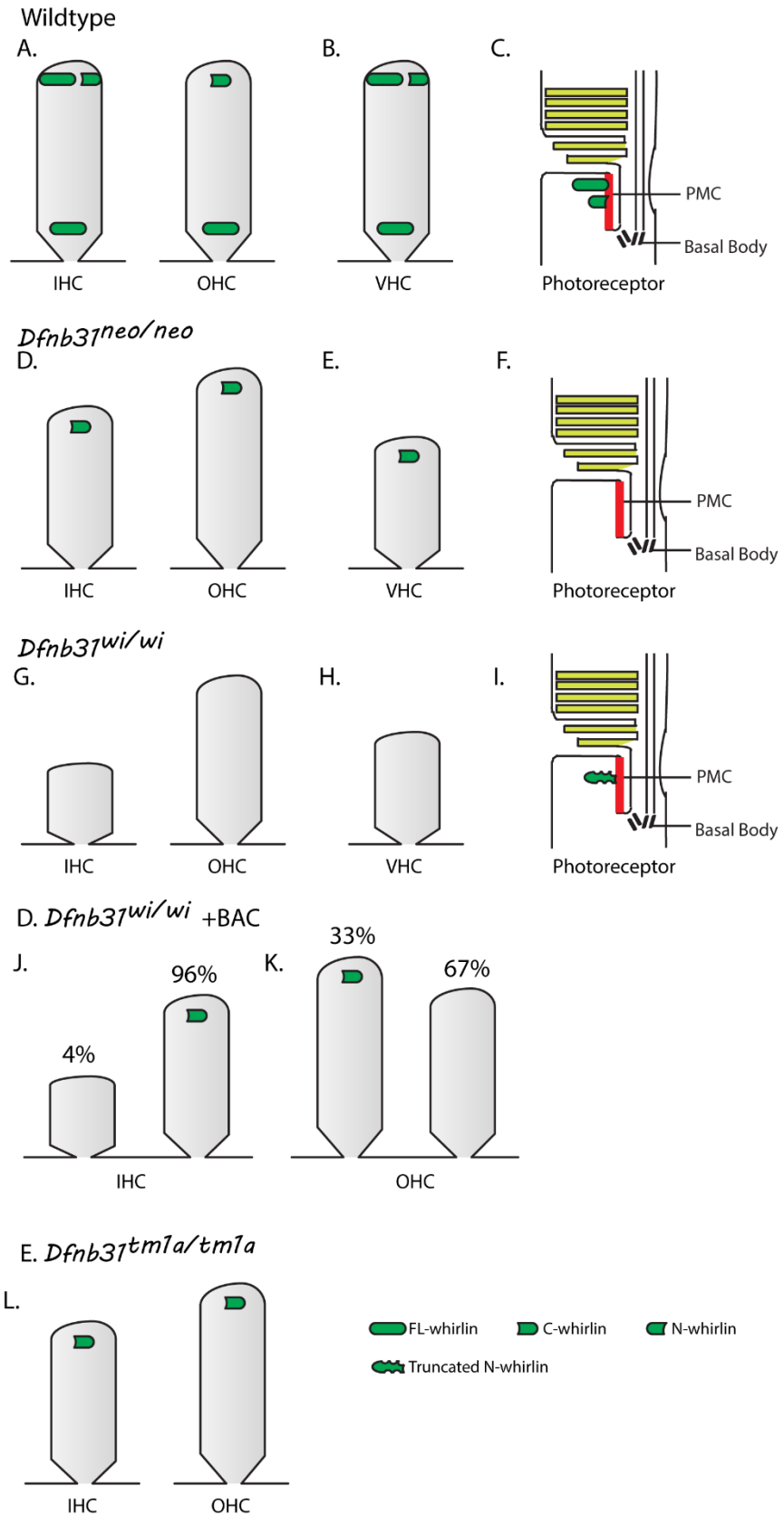
Wildtype
A.
B.
C.
IHC
OHC
VHC
PMC
Basal Body
Photoreceptor
Dfnb31neo/neo
D.
E.
F.
IHC
OHC
VHC
PMC
Basal Body
Photoreceptor
Dfnb31wi/wi
G.
H.
I.
IHC
OHC
VHC
PMC
Basal Body
Photoreceptor
D. Dfnb31wi/wi +BAC
J.
96%
4%
IHC
K.
33%
67%
OHC
E. Dfnb31tm1a/tm1a
L.
IHC
OHC
FL-whirlin
C-whirlin
N-whirlin
Truncated N-whirlin

Figure 4

Dfnb31$^{wi/wi}$ mice leads to loss of both FL- and C-whirlin isoforms in the inner ear hair cells (Fig 5.3 and Fig 5.4).

Whirlin was previously found at the PMC in photoreceptors (Yang et al., 2010a); however, isoform-specific information on whirlin in the PMC was unknown. I found that the FL- and likely the N-whirlin isoforms are expressed and localize to the PMC in the WT (Fig. 5.4C). *Dfnb31*$^{neo/neo}$ mice did not show any whirlin isoforms in the retina (Fig 5.4F). In *Dfnb31*$^{wi/wi}$ mice, a truncated N-whirlin fragment (Fig. 5.3C) localized normally at the PMC (Fig 5.4I), although the expression level was low. This suggests that the truncated FL-whirlin mRNA transcript in *Dfnb31*$^{wi/wi}$ is translated into truncated N-whirlin protein fragment. Together, these findings indicate that whirlin has multiple spatiotemporal expression patterns in the inner ear and retina.

Whirlin forms different multiprotein complexes in the inner ear and retina

Whirlin is a scaffold protein with three PDZ domains, which aid in assembling several large multiprotein complexes. Different whirlin protein isoforms likely form different complexes at unique subcellular locations in the inner ear hair cells and at the PMC of the photoreceptors. To understand the function of different whirlin isoforms and the mechanism underlying different phenotypes observed in *Dfnb31* mutants, it is important to identify proteins that interact with whirlin and to determine how whirlin isoforms mediate these interactions.

Proteins interacting with whirlin at the stereociliary tips in hair cells. Actin regulatory protein EPS8, actin motor protein myosin-XVa and a MAGUK scaffold

protein p55, bind to and colocalize with whirlin at the stereociliary tips to maintain the stereocilia length (Fig 5.5A) (Manor et al., 2011; Mburu et al., 2006). Loss of any of these proteins leads to short stereociliary length, as observed in *Eps8* knockout (*Eps8*$^{-/-}$), *shaker2* (*Myo15a*$^{sh2/sh2}$), *Dfnb31*$^{wi/wi}$ and *Dfnb31*$^{neo/neo}$ mice (Holme et al., 2002; Mathur, Zou, et al., 2015; Mustapha et al., 2007; Zampini et al., 2011). The N-terminal region of EPS8 binds to the PDZ1, PDZ2 and PR domains of whirlin, while its C-terminal region binds to myosin-XVa (Manor et al., 2011). The C-terminal PDZ-binding motif of myosin-XVa interacts with the PDZ3 domain of whirlin and delivers whirlin to the tips of stereocilia (Belyantseva et al., 2005). By contrast, another study shows that whirlin PDZ1 and PDZ2 domains interact with the MyTH4-FERM domain of myosin-XVa and the whirlin PDZ3 domain binds to the SH3-MyTH4 domain of myosin-XVa (Delprat et al., 2005). My findings in Chapter 3 suggest that only C-terminal whirlin region is required for the interaction between myosin-XVa and whirlin, and that both whirlin N- and C-terminal regions are involved in the interaction between EPS8 and whirlin (Mathur, Zou, et al., 2015). The GUK domain of p55 interacts with whirlin PDZ3 (Mburu et al., 2006, 2010; Yang, Le, Song, & Sokolov, 2012). In addition, 4.1R, one of the four 4.1 protein isoforms, and CASK, other MAGUK proteins similar to P55, are shown to localize at the OHC stereociliary tips. Localization of P55 and 4.1R is sporadic at E17.5 (embryonic day 17.5) OHC stereociliary tips and their signals get completely ablated at P5 in *Dfnb31*$^{wi/wi}$ mice (Jing-Ping et al., 2005; Mburu et al., 2006). Because only C- whirlin is localized at the stereociliary tips of OHCs (Mathur et al. 2015), it is likely that 4.1R and CASK also interact with the PDZ3 of C-whirlin. Interaction of CASK with the whirlin C-terminal region is thought to be required for the actin cytoskeleton reorganization in neurons

Figure 5.5: Interacting partners of whirlin at various subcellular regions.
(A) Whirlin interacts with EPS8, MYOXVA, P55, CASK and 4.1R proteins at the stereociliary tips of the inner ear hair cells. (B) Whirlin interacts with ADGRV1, usherin and PDZD7 at the ankle-link complex region of the stereociliary bases in the inner ear hair cells. (C) At the periciliary membrane complex of the retina, whirlin interacts with ADGRV1 and usherin. A fourth protein (indicated as '?'), required to form a stable USH2 protein complex is still unkown.

A. Whirlin interactions at the stereociliary tips

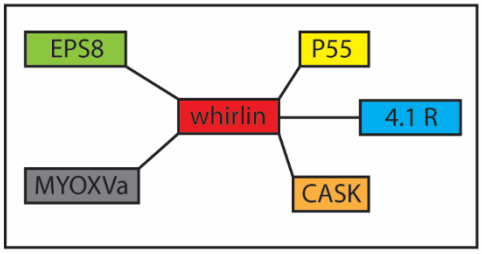

B. Whirlin interactions at the stereociliary bases

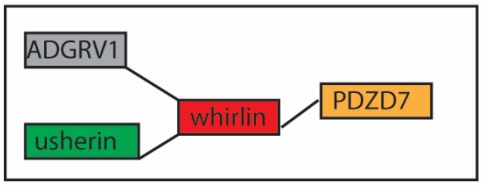

C. Whirlin interactions at the periciliary membrane complex

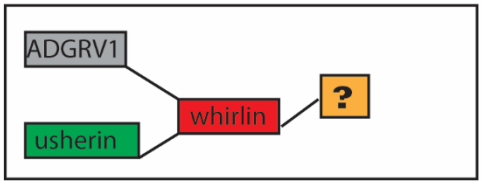

(Yap et al., 2003). However, the exact function of interactions of whirlin with P55, CASK and 4.1R in hair cells remains unknown.

Proteins interacting with whirlin at the stereociliary base in hair cells. ADGRV1, usherin and PDZD7 bind to one another and to whirlin to form the ankle-link complex (ALC) toward the stereociliary base (Fig. 5.5B). This complex is required for stereociliary bundle organization. Several studies have confirmed the existence and function of this USH2 protein complex in vivo (Grati et al., 2012; Michalski et al., 2007; van Wijk et al., 2006b; Yang et al., 2010b; Zou et al., 2015). PDZ1 of whirlin binds to the PDZ2 of PDZD7 and the cytoplasmic C-termini of usherin and of ADGRV1. The whirlin PDZ2 can bind to usherin, but not ADGRV1, C-terminus (Chen, Zou, Shen, Zhang, & Yang, 2014). I found that loss of whirlin at the stereociliary base leads to partial mislocalization of ADGRV1 to the stereociliary tips, while usherin and PDZD7 remain relatively unaffected (Zou et al., 2015). ADGRV1 along with other proteins forms and stabilizes ankle links of the developing hair cell stereocilia. Ankle links are essential for stereociliary organization and the typical 'V'-shape stereociliary bundle. (McGee et al., 2006; Michalski et al., 2007). Together, these findings suggest that loss of whirlin at the stereociliary base cause partial destabilization of ankle links. ADGRV1 is also implicated in G-protein-coupled receptor (GPCR) signaling pathway (Hu et al., 2014; Weston, Luijendijk, Humphrey, Möller, & Kimberling, 2004). Therefore, it is likely that formation of the ALC is required for efficient and proper GPCR signaling. Whether or not loss of whirlin from the ALC affects GPCR signaling remains to be studied.

Proteins interacting with whirlin at the PMC in photoreceptors. ADGRV1 and usherin are also colocalized with whirlin at the PMC in photoreceptors (Fig. 5.5C) (Yang

et al., 2010a). Our in vitro studies demonstrated that formation of a stable USH2 complex requires a fourth protein apart from whirlin, usherin and ADGRV1 (Chen et al., 2014). Interestingly, PDZD7, the fourth USH2 protein required for stable USH2 complex formation in the inner ear ALC, was not found in the retina (Zou et al., 2014), which suggests that a fourth unknown protein exists in the retina for stabilization of the USH2 complex. The RPGR (Retinitis Pigmentosa GTPase regulator) isoform $RPGR^{orf15}$, which is preferentially expressed in the retina, colocalizes and interacts with whirlin at the connecting cilium of photoreceptors. Specifically, PDZ1 and PDZ2 of whirlin were shown to interact with the C-terminal region of $RPGR^{orf15}$ (Wright et al., 2012). Furthermore, RPGR is thought to be essential for the protein trafficking and mutations in RPGR lead to RP (Hong et al., 2000). However, my localization studies on whirlin suggest that whirlin is localized at the PMC and not at the connecting cilium. Therefore, the functional significance of the whirlin-$RPGR^{orf15}$ interaction remains unexplored, and whether $RPGR^{orf15}$ interacts with other USH2 proteins present at the PMC is yet to be tested. Further studies are required to identify all the components of the USH2 protein complex at the PMC in the retina.

Correlation of genotypes with phenotypes conveys the function of different whirlin isoforms

Phenotypes caused by the absence of whirlin isoforms at a specific subcellular location in the retina or the inner ear convey information about the function of the whirlin isoforms. For example, whirlin isoforms are completely missing in *Dfnb31*$^{neo/neo}$ mouse retinas. This causes mislocalization of ADGRV1 and usherin at the PMC, and is likely

the cause for retinal degeneration in *Dfnb31*$^{neo/neo}$ mice. In contrast, *Dfnb31*$^{wi/wi}$ retinas retain the truncated N-terminal whirlin fragment and this partially rescues the normal localizations of ADGRV1 and usherin to the PMC (Mathur, Zou, et al., 2015). The partial rescue of the USH2 complex at the PMC is likely sufficient to prevent or delay retinal degeneration in *Dfnb31*$^{wi/wi}$ mice. A 2014 study, however, reported that *Dfnb31*$^{wi/wi}$ mice had delayed transducin translocation from the outer segment to the inner segment upon light stimulation and that light exposure can induce photoreceptor degeneration (Tian et al., 2014). This study, however, did not include the *Dfnb31*$^{neo/neo}$ mice. It would, therefore, be interesting to see whether *Dfnb31*$^{neo/neo}$ mice have a more severe transducin translocation and photoreceptor degeneration phenotype compared to *Dfnb31*$^{wi/wi}$ mice upon light stimulation.

Localization of both FL- and C-whirlins at the stereociliary tips is essential for IHC stereociliary elongation, whereas only C-whirlin is required for OHC stereociliary elongation. Loss of FL-whirlin but normal C-whirlin localization at the *Dfnb31*$^{neo/neo}$ IHC stereociliary tips leads to relatively shorter IHC stereocilia in *Dfnb31*$^{neo/neo}$ mice compared to WT. *Dfnb31*$^{neo/neo}$ OHCs, like WT OHCs, have only the C-whirlin isoform localized at their stereociliary tips and, as a result, *Dfnb31*$^{neo/neo}$ OHCs have normal stereocilia lengths (Mathur, Zou, et al., 2015). *Dfnb31*$^{wi/wi}$ mice lack both FL- and C-whirlins at their IHC and OHC stereociliary tips and, therefore, have significantly short IHC and OHC stereocilia compared to *Dfnb31*$^{neo/neo}$ and WT mice (Fig 5.4G). As a result, *Dfnb31*$^{wi/wi}$ mice have a more severe hearing loss compared with *Dfnb31*$^{neo/neo}$, *Dfnb31*$^{tm1a/tm1a}$ and *Dfnb31*$^{wi/wi}$+BAC mice that harbor C-whirlin isoform at their hair cell stereociliary tips (Fig. 5.4D, J-L) (Mathur, Zou, et al., 2015). At the stereociliary base, all

Dfnb31 mutants lack the FL-whirlin isoform. OHC stereocilia disorganization is similar in *Dfnb31*$^{neo/neo}$, *Dfnb31*$^{tm1a/tm1a}$, *Dfnb31*$^{wi/wi}$+BAC and *Dfnb31*$^{wi/wi}$ mice, and these mice have similar distortion products of otoacoustic emissions (DPOAE) responses, which specifically indicates the function of OHCs (Mathur, Zou, et al., 2015). This observation suggests that FL-whirlin is required at the OHC ALC for the stereociliary bundle organization during development. The function of FL-whirlin at the stereociliary base needs to be further investigated.

Localization of whirlin isoforms in VHCs is the same as that in IHCs, and *Dfnb31*$^{neo/neo}$ VHC stereocilia are taller than *Dfnb31*$^{wi/wi}$ but shorter than WT VHC stereocilia (Fig. 5.4E,H) (Mathur, Vijayakumar, et al., 2015). This suggests that in terms of stereociliary elongation, the function of FL- and C-whirlins at stereociliary tips in VHCs is similar to that in IHCs. Consistently, *Dfnb31*$^{wi/wi}$ mice have overt vestibular behaviors (Holme et al., 2002), whereas *Dfnb31*$^{neo/neo}$ mice do not (Mathur, Vijayakumar, et al., 2015). However, both *Dfnb31*$^{neo/neo}$ and *Dfnb31*$^{wi/wi}$ mice show similar severe to profound loss of linear vestibular evoked potential (VsEP) responses. One reason for this discrepancy could be that the central nervous system (CNS) compensates in *Dfnb31*$^{neo/neo}$ mice, owing to some uncharacterized functional role of C-whirlin in the murine CNS. Another possibility could be the presence of tall VHC stereocilia in the peripheral region of *Dfnb31*$^{neo/neo}$ cristae. Since linear VsEPs test only the otolith organs, measurements of angular VsEP measurements are required to test this hypothesis.

Whirlin isoforms have functions outside the inner ear and retina

My studies on *Dfnb31* mutant VHCs suggest the possibility that whirlin functions in the CNS. Consistent with this, several recent studies emphasize the expression and role of whirlin in the CNS. Loss of whirlin disrupts the axonal domain organization and causes paranodal abnormalities during development in both central and peripheral nervous systems (Green, Yang, Grati, Kachar, & Bhat, 2013). Another study revealed that *Dfnb31*$^{tm1a/tm1a}$ mice have elevated nociceptive thresholds (White et al., 2013). Subsequently, it was found that whirlin is selectively expressed in proprioceptive sensory neurons, where it functions in afferent firing in response to touch (de Nooij et al., 2015). Recently, both C-terminal and FL-whirlin isoforms were found to associate with and increase the stability and clustering of TRPV1, a thermosensory channel, at the cell membrane of nociceptive neurons (Ciardo et al., 2016). *Dysc* (dyschronic), the closest homolog of whirlin, is required in Drosophila for locomotor behavior and circadian rhythm (Jepson et al., 2012). *Dysc* is expressed at the presynaptic region and is essential in synaptic development and output. *Dysc* mutants show increased evoked and spontaneous synaptic transmission (Jepson et al., 2014).

Together, these findings suggest that whirlin isoforms have multiple functions in the inner ear, retina, and nervous system, and that different mutations in *Dfnb31* may affect some isoforms while sparing other isoforms. Unaffected isoforms localize and function normally in their respective tissues. Disruption of different whirlin isoforms is, therefore, a likely explanation for different disease manifestations and genotype-phenotype correlation. Furthermore, expression and function of whirlin in the murine nervous system suggest that patients with mutations in *DFNB31* might have

abnormalities in the nervous system.

Previous attempts to rescue *Dfnb31* mutant phenotypes were only partially successful

Gene therapy appears to be one of the most promising therapeutic approaches in human medicine, and several attempts have been made to rescue the phenotypes of whirlin mutant mice using gene replacement therapy. Adeno-Associated Virus (AAV) carrying FL-whirlin cDNA was able to successfully restore the USH2 complex at the PMC in *Dfnb31*$^{neo/neo}$ retinas (Zou et al., 2011). *Dfnb31*$^{neo/neo}$ mice completely lack whirlin in their retina and the N-terminal region of whirlin is sufficient to stabilize and restore the normal localization of usherin and ADGRV1 in the retina (Chen et al., 2014; Mathur, Zou, et al., 2015), suggesting that AAV-carrying N-whirlin may also be able to rescue normal localizations of usherin and ADGRV1, and potentially to prevent retinal degeneration in *Dfnb31*$^{neo/neo}$ mice.

Dfnb31 restoration studies in the inner ear (Belyantseva et al., 2005; Chien et al., 2015; Mburu et al., 2003) have been unsuccessful in completely rescuing hearing or stereociliary bundle morphology. The *Dfnb31*$^{wi/wi}$+BAC mouse does not circle and has longer stereocilia and better hearing compared with *Dfnb31*$^{wi/wi}$ mouse. However, *Dfnb31*$^{wi/wi}$+BAC mice still have the abnormal 'U'-shaped OHC stereociliary arrangement and impaired hearing function comparable to *Dfnb31*$^{neo/neo}$ mice (Mathur, Zou, et al., 2015; Mburu et al., 2003). This phenotype probably results from the absence of FL-whirlin, which is required for ALC stabilization and IHC stereociliary elongation.

Gene gun transfection of VHCs with GFP-FL-whirlin cDNA was able to elongate

stereocilia and rescue the missing staircase pattern in *Dfnb31*$^{wi/wi}$ mice to some extent (Belyantseva et al., 2005). However, whether the rescued hair cells had stereociliary lengths similar to those of WT hair cells was not studied. My studies showed that both FL- and C-whirlins are required for stereocilia elongation, with FL-whirlin playing a major role in VHC stereocilia elongation. Furthermore, the presence of C-whirlin isoform alone is sufficient to partially bring back the missing staircase pattern in the VHC stereocilia of *Dfnb31*$^{wi/wi}$ mice (Mathur, Vijayakumar, et al., 2015).

In a very recent study, Chien et al., packaged FL-whirlin cDNA into an AAV8 vector and delivered this AAV particle to the inner ear hair cells of *Dfnb31*$^{wi/wi}$ mice. This AAV FL-whirlin particle partially increased the stereocilia length in IHCs but not OHCs. Moreover, the hearing loss in *Dfnb31*$^{wi/wi}$ mice could not be restored (Chien et al., 2015). Based on my findings in Chapter Three, the partial rescue observed by Chien et al., is likely due to the absence of C-whirlin at the OHC stereociliary tips, which contributes to normal OHC stereociliary lengths and hearing function (Mathur, Zou, et al., 2015).

Conclusion and future directions

My studies on *Dfnb31* in this dissertation suggest that disruption of different isoforms might be a mechanism underlying the different disease manifestations observed in mutations in other USH genes as well. Nine out of eleven currently known USH genes show variable disease manifestations when mutated and, similar to *Dfnb31,* most of these USH genes express multiple splicing isoforms (Table 5.1). Furthermore, a high percentage of similarity between human and mouse genes provides a rationale that findings from the study of USH genes in mice can possibly be extended to answer

questions about human USH. For example, analysis of human *DFNB31* cDNA sequences (AB040959; AL11028; AK022854 and AL110228) predicts that human whirlin is also expressed as FL-, N- and C-terminal protein isoforms, similarly to mice. However, the information about the promoter regions that lead to expression of multiple *DFNB31*/*Dfnb31* variants still remains unknown. Nonetheless, with an 88% amino acid sequence identity between mouse and human whirlins that rises to 94.4% in the PDZ domains (Mburu et al., 2003), it is likely that there is little difference in the function of whirlin isoforms in humans and mice. My findings in Chapters 3 and 4 are, therefore, valuable for early differential diagnosis of USH2D and DFNB31, genetic counselling of parents and educational planning of newborns with mutated *DFNB31* gene. This is important because retinal degeneration in USH2D patients does not occur until about 20 years of age, and prior knowledge of USH2D will allow ample time for treatment and preventive measures.

Abnormal vestibular responses in *Dfnb31*$^{neo/neo}$ mice (Mathur, Vijayakumar, et al., 2015), which represent USH2D patients, suggest for the first time that USH2 patients may have vestibular deficits. In support of this finding, a recent study reported abnormal vestibular responses in 8 out of 11 USH2 patients examined. These eight patients never self-reported any balance problems (like other USH2 patients), but later recalled occasional vertigo attacks (Magliulo et al., 2015). Therefore, vestibular tests of other USH2 mouse models and all USH2 patients in clinics are important. The role of other USH2 proteins in vestibular function and the role of the ALC in VHCs also need to be studied. This is important because to date USH2 patients are considered to have normal vestibular function. However, my findings, coupled with those of Magliulo et al., suggest

that vestibular deficits in USH2 patients may not be ruled out even if USH2 patients do not self-report vertigo attacks. Therefore, USH2 patients need testing and counselling about a potential vestibular dysfunction in them. Moreover, for a clear understanding of the USH pathogenesis and mechanism, all the affected systems need to be studied.

Therapeutic strategy using my study. Among the several therapeutic measures studied to treat USH, only viral-mediated gene therapy has shown promise, due to its high efficacy and relative safety. However, all previous attempts to rescue the hearing and inner ear morphology in *Dfnb31* mutants by putting the *Dfnb31* cDNA or gene back into them have only been partially successful, mostly due to incomplete knowledge about the expression and function of different whirlin isoforms. My studies elucidated the role of each whirlin isoform in the retinal photoreceptors and inner ear hair cells. A rescue study utilizing the isoform-specific information discussed in this dissertation may be promising for future therapy. Specifically, $Dfnb31^{neo/neo}$ mice that show a moderate level of hearing loss and retinal degeneration should receive a therapy which provides the FL-whirlin isoform to the $Dfnb31^{neo/neo}$ ALC and PMC regions. On the other hand, $Dfnb31^{wi/wi}$ inner ear hair cells require both FL- and C-whirlin isoforms for complete rescue of morphology and hearing. Adeno-associated virus serotype 2 (AAV2) is in clinical trials to deliver the packaged DNA to retinal photoreceptors (Hauswirth et al., 2008). AAV2 has also been shown to transduce both OHC and IHC with an overall efficiency better than other AAV serotypes tested (Stone, Lurie, Kelley, & Poulsen, 2005). The ability of AAV2 to transduce photoreceptors, OHCs, and IHCs makes it a promising candidate for gene therapy for USH. With a packaging capacity of about 4.7kb, AAV2 can carry the *DFNB31* cDNA variants, but packaging other USH genes

with large full-length cDNA may be challenging. However, a knowledge of the function of the various isoforms of other USH genes may help address this issue. For example, a FL-usherin cDNA is about 16kb, which is beyond the packing capacity of AAV2, but the shorter usherin isoform cDNA is about 4.5kb in size and can be packaged in AAV2. Therefore, to understand the molecular function of the USH genes that show variable disease manifestations and have multiple isoforms using a study design similar to my *Dfnb31* study described in this dissertation may be promising in order to make therapeutic progress.

References

Ahmed, Z. M., Goodyear, R., Riazuddin, S., Lagziel, A., Legan, P. K., Behra, M., … Friedman, T. B. (2006). The Tip-Link Antigen, a Protein Associated with the Transduction Complex of Sensory Hair Cells, Is Protocadherin-15. *Journal of Neuroscience*, *26*(26), 7022–7034. http://doi.org/10.1523/JNEUROSCI.1163-06.2006

Ahmed, Z. M., Riazuddin, S., Ahmad, J., Bernstein, S. L., Guo, Y., Sabar, M. F.,Friedman, T.B., & Wilcox, E. R. (2003). PCDH15 is expressed in the neurosensory epithelium of the eye and ear and mutant alleles are responsible for both USH1F and DFNB23. *Human Molecular Genetics*, *12*(24), 3215–3223. http://doi.org/10.1093/hmg/ddg358

Ahmed, Z. M., Smith, T. N., Riazuddin, S., Makishima, T., Ghosh, M., Bokhari, S., & Wilcox, E. R. (2002). Nonsyndromic recessive deafness DFNB18 and usher syndrome type IC are allelic mutations of USHIC. *Human Genetics*, *110*(6), 527–531. http://doi.org/10.1007/s00439-002-0732-4

Audo, I., Bujakowska, K., Mohand-Saïd, S., Tronche, S., Lancelot, M.-E., Antonio, A., & Zeitz, C. (2011). A novel DFNB31 mutation associated with Usher type 2 syndrome showing variable degrees of auditory loss in a consanguineous Portuguese family. *Molecular Vision*, *17*(March), 1598–606. Retrieved from http://www.pubmedcentral.nih.gov/articlerender.fcgi?artid=3123164&tool=pmcentrez&rendertype=abstract

Belyantseva, I. a, Boger, E. T., Naz, S., Frolenkov, G. I., Sellers, J. R., Ahmed, Z. M., Griffith A.J., & Friedman, T. B. (2005). Myosin-XVa is required for tip localization of whirlin and differential elongation of hair-cell stereocilia. *Nature Cell Biology*, *7*(2), 148–156. http://doi.org/10.1038/ncb1219

Besnard, T., Vaché, C., Baux, D., Larrieu, L., Abadie, C., Blanchet, C., Clausteras, M., & Roux, A.-F. (2012). Non-USH2A mutations in USH2 patients. *Human Mutation*, *33*(3), 504–10. http://doi.org/10.1002/humu.22004

Bork, J. M., Peters, L. M., Riazuddin, S., Bernstein, S. L., Ahmed, Z. M., Ness, S. L., … Morell, R. J. (2001). Usher syndrome 1D and nonsyndromic autosomal recessive deafness DFNB12 are caused by allelic mutations of the novel cadherin-like gene CDH23. *American Journal of Human Genetics*, *68*(1), 26–37. http://doi.org/10.1086/316954

Chen, Q., Zou, J., Shen, Z., Zhang, W., & Yang, J. (2014). Whirlin and PDZ domain-containing 7 (PDZD7) proteins are both required to form the quaternary protein complex associated with Usher syndrome type 2. *The Journal of Biological Chemistry*, *289*(52), 36070–88. http://doi.org/10.1074/jbc.M114.610535

Chien, W. W., Isgrig, K., Roy, S., Belyantseva, I. A., Drummond, M. C., May, L. A., …

Cunningham, L. L. (2015). Gene Therapy Restores Hair Cell Stereocilia Morphology in Inner Ears of Deaf Whirler Mice. *Molecular Therapy*, *8*, 1–9. http://doi.org/10.1038/mt.2015.150

Ciardo, M. G., Andrés-Bordería, A., Cuesta, N., Valente, P., Camprubí-Robles, M., Yang, J., … Ferrer-Montiel, A. (2016). Whirlin increases TRPV1 channel expression and cellular stability. *Biochimica et Biophysica Acta (BBA) - Molecular Cell Research*, *1863*(1), 115–127. http://doi.org/10.1016/j.bbamcr.2015.10.016

de Nooij, J. C., Simon, C. M., Simon, A., Doobar, S., Steel, K. P., Banks, R. W., … Jessell, T. M. (2015). The PDZ-Domain Protein Whirlin Facilitates Mechanosensory Signaling in Mammalian Proprioceptors. *The Journal of Neuroscience : The Official Journal of the Society for Neuroscience*, *35*(7), 3073–84. http://doi.org/10.1523/JNEUROSCI.3699-14.2015

Delprat, B., Michel, V., Goodyear, R., Yamasaki, Y., Michalski, N., El-Amraoui, A., … Petit, C. (2005). Myosin XVa and whirlin, two deafness gene products required for hair bundle growth, are located at the stereocilia tips and interact directly. *Human Molecular Genetics*, *14*(3), 401–10. http://doi.org/10.1093/hmg/ddi036

Doucette, L., Merner, N. D., Cooke, S., Ives, E., Galutira, D., Walsh, V., … Young, T.-L. (2009). Profound, prelingual nonsyndromic deafness maps to chromosome 10q21 and is caused by a novel missense mutation in the Usher syndrome type IF gene PCDH15. *European Journal of Human Genetics : EJHG*, *17*(5), 554–564. http://doi.org/10.1038/ejhg.2008.231

Ebermann, I., Phillips, J. B., Liebau, M. C., Koenekoop, R. K., Schermer, B., Lopez, I., … Bolz, H. J. (2010). PDZD7 is a modifier of retinal disease and a contributor to digenic Usher syndrome. *The Journal of Clinical Investigation*, *120*(6), 1812-1823. http://doi.org/10.1172/JCI39715DS1

Ebermann, I., Scholl, H. P. N., Charbel Issa, P., Becirovic, E., Lamprecht, J., Jurklies, B., … Bolz, H. (2007). A novel gene for Usher syndrome type 2: Mutations in the long isoform of whirlin are associated with retinitis pigmentosa and sensorineural hearing loss. *Human Genetics*, *121*(2), 203–211. http://doi.org/10.1007/s00439-006-0304-0

Eudy, J. D. (1998). Mutation of a Gene Encoding a Protein with Extracellular Matrix Motifs in Usher Syndrome Type IIa. *Science*, *280*(5370), 1753–1757. http://doi.org/10.1126/science.280.5370.1753

Goodyear, R. J., Marcotti, W., Kros, C. J., & Richardson, G. P. (2005). Development and properties of stereociliary link types in hair cells of the mouse cochlea. *Journal of Comparative Neurology*, *485*(1), 75–85. http://doi.org/10.1002/cne.20513

Grati, M., Shin, J.-B., Weston, M. D., Green, J., Bhat, M. a, Gillespie, P. G., & Kachar, B. (2012). Localization of PDZD7 to the stereocilia ankle-link associates this scaffolding protein with the Usher syndrome protein network. *The Journal of*

Neuroscience : The Official Journal of the Society for Neuroscience, *32*(41), 14288–93. http://doi.org/10.1523/JNEUROSCI.3071-12.2012

Green, J. a, Yang, J., Grati, M., Kachar, B., & Bhat, M. a. (2013). Whirlin, a cytoskeletal scaffolding protein, stabilizes the paranodal region and axonal cytoskeleton in myelinated axons. *BMC Neuroscience*, *14*(1), 96. http://doi.org/10.1186/1471-2202-14-96

Hauswirth, W. W., Aleman, T. S., Kaushal, S., Cideciyan, A. V, Schwartz, S. B., Wang, L., … Jacobson, S. G. (2008). Treatment of leber congenital amaurosis due to RPE65 mutations by ocular subretinal injection of adeno-associated virus gene vector: short-term results of a phase I trial. *Human Gene Therapy*, *19*(10), 979–90. http://doi.org/10.1089/hum.2008.107

Holme, R. H., Kiernan, B. W., Brown, S. D. M., & Steel, K. P. (2002). Elongation of hair cell stereocilia is defective in the mouse mutant whirler. *The Journal of Comparative Neurology*, *450*(1), 94–102. http://doi.org/10.1002/cne.10301

Hong, D. H., Pawlyk, B. S., Shang, J., Sandberg, M. a, Berson, E. L., & Li, T. (2000). A retinitis pigmentosa GTPase regulator (RPGR)-deficient mouse model for X-linked retinitis pigmentosa (RP3). *Proceedings of the National Academy of Sciences of the United States of America*, *97*(7), 3649–3654. http://doi.org/10.1073/pnas.97.7.3649

Hu, Q. X., Dong, J. H., Du, H. B., Zhang, D. L., Ren, H. Z., Ma, M. L., … Sun, J. P. (2014). Constitutive Gai coupling activity of very large G protein-coupled receptor 1 (VLGR1) and its regulation by PDZD7 protein. *Journal of Biological Chemistry*, *289*(35), 24215–24225. http://doi.org/10.1074/jbc.M114.549816

Jepson, J. E. C., Shahidullah, M., Lamaze, A., Peterson, D., Pan, H., & Koh, K. (2012). dyschronic, a Drosophila homolog of a deaf-blindness gene, regulates circadian output and Slowpoke channels. *PLoS Genetics*, *8*(4), e1002671. http://doi.org/10.1371/journal.pgen.1002671

Jepson, J. E. C., Shahidullah, M., Liu, D., le Marchand, S. J., Liu, S., Wu, M. N., … Koh, K. (2014). Regulation of synaptic development and function by the Drosophila PDZ protein Dyschronic. *Development (Cambridge, England)*, *141*(23), 4548–4557. http://doi.org/10.1242/dev.109538

Jing-Ping, Z., Tian, Q. B., Sakagami, H., Kondo, H., Endo, S., & Suzuki, T. (2005). p55 protein is a member of PSD scaffold proteins in the rat brain and interacts with various PSD proteins. *Molecular Brain Research*, *135*(1-2), 204–216. http://doi.org/10.1016/j.molbrainres.2004.12.023

Kikkawa, Y., Mburu, P., Morse, S., Kominami, R., Townsend, S., & Brown, S. D. M. (2005). Mutant analysis reveals whirlin as a dynamic organizer in the growing hair cell stereocilium. *Human Molecular Genetics*, *14*(3), 391–400. http://doi.org/10.1093/hmg/ddi035

Kimberling, W. J., Hildebrand, M. S., Shearer, A. E., Jensen, M. L., Halder, J. A., Trzupek, K., … Smith, R. J. H. (2010). Frequency of Usher syndrome in two pediatric populations: Implications for genetic screening of deaf and hard of hearing children. *Genetics in Medicine : Official Journal of the American College of Medical Genetics*, *12*(8), 512–6. http://doi.org/10.1097/GIM.0b013e3181e5afb8

Lagziel, A., Ahmed, Z. M., Schultz, J. M., Morell, R. J., Belyantseva, I. A., & Friedman, T. B. (2005). Spatiotemporal pattern and isoforms of cadherin 23 in wild type and waltzer mice during inner ear hair cell development. *Developmental Biology*, *280*(2), 295–306. http://doi.org/10.1016/j.ydbio.2005.01.015

Lagziel, A., Overlack, N., Bernstein, S. L., Morell, R. J., Wolfrum, U., & Friedman, T. B. (2009). Expression of cadherin 23 isoforms is not conserved: implications for a mouse model of Usher syndrome type 1D. *Molecular Vision*, *15*(April), 1843–57. Retrieved from http://www.pubmedcentral.nih.gov/articlerender.fcgi?artid=2743805&tool=pmcentrez&rendertype=abstract

Liu, X., Udovichenko, I. P., Brown, S. D., Steel, K. P., & Williams, D. S. (1999). Myosin VIIa participates in opsin transport through the photoreceptor cilium. *The Journal of Neuroscience : The Official Journal of the Society for Neuroscience*, *19*(15), 6267–74. Retrieved from http://www.ncbi.nlm.nih.gov/pubmed/10414956

Liu, X., Walsh, J., Mburu, P., Kendrick-jones, J., Cope, J. T., Steel, K. P., & Brown, S. D. M. (1997). © 199 7 Nature Publishing Group http://www.nature.com/naturegenetics. *Nature Genetics*, *15*, 57–61.

Liu, X. Z., Hope, C., Walsh, J., Newton, V., Ke, X. M., Liang, C. Y., … Brown, S. D. (1998). Mutations in the myosin VIIA gene cause a wide phenotypic spectrum, including atypical Usher syndrome. *American Journal of Human Genetics*, *63*(3), 909–912. http://doi.org/10.1086/302026

Magliulo, G., Iannella, G., Gagliardi, S., Plateroti, R., Plateroti, P., Iozzo, N., & Vingolo, E. M. (2015). Usher's syndrome: Evaluation of the vestibular system with Cervical and Ocular Vestibular Evoked Myogenic Potentials and the Video Head Impulse Test. *Otology & Neurotology*, *36*(2), 1421–1427. http://doi.org/10.1097/MAO.0000000000000613

Manor, U., Disanza, A., Grati, M., Andrade, L., Lin, H., Di Fiore, P. P., … Kachar, B. (2011). Regulation of stereocilia length by myosin XVa and whirlin depends on the actin-regulatory protein Eps8. *Current Biology : CB*, *21*(2), 167–72. http://doi.org/10.1016/j.cub.2010.12.046

Mathur, P. D., Vijayakumar, S., Vashist, D., Jones, S. M., Jones, T. A., & Yang, J. (2015). A study of whirlin isoforms in the mouse vestibular system suggests potential vestibular dysfunction in *DFNB31* -deficient patients. *Human Molecular Genetics*, (September), ddv403. http://doi.org/10.1093/hmg/ddv403

Mathur, P. D., Zou, J., Zheng, T., Almishaal, A., Wang, Y., Chen, Q., … Yang, J. (2015).

Distinct expression and function of whirlin isoforms in the inner ear and retina: an insight into pathogenesis of USH2D and DFNB31. *Human Molecular Genetics*, *24*(21), 6213–28. http://doi.org/10.1093/hmg/ddv339

Mburu, P., Kikkawa, Y., Townsend, S., Romero, R., Yonekawa, H., & Brown, S. D. M. (2006). Whirlin complexes with p55 at the stereocilia tip during hair cell development. *Proceedings of the National Academy of Sciences of the United States of America*, *103*(29), 10973–8. http://doi.org/10.1073/pnas.0600923103

Mburu, P., Mustapha, M., Varela, A., Weil, D., El-Amraoui, A., Holme, R. H., … Brown, S. D. M. (2003). Defects in whirlin, a PDZ domain molecule involved in stereocilia elongation, cause deafness in the whirler mouse and families with DFNB31. *Nature Genetics*, *34*(4), 421–8. http://doi.org/10.1038/ng1208

Mburu, P., Romero, M. R., Hilton, H., Parker, A., Townsend, S., Kikkawa, Y., & Brown, S. D. M. (2010). Gelsolin plays a role in the actin polymerization complex of hair cell stereocilia. *PLoS ONE*, *5*(7), 1–9. http://doi.org/10.1371/journal.pone.0011627

McGee, J., Goodyear, R. J., McMillan, D. R., Stauffer, E. a, Holt, J. R., Locke, K. G., … Richardson, G. P. (2006). The very large G-protein-coupled receptor VLGR1: a component of the ankle link complex required for the normal development of auditory hair bundles. *The Journal of Neuroscience : The Official Journal of the Society for Neuroscience*, *26*(24), 6543–53. http://doi.org/10.1523/JNEUROSCI.0693-06.2006

Michalski, N., Michel, V., Bahloul, A., Lefèvre, G., Barral, J., Yagi, H., … Petit, C. (2007). Molecular characterization of the ankle-link complex in cochlear hair cells and its role in the hair bundle functioning. *The Journal of Neuroscience : The Official Journal of the Society for Neuroscience*, *27*(24), 6478–88. http://doi.org/10.1523/JNEUROSCI.0342-07.2007

Mustapha, M., Beyer, L. a, Izumikawa, M., Swiderski, D. L., Dolan, D. F., Raphael, Y., & Camper, S. a. (2007). Whirler mutant hair cells have less severe pathology than shaker 2 or double mutants. *Journal of the Association for Research in Otolaryngology : JARO*, *8*(3), 329–37. http://doi.org/10.1007/s10162-007-0083-x

Mustapha, M., Chouery, E., Chardenoux, S., Naboulsi, M., Paronnaud, J., Lemainque, A., … Petit, C. (2002). DFNB31, a recessive form of sensorineural hearing loss, maps to chromosome 9q32-34. *European Journal of Human Genetics : EJHG*, *10*(3), 210–212. http://doi.org/10.1038/sj.ejhg.5200780

Nakayama, J., Fu, Y. H., Clark, A. M., Nakahara, S., Hamano, K., Iwasaki, N., … Ptáček, L. J. (2002). A nonsense mutation of the MASS1 gene in a family with febrile and afebrile seizures. *Annals of Neurology*, *52*(5), 654–657. http://doi.org/10.1002/ana.10347

Nishiguchi, K. M., Tearle, R. G., Liu, Y. P., & et al. (2013). Whole genome sequencing in patients with retinitis pigmentosa reveals pathogenic DNA structural changes and

NEK2 as a new disease gene. *Proceedings of the National Academy of Sciences of the United States of America*, *110*(40), 16139–44. http://doi.org/10.1073/pnas.1308243110

Ouyang, X. M., Xia, X. J., Verpy, E., Du, L. L., Pandya, A., Petit, C., … Liu, X. Z. (2002). Mutations in the alternatively spliced exons of USH1C cause non-syndromic recessive deafness. *Human Genetics*, *111*(1), 26–30. http://doi.org/10.1007/s00439-002-0736-0

Randy McMillan, D., Kayes-Wandover, K. M., Richardson, J. A., & White, P. C. (2002). Very large G protein-coupled receptor-1, the largest known cell surface protein, is highly expressed in the developing central nervous system. *Journal of Biological Chemistry*, *277*(1), 785–792. http://doi.org/10.1074/jbc.M108929200

Reiners, J., Reidel, B., El-Amraoui, A., Boëda, B., Huber, I., Petit, C., & Wolfrum, U. (2003). Differential Distribution of Harmonin Isoforms and Their Possible Role in Usher-1 Protein Complexes in Mammalian Photoreceptor Cells. *Investigative Ophthalmology and Visual Science*, *44*(11), 5006–5015. http://doi.org/10.1167/iovs.03-0483

Riazuddin, S., Belyantseva, I. A., Giese, A. P. J., Lee, K., Indzhykulian, A. A., Nandamuri, S. P., … Ahmed, Z. M. (2012). Alterations of the CIB2 calcium- and integrin-binding protein cause Usher syndrome type 1J and nonsyndromic deafness DFNB48. *Nature Genetics*, *44*(11), 1265–1271. http://doi.org/10.1038/ng.2426

Riazuddin, S., Nazli, S., Ahmed, Z. M., Yang, Y., Zulfiqar, F., Shaikh, R. S., … Friedman, T. B. (2008). Mutation spectrum of MYO7A and evaluation of a novel nonsyndromic deafness DFNB2 allele with residual function. *Human Mutation*, *29*(4), 502–511. http://doi.org/10.1002/humu.20677

Rivolta, C., Sweklo, E. A., Berson, E. L., & Dryja, T. P. (2000). Missense mutation in the USH2A gene: association with recessive retinitis pigmentosa without hearing loss. *American Journal of Human Genetics*, *66*(6), 1975–8. http://doi.org/10.1086/302926

Schneider, E., Märker, T., Daser, A., Frey-Mahn, G., Beyer, V., Farcas, R., … Haaf, T. (2009). Homozygous disruption of PDZD7 by reciprocal translocation in a consanguineous family: a new member of the Usher syndrome protein interactome causing congenital hearing impairment. *Human Molecular Genetics*, *18*(4), 655–66. http://doi.org/10.1093/hmg/ddn395

Schultz, J. M., Bhatti, R., Madeo, A. C., Turriff, A., Muskett, J. a, Zalewski, C. K., … Friedman, T. B. (2011). Allelic hierarchy of CDH23 mutations causing non-syndromic deafness DFNB12 or Usher syndrome USH1D in compound heterozygotes. *Journal of Medical Genetics*, *48*(11), 767–75. http://doi.org/10.1136/jmedgenet-2011-100262

Schultz, J. M., Yang, Y., Caride, A. J., Filoteo, A. G., Penheiter, A. R., Lagziel, A., … Griffith, A. J. (2005). Modification of human hearing loss by plasma-membrane

calcium pump PMCA2. *The New England Journal of Medicine*, *352*(15), 1557–64. http://doi.org/10.1056/NEJMoa043899

Skradski, S. L., Clark, A. M., Jiang, H., White, H. S., Fu, Y. H., & Ptacek, L. J. (2001). A novel gene causing a mendelian audiogenic mouse epilepsy. *Neuron*, *31*(4), 537–544. http://doi.org/10.1016/S0896-6273(01)00397-X

Stone, I. M., Lurie, D. I., Kelley, M. W., & Poulsen, D. J. (2005). Adeno-associated virus-mediated gene transfer to hair cells and support cells of the murine cochlea. *Molecular Therapy*, *11*(6), 843–848. http://doi.org/10.1016/j.ymthe.2005.02.005

Tian, M., Wang, W., Delimont, D., Cheung, L., Zallocchi, M., Cosgrove, D., & Peng, Y.-W. (2014). Photoreceptors in whirler mice show defective transducin translocation and are susceptible to short-term light/dark changes-induced degeneration. *Experimental Eye Research*, *118*, 145–53. http://doi.org/10.1016/j.exer.2013.10.021

Tlili, A., Charfedine, I., Lahmar, I., Benzina, Z., Mohamed, B. A., Weil, D., … Ayadi, H. (2005). Identification of a novel frameshift mutation in the DFNB31/WHRN gene in a Tunisian consanguineous family with hereditary non-syndromic recessive hearing loss. *Human Mutation*, *25*(5), 503. http://doi.org/10.1002/humu.9333

van Wijk, E., Pennings, R. J. E., te Brinke, H., Claassen, A., Yntema, H. G., Hoefsloot, L. H., … Kremer, H. (2004). Identification of 51 novel exons of the Usher syndrome type 2A (USH2A) gene that encode multiple conserved functional domains and that are mutated in patients with Usher syndrome type II. *American Journal of Human Genetics*, *74*, 738–744. http://doi.org/10.1086/383096

van Wijk, E., van der Zwaag, B., Peters, T., Zimmermann, U., Te Brinke, H., Kersten, F. F. J., … Kremer, H. (2006a). The DFNB31 gene product whirlin connects to the Usher protein network in the cochlea and retina by direct association with USH2A and VLGR1. *Human Molecular Genetics*, *15*(5), 751–65. http://doi.org/10.1093/hmg/ddi490

van Wijk, E., van der Zwaag, B., Peters, T., Zimmermann, U., Te Brinke, H., Kersten, F. F. J., … Kremer, H. (2006b). The DFNB31 gene product whirlin connects to the Usher protein network in the cochlea and retina by direct association with USH2A and VLGR1. *Human Molecular Genetics*, *15*(5), 751–65. http://doi.org/10.1093/hmg/ddi490

Verpy, E., Leibovici, M., Zwaenepoel, I., Liu, X. Z., Gal, a, Salem, N., … Petit, C. (2000). A defect in harmonin, a PDZ domain-containing protein expressed in the inner ear sensory hair cells, underlies Usher syndrome type 1C. *Nature Genetics*, *26*(1), 51–55. http://doi.org/10.1038/79171

Vozzi, D., Aaspõllu, A., Athanasakis, E., Berto, A., Fabretto, A., Licastro, D., … Gasparini, P. (2011). Molecular epidemiology of Usher syndrome in Italy. *Molecular Vision*, *17*(June), 1662–1668.

Weston, M. D., Luijendijk, M. W. J., Humphrey, K. D., Möller, C., & Kimberling, W. J. (2004). Mutations in the VLGR1 gene implicate G-protein signaling in the pathogenesis of Usher syndrome type II. *American Journal of Human Genetics*, *74*(2), 357–366. http://doi.org/10.1086/381685

White, J. K., Gerdin, A. K., Karp, N. A., Ryder, E., Buljan, M., Bussell, J. N., … Steel, K. P. (2013). Genome-wide Generation and Systematic Phenotyping of Knockout Mice Reveals New Roles for Many Genes. *Cell*, *154*(2), 452–464. http://doi.org/10.1016/j.cell.2013.06.022

Wright, R. N., Hong, D.-H., & Perkins, B. (2012). RpgrORF15 connects to the usher protein network through direct interactions with multiple whirlin isoforms. *Investigative Ophthalmology & Visual Science*, *53*(3), 1519–29. http://doi.org/10.1167/iovs.11-8845

Yagi, H., Takamura, Y., Yoneda, T., Konno, D., Akagi, Y., Yoshida, K., & Sato, M. (2005). Vlgr1 knockout mice show audiogenic seizure susceptibility. *Journal of Neurochemistry*, *92*(1), 191–202. http://doi.org/10.1111/j.1471-4159.2004.02875.x

Yang, J., Le, W., Song, H., & Sokolov, M. (2012). Current Understanding of Usher Syndrome Type II. *Frontiers in Bioscience*, *17*, 1165–1183.

Yang, J., Liu, X., Zhao, Y., Adamian, M., Pawlyk, B., Sun, X., … Li, T. (2010a). Ablation of whirlin long isoform disrupts the USH2 protein complex and causes vision and hearing loss. *PLoS Genetics*, *6*(5), e1000955. http://doi.org/10.1371/journal.pgen.1000955

Yang, J., Liu, X., Zhao, Y., Adamian, M., Pawlyk, B., Sun, X., … Li, T. (2010b). Ablation of whirlin long isoform disrupts the USH2 protein complex and causes vision and hearing loss. *PLoS Genetics*, *6*(5), e1000955. http://doi.org/10.1371/journal.pgen.1000955

Yap, C. C., Liang, F., Yamazaki, Y., Muto, Y., Kishida, H., Hayashida, T., … Yano, R. (2003). CIP98, a novel PDZ domain protein, is expressed in the central nervous system and interacts with calmodulin-dependent serine kinase. *Journal of Neurochemistry*, *85*(1), 123–134. http://doi.org/10.1046/j.1471-4159.2003.01647.x

Zampini, V., Rüttiger, L., Johnson, S. L., Franz, C., Furness, D. N., Waldhaus, J., … Marcotti, W. (2011). Eps8 regulates hair bundle length and functional maturation of mammalian auditory hair cells. *PLoS Biology*, *9*(4). http://doi.org/10.1371/journal.pbio.1001048

Zou, J., Luo, L., Shen, Z., Chiodo, V. A., Ambati, B. K., Hauswirth, W. W., & Yang, J. (2011). Whirlin replacement restores the formation of the USH2 protein complex in whirlin knockout photoreceptors. *Investigative Ophthalmology and Visual Science*, *52*(5), 2343–2351. http://doi.org/10.1167/iovs.10-6141

Zou, J., Mathur, P. D., Zheng, T., Wang, Y., Almishaal, A., Park, A. H., & Yang, J.

(2015). Individual USH2 proteins make distinct contributions to the ankle link complex during development of the mouse cochlear stereociliary bundle. *Human Molecular Genetics*, (September), ddv398. http://doi.org/10.1093/hmg/ddv398

Zou, J., Zheng, T., Ren, C., Askew, C., Liu, X., & Yang, J. (2014). Deletion of PDZD7 disrupts the Usher Syndrome Type 2 protein complex in cochlear hair cells and causes hearing loss in mice. *Human Molecular Genetics*, *23*(9), 2374–90.